Notes on

Gravitational Waves

v0.2

S.Bernuzzi[1] & M.Breschi ©

Jena FSU

Last update: April 21, 2022

[1] sebastiano.benuzzi@uni-jena.de

Contents

About

These are semiprivate notes sketching topics and calculations discussed in about 15 lectures of 1.5 hours each at Jena FSU. They are not meant to substitute books. Please visit

`http://sbernuzzi.gitpages.tpi.uni-jena.de/gw/`

for an updated list of books, references and other material, including the exercise sheets distributed each week.

I welcome constructive feedbacks. Red text is work in progr...

Conventions. The spacetime and the metric are indicated as $(\mathcal{M}, g_{ab})$ and the notation mostly follows Wald's book: signature convention $(-,+,+,+)$, $a,b,...$ indexes in abstract notation, $\alpha,\beta,...$ indexes of tensor components, $i,j,...$ spatial coordinate indexes, etc. Vector and tensors are sometimes indicated as $\boldsymbol{v}$ and $\boldsymbol{g}$, i.e. in geometrical instead of index notation. Coordinate basis of the tange vector space $T_p(M)$ are indicated as e_μ; the natural basis of partial derivatives is $e_\mu = \partial_\mu$. The dual basis $e^{*\nu}$ ($e_\mu e^{*\nu} = \delta^\nu_\mu$) is constructed by the gradients of the coordinates is $e^{*\mu} = \mathrm{d}x^\mu$. The exterior derivative of an n-form is indicated with $\mathbf{d}$; applied to scalars it reduces to the gradient (1-form) $\mathbf{d}f = \mathrm{d}f = \mathrm{grad}(f)$ with components $(\mathbf{d}f)_\mu = (\mathrm{d}f)_\mu = \partial_\mu f$. Covariant derivatives (Levi-Civita connection) are indicated with ∇. ∇ applied to scalars reduces to the gradient $\nabla f = \mathrm{d}f$ (components $\nabla_\mu f = (\mathrm{d}f)_\mu = \partial_\mu f$) and it is consistent with the concept of tangent vector $v(f) = v^\mu \nabla_\mu f$. The symbol $:=$ is an assignment, while $\equiv$ an identity.

Units are $c = G = 1$ if not specified. $GM_\odot = 4.925490947\mu$s or 1.476625038km. The dimensionless frequency $\hat{\omega} = GM\omega$ relates to the frequency in Hz

$$f = \frac{\omega}{2\pi} \simeq 32.3125\, \hat{\omega}\, \frac{M_\odot}{M} \ \text{kHz}.$$

1. Introduction

Gravitational waves (GWs) are a key prediction of Einstein's general relativity (GR). Einstein discusses these solutions of the theory already in 1916, but a rigorous understanding of gravitational radiation is available only starting from the 50s in connection to fundamental studies on the asymptotic structure of spacetime (Bondi, Goldberg, Newmann, Penrose, Pirani, Robison, Sachs, Trautman and many others.)

Observational evidence for GWs exists since 1974 with the measurements of radio signals from the pulsar PSR B1913+16. The source is a binary system in our galaxy at 21000 light years (6400 pc) made of two neutron stars, one of those being a pulsar that emits period radio pulses. The variation in the time arrival of the pulses allows to identify the source is a binary system and to precise measure its orbital period (~ 7.75 hrs) and the masses. The observations performed during the decades have proven that the period of the orbit decay as predicted by GR due to the emission of GWs, as shown by the famous plot in the left panel of Fig. (1.1). Few of these systems have been identified to date and they provide us with stringent tests of GR.

Direct measurements of GW travelling trhough Earth are possible since 2015 using gravitational-wave interferometric techniques. The first detection was obtained by the LIGO experiment on September 14th 2015. The source is identified as the collision (merger) of black holes in circularized orbits as predicted by GR. The signal corresponds to the one calculated by means of numerical relativity simulations and consist of a chirp signal followed by the final black hole's ringdown. The former is predicted by the post-Newtonian formalism, the latter by black hole perturbation theory. The binary was a distance of $\sim$ 440 Mpc (redshift 0.09) and the collision of the two masses of $\sim 35 + 30 M_\odot$ formed a black hole of $\sim 62\ M_\odot$ emitting in GWs an energy of $\sim 3\ M_\odot c^2$. Several GW detections from black hole mergers and two from neutron star binary mergers have been reported since then by the LIGO-Virgo collaboration.

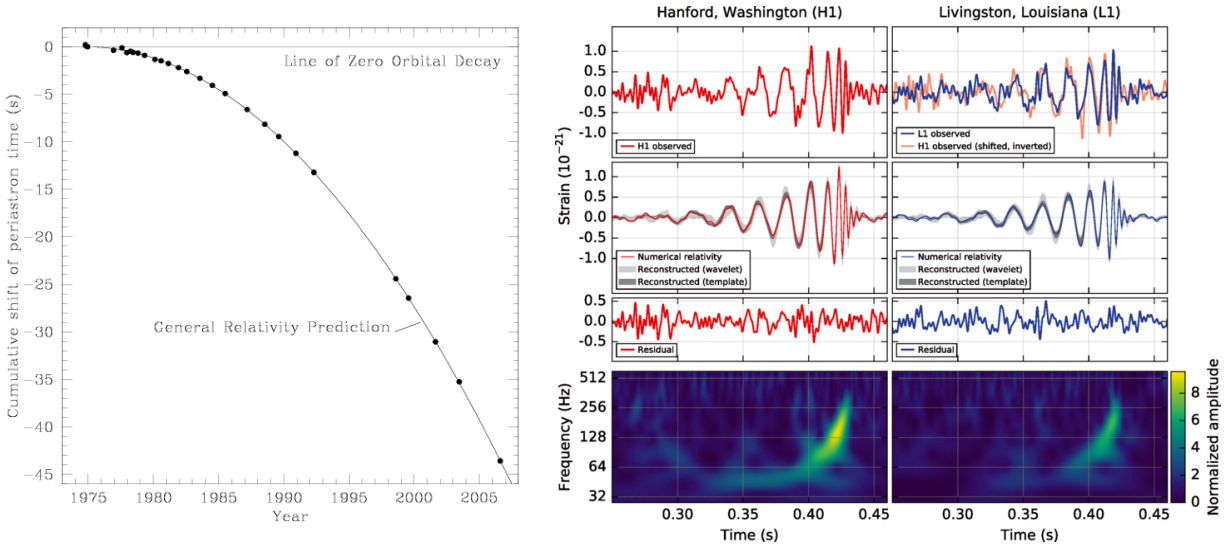

Figure 1.1: Observations of GWs. Left: The decay of the orbital period of the binary system observed in PSR B1913+16; Right: The binary black hole merger waveform GW150914 observed by LIGO in 2015.

The course introduces the basic theoretical concepts necessary to understand the two observations above. The linearized theory (Chap. 2-3) is complemented with a discussion on the energy and the stress-energy tensor (Chap. 5). The systematic multipolar expansion on flat spacetime is then discussed both in terms of STF tensors and tensor spherical harmonics (Chap. 4). Those tensors are key tools for computing solutions in the post-Newtonian (PN) formalism (Chap. 6) and in perturbation theory of spherical spacetimes (Chap. 7). Post-Newtonian and black hole perturbations combine in the most avanced framework for the GR two-body dynamics of compact binaries: the effective-one-body formalism (Chap.8). Finally, the basics of laser-interferometer detectors and modern data analysis techniques are discussed (Chap. 9).

2. Weak field GR

Weak field limit of GR and the Einstein Field Equations (EFE) linearized around Mikowski spacetime. The linearized EFE equations apply for the description of Solar-system phenomena, gravitoeletric/magnetic phenomena and gravitational waves.

Suggested readings. *Chap. 4 of Wald (1984); Chap. 4 of Carroll (1997); Chap. 7-8 of Schutz (1985); Chap. 1,3 of Maggiore (2007).*

2.1 Weak field GR

In the regime of weak gravity one assumes that there exists a global inertial frame in which the metric can be written as

$$g_{\mu\nu} = \eta_{\mu\nu} + h_{\mu\nu} \quad \text{with} \quad |h_{\mu\nu}| \ll |\eta_{\mu\nu}| \sim 1 \ . \tag{2.1}$$

Since the component of the perturbation of Mikowski spacetime are "small" (in the sense above), the GR equations can be linearized at linear order in $\boldsymbol{h}$. Linearized equations apply, for example, to the Solar system where

$$|h_{\mu\nu}| \sim \frac{\phi}{c^2} \lesssim \frac{GM_\odot}{c^2 R_\odot} \sim 10^{-6} \ , \tag{2.2}$$

and can be used to describe

- Newtonian gravity;
- Gravitoelectric and gravitomagnetic phenomena;
- Propagation of gravitational waves.

Formally, the linearized theory can be regarded as a field theory in which

- $\eta_{\mu\nu}$ is a background metric;
- The grav.field generated by the matter does not backreact on the source;
- $h_{\mu\nu}$ is the main field and transforms as a tensor on flat spacetime under Lorentz transformation (Lorentz covariance). Consider a Lorentz transformation of coordinates ($\Lambda^{\mathrm{T}}\eta\Lambda = \eta$):

$$x^\mu = \Lambda^\mu{}_\nu (x')^\nu = \frac{\partial x^\mu}{\partial x^{\nu'}} x^{\nu'} \quad \Rightarrow \quad g_{\mu'\nu'} = \frac{\partial x^\mu}{\partial x^{\mu'}} \frac{\partial x^\nu}{\partial x^{\nu'}} g_{\mu\nu} = \Lambda^\mu{}_{\mu'} \Lambda^\nu{}_{\nu'} g_{\mu\nu} = \Lambda^\mu{}_{\mu'} \Lambda^\nu{}_{\nu'} (\eta_{\mu\nu} + h_{\mu\nu}) = \tag{2.3a}$$

$$= \underbrace{\Lambda^\mu{}_{\mu'} \Lambda^\nu{}_{\nu'} \eta_{\mu\nu}}_{=\eta_{\mu'\nu'}} + \Lambda^\mu{}_{\mu'} \Lambda^\nu{}_{\nu'} h_{\mu\nu} = \eta_{\mu\nu} + \Lambda^\mu{}_{\mu'} \Lambda^\nu{}_{\nu'} h_{\mu\nu} \tag{2.3b}$$

  that implies that the following substitution leaves the linearized theory invariant,

$$h_{\mu\nu} \to h_{\mu'\nu'} = \Lambda^\mu{}_{\mu'} \Lambda^\nu{}_{\nu'} h_{\mu\nu} \ . \tag{2.4}$$

2.2 Infinitesimal diffeomorphism invariance

Symmetry of linearized GR. Consider an infinitesimal coordinate transformation:

$$x^\mu \mapsto x^{\mu'} = x^\mu + \xi^\mu(x^\alpha) \quad \text{with} \quad |\partial_\beta \xi^\alpha| \sim |h_{\mu\nu}| \ll 1 \tag{2.5a}$$

$$\frac{\partial x^{\mu'}}{\partial x^\mu} = \delta^{\mu'}_\mu + \partial_\mu \xi^{\mu'} \tag{2.5b}$$

$$\frac{\partial x^\mu}{\partial x^{\mu'}} = \delta^\mu_{\mu'} - \partial_{\mu'} \xi^\mu + \mathcal{O}(|\partial\xi|^2) \tag{2.5c}$$

where one uses the Taylor expansion of a matrix $A = (1 + \delta\xi)$ for the inverse $(1 + \delta\xi)^{-1} \approx 1 - \delta\xi$. Note prime indexes refer to tensor components in primed coordinates x', while the unprimed indexes refer to tensor component in unprime

coordinates x. Indexes on r.h.s. and l.h.s. take the same values, although they do not "symbolically match" on the two side of the equation. For example, $g_{\mu'\nu'} = \eta_{\mu\nu} + h_{\mu\nu} = \eta_{\mu'\nu'} + h_{\mu\nu}$ really means $g_{\mu\nu}(x') = \eta_{\mu\nu} + h_{\mu\nu}(x)$. Using this notation is useful to keep formulas compact. To linear order in h and in $\partial\xi$ the metric change is:

$$
\begin{aligned}
g_{\mu'\nu'} &= \frac{\partial x^\mu}{\partial x^{\mu'}}\frac{\partial x^\nu}{\partial x^{\nu'}} g_{\mu\nu} = (\delta^\mu_{\mu'} - \partial_{\mu'}\xi^\mu)(\delta^\nu_{\nu'} - \partial_{\nu'}\xi^\nu)(\eta_{\mu\nu} + h_{\mu\nu}) = && \text{(2.6a)}\\
&= (\delta^\mu_{\mu'}\delta^\nu_{\nu'} - \partial_{\mu'}\xi^\mu\delta^\nu_{\nu'} - \partial_{\nu'}\xi^\nu\delta^\mu_{\mu'} + \partial_{\mu'}\xi^\mu\partial_{\nu'}\xi^\nu)(\eta_{\mu\nu} + h_{\mu\nu}) = && \text{(2.6b)}\\
&= \underbrace{\delta^\mu_{\mu'}\delta^\nu_{\nu'}\eta_{\mu\nu}}_{=\eta_{\mu'\nu'}} - \underbrace{\partial_{\mu'}\xi^\mu\delta^\nu_{\nu'}\eta_{\mu\nu}}_{=\partial_{\mu'}\xi_{\nu'}} - \partial_{\nu'}\xi^\nu\delta^\mu_{\mu'}\eta_{\mu\nu} + \underbrace{\delta^\mu_{\mu'}\delta^\nu_{\nu'}h_{\mu\nu}}_{h_{\mu'\nu'}} - \underbrace{\partial_{\mu'}\xi^\mu\delta^\nu_{\nu'}h_{\mu\nu} - \partial_{\nu'}\xi^\nu\delta^\mu_{\mu'}h_{\mu\nu} + \partial_{\mu'}\xi^\mu\partial_{\nu'}\xi^\nu h_{\mu\nu}}_{=\mathcal{O}(h^2)} = && \text{(2.6c)}\\
&= \eta_{\mu'\nu'} + h_{\mu'\nu'} - 2\partial_{(\mu'}\xi_{\nu')} = && \text{(2.6d)}\\
&= \eta_{\mu\nu} + h_{\mu'\nu'} - 2\partial_{(\mu'}\xi_{\nu')} && \text{(2.6e)}
\end{aligned}
$$

Hence, the metric is invariant under any infinitesimal coordinate transformation of the perturbed metric:

$$
\boxed{h_{\mu\nu} \mapsto h_{\mu'\nu'} = h_{\mu\nu} + 2\partial_{(\mu}\xi_{\nu)} \ , } \tag{2.7}
$$

In other words, the weak metric is represented by the equivalence classes of metrics linked by the infinitesimal coordinate transformations above. If one considers ξ^α as the components of a vector, then the transformation can be written in terms of the Lie derivatives, and the infinitesimal coordinate transformation can be interpreted as an *infinitesimal diffeomorphism* generated by ξ:

$$
2\partial_{(\mu}\xi_{\nu)} = \mathcal{L}_\xi \eta_{\mu\nu} \quad \Rightarrow \quad h_{\mu\nu} \mapsto h_{\mu\nu} + \mathcal{L}_\xi \eta_{\mu\nu} \quad . \tag{2.8}
$$

In summary, weak field GR is *invariant under infinitesimal diffeomorphisms.*

Remark 2.2.1. *The above transformation is the analogous to the gauge transformation for the potentials in electromagnetism:*

$$
A_\alpha \mapsto A_\alpha + \partial_\alpha \chi \ . \tag{2.9}
$$

2.3 Weak field equations

Calculation of the Einstein tensor linearized in h. Indexes are raised on lowered with the flat metric η; for example the trace of the perturbation is $h := h^\alpha_\alpha = \eta^{\alpha\beta}h_{\alpha\beta}$. It is left as [exercise] to show:

$$
\begin{aligned}
g^{\mu\nu} &= \eta^{\mu\nu} + h^{\mu\nu} + \mathcal{O}(h^2) && \text{(2.10a)}\\
\Gamma^\mu_{\alpha\beta} &= \frac{1}{2}\eta^{\mu\lambda}\left(\partial_\alpha h_{\lambda\beta} + \partial_\beta h_{\lambda\alpha} - \partial_\lambda h_{\alpha\beta}\right) + \mathcal{O}(h^2) && \text{(2.10b)}\\
R_{\mu\nu} &= \partial\Gamma - \partial\Gamma + \underbrace{\Gamma\Gamma - \Gamma\Gamma}_{\mathcal{O}(h^2)} = \partial_\alpha\Gamma^\alpha_{\mu\nu} - \partial_\mu\Gamma^\alpha_{\alpha\nu} + \mathcal{O}(h^2) \approx \partial^\alpha\partial_{(\mu}h_{\nu)\alpha} - \frac{1}{2}\partial_\lambda\partial^\lambda h_{\mu\nu} - \frac{1}{2}\partial_\mu\partial_\nu h && \text{(2.10c)}\\
R &= \eta^{\mu\nu}R_{\mu\nu} = \frac{1}{2}\left(\eta^{\mu\nu}\partial^\alpha\partial_\mu h_{\nu\alpha} + \eta^{\mu\nu}\partial^\alpha\partial_\nu h_{\mu\alpha}\right) - \frac{1}{2}\partial_\lambda\partial^\lambda(\underbrace{\eta^{\mu\nu}h_{\mu\nu}}_{=h}) - \frac{1}{2}\underbrace{\eta^{\mu\nu}\partial_\mu\partial_\nu}_{\partial_\lambda\partial^\lambda} h = \cancel{\frac{1}{2}2}\partial^\alpha\partial^\nu h_{\nu\alpha} - \partial_\lambda\partial^\lambda h && \text{(2.10d)}\\
G_{\mu\nu} &= R_{\mu\nu} - \frac{1}{2}\eta_{\mu\nu}R = \partial^\alpha\partial_{(\mu}h_{\nu)\alpha} - \frac{1}{2}\partial_\lambda\partial^\lambda h_{\mu\nu} - \frac{1}{2}\partial_\mu\partial_\nu h - \frac{1}{2}\eta_{\mu\nu}(\partial^\alpha\partial^\beta h_{\alpha\beta} - \partial_\lambda\partial^\lambda h) \ . && \text{(2.10e)}
\end{aligned}
$$

The linearized Einstein tensor

$$
G_{\mu\nu} = \underbrace{\partial^\alpha\partial_{(\mu}h_{\nu)\alpha}}_{\text{I.}} - \underbrace{\frac{1}{2}\partial_\lambda\partial^\lambda h_{\mu\nu}}_{\text{II.}} - \underbrace{\frac{1}{2}\partial_\mu\partial_\nu h}_{\text{III.}} - \underbrace{\frac{1}{2}\eta_{\mu\nu}\partial^\alpha\partial^\beta h_{\alpha\beta}}_{\text{IV.}} + \underbrace{\frac{1}{2}\eta_{\mu\nu}\partial_\lambda\partial^\lambda h}_{\text{V.}} \ , \tag{2.11}
$$

can be written in a simpler form considering the trace reverse metric

$$
\bar{h}_{\mu\nu} := h_{\mu\nu} - \frac{1}{2}\eta_{\mu\nu}h \ . \tag{2.12}
$$

Note that

$$
\bar{h} = \eta^{\mu\nu}\bar{h}_{\mu\nu} = \underbrace{\eta^{\mu\nu}h_{\mu\nu}}_{=h} - \frac{1}{2}\underbrace{\eta^{\mu\nu}\eta_{\mu\nu}}_{=4} h = -h \ . \tag{2.13}
$$

Calculate each term:

$$\mathrm{I} = \partial^\alpha \partial_{(\mu}\bar{h}_{\nu)\alpha} + \frac{1}{4}\partial^\alpha\partial_\mu(\eta_{\nu\alpha}h) + \frac{1}{4}\partial^\alpha\partial_\nu(\eta_{\mu\alpha}h) = \underbrace{\partial^\alpha\partial_{(\mu}\bar{h}_{\nu)\alpha}}_{\mathrm{Ia}} + \underbrace{\frac{1}{2}\partial_{(\mu}\partial_{\nu)}h}_{\mathrm{Ib}} \tag{2.14a}$$

$$\mathrm{II} = \underbrace{-\frac{1}{2}\eta_{\alpha\beta}\partial^\alpha\partial^\beta\bar{h}_{\mu\nu}}_{\mathrm{IIa}} \underbrace{-\frac{1}{4}\eta_{\mu\nu}\eta_{\alpha\beta}\partial^\alpha\partial^\beta h}_{\mathrm{IIb}} \tag{2.14b}$$

$$\mathrm{IV} = -\frac{1}{2}\eta_{\mu\nu}\partial^\alpha\partial^\beta(\bar{h}_{\alpha\beta} + \frac{1}{2}\eta_{\alpha\beta}h) = \underbrace{-\frac{1}{2}\eta_{\mu\nu}\partial^\alpha\partial^\beta\bar{h}_{\alpha\beta}}_{\mathrm{IVa}} \underbrace{-\frac{1}{4}\eta_{\mu\nu}\eta_{\alpha\beta}\partial^\alpha\partial^\beta h}_{\mathrm{IVb}} \tag{2.14c}$$

$$0 = \mathrm{V} + \mathrm{IIb} + \mathrm{IVb} \tag{2.14d}$$

$$0 = \mathrm{III} + \mathrm{Ib} \tag{2.14e}$$

$$G_{\mu\nu} = \mathrm{IIa} + \mathrm{Ia} + \mathrm{IVa} = -\frac{1}{2}\eta_{\alpha\beta}\partial^\alpha\partial^\beta\bar{h}_{\mu\nu} + \partial^\alpha\partial_{(\mu}\bar{h}_{\nu)\alpha} - \frac{1}{2}\eta_{\mu\nu}\partial^\alpha\partial^\beta\bar{h}_{\alpha\beta} \tag{2.14f}$$

The linearized Einstein tensor is invariant w.r.t the inifinitesimal coordinate transformation of Eq. (2.7) [exercise]. From the above expression one sees that the last two terms contain the divergence of the metric. Imposing the *Hilbert gauge* (or Lorentz)

$$\partial^\alpha\bar{h}_{\mu\alpha} = 0 \ , \quad \text{(Hilbert gauge)} \tag{2.15}$$

leads to the following equations for linearized GR:

$$\Box_\eta\bar{h}_{\mu\nu} = -\frac{16\pi G}{c^4}T_{\mu\nu} \ . \tag{2.16}$$

Note:

- It is always possible to reduce to Hilbert gauge by performing an infinitesimal coordinate transformation. The set of 4 functions ξ^μ is given by the solution of 4 inhomogeneous wave equations (Cf. Lorentz gauge in electrodynamics):

$$h_{\mu\nu} \mapsto h_{\mu\nu} + 2\partial_{(\mu}\xi_{\nu)} \tag{2.17a}$$

$$h \mapsto h + \eta^{\alpha\beta}\partial_\alpha\xi_\beta + \eta^{\alpha\beta}\partial_\beta\xi_\alpha = h + 2\partial_\mu\xi^\mu \tag{2.17b}$$

$$\bar{h}_{\mu\nu} \mapsto \bar{h}_{\mu\nu} + 2\partial_{(\mu}\xi_{\nu)} - \eta_{\mu\nu}\partial_\alpha\xi^\alpha \tag{2.17c}$$

$$\partial^\alpha\bar{h}_{\mu\alpha} \mapsto \partial^\alpha\bar{h}_{\mu\alpha} + \Box\xi_\mu + \cancel{\partial^\beta\partial_\mu\xi_\beta} - \cancel{\partial_\mu\partial_\lambda\xi^\lambda} \quad \Rightarrow \quad \Box\xi_\nu = -\partial^\alpha\bar{h}_{\nu\alpha} =: V_\nu \neq 0 \tag{2.17d}$$

- Eq. (2.16) is a linear wave equation for the components of $\boldsymbol{h}$. At linear order in $\boldsymbol{h}$, the stress energy tensor does **not** depend on $\boldsymbol{h}$, so in linear GR one can specify the matter source and solve for the metric. For example, it is possible to calculate solutions using Green functions as in electrodynamics (see below).
- The Bianchi identity in the weak field simplifies and it is written as the partial derivative of the Einstein tensor since $\boldsymbol{\partial}$ is the connection associated to $\boldsymbol{\eta}$. Hence, the weak field equations imply the conservation of the stress-energy tensor on flat background, and that matter does not backreact on the curvature:

$$\partial_\nu G^{\mu\nu} = 0 \quad \Rightarrow \quad \partial_\nu T^{\mu\nu} = 0 \ . \tag{2.18}$$

- In vacuum, linearized EFEs are the equations for a massless spin-2 field propagating in flat spacetime (Chap. 13 Wald (1984)).

2.4 Weak field solutions

Formal solutions of Eq. (2.16) for static and stationary matter distributions.

2.4.1 Static source

A static matter distribution is modeled by a time-independent stress-energy tensor in the form

$$T_{\mu\nu} = \rho t_\mu t_\nu \ \text{ i.e. } \ T_{00} = \rho(x^i) \ , \ \ T_{0i} = T_{ij} = 0 \ , \tag{2.19}$$

where $t^\mu = (\partial_t)^\mu$ is the vector along the time direction of the global inertial coordinates. With this prescription, the r.h.s. of Eq. (2.16) is time-independent, thus also the grav. field must be time independent

$$\partial_t\bar{h}_{\mu\nu} = 0 \ , \tag{2.20}$$

and the linearized EFE reduce to Poisson equations for the components of the metric field:

$$\begin{cases} \Delta\bar{h}_{\mu\nu} = -16\pi\rho & , \quad \mu=\nu=0 \\ \Delta\bar{h}_{\mu\nu} = 0 & , \quad \text{otherwise} \ . \end{cases} \tag{2.21}$$

The Poisson equations have boundary values $\bar{h}_{ij}|_{r\to\infty} = 0$. Hence, the solution of the 00 equation is immediately given in terms of the Newton grav. potential by formally comparing to Newton's $\Delta\phi = 4\pi\rho$. The solution of the other equations (without source terms) is simply zero:

$$\begin{cases} \bar{h}_{\mu\nu} & = -4\phi \ , \quad \mu=\nu=0 \\ \bar{h}_{\mu\nu} & = 0 \ , \quad \text{otherwise} \end{cases} \quad \Rightarrow \quad \bar{h}_{\mu\nu} = -4\phi t_\mu t_\nu \ . \tag{2.22}$$

Reversing the trace:

$$\bar{h} = \eta^{\mu\nu}\bar{h}_{\mu\nu} = \eta^{00}\bar{h}_{00} = +4\phi \tag{2.23a}$$

$$h_{\mu\nu} = \bar{h}_{\mu\nu} - \frac{1}{2}\eta_{\mu\nu}\bar{h} = -4\phi t_\mu t_\nu - \frac{1}{2}\eta_{\mu\nu}(4\phi) \tag{2.23b}$$

$$g_{\mu\nu} = \eta_{\mu\nu} + h_{\mu\nu} = \eta_{\mu\nu} + \bar{h}_{\mu\nu} - \frac{1}{2}\eta_{\mu\nu}\bar{h} = \eta_{\mu\nu}(1-\frac{\bar{h}}{2}) + \bar{h}_{\mu\nu} = \eta_{\mu\nu}(1-2\phi) - 4\phi t_\mu t_\nu \tag{2.23c}$$

or

$$g = -\left(1+\frac{2\phi}{c^2}\right)\mathrm{d}(ct)^2 + \left(1-\frac{2\phi}{c^2}\right)\delta_{ij}\mathrm{d}x^i\mathrm{d}x^j \approx -(1+2\phi)c^2\mathrm{d}t^2 + \delta_{ij}\mathrm{d}x^i\mathrm{d}x^j \ , \tag{2.24}$$

where the second line highlights the leading order terms in a $1/c$ expansion.

Far from a source of mass M the multipolar expansion of the grav. potential starts with $\phi \approx -\frac{M}{r} + \mathcal{O}(1/r^2)$, so the distant metric is fully specified by the source mass and reduces to Mikowski at $r\to\infty$ if $M\neq 0$, or everywhere if $M\equiv 0$. It is remarkable that this metric describes the motion of particles (geodesic motion) in both Newtonian gravity and SR (using the appropriate limits). Note, however, a subtle point: the geodesic equations on the weak metric (weak gravity field) imply

$$\frac{d^2x^i}{dt^2} = -\partial_i\phi \ , \quad \text{(weak gravity)} \tag{2.25}$$

but they are **not** consistent with the equation $\partial_\mu T^{\mu\nu} = 0$. The latter implies the geodesics on flat metric (Mikowksi spacetime, unaccelerated motion, no gravity)

$$\frac{d^2x^i}{dt^2} = 0 \ , \quad \text{(no gravity)} \ . \tag{2.26}$$

This illustrates some of the difficulties/inconsistencies in predicting the EOM of matter from linearized EFE as an expansion on $\boldsymbol{\eta}$. Eq. (2.26) is the EOM of the matter that determines curvature, Eq. (2.25) is the EOM of matter in the resulting slightly curved spacetime.

Example 2.4.1. Deflection of light (Einstein's 1915 calculation). *Consider a photon moving in a weak and static gravitational field generated by a mass M. The metric is given by Eq. (2.24) with the grav. potential is $\phi = GM/rc^2$. The photon moves in the $z=0$ plane in direction x with impact parameter $y=b$. Setting $\mathrm{d}\ell^2 = \delta_{ij}\mathrm{d}x^i\mathrm{d}x^j$ and interpreting the* d *as differential, the coordinate speed of the photon can be computed from the condition $g=0$,*

$$v = \frac{d\ell}{dt} = c\left(\frac{1-2\phi}{1+2\phi}\right)^{1/2} \approx c(1-2\phi) = c\left(1-\frac{2GM}{c^2r}\right) \ , \tag{2.27}$$

where the square root is expanded in $\phi \ll 1$. The speed of light measured in these non-inertial coordinates decreases the closer the photon approach to the mass. This is analogous to a wave front passing through a medium in which the speed of the wave varies with position. Hence, a beam of light rays is bent towards the mass the closer is to the mass. The deflection can be calculated using Huygens principle in analogous way to the refraction angle of waves in a medium,

$$\frac{d\theta}{dx} = \frac{1}{c}\frac{dv}{dy} = \frac{2GM}{c^2}\frac{y}{(x^2+y^2)^{3/2}} \quad \Rightarrow \quad \theta = \frac{2GM}{c^2}\int\frac{bdx}{(x^2+b^2)^{3/2}} = \frac{4GM}{c^2b} \ . \tag{2.28}$$

The same solution can be found considering null geodesics, e.g. (Carroll, 1997), and also by starting from the Schwazrschild metric in isotropic coordinates. Note that one can also perform a calculation using Newton gravity (the acceleration does not depend on the photon mass) and find that GR result is twice the Newtonian prediction. Detailed calculations are left as [exercise].

Observations conducted by Eddington in 1916 and others later, indicate that the Sun deflects photons of an angle $\theta_d \approx 8.5\times10^{-6}$ radians (1.75 arcsec) in agreement with the GR formula above ($M_\odot = 1.98847\times10^{33}$ g and $R_\odot = 6.960\times10^{10}$ cm). Accurate measurements of light deflection are also available from the 60s using radio interferometers and astrophysical sources called blazars (gravitational lensing).

2.4.2 No-stresses source

A matter distribution with mass-energy density current vector J^μ and no stresses is modeled by a stress-energy tensor in the form

$$T_{\mu\nu} = 2J_{(\mu}t_{\nu)} - 2\rho t_\mu t_\nu \quad \text{i.e.} \quad T_{0\mu} = J_\mu \ , \quad T_{ij} = 0 \ . \tag{2.29}$$

Note that $J^\mu = \rho u^\mu = \rho(W, Wv^i/c)$ and that $T_{ij} = \mathcal{O}(v^2/c^2)$, thus (i) the static case considered above is equivalent to consider the slow velocity limit $v/c \ll 1$ for the (nonrelativistic) source, and (ii) taking $T_{ij} \equiv 0$ is equivalent to neglect velocity terms $\mathcal{O}(1/c^2)$ in the source motion.

The linearized equations read

$$\begin{cases} \Box\bar{h}_{0\mu} &= -16\pi T_{0\mu} \ , \quad \mu = 0, ..., 3 \\ \Box\bar{h}_{ij} &= 0 \ , \quad i, j = 1, ..., 3 \ . \end{cases} \tag{2.30}$$

If the spatial component of the metric are assumed time-independent, then they are solution of the boundary value problem with the Poisson equation and boundary values $\bar{h}_{ij}|_{r\to\infty} = 0$. This implies they are zero:

$$\partial_t \bar{h}_{ij} = 0 \quad \Rightarrow \quad \begin{cases} \Delta\bar{h}_{ij} = 0 \\ \bar{h}_{ij}|_{r\to\infty} = 0 \end{cases} \quad \Rightarrow \quad \bar{h}_{ij} = 0 \ . \tag{2.31}$$

The linearized equations reduce to only those for $\bar{h}_{0\mu}$, that are formally equivalent to the Maxwell equations in Lorentz gauge for the field

$$A_\mu := -\frac{1}{4}\bar{h}_{0\mu} = -\frac{1}{4}\bar{h}_{\mu\nu}t^\nu \ . \tag{2.32}$$

Once a solution is found, the metric is given by [exercise]

$$g_{00} = -1 + 2A_0 \ , \quad g_{0i} = 4A_i \ , \quad g_{ij} = 1 + 2A_0\delta_{ij} \ . \tag{2.33}$$

If one further assumes that $\bar{h}_{0\mu}$ is time-independent a formal solution can be obtained with the usual Green function method for the Poisson equation

$$\partial_t \bar{h}_{0\mu} = 0 \quad \Rightarrow \quad \begin{cases} A_0 &= -\phi \\ A_i &= \int d^3x' \frac{T_{0i}(x')}{|\vec{x} - \vec{x}'|} \ . \end{cases} \tag{2.34}$$

Reintroducing the factors c, the metric reads

$$g = -\left(1 + \frac{2\phi}{c^2}\right) \mathrm{d}(ct)^2 + 4A_i \mathrm{d}(ct)\mathrm{d}x^i + \left(1 - \frac{2\phi}{c^2}\right)\delta_{ij}\mathrm{d}x^i\mathrm{d}x^j \ . \tag{2.35}$$

Using the same formulas as in electrodynamics, one then defines from A_μ the *gravitoelectric* $\vec{E}$ and *gravitomagnetic* $\vec{B}$ fields. The geodesics on this metric in the small velocity limit reduce to those of a particle subject to the (gravitational) Lorentz force. Consider the Lagrangian for a particle in the weak metric Eq. (2.35) and expand in v/c [1] :

$$L = -mc\sqrt{-g_{\mu\nu}\frac{dx^\mu}{dt}\frac{dx^\nu}{dt}} = -mc^2\sqrt{-g_{00} - 2g_{0i}\frac{v^i}{c} - g_{ij}\frac{v^iv^j}{c^2}} \tag{2.36a}$$

$$= -mc^2\sqrt{1 - 2A_0 - 8A_i\frac{v^i}{c} - \frac{v^jv_j}{c^2} + 2A_0\frac{v^jv_j}{c^2}} \tag{2.36b}$$

$$\approx -mc^2 + \frac{m}{2}v^2 + m\phi + 4mcA_iv^i \ . \tag{2.36c}$$

The above equation implies an EOM with the (gravitational) Lorentz force,

$$\ddot{\vec{x}} = \vec{E} + 4\vec{v} \times \vec{B} \ . \tag{2.37}$$

The difference w.r.t. the EOM for a charge particle are that (i) there is no charge; (ii) there is a factor "4" in front of the gravitomagnetic field.

Example 2.4.2. Lense-Thirring effect. *The spacetime of a "weaky" gravitating planet or star in slow rotation is described by the metric of Eq. (2.33). The grav. field is stationary and the motion of a test body in such field is precisely described by the gravitoeletric/magnetic equations. For example, the precession motion of a gyroscope due to the gravitomagnetic field of the rotating object is precisely given by the spin-precession formula of electromagnetism*

$$\frac{d\vec{s}}{dt} = \vec{\mu} \times \vec{B} = \frac{q}{2m}\vec{s} \times \vec{B} = \vec{s} \times \vec{\Omega} \ , \tag{2.38}$$

[1] Recall that $x^0 = ct$ and $v^i = dx^i/dt$.

where $\vec{\Omega} = -q/m\vec{B}$, q is the particle charge and $\vec{\mu}$ the magnetic moment. The formal substitution

$$q \mapsto m \ , \quad \vec{B} \mapsto 4\vec{B}_g \ , \tag{2.39}$$

maps the eletrogmagnetic problem top the gravitomagnetic one. The precession frequency in the latter is thus $\Omega_g = -2B_g$. In the grav. field of Earth one obtains that a free-falling body at distance r acquires an angular velocity

$$\Omega = \dot{\varphi} \sim 0.22''/yr \left(\frac{R_\oplus}{r}\right)^3 \ . \tag{2.40}$$

This effect is called also frame dragging*, and it has been measured by the satellite mission Gravity Probe B in 2004 with 20% confidence (Everitt et al., 2011)* [2].

Example 2.4.3. *An extreme frame dragging phenomenon happens around* rotating black holes*. But in this case it is not a weak field effect and Eq. (2.33) do not apply. Particles close to the black hole horizon are dragged around at a speed comparable to the hole's rotation $\Omega \sim \Omega_{BH}$. The Lense-Thirring effect in strong field play an important role to understand high-energy particle emission from matter accreting onto black holes.*

2.5 Relativistic precession

To conclude this Chapter we briefly review relativistic precession. Relativistic precession is a consequence of the weak field metric, but it is usually derived using the Schwarzschild metric. Indeed, a simple way to derive Eq. (2.24) is to start from the Schwarzschild metric in isotropic coordinates

$$g = -\left(1 - \frac{M}{2r}\right)^2 \Psi^2(r)\mathrm{d}t^2 + \Psi^4(r)\left(\mathrm{d}r^2 + r^2\mathrm{d}\Omega^2\right) \ , \tag{2.41}$$

where r the isotropic radius [3] and $\Psi(r) = 1 + M/(2r)$ is the conformal factor that for $\phi = -M/r \ll 1$ is

$$\Psi \approx 1 - \frac{\phi}{2c^2} \ . \tag{2.42}$$

The conformal spatial spatial metric is flat and can be thus written in Carterian coordinates

$$\mathrm{d}r^2 + r^2\mathrm{d}\Omega^2 = \delta_{ij}dx^i dx^j \ . \tag{2.43}$$

Using this coordinates and taking the limit to large radii one gets Eq. (2.24).

The simplest way to analyze relativistic precession is to consider test bodies in the Schwarzschild metric in standard coordinates, e.g. (Wald, 1984). Starting from the Schwarzschild radial geodesic and (i) restricting to equatorial plane, (ii) including the constant of motions, (iii) multiplying by $(\dot{\phi})^{-2}$, (iv) changing variable to $u = 1/r = GM/c^2 r$ (from now on r is the Schwarzschild radius [4]), one obtains [exercise]

$$\frac{d^2u}{d\phi^2} + u = \frac{M}{\ell^2} + \underbrace{3Mu^2}_{\text{GR term}} \ . \tag{2.44}$$

The above equation is similar to the Newtonian equations for elliptic orbits but includes the "GR term". Without the GR term one has the orbit equation

$$u_N = M\ell^2(1 + \varepsilon\cos\phi) \ , \tag{2.45}$$

describing the Kepler ellipses and where the eccentricity ε is fixed by the initial condition. The GR term can be treated as a perturbation when compared to the Newtonian term at the r.h.s. if $3Mu^2 \ll M\ell^{-2}$. For example, this condition is verified for Mercury's orbit around the Sun since the ratio of the two terms reduced to the tangential velocity that is small,

$$\frac{3Mu^2}{M\ell^{-2}} = 3u^2\ell^2 = 3r^{-2}(r^2\dot{\phi})^2 \simeq 3(r\frac{d\phi}{dt})^2 = 3(\frac{v_\perp}{c})^2 \approx 10^{-7} \ . \tag{2.46}$$

Let $u = u_N + v$ and find a linear equation in v:

$$\underbrace{\frac{d^2u_N}{d\phi^2} + u_N - \frac{M}{\ell^2}}_{=0} + \frac{d^2v}{d\phi^2} + v = 3M(u_N^2 + 2u_N v + v^2) \approx 3Mu_N^2 \ . \tag{2.47}$$

[2] Summary webpage: `http://einstein.stanford.edu/highlights/status1.html`

[3] The isotropic radius is defined from the Schwarzschild radial coordinate as $R = r(1 + M/(2r))^2$.

[4] To switch from/to geometric units is often sufficient to remember that $M \leftrightarrow GM/c^2$.

This is an equation for a forced oscillator; the solution is given by the general solution of the homogeneous equations plus a particular solution of the complete equation. A particular solution is given by

$$v = 3M^2\ell^{-4}[1 + \underbrace{\varepsilon\phi\sin\phi}_{\text{secular term}} + \varepsilon^2(\frac{1}{2} - \frac{1}{6}\cos(2\phi))] \ , \tag{2.48}$$

which is the combination of a constant term, a secular term $\propto \phi$ and an oscillating term. An approximate solution to the perturbation problem is obtained by just picking the secular term,

$$u \approx u_N + v_{\text{secular}} = M\ell^{-2}(1 + \varepsilon\cos\phi) + 3M^2\ell^{-4}\varepsilon\phi\sin\phi \simeq M\ell^{-2}\left(1 + \varepsilon\cos(\phi - 3M^2\ell^{-2}\phi)\right) \ , \tag{2.49}$$

where in the first passage we approximate $3M^2\ell^{-2}\phi \sim \sin(3M^2\ell^{-2}\phi)$ for small arguments of the sin(.), and trigonometric identities were used in the second passage. The approximate solution above shows that if $\varepsilon \neq 0$, then the orbit is not periodic of 2π and it is not an ellipses. For a revolution of $\phi = 2\pi$, the periastron (perihelion) shift is

$$2\pi(1 - 3M^2\ell^{-2}) = 2\pi - 6M^2\ell^{-2} \quad \Rightarrow \quad \Delta\phi = 6\pi 3M^2\ell^{-2} \ . \tag{2.50}$$

The angular momentum in the formula above is difficult to measure from astronomical observations and it is best to replace it with the semi-major axis a. This is done by comparing $u_N(\phi)$ to the generic equation for an ellipsis $u(\phi)$:

$$ua(1 - \varepsilon^2) = (1 + \varepsilon\cos\phi) \ , \tag{2.51}$$

which implies $M\ell^2 = a(1 - \varepsilon^2)$. Plugging in the angular momentum expression in terms of the semi-major axis, the final result for the perihelion shift is

$$\Delta\phi = \frac{6\pi M}{a(1 - \varepsilon^2)} = \frac{6\pi GM}{a(1 - \varepsilon^2)c^2} \ . \tag{2.52}$$

Example 2.5.1. Mercury perihelion shift. *Mercury data are* $GM_\odot/c^2 \simeq 1.48 \cdot 10^5$ *cm,* $a \simeq 5.79 \cdot 10^{12}$ *cm,* $\varepsilon \simeq 0.20$, $T \simeq 88$ *days, resulting in* $\Delta\phi \simeq 0.103''/$ *orbit* $\simeq 43''/100$ *yrs. This is a famous and successful experimental test of GR.*

Example 2.5.2. PSR 1913+16 *is a relativistic binary system that shows precession. This precession is not described by the Schwarzschild geodesic because the binary has components of comparable masses. However, it can be studied using the post-Newtonian formalism Damour and Deruelle (1986). PSR 1913+16 has a precession of* $\Delta\phi \sim 4.2^\circ/100$ *yrs, which is* $\sim 270\times$ *the one of Mercury and indicate the extreme gravity of that binary system. Differently from Mercury, PSR 1913+16 cannot be used this way to verify GR from measured precession because the masses of PSR are not known. The measurement is in fact used to estimate the masses, as we shall see.*

3. GWs in linear GR

Gravitational-wave in linearized GR: propagation properties, effect on test masses, and the quadrupole formula.

Suggested readings. *Chap. 1,3 of Maggiore (2007). Chap. 4 of Wald (1984); Chap. 7 of Carroll (1997); Chap. 7-8 of Schutz (1985);*

3.1 Propagation of GWs

The linearized EFE in vacuum are homogeneous wave equations for each component of the metric,

$$0 = \Box_\eta \bar{h}_{\mu\nu} = \eta^{\alpha\beta}\partial_\alpha\partial_\beta \bar{h}_{\mu\nu} \ . \tag{3.1}$$

Solutions to the above equation can be constructed by superposition of plane waves with (constant) wave vector $k^\mu = (\omega, \vec{k})$ [1] and amplitudes $A_{\mu\nu}$:

$$\bar{h}_{\mu\nu} = A_{\mu\nu}\exp\left(\mathrm{i}k_\mu x^\mu\right) = A_{\mu\nu}\exp\left[\mathrm{i}(-k_0 x^0 + \vec{k}\cdot\vec{x})\right] = A_{\mu\nu}\exp\left[\mathrm{i}(-\omega t + \vec{k}\cdot\vec{x})\right] \tag{3.2a}$$

$$\partial_\mu \bar{h}_{\alpha\beta} = A_{\alpha\beta}\partial_\mu(\exp\left(\mathrm{i}k_\rho x^\rho\right)) = \bar{h}_{\alpha\beta}\partial_\mu(\mathrm{i}k_\rho x^\rho) = \mathrm{i}\bar{h}_{\alpha\beta}k_\rho\delta^\rho_\mu \tag{3.2b}$$

Substituting the plane-wave ansatz into the wave equations, one finds immediately that the the *wave vector is null* (Mikowski metric):

$$0 = \Box\bar{h}_{\alpha\beta} \overset{p.w.}{=} -\eta^{\mu\nu}k_\mu k_\nu \bar{h}_{\alpha\beta} \quad \Rightarrow \quad \eta^{\mu\nu}k_\mu k_\nu = k_\mu k^\mu = 0 \quad \Rightarrow \quad \omega^2 = |\vec{k}|^2 c^2 \ . \tag{3.3}$$

The last equation is the *dispersion relation* for GWs and indicates that GWs propagate at the speed of light. Another way to see this is to consider the worldline of a photon moving along k^μ, and observe that it moves in phase with the wave's phase $\varphi = k_\mu x^\mu$:

$$x^\mu(\lambda) = k^\mu\lambda + x^\mu(0) \quad \Rightarrow \quad k_\mu x^\mu(\lambda) = \underbrace{k_\mu k^\mu}_{=0}\lambda + k_\mu x^\mu(0) = k_\mu x^\mu(0) = const \ . \tag{3.4}$$

The Hilbert gauge Eq. (2.15) translates into the 4 equations that imply the waves are *transverse to the direction of propagation*:

$$0 = -\partial^\alpha \bar{h}_{\mu\alpha} = \mathrm{i}k^\mu A_{\mu\nu}\exp\left[\mathrm{i}(k_\rho x^\rho)\right] = \mathrm{i}k^\mu \bar{h}_{\mu\alpha} \quad \Rightarrow \quad k^\mu A_{\mu\nu} = 0 \ . \tag{3.5}$$

Transverse-traceless (TT) gauge and physical degrees of freedom. Linearized EFE in vacuum are 10 equations. Imposing the Hilbert gauge (4 equations) reduces the problem to $10 - 4 = 6$ equations, but there remains freedom in the gauge choice. Looking at Eq. (2.17), it is immediate that the Hilbert gauge is defined up to 4 harmonic functions ξ^μ: any infinitesimal transformation such that $\Box\xi_\nu = 0$ maintains the Hilbert gauge $-\partial^\alpha\bar{h}_{\mu\alpha} = 0$. Let us further specify the gauge choice. The additional gauge freedom can be fixed by

(i) writing the harmonic function as (note the following expression clearly solves $\Box\xi_\nu = 0$)

$$\xi^\mu = B^\mu \exp\left[\mathrm{i}(k_\rho x^\rho)\right] \ , \tag{3.6}$$

such that the transformation of the trace reverse metric translates into the following transformation of the plane-wave amplitude,

$$\bar{h}_{\mu\nu} \mapsto \bar{h}_{\mu\nu} + 2\partial_{(\mu}\xi_{\nu)} - \eta_{\mu\nu}\partial_\alpha\xi^\alpha \quad \Rightarrow \quad A_{\mu\nu} \mapsto A_{\mu\nu} - \mathrm{i}2k_{(\mu}B_{\nu)} - \mathrm{i}\eta_{\mu\nu}k_\rho B^\rho \ . \tag{3.7}$$

[1] Note that in general the wave frequency measured by an observer of 4-velocity u^μ is $\omega = k_\mu u^\mu$.

(ii) and then fixing the functions B^μ requiring the additional 4 conditions

$$\begin{cases} \bar{h} = 0 = A^\mu_\mu & \text{Traceless condition} \\ \bar{h}_{0\mu} = 0 = A_{0\mu} & \text{Transverse condition} \ . \end{cases} \tag{3.8}$$

The above conditions give a linear algebraic system for B^μ, which can be inverted to find the solution. The gauge above is called *traceless & transverse (TT) gauge*. The remaining degrees of freedom are $10 - 4 - 4 = 2$, that represent the two physical states of gravity waves.

Let us explicitely consider a wave propagating along the $\hat{z}$-direction,

$$k^\mu = (\omega, 0, 0, k_3) \ . \tag{3.9}$$

Then

1. Null condition, $k_\mu k^\mu = 0 \Rightarrow -k_3 = \omega$;
2. Phase, $k_\rho x^\rho = \omega(t - z)$;
3. Hilbert gauge, $k^\mu A_{\mu\nu} = 0 \Rightarrow k^0 A_{0\nu} + k^3 A_{3\nu} = \omega A_{0\nu} - \omega A_{3\nu} = 0$ or $A_{0\nu} = A_{3\nu}$;
4. Transverse condition, $A_{0\mu} = 0 \Rightarrow A_{3\mu} = 0$;
5. Traceless condition, $-A_{00} + A_{11} + A_{22} + A_{33} = 0$;

From (3.-4.) one gets the first and last row/col of the amplitude matrix components are zero, and (note $A_{\mu\nu}$ is symmetric)

$$A_{\mu\nu} = \begin{bmatrix} 0 & 0 & 0 & 0 \\ 0 & A_{11} & A_{12} & 0 \\ 0 & A_{12} & A_{22} & 0 \\ 0 & 0 & 0 & 0 \end{bmatrix} \tag{3.10}$$

The trace condition (5.) then gives $A_{22} = -A_{11}$. Setting $A_+ := A_{11}$ and $A_\times := A_{12}$, the plane-wave solution in TT gauge can be written

$$h^{\rm TT}_{\mu\nu} = \begin{bmatrix} 0 & 0 & 0 & 0 \\ 0 & A_+ & A_\times & 0 \\ 0 & A_\times & -A_+ & 0 \\ 0 & 0 & 0 & 0 \end{bmatrix} \exp\left[\mathrm{i}\omega\left(t - \frac{z}{c}\right)\right] \ . \tag{3.11}$$

The two *polarization of the GW* are indicated as "+" and "×"

$$h_+(t - z/c) = A_+ \exp\left[\mathrm{i}\omega\,(t - z/c)\right] \ , \quad h_\times(t - z/c) = A_\times \exp\left[\mathrm{i}\omega\,(t - z/c)\right] \ . \tag{3.12}$$

Note:

- In the TT gauge $h_{\mu\nu} = \bar{h}_{\mu\nu}$.
- The TT gauge can defined only in vacuum, because in case matter is present $\Box\bar{h}_{\mu\nu} \neq 0$ and, while there is still the freedom to rescale the $\bar{h}_{\mu\nu}$ with an infinitesimal coordinate transformation generated by four harmonic functions, we cannot set to zero the components $\bar{h}_{\mu\nu}$ inside the source.
- The *metric* in the TT gauge reads

$$g = -\mathrm{d}t^2 + \mathrm{d}z^2 + (1 + h_+)\mathrm{d}x^2 + (1 - h_+)\mathrm{d}y^2 + 2h_\times \mathrm{d}x\mathrm{d}y \tag{3.13}$$
$$= -\mathrm{d}t^2 + (\delta_{ij} + h^{\rm TT}_{ij})\mathrm{d}x^i\mathrm{d}x^j \ , \tag{3.14}$$

where the first expression holds for a GW along the $\hat{z}$-direction and the second is general.

- Given a solution $\bar{h}_{\mu\nu}$ of linearized EFE in vaccum in Hilbert gauge propagating in direction $\hat{n}$, it is possible to obtain the solution in TT outside the source by means of the following projection operator (below summation on repeated indexes is understood although they are not raised)

$$\bar{h}^{\rm TT}_{\mu\nu} = \Lambda_{\mu\nu,\alpha\beta}\bar{h}_{\alpha\beta} \tag{3.15a}$$
$$\Lambda_{\mu\nu,\alpha\beta}(\hat{n}) := P_{\mu\alpha}P_{\nu\beta} - \frac{1}{2}P_{\mu\nu}P_{\alpha\beta} \tag{3.15b}$$
$$P_{\mu\nu}(\hat{n}) := \delta_{\mu\nu} - n_\mu n_\nu \ . \tag{3.15c}$$

The following properties also hold [exercise]

1. $P_{\mu\nu}$ is symmetric;
2. $P_{\mu\nu}$ is transverse, $n^\mu P_{\mu\nu} = 0$;
3. $P_{\mu\nu}$ is a projector, $P_{\mu\alpha}P_{\alpha\nu} = P_{\mu\nu}$;

4. $P_{\mu\nu}$ has trace $P_{\mu\mu} = 2$;
5. $\Lambda_{\mu\nu,\alpha\beta}$ is a projector, $\Lambda_{\mu\nu,\alpha\beta}\Lambda_{\alpha\beta,\rho\sigma} = \Lambda_{\mu\nu,\rho\sigma}$;
6. $\Lambda_{\mu\nu,\alpha\beta}$ is transverse in al indexes;
7. $\Lambda_{\mu\nu,\alpha\beta}$ is traceless in $\mu\nu$ and $\alpha\beta$,$\Lambda_{\mu\mu,\alpha\beta} = 0 = \Lambda_{\mu\nu,\alpha\alpha}$;
8. $\Lambda_{\mu\nu,\alpha\beta}$ is symmetric in $\mu\nu - \alpha\beta$, $\Lambda_{\mu\nu,\alpha\beta} = \Lambda_{\alpha\beta,\mu\nu}$.

- More in general, for any symmetric tensor $S_{\mu\nu}$ one can obtain a *symmetric, transverse and tracefree (STF)* tensor using the $\Lambda_{\mu\nu,\alpha\beta}$ projector. STF tensors are a powerful tool to develop multipolar expansions of tensor satisfying wave equations, thus generalizing the multipolar expansion of the Newtonian and electrostatic potentials and scalar wave equations (Thorne, 1980; Maggiore, 2007) (Chap. 4.)

3.2 Effect of GWs on test masses

A simple argument to understand the effect of GW on test masses is given by the following

Example 3.2.1. Distance measurement with the radar method. *Consider two masses initially at rest and at distance L_0 in absence of GW. Denote the two spacetime points (at $t = 0$) as p, q. The distance L can be measured by sending a light pulse from the first mass (p) to the second, and then back from the second to the first. A time measurement with the clock at the first mass allows one to calculate L. Let q', p' and p'' the events in which, respectively, the second mass receives the signal, the simultaneous event at the position of the first mass, and the first mass receives the signal. The length measurement with this radar procedure is*

$$L = \frac{1}{2}c(t_{p''} - t_p) \ . \tag{3.16a}$$

Let us now take spatial coordinate of the two masses at $t = 0$ as $x^i_p = (0, 0, 0)$ and $x^i_q = L_0 n^i$, where n^i ($\eta_{ij}n^i n^j = 1$) is the direction between the masses, so that $L_0^2 = \delta_{ij}x^i_q x^j_q$. Calculate the variation of the distance measured at a time $t_{p'} = t_{q'}$ when the second mass receives the light ray in the case a GW is present:

$$L^2 = g_{\mu\nu}(x^\mu_{q'} - x^\mu_{p'})(x^\nu_{q'} - x^\nu_{p'}) \overset{t_{p'}=t_{q'}}{=} g_{ij}(x^i_{q'} - x^i_{p'})(x^j_{q'} - x^j_{p'}) \overset{x^i_{p'}=0}{=} g_{ij}x^i_{q'}x^j_{q'} = (\delta_{ij} + h^{TT}_{ij})L_0^2 n^i n^j \ , \tag{3.16b}$$

that implies the relative variation of the lenght

$$\frac{\delta L}{L_0} = \frac{L}{L_0} - 1 = \sqrt{1 + h^{TT}_{ij}n^i n^j} - 1 \approx \frac{1}{2}h^{TT}_{ij}n^i n^j \ . \tag{3.16c}$$

The distance's relative variation due to the GW is proportional to the GW amplitude.

A more formal study the effect of GW on test masses employs the geodesic deviation equation

$$u^\mu \nabla_\mu (u^\nu \nabla_\nu s^\alpha) = R^\alpha_{\nu\rho\sigma} u^\nu u^\rho s^\sigma \ , \tag{3.17}$$

where u is the tangent to the particles worldline and s is is the displacement vector between worldlines. Here, one considers the "relative motion" of nearby particles at the passage of the GW using tensorial equations.

In linearized GR, the Riemann tensor is proportional to $h_{\mu\nu}$ and a particle initially at rest (in the global inertial reference system of the backround metric) acquires a velocity due to the perturbation

$$\frac{dx^0}{d\tau} = 1 + \mathcal{O}(h) \ , \quad \frac{dx^i}{d\tau} = \mathcal{O}(h) \quad \Rightarrow \quad u^\mu = c\frac{dx^\mu}{d\tau} \simeq (1, 0, 0, 0) + \mathcal{O}(h) \ . \tag{3.18}$$

At leading order, coordinate and proper time coincide. Using this velocity and coordinate time instead of proper time, the geodesic equation at lowest order and in TT gauge reduces to

$$\frac{d^2 s_\alpha}{dt^2} = R_{\alpha 00\mu} s^\mu \ , \tag{3.19a}$$

where

$$R_{\mu 00\nu} = \frac{1}{2}\frac{\partial^2 h^{\rm TT}_{\mu\nu}}{\partial t^2} \ . \tag{3.19b}$$

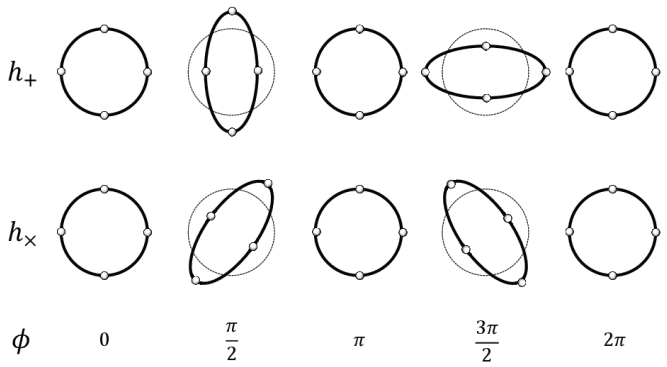

Figure 3.1: Effect on a ring of test masses on the $x-y$ plane at the passage of a GW in perpendiculr direction.

The formula above shows that the two degrees of freedom of the GW are physical: they cannot be gauged away. Restricting to the spatial indexes and calling $s^i_0 = s^i(t=0)$ the deviation vector before the GW arrives, the formula above reduces to

$$\frac{d^2 s^i}{dt^2} = \frac{1}{2}\ddot{h}^{\rm TT}_{ij} s^j_0 + \mathcal{O}(h^2) \ , \tag{3.20}$$

where terms $\propto \ddot{h}^{\rm TT}_{ij} s^i(t)$ can be discarded if one works at leading order in the perturbation. Because the particle are initially at rest, $\dot{s}^i(0) = 0$, the solution for the deviation vector is simply

$$s^i(t) = (\delta_{ij} + \frac{1}{2} h^{\rm TT}_{ij}) s^j_0 \ . \tag{3.21}$$

Specify for a GW propagating in $\hat{z}$-direction and setting $s^i_0 = (x_0, y_0, z_0)$, one gets

$$\begin{cases} \delta x(t) &= x_0 + \frac{1}{2}(h_+(t) x_0 + h_\times(t) y_0) \\ \delta y(t) &= y_0 + \frac{1}{2}(-h_+(t) y_0 + h_\times(t) x_0) \\ \delta z(t) &= z_0 \ . \end{cases} \tag{3.22}$$

The test masses oscillates in the x-y plane, transverse to the direction of propagation of the GW. The effect of the two polarizations is clearly visualized by considering a ring of test masses places in the plane, Fig. (3.1). If initially $(x_0, y_0) = r_0(\cos\phi, \sin\phi)$, the effect of the *plus* polarization is

$$\begin{cases} \delta x(t) &= x_0 + \frac{1}{2} h_+(t) x_0 = r_0(1 + h_+(t))\cos\phi \\ \delta y(t) &= y_0 - \frac{1}{2} h_+(t) y_0 = r_0(1 - h_+(t))\sin\phi \ . \end{cases} \tag{3.23}$$

Take the square of the equations and sum them up:

$$1 = \cos\phi^2 + \sin^2\phi = \frac{\delta x(t)^2}{r_0^2(1+h_+(t))^2} + \frac{\delta y(t)^2}{r_0^2(1-h_+(t))^2} \ , \tag{3.24}$$

this is an ellipsis of semi-axes $a_\pm := r_0(1 \pm h_+)$, and because $h_+(t)$ is an oscillating function with period $T = 2\pi/\omega$, one axis gets shorter and the other longer with the period T.

Similarly, for the *cross* polarization

$$\begin{cases} \delta x(t) &= x_0 + \frac{1}{2} h_\times(t) y_0 \\ \delta y(t) &= y_0 + \frac{1}{2} h_\times(t) x_0 \ , \end{cases} \tag{3.25}$$

one can proceed by diagonalizing the r.h.s. matrix with a rotation of $\pi/4$

$$\begin{bmatrix} 1 & h_\times/2 \\ h_\times/2 & 1 \end{bmatrix} \ \Rightarrow \ \lambda_\pm = \pm\frac{1}{2} h_\times \ , R = \frac{1}{\sqrt{2}}\begin{bmatrix} 1 & 1 \\ -1 & 1 \end{bmatrix} = \begin{bmatrix} \cos\alpha & \sin\alpha \\ -\sin\alpha & \cos\alpha \end{bmatrix}\Big|_{\alpha=\pi/4} \ . \tag{3.26}$$

In the rotated frame, the equations are identical to Eq. (3.23). Thus, the cross polarization moves the ring in the same way as the plus but for a phase of $\pi/4$.

Remark 3.2.1. *Eq. (3.19b) is valid in harmonic coordinates. Using the GW polarizations it is possible to write the* connection between the GW d.o.f. and the Riemann tensor in covariant form. *Imagine the GW propagating along light cones $u \sim t - r = const$ at large r and introduce the following unit vectors on the asymptotic two-sphere*

$$\vec{\theta} = (\cos\theta\cos\phi, \cos\theta\sin\phi, -\sin\theta) \quad , \quad \vec{\phi} = (-\sin\phi, \cos\phi, 0) \, . \tag{3.27}$$

A transverse projector Λ can be defined starting from the projector

$$P^{ij} := \theta^i\theta^j + \phi^i\phi^j \tag{3.28}$$

such that any STF tensor S^{ij} on the Euclidean 3D space can be decomposed as

$$S^{ij} = S_+(\theta^i\theta^j - \phi^i\phi^j) + S_\times(\theta^i\theta^j + \phi^i\phi^j) \tag{3.29}$$

where S_+ ($S_\times$) is the $\theta\theta$ ($\phi\phi$) component. The latter are given by the projections:

$$S_+ = \frac{1}{2}(\theta_i\theta_j - \phi_i\phi_j)S^{ij} \quad , \quad S_\times = \frac{1}{2}(\theta_i\theta_j + \phi_i\phi_j)S^{ij} \, . \tag{3.30}$$

Now take a timelike vector t^μ that asymptotically coincides with the timelike Killing vector of Minkowski spacetime together with vectors θ^α and ϕ^α that asymptotically coincide with the $\vec{\theta}$ and $\vec{\phi}$ vectors. Then, the two polarizations in Eq. (3.19b) can be expressed as projection of the Riemann as

$$\ddot{h}_+ = R_{\alpha\mu\nu\beta}(\theta^\alpha\theta^\beta - \phi^\alpha\phi^\beta)t^\mu t^\nu \tag{3.31a}$$

$$\ddot{h}_\times = R_{\alpha\mu\nu\beta}(\theta^\alpha\theta^\beta + \phi^\alpha\phi^\beta)t^\mu t^\nu \, . \tag{3.31b}$$

3.3 Sources of GWs

A formal solution of the linearized EFE

$$\Box\bar{h}_{\mu\nu} = -16\pi T_{\mu\nu} \ , \tag{3.32}$$

is given in terms of the Green functions with retarded time $u := t - |\vec{x} - \vec{x}'|/c$ (See e.g. Jackson (1975))

$$\bar{h}_{\mu\nu}(t,\vec{x}) = -16\pi \int G_R(x^\mu - x^{\mu'})T_{\mu\nu}d^4x' = 4\int \frac{T_{\mu\nu}(u,\vec{x}')}{|\vec{x}-\vec{x}'|}d^3x' \ , \tag{3.33}$$

where in the last passage G_R is given by the retarded time solution of

$$\Box_{(x)}G(x^\mu, x^{\mu'}) = \delta^{(4)}(x^\mu - x^{\mu'}) \quad \Rightarrow \quad G_R(x^\mu, x^{\mu'}) = -\frac{1}{4\pi}\frac{1}{|\vec{x}-\vec{x}'|}\delta(u-t') \ . \tag{3.34}$$

The physics picture is that the solution at point p (time t and location x^i) is determined by the events in the past lightcone. Note that since these are weak field equations, they apply to a source with negligible selfgravity $\sigma = 2GM/(c^2R) \ll 1$, where M, R are the typical mass and size of the source.

3.3.1 Quadrupole formula

Let us specify the above formula under the conditions
(i) Large distance from a compact source $r = |\vec{x}| = \sqrt{\delta_{ij}x^i x^j} \gg R$;
(ii) Slow velocity, the source motion is slow $v \sim |T_{0i}|/|T_{00}| \ll c$ and $T_{00} \approx \rho c^2$.
The hypothesis (i) implies that

$$|\vec{x}-\vec{x}'| = r|\hat{n} - \frac{\vec{x}'}{r}| = r\sqrt{(\hat{n}-\frac{\vec{x}'}{r})\cdot(\hat{n}-\frac{\vec{x}'}{r})} = r\sqrt{1 - 2\hat{n}\cdot\frac{\vec{x}'}{r} + \left(\frac{\vec{x}'}{r}\right)^2} \approx r - \hat{n}\cdot\vec{x}' \ , \tag{3.35}$$

and restricting to the spatial indexes (those relevant in the TT gauge) Eq. (3.33) becomes

$$\bar{h}_{ij}(t,\vec{x}) \approx \frac{4}{r}\int T_{ij}(t_r + \frac{\hat{n}\cdot\vec{x}'}{c}, \vec{x}')d^3x' \ , \tag{3.36}$$

where one retains only the leading-order term at the denominator $1/|\vec{x}-\vec{x}'| \sim 1/r$, and where $u \approx t_r := t - r/c$.

The hypothesis (ii) allows one to expand the stress-energy tensor in $\hat{n}\cdot\vec{x}'/c$:

$$T_{kl}(t_r + \frac{\hat{n}\cdot\vec{x}'}{c}, \vec{x}') = T_{kl}(t_r, \vec{x}') + \frac{n_i x'^i}{c}\partial_t T_{kl}(t_r,\vec{x}') + \frac{n_i x'^i n_j x'^j}{c^2}\partial_{tt}T_{kl}(t_r,\vec{x}') + ... \ , \tag{3.37}$$

A simple way to justify the above expansion from the hypothesis (ii) is to look at the expression of T_{kl} in terms of its Fourier transform,

$$T_{kl}(t_r + \frac{\hat{n}\cdot\vec{x}'}{c}, \vec{x}') = \int d^4k\, \tilde{T}_{kl}(\omega,\vec{k})e^{-\mathrm{i}\omega(t_r + \frac{\hat{n}\cdot\vec{x}'}{c}) + \mathrm{i}\vec{k}\cdot\vec{x}'} \ , \tag{3.38}$$

and realize that the integral of T_{kl} is dominated by the slow characteristic frequencies of the source ($v \sim \Omega R$)

$$\omega\frac{|\vec{x}'|}{c} \sim \Omega\frac{R}{c} \ll 1 \ . \tag{3.39}$$

Hence, the exponential in the Fourier transform can be expanded as

$$e^{-\mathrm{i}\omega(u+\frac{\hat{n}\cdot\vec{x}'}{c})} \simeq e^{-\mathrm{i}\omega u}\left(1-\mathrm{i}\frac{\omega}{c}x'^{i}n_i - \frac{1}{2}\mathrm{i}^2\frac{\omega^2}{c^2}x'^{i}n_i x'^{j}n_j + ...\right) , \tag{3.40}$$

and the above expansion is equivalent to Eq. (3.37) (each multiplication by ω in Fourier domain corresponds to a time derivative in the direct space). The latter equation is a multipolar expansion of the of T_{kl} in Cartesian coordinates. Truncating the expansion at leading order one gets:

$$\bar{h}_{ij}(t,\vec{x}) \approx \frac{4}{r}\int T_{ij}(t_r,\vec{x}')d^3x' . \tag{3.41}$$

Focus now on the matter distribution and derive an equation for the integral of the spatial components T_{ij} by using the conservation law on flat background,

$$0 = \partial^\mu T_{\mu\alpha} = \eta^{\mu\nu}\partial_\nu T_{\alpha\mu} = \begin{cases} -\partial_t T_{00} + \partial_i T_{0i} & \alpha = 0 \\ -\partial_t T_{0k} + \partial_i T_{ki} & \alpha = k . \end{cases} \tag{3.42a}$$

Derive the $\alpha = 0$ equation in time ∂_t and substitute the $\alpha = k$ equation to obtain

$$0 = -\partial_{tt}T_{00} + \partial_t\partial_k T_{0k} = -\partial_{tt}T_{00} + \partial_k\partial_l T_{kl} . \tag{3.42b}$$

Multiply the above equation by $x^i x^j$ and integrate:

$$\frac{d^2}{dt^2}\int T_{00}x^i x^j d^3x = \int \partial_k\partial_l T_{kl}x^i x^j d^3x = \tag{3.42c}$$

$$= \int \partial_k\left(\partial_l T_{kl}x^i x^j\right)d^3x - \int \partial_l T_{kl}\partial_k(x^i x^j)d^3x = \tag{3.42d}$$

$$= \underbrace{\oint \partial_l T_{kl}y^i y^j n^k d^2y}_{=0} - \int \partial_l T_{kl}(\delta^i_k x^j + \delta^j_k x^i)d^3x = \tag{3.42e}$$

$$= -\int(\partial_l T_{il}x^j + \partial_l T_{kl}x^i)d^3x = -\int(\partial_l(T_{il}x^j) - T_{il}\underbrace{\partial_l x^j}_{=\delta^j_l} + \partial_l(T_{kl}x^i) - T_{kl}\underbrace{\partial_l x^i}_{=\delta^i_l})d^3x = \tag{3.42f}$$

$$= -\underbrace{\oint T_{il}x^j n^l d^2y}_{=0} - \underbrace{\oint T_{kl}x^i n^l d^2y}_{=0} + 2\int T_{ij}d^3x \tag{3.42g}$$

The surface integrals in the third and fifth lines are zero since the matter distribution is compact and there is no matter outside a sphere of radius $r > R$. The integral of the spatial components of the stress-energy tensor is thus related to the *moment of inertia* tensor of the matter distribution ρ

$$2\int T_{ij}d^3x = \frac{1}{c^2}\frac{d^2}{dt^2}\int T_{00}x^i x^j d^3x = \frac{d^2}{dt^2}\int \rho x^i x^j d^3x =: \frac{d^2}{dt^2}I_{ij} . \tag{3.42h}$$

Putting together Eq. (3.41) and Eq. (3.42c), one obtains

$$\bar{h}_{ij}(t,\vec{x}) = \frac{2G}{c^4 r}\ddot{I}_{ij}(t-\frac{r}{c}) . \tag{3.43}$$

Far from the source, the solution can be projected to the TT gauge to obtain the *quadrupole formula*

$$\bar{h}^{\mathrm{TT}}_{ij}(t,\vec{x}) = \frac{2G}{c^4 r}\Lambda_{ijkl}\ddot{Q}_{kl}(t-\frac{r}{c}) , \tag{3.44}$$

where the moment of inertia is substituted by its traceless version, the *quadrupole moment*:

$$Q_{ij} = I_{ij} - \frac{1}{3}(\underbrace{\delta^{kl}I_{kl}}_{=I})\delta_{ij} = \int \rho(x^i x^j - \frac{1}{3}\vec{x}\cdot\vec{x}\delta_{ij})d^3x . \tag{3.45}$$

Note: $\Lambda_{ijkl}\ddot{I}_{ij} = \Lambda_{ijkl}\ddot{Q}_{kl}$. The quadrupole formula gives the leading order contribution to the GW from a (spatially) compact, slowly moving and nonselfgravitating source.

Using dimensional analysis, $[\ddot{Q}] = ML^2T^{-2}$ and one immediately finds that the GW observed at distance D from the source is

$$h \sim \left(\frac{G}{c^4 D}\right)(Mv^2) = \left(\frac{R}{D}\right)\left(\frac{GM}{c^2 R}\right)\left(\frac{v}{c}\right)^2 . \tag{3.46}$$

The formula above indicates thet GW are produced by physical objects that are

- very compact;
- strongly gravitating;
- rapidly moving.

Note that the quadrupole formula does not apply for those objects!

Example 3.3.1. Quadrupole formula for a binary star system. *Consider two masses m_1 and m_2 separated by $\vec{r}=\vec{x}_1-\vec{x}_2$ in Newtonian gravity. The mass density is $\rho=m_1\delta(\vec{x}-\vec{x}_1)+m_2\delta(\vec{x}-\vec{x}_2)$, the total mass is $m=m_1+m_2$ and the reduced mass is $\mu=m_1m_2/m$. The moment of inertia reads*

$$I^{ij}=\int \rho x^i x^j d^3x = m_1x_1^ix_1^j+m_2x_2^ix_2^j = mx^i_{\rm cm}x^j_{\rm cm}+\mu r^i r^j \tag{3.47}$$

where $x^i_{\rm cm}=(m_1\vec{x}_1+m_2\vec{x}_2)/m$ is the center of mass coordinate. In the center of mass frame $I^{ij}=\mu r^i r^j$ and the trace is $I=\mu\delta_{ij}r^ir^j=\mu r^2$. The quadrupole of the 2-body system is thus

$$Q^{ij}=I^{ij}-\frac{1}{3}I\delta^{ij}=\mu(r^ir^j-\frac{1}{3}r^2\delta^{ij})\ . \tag{3.48}$$

Specialize now for a circular orbit in the $z=0$ plane, for which $\vec{r}=(x,y,0)=R(\cos(\Omega t+\pi/2),\sin(\Omega t+\pi/2),0)$ (the $\pi/2$ phase factors are there for later convenient) and

$$\Omega=\frac{2\pi}{T}=\left(\frac{Gm}{R^3}\right)^{1/2} \tag{3.49}$$

is the orbital frequency as given by Kepler law [2]. The inertial moment for circular orbits is immediately calculated, the nonzero components are

$$\begin{cases} I^{11} &= \mu R^2\cos^2(\Omega t+\pi/2)=\mu R^2\frac{1+\cos^2(2\Omega t+\pi)}{2}=\mu R^2\frac{1-\cos^2(2\Omega t)}{2}\\ I^{22} &= \mu R^2\sin^2(\Omega t+\pi/2)=\mu R^2\frac{1-\cos^2(2\Omega t+\pi)}{2}=\mu R^2\frac{1+\cos^2(2\Omega t)}{2}\\ I^{12} &= \mu R^2\cos(\Omega t+\pi/2)\sin(\Omega t+\pi/2)=\mu R^2\frac{1}{2}(\sin(2\Omega t+\pi)+\sin(0))=-\mu R^2\sin(2\Omega t)\ . \end{cases} \tag{3.50}$$

Taking the derivatives

$$\begin{cases} \ddot{I}^{11} &= 2\mu R^2\Omega^2\cos(2\Omega t)\\ \ddot{I}^{21} &= 2\mu R^2\Omega^2\sin(2\Omega t)\\ \ddot{I}^{22} &= -\ddot{I}^{11}\ . \end{cases} \tag{3.51}$$

From the quadrupole formula one concludes that GW are emitted at frequency $\omega=2\Omega$. Note this comes from the term $x^ix^j\sim\cos^2(\Omega t)$, hence any monocromatic source emits at 2Ω as a consequence of the quadrupole nature of the GW. Performing the TT projection (the first expressions omit the constants) one gets (Maggiore, 2007)

$$\begin{cases} h_+ &= \frac{1}{r}(\ddot{I}_{11}-\ddot{I}_{22})=\frac{G}{rc^2}4\mu R^2\Omega^2\frac{1+\cos^2\theta}{2}\cos(2\Omega t_R+\varphi)\\ h_\times &= \frac{2}{r}\ddot{I}_{12}=\frac{G}{rc^2}4\mu R^2\Omega^2\cos\theta\sin(2\Omega t_R+\varphi)\ , \end{cases} \tag{3.52}$$

where (θ,φ) is the sky location of the source (related to the direction $\hat{n}(\theta,\varphi)$ in the STF projector).

The formula above can be re-written using again Kepler law to eliminate R for Ω. The result is

$$\begin{cases} h_+ &= \frac{4}{r}\left(\frac{G\mathcal{M}_c}{c^2}\right)^{5/3}\left(\frac{\pi\omega}{2c}\right)^{2/3}\frac{1+\cos^2\theta}{2}\cos(\omega t_R+\varphi)\sim\nu\frac{m}{r}(m\omega)^{2/3}\\ h_\times &= \frac{4}{r}\left(\frac{G\mathcal{M}_c}{c^2}\right)^{5/3}\left(\frac{\pi\omega}{2c}\right)^{2/3}\sin(\omega t_R+\varphi)\sim\nu\frac{m}{r}(m\omega)^{2/3} \end{cases} \tag{3.53}$$

Above we have introduced key quantities: the chirp mass

$$\mathcal{M}_c:=\frac{(m_1m_2)^{3/5}}{m^{1/5}}=\mu^{3/5}m^{2/5}=m\nu^{3/5}\ , \tag{3.54}$$

and the symmetric mass ratio $\nu:=(m_1m_2)/m^2$. *The GW (in the quadrupole formula approximation) of a binary system depends exclusively on the chirp mass, not on the individual masses. Hence, this is the mass combination that is best measured in a GW observation. Moreover, the second line of Eq. (3.53) clearly indicates that the GW amplitude scales in a trivial way with the total mass of the system. We shall see this result holds also for the phase, and it holds also for binary black holes in GR. The key parameter determining the morphology of the waveform is thus the mass ratio.*

[2] Kepler law can be derived from dimensional analysis of the quantities Ω, Gm, R or equating the grav.force to the centripetal force.

3.4 Multipolar expansion

The quadrupole moment is the tensor that appears in the multipolar expansion of the Newtonian potential

$$\phi(t,\vec{x}) = -\frac{GM}{r} + \frac{3GQ_{ij}(t)n^i n^j}{2r^3} + \dots \,. \tag{3.55}$$

The dipolar term (multipole with "one index") is just the center of mass vector that can be removed by using the center of mass frame. The quadrupole is the lowest multipole described by a tensor with 2 indexes. A similar expansion hold for the electrostatic potential, but in that case the dipole cannot be removed and represents the next-to-leading order approximation of the charge distribution. The multipolar expansion is a key tool in classical field theories and in particular for gravitational waves.

The derivation of the quadrupole formula used the expansion Eq. (3.37), or equilvalently Eq. (3.40), at leading order which is valid far from the source and for low frequencies. The expansion starts at the quadrupolar order ($\ell = 2$) because of mass and momentum conservation. Indeed, integrating T_{00} and using the conservation law for $T_{\mu\nu}$ one finds immediately $\dot{M} = 0$ and similarly integrating $T_{00}x^i$ gives momentum conservation $\dot{P}^i = 0$ (see below).

A generic source can be however decomposed in a infinite series of multipoles. Let us sketch, in three steps, how to build a systematic multipolar formulas for the linearized GWs.

1. Starting from the multipolar expansion of the stress-energy tensor in Eq. (3.37),

$$T_{kl}(u + \frac{\hat{n}\cdot\vec{x}'}{c}, \vec{x}') = T_{kl}(u,\vec{x}') + \frac{n_i x'^i}{c}\partial_t T_{kl}(u,\vec{x}') + \frac{n_i x'^i n_j x'^j}{c^2}\partial_{tt} T_{kl}(u,\vec{x}') + \dots \,,$$

   define the following quantities

$$S^{ij} = \int d^3x' T^{ij} \;,\quad S^{ij,k} = \int d^3x' T^{ij}x^k \;,\quad S^{ij,kl} = \int d^3x' T^{ij}x^k x^l \;,\quad \dots \tag{3.56a}$$

   such that the Eq. (3.41) (in TT gauge) generalizes to

$$\bar{h}^{\rm TT}_{ij} \sim \Lambda_{ij,kl}\left(S^{kl} + \frac{1}{c}n_m \dot{S}^{kl,m} + \frac{1}{c^2}n_{m_1}n_{m_2}\ddot{S}^{kl,m_1m_2} + \dots\right) \,. \tag{3.57}$$

2. The next step is to express T^{ij} in favour of T^{00} in the integrals, similarly to what done for the quadrupole formula. Define two sets of quantities, the *mass multipoles*

$$M = \int d^3x' T^{00} \;,\quad M^i = \int d^3x' T^{00}x^i \;,\quad M^{ij} = \int d^3x' T^{00}x^i x^j \;,\quad \dots \,, \tag{3.58a}$$

   and the *current multipoles*

$$P^i = \int d^3x' T^{0i} \;,\quad P^{i,j} = \int d^3x' T^{0i}x^j \;,\quad P^{i,jk} = \int d^3x' T^{0i}x^j x^k \;,\quad \dots \,. \tag{3.59}$$

   Mass and current multipoles are connected by identities that follow from the stress-energy conservation:

$$\dot{M} = 0 \;,\quad \dot{P}^i = 0 \tag{3.60a}$$
$$\dot{M}^i = P^i \;,\quad \dot{P}^{i,j} = S^{ij} \tag{3.60b}$$
$$\dot{M}^{ij} = P^{i,j} + P^{j,i} \;,\quad \dot{P}^{i,jk} = S^{ij,k} + S^{ik,j} \tag{3.60c}$$
$$\dot{M}^{ijk} = P^{i,jk} + P^{j,ki} + P^{k,ij} \;,\quad \dots \tag{3.60d}$$

   The first line expresses the conservation of energy and momentum. It is left as [exercise] to prove these relations.

3. The last step is to use the above identities to substitute the derivatives of the $S^{ij,*}$ quantities with the mass and current multipoles. The first three terms in the expansion are the second time derivative of the mass quadrpole (quadrupole formula), the third time derivatives of *mass octupole* and the second time derivatives of the *current quadrupole*:

$$S^{ij} = \frac{1}{2}\ddot{M}^{ij} \;, \tag{3.61a}$$
$$\dot{S}^{ij,k} = \underbrace{\frac{1}{6}\dddot{M}^{ijk}}_{\text{mass octupole term}} + \underbrace{\frac{1}{3}\left(\ddot{P}^{i,jk} + \ddot{P}^{j,ik} + 2\ddot{P}^{k,ij}\right)}_{\text{current quadrupole term}} \,, \tag{3.61b}$$
$$\ddot{S}^{ij,kl} = \dots$$

The direct calculation of arbitrary high-order multipoles with the method above is clearly cumbersome. A general formalism to help with that is presented in Chap. 4.

4. Multipolar expansion

Basics of systematic multipolar expansions for tensor fields on flat spacetimes. Spherical harmonics and Symmetric—Trace-Free (STF) expansion for scalar fields. Tensors spherical components. STF expansion for tensors. Tensor spherical harmonics.

Suggested readings. *Sec. 3.4-3.5 of Maggiore (2007). Sec. 12.1-12.2 of Maggiore (2018). Thorne (1980), Blanchet and Damour (1989); Damour and Iyer (1991).*

4.1 Multipolar expansion for scalar fields

4.1.1 Static potential

Consider a scalar field solution of the Poisson equation

$$\Delta\phi = 4\pi\rho \,, \tag{4.1}$$

where ρ is a localized source (compact support in $r < R$) and thus the boundary condition for the field is $\phi \to 0$ at infinity. The solution to the boundary value problem (BVP) can be obtained by introducing the Green function (Jackson, 1975)

$$\Delta G(x-y) = 4\pi\delta(x-y) \quad \Rightarrow \quad G(x-y) = \frac{1}{|x-y|} \,, \tag{4.2}$$

that helps to invert the Poisson operator:

$$\phi = \Delta^{-1}\rho := \int d^3y G(x-y)\rho(y) = \int d^3y \frac{\rho(y)}{|x-y|} \,. \tag{4.3}$$

Spherical coordinates and spherical harmonics. We start considering the multipolar expansion of the solution in terms of spherical harmonics and adopt spherical coordinates. The exterior solution of the BVP is the solution for $r > R$. Functions in the form $r^{-\ell-1}Y_{\ell m}$ are particular solutions of the homogeneous equation ($\rho(r > R) = 0$) that respect the boundary conditions, i.e. they are decaying solutions. This is directly verified by the following lines:

$$\Delta\left(\frac{Y_{\ell m}}{r^{\ell+1}}\right) = \left(\frac{1}{r^2}\partial_r(r^2\partial_r) + \frac{L^2}{r^2}\right)\frac{Y_{\ell m}}{r^{\ell+1}} = \frac{Y_{\ell m}}{r^2}\frac{d}{dr}(r^2\frac{d}{dr})r^{-\ell-1} - \frac{\ell(\ell+1)}{r^2}\frac{Y_{\ell m}}{r^{\ell+1}} = \tag{4.4a}$$

$$= \frac{Y_{\ell m}}{r^2}\left(\frac{d}{dr}(r^2\frac{d}{dr}r^{-\ell-1}) - \ell(\ell+1)r^{-\ell-1}\right) = \frac{Y_{\ell m}}{r^2}\left(-(\ell+1)\frac{d}{dr}(r^2r^{-\ell-2}) - \ell(\ell+1)r^{-\ell-1}\right) = \tag{4.4b}$$

$$= \frac{Y_{\ell m}}{r^2}\left(\ell(\ell+1)r^{-\ell-1} - \ell(\ell+1)r^{-\ell-1}\right) \equiv 0 \,. \tag{4.4c}$$

In the expression above L^2 is the Laplacian on the 2-sphere and we used that the spherical harmonics satisfy by definition the eigenvalue equation

$$L^2Y_{\ell m} = -\ell(\ell+1)Y_{\ell m} \,. \tag{4.5}$$

The general exterior solution is given by a linear combination of the function above with coefficients $Q_{\ell m}$,

$$\phi^{\rm ext} = \sum_{\ell=0}\sum_{m=-\ell}^{\ell}\frac{Q_{\ell m}}{2\ell+1}\frac{Y_{\ell m}}{r^{\ell+1}} \,. \tag{4.6}$$

The coefficients $Q_{\ell m}$ can be determined by matching the exterior solution to the general solution in Eq. (4.3). In order to perform this matching, one needs to consider the expansion of the Green function in spherical harmonics (Jackson, 1975)

$$\frac{1}{|x-y|} = \sum_{\ell=0}\sum_{m=-\ell}^{\ell}\frac{1}{2\ell+1}\,r'^{\ell}\,Y^*_{\ell m}(\theta',\varphi')\,\frac{Y_{\ell m}(\theta,\varphi)}{r^{\ell+1}} \,, \tag{4.7}$$

where $r = |x|$ and primed quantities refer to $\vec{y}$, e.g. $r' = |y|$. Next, we can write the exterior solution as an expansion in spherical hamornics where the coefficients are determined by the spherical harmonics decomposition of the source. The result is immediately found by plugging Eq. (4.7) into Eq. (4.3); comparing to Eq. (4.6) one can read-off that the multipolar coefficients $Q_{\ell m}$ are integrals of the source ρ:

$$\Delta^{-1}\rho = \sum_{\ell=0}\sum_{m=-\ell}^{\ell} \frac{1}{2\ell+1}\int d^3y\, r'^{\ell} Y^*_{\ell m}(\theta',\varphi')\rho(r',\theta',\varphi')\frac{Y_{\ell m}(\theta,\varphi)}{r^{\ell+1}} = \sum_{\ell=0}\sum_{m=-\ell}^{\ell}\frac{Q_{\ell m}}{2\ell+1}\frac{Y_{\ell m}(\theta,\varphi)}{r^{\ell+1}} \tag{4.8a}$$

with

$$Q_{\ell m} := \int d^3y\, r'^{\ell}\, \rho(r',\theta',\varphi')\, Y^*_{\ell m}(\theta',\varphi')\ . \tag{4.8b}$$

It should be evident that the $\ell = 0$ multipole is the mass (or charge) of the source distribution; the $\ell = 1$ terms are the dipole moment; the $\ell = 2$ are the quadrupole moment, etc.

Cartesian coordinates and STF. An analogous result can be obtained using Cartesian coordinates. Consider the Taylor expansion of the Green function $G(x-y)$ in the variable $\vec{y}$

$$f(y) := \frac{1}{|x-y|} = f(0) + y^i \frac{\partial f}{\partial y^i}\Big|_0 + \frac{1}{2!}y^i y^j \frac{\partial^2 f}{\partial y^i \partial y^j} + ... \tag{4.9a}$$

$$= \frac{1}{|x|} - y^i \frac{\partial}{\partial x^i}\frac{1}{|x|} + \frac{1}{2}y^i y^j \frac{\partial}{\partial x^i}\frac{\partial}{\partial x^i}\frac{1}{|x|} + ... \tag{4.9b}$$

$$= \sum_{\ell=0}\frac{(-1)^\ell}{\ell!} y^{i_1}...y^{i_\ell}\frac{\partial}{\partial x^{i_1}}...\frac{\partial}{\partial x^{i_\ell}}\frac{1}{|x|}\ , \tag{4.9c}$$

where in the second line we used the results:

$$\frac{\partial f}{\partial y^i}\Big|_0 = \frac{\partial}{\partial y^i}\left(\frac{1}{|x-y|}\right)\Big|_{y=0} = -\frac{\partial}{\partial x^i}\left(\frac{1}{|x-y|}\right)\Big|_{y=0} = -\frac{\partial}{\partial x^i}\frac{1}{|x|} \tag{4.10a}$$

$$\frac{\partial^\ell f}{\partial y^{i_1}...\partial y^{i_\ell}}\Big|_0 = (-1)^\ell \frac{\partial^\ell}{\partial x^{i_1}...\partial x^{i_\ell}}\frac{1}{|x|}\ . \tag{4.10b}$$

The terms $\partial_{i_1}...\partial_{i_\ell}1/|x|$ of the expansion in Eq. (4.9) have two important properties

- Symmetric in the indexes $i_1....i_\ell$
- Traceless, in the following sense

$$\delta^{ij}\frac{\partial^2}{\partial x^i \partial x^j}\frac{1}{|x|} = \Delta\frac{1}{|x|} = 0 \quad (|x| \neq 0)\ , \tag{4.11a}$$

$$\delta^{ij}\frac{\partial^\ell}{\partial x^i \partial x^j \partial x^{i_2}...\partial x^{i_\ell}}\frac{1}{|x|} = 0 \quad (\text{for any } i,j = i_1,...,i_\ell)\ . \tag{4.11b}$$

An expansion in the form of the last line of Eq. (4.9) is thus called an expansion in *Symmetric—Trace-Free (STF) tensors*. Using the notation $x^i = rn^i$ with $r = |x|$ and the relations

$$\partial_i r = \partial_i (x_j x^j)^{1/2} = \frac{x_i}{r} = n_i\ ,\quad \partial_i n_j = \partial_j(\frac{x_j}{r}) = \frac{1}{r}\delta_{ij} - \frac{1}{r^2}x_j\partial_i r = \frac{1}{r}(\delta_{ij} - n_i n_j)\,, \tag{4.12}$$

the derivatives in Eq. (4.9) can be written

$$\partial_i \frac{1}{r} = -\frac{n_i}{r^2} \tag{4.13a}$$

$$\partial_i\partial_j \frac{1}{r} = -\frac{3}{r^3}n^{\langle i}n^{j\rangle} \tag{4.13b}$$

$$\partial_i\partial_j\partial_k \frac{1}{r} = -\frac{3\cdot 5}{r^4}n^{\langle i}n^j n^{k\rangle} \tag{4.13c}$$

$$\partial_{i_1}...\partial_{i_\ell}\frac{1}{r} = \frac{(-1)^\ell(2\ell-1)!!}{r^{\ell+1}}n^{\langle i_1}...n^{i_l\rangle}\,, \tag{4.13d}$$

where the symbol $\langle ...\rangle$ indicate the symmetric–trace-free part. Hence, the Green function admits an alternative expansion in terms of STF tensors (Cf. Eq. (4.7))

$$\frac{1}{|x-y|} = \sum_{\ell=0}\frac{(2\ell-1)!!}{\ell!}\frac{r'^\ell}{r^{\ell+1}}n'^{i_1}...n'^{i_\ell}n^{\langle i_1}...n^{i_l\rangle}\,, \tag{4.14}$$

where we used $y^i = r' n'^i$. An alternative expression for the exterior solution of the Poisson equation in terms of STF can be found by plugging Eq. (4.14) into Eq. 4.3:

$$\Delta^{-1}\rho = \sum_{\ell=0}\sum_{\ell=0} \frac{(2\ell-1)!!}{\ell!} \int d^3y\, r'^\ell\, \rho(y)\, n'^{i_1}...n'^{i_\ell} \frac{n^{\langle i_1}...n^{i_l\rangle}}{r^{\ell+1}} = \sum_{\ell=0} \frac{(2\ell-1)!!}{\ell!} Q_{i_1...i_\ell} \frac{n^{\langle i_1}...n^{i_l\rangle}}{r^{\ell+1}} \tag{4.15a}$$

with

$$Q_{i_1...i_\ell} := \int d^3y\, r'^\ell\, \rho(y)\, n'^{\langle i_1}...n'^{i_\ell\rangle} \tag{4.15b}$$

Note that the coefficients can be directly defined as the STF part because they are contracted with a STF combination of derivatives and their antisymmetric and trace part does not contribute in the sum. The above equation should be compared to Eq. (4.8a).

Example 4.1.1. *Consider the tensor $T^{ij} := y^i y^j$. The symmetrized tensor is $T^{(ij)} = y^{(i}y^{j)} = 1/2(y^iy^j + y^jy^i)$, with trace $T = y^{(i}y^{j)}\delta_{ij} = 2y^jy_j/2 = y^2$. Then the STF is constructed by first taking the symmetric and then subtracting $\delta_{ij}T/3$:*

$$T^{\langle ij\rangle} = y^{\langle i}y^{j\rangle} = \frac{1}{2}(y^iy^j + y^jy^i) - \frac{1}{3}y^2\delta^{ij}\ . \tag{4.16}$$

Relation between the two expansions. Evidently, there is close relation between Eq. (4.7) and Eq. (4.14) and between Eq. (4.8a) and Eq. (4.15a). The first thing to note is that the angles (θ,φ) can be considered a function of the unit vector n^i that points in the direction identified by the angles,

$$n^i = (\sin\theta\cos\varphi, \sin\theta\sin\varphi, \cos\theta)\ . \tag{4.17}$$

Example 4.1.2. *An* axisymmetric *system is invariant under rotation about an axis, say $\hat{n} = \hat{z}$. Axisymmetric functions $F(\theta,\varphi) = F(\theta)$ are usually expanded in Legendre polynomials $P_\ell(\cos\theta)$, but they can be expanded also in STF*

$$F(\theta) = c_0 + c_1 z^{\langle i\rangle}n_i + c_2 z^{\langle i}z^{j\rangle}n_in_j + ... + c_\ell z^{\langle i_1}...z^{i_\ell\rangle}n_{i_1}...n_{i_\ell} + ...\ , \tag{4.18}$$

as a particular case of generic functions of (θ,φ). Considering $z_in^i = \cos\theta$, it is immediate to see the two expansions are equivalent:

$$1 = 1 \tag{4.19a}$$

$$z^{\langle i\rangle}n_i = z^in_i = \cos\theta \tag{4.19b}$$

$$z^{\langle i}z^{j\rangle}n_in_j = (z_iz_j - \frac{1}{3}\delta_{ij})n^in^j = \cos^2\theta - \frac{1}{3} \tag{4.19c}$$

...

The relation between Eq. (4.7) and Eq. (4.14) is now clarified by the following

Theorem 4.1.1. *The functions $F_\ell(\hat{n}) := Q_{i_1...i_\ell}n^{\langle i_1}...n^{i_\ell\rangle}$ are eigenfunctions of the L^2 operator (Laplacian on the 2-sphere) with eigenvalues $-\ell(\ell+1)$.*

Proof.

(i) Take $\tilde{F}_\ell = r^\ell F_\ell$ and show that $L^2\tilde{F}_\ell \equiv 0\ \forall\ \ell$. This is immediate for $\ell = 0$ (F_0 is a constant) and for $\ell = 1$ since $F_1(x^i)$ is a linear function and its second derivative is zero. The first nontrivial term is $\ell = 2$ that vanishes because the coefficient are tracefree:

$$\Delta\tilde{F}_2 = \Delta(Q_{ij}r^2n^in^j) = \Delta(Q_{ij}x^ix^j) = Q_{ij}\partial_k\partial_k(x^ix^j) = Q_{ij}\partial_k(\delta^i_kx^j + \delta^j_kx^i) = 2Q_{ij}\delta^i_k\delta^j_k = 2Q_{ij}\delta^{ij} = 0\ . \tag{4.20}$$

Similarly, the STF property of the expansion makes all the $\ell > 2$ terms to vanish [exercise].

(ii) Using the result above:

$$0 = \Delta\tilde{F}_\ell = \left(\frac{1}{r^2}\partial_r(r^2\partial_r) + \frac{L^2}{r^2}\right)\tilde{F}_\ell = \frac{F_\ell}{r^2}\frac{d}{dr}(r^2\frac{d}{dr}r^\ell) + \frac{r^\ell}{r^2}L^2F_\ell = r^{\ell-2}\left(\ell(\ell+1)F_\ell + L^2F_\ell\right)\ . \tag{4.21}$$

The theorem implies something very general. Given the spherical harmonic $Y_{\ell m}(\theta,\varphi)$, there exists a SFT tensor $\mathcal{Y}^{\ell m}_{i_1....i_\ell}$ independendent on (θ,φ) such that

$$Y_{\ell m}(\theta,\varphi) = \mathcal{Y}^{\ell m}_{i_1....i_\ell}n^{i_1}...n^{i_\ell}\ . \tag{4.22}$$

It is possible to show that

Theorem 4.1.2. *The $2\ell+1$ STF tensors $\mathcal{Y}^{\ell m}_{i_1....i_\ell}$ form an orthonormal basis for the rank-ℓ STF tensors. In other terms, a generic STF $T_{i_1...i_\ell}$ can be expanded as*

$$T_{i_1....i_\ell} = \sum_{m=-\ell}^{\ell} T_{\ell m} \mathcal{Y}^{\ell m}_{i_1....i_\ell} \tag{4.23}$$

where the $T_{\ell m}$ are called the spherical components *of T_{ij}.*

A direct calculation for $\ell = 2$ should convince of the general validity of this theorem and it is left as [exercise].

Properties of spherical components. Tensor spherical components play a role not in GWs physics but also in quantum mechanics. Few important properties are discussed in the following.

(i) Multiplying Eq. (4.23) by $n_{i_1}...n_{i_\ell}$ and using the definition of $\mathcal{Y}^{\ell m}_{i_1....i_\ell}$ one obtains the identity

$$T_{i_1....i_\ell} n^{i_1}...n^{i_\ell} = \sum_{m=-\ell}^{\ell} T_{\ell m} Y^{\ell m} \ . \tag{4.24}$$

This express the fact that in the STF expansion only the spherical harmonics with index ℓ contribute to the term with indexes $i_1....i_\ell$.

(ii) The spherical components can be be obtained using the orhogonality of $Y_{\ell m}$:

$$T_{\ell m} = 4\pi \frac{\ell!}{(2\ell+1)!!} T_{i_1...i_\ell} (\mathcal{Y}^{\ell m, i_1....i_\ell})^* \ . \tag{4.25}$$

The general calculation is a as follow. First, multiply the identity Eq. (4.24) by the complex cojugate of the spherical harmonics and integrate; then

$$T_{\ell m} = T_{i_1...i_\ell} \int d\Omega Y^*_{\ell m} n_{i_1}...n_{i_\ell} = T_{i_1...i_\ell} \mathcal{Y}^{\ell m}_{j_1....j_\ell} \int d\Omega n_{j_1}...n_{j_\ell} n_{i_1}...n_{i_\ell} \tag{4.26a}$$

$$= 4\pi \frac{\ell!}{(2\ell+1)!!} T_{i_1...i_\ell} (\mathcal{Y}^{\ell m, i_1....i_\ell})^* \ . \tag{4.26b}$$

The last line uses the following identity:

$$\frac{1}{4\pi} \int d\Omega n_{i_1}...n_{i_\ell} = \frac{1}{(2\ell+1)!!} \left(\delta_{i_1 i_2} \delta_{i_3 i_4} ... \delta_{i_{2\ell-1} i_{2\ell}} + \text{... all possible pairing of indexes} \right) \ , \tag{4.26c}$$

and the fact that, since $\mathcal{Y}^{\ell m, j_1....j_\ell}$ is symmetric in $j_1...j_\ell$, all the $\ell!$ permutations give the same result. To show this, do first the full calculation for $\ell = 2$. For any vector v^i:

$$I_2 := \int_0^{2\pi} d\varphi \int_0^{\pi} d\theta \ \sin\theta \, v_i n^i v^i n_j = \int d\varphi \int \sin\theta \, d\theta \, (v_1 \sin\theta\cos\varphi + v_2 \sin\theta \sin\varphi + v_3 \cos\theta)^2 = \tag{4.26d}$$

$$= \int d\varphi \int \sin\theta \, d\theta \, (v_1^2 \sin^2\theta \cos^2\varphi + v_2^2 \sin^2\theta \sin^2\varphi + v_3^2 \cos^2\theta \tag{4.26e}$$

$$+ 2v_1 v_2 \sin^2\theta \underbrace{\cos\varphi \sin\varphi}_{\int d\varphi ... = 0} + 2v_1 v_3 \sin\theta\cos\theta \underbrace{\cos\varphi}_{\int d\varphi ... = 0} + 2v_2 v_3 \sin\theta\cos\theta \underbrace{\cos\varphi}_{\int d\varphi ... = 0}) =$$

$$= v_1^2 \underbrace{\int \cos\varphi d\varphi}_{=\pi} \underbrace{\int \sin^3\theta d\theta}_{=4/3} + v_2^2 \underbrace{\int \sin^2\varphi d\varphi}_{=\pi} \underbrace{\int \sin^3\theta d\theta}_{=4/3} + v_3^2 2\pi \underbrace{\int \sin\theta\cos^2\theta d\theta}_{=2/3} \tag{4.26f}$$

$$= \frac{4\pi}{3}(v_1^2 + v_2^2 + v_3^2) = \frac{4\pi}{3} v_i v_j \delta^{ij} \tag{4.26g}$$

Then observe that all the odd integrals I_{2k+1} are zero because under a parity transformation $\theta \mapsto \theta - \pi$ the integral is equal to minus itself $I_{2k+1} \mapsto -I_{2k+1}$: $\int_0^\pi d\theta \sin\theta = \int_{-1}^1 du \mapsto \int_1^{-1} du$. Finally, all the even integrals I_{2k} are equal to the symmetric combination of the product of the δ's times a coefficient C_ℓ that depends on ℓ. The latter can be found by contracting all the indexes of the integrand. For example, for $\ell = 2$

$$\int d\Omega n^i n_i = C_2 \delta^i_i = 4\pi \frac{1}{3} \ . \tag{4.26h}$$

Patience calculation gives the result in Eq. (4.26c).

(iii) The properties of the tensor components under rotation are determined by the properties of the spherical harmonics. Since $T_{i_1....i_\ell} n^{i_1}...n^{i_\ell}$ is a scalar, it does not change under rotations, and if one performs a rotation around the z-axis of an angle $\delta\varphi$ (azimuthal angle) the identity in Eq. (4.24) implies that

$$Y_{\ell m} \mapsto e^{\mathrm{i}m\delta\varphi} Y_{\ell m} \quad \Rightarrow \quad T_{\ell m} \mapsto e^{-\mathrm{i}m\delta\varphi} T_{\ell m} \ . \tag{4.27}$$

In general, $T_{\ell m}$ transforms like $Y^*_{\ell m}$.

Summary 4.1.1. *A rank-ℓ STF tensor $T^{\langle i_1 \dots i_\ell \rangle}$ has $2\ell+1$ independent components and it is an* irreducible representation *of dimension $2\ell+1$ of the rotation group $SO(3)$. The spherical harmonics $Y_{\ell m}$ with $-\ell \leq m \leq \ell$ are a particular equivalent representation.*

Remark 4.1.1. *There is a useful compact notation for these multi-index sum: the indexes $i_1 ... i_\ell$ are often indicated with a capital letter L, e.g.*

$$\sum_{\ell=0} \frac{(-1)^\ell}{\ell!} Q_L \partial_L F(x) := \sum_{\ell=0} \frac{(-1)^\ell}{\ell!} Q_{i_1 \dots i_\ell} \frac{\partial}{\partial x^{i_1}} \dots \frac{\partial}{\partial x^{i_\ell}} F(x) \ . \tag{4.28}$$

4.1.2 Extension to wave equations & tensors

In order to be applied to gravitational waves, the above method must be generalized to tensorial fields that satisfy wave equations. Schematically we are interested in the extension

$$\Delta \longrightarrow \Box \ , \quad \phi(x) \longrightarrow h_{\mu\nu}(t,x) \ .$$

One possibility is to perform a Fourier transform in time such that $\Box \mapsto \Delta + k^2$ and to generalize the method for static potentials utilizing *tensor spherical harmonics* (Jackson, 1975). Tensor spherical harmonics are eigenfunctions of L^2 and can be used to separate the wave equation for tensor fields. Hence, they generalize the scalar wave case $\Box\phi = 0$ where one looks at solutions in the form

$$\phi = \sum_{\ell=0} \sum_{m=-\ell}^{\ell} \frac{c_{\ell m}(t - r/c)}{r} Y_{\ell m}(\theta, \varphi) \, . \tag{4.29}$$

Tensor spherical harmonics are useful in various contexts, including perturbations of spherically symmetric spacetimes. They will be introduced in Sec. 4.3. However, the Fourier approach does not allow one to explicitely link the multipoles to the time evolution of the source. The STF approach extended to tensor fields is preferable in this case and it is heavily employed in the post-Newtonian approach.

4.2 STF expansion

Scalars. Consider a scalar field solution of the wave equation

$$\Box\phi = -4\pi\rho \ , \tag{4.30}$$

where ρ is a localized source (compact support in $r < R$) and thus $\phi \to 0$ at infinity. The solution to the initial-boundary value problem (IBVP) is given in terms of the retarded Green function (Jackson, 1975)

$$\phi = \Box^{-1}\rho = \int d^3x' \frac{\rho(t - |x - x'|/c, x')}{|x - x'|} \ . \tag{4.31}$$

The exterior solution for $r > R$ (homogeneous equation) can be obtained by observing that functions of the retarded time $u = t - r/c$ of type $F(u)/r$ are particular decaying solutions

$$\Box \left(F(t - r/c)/r\right) = \left(-\partial_{tt} + c^2\Delta\right)\left(F(t - r/c)/r\right) = \left(-\partial_{tt} + \frac{c^2}{r^2}\partial_r(r^2\partial_r) + \frac{L^2}{r^2}\right)\left(F(t - r/c)/r\right) = \tag{4.32a}$$

$$= \left(-\partial_{tt} + \frac{c^2}{r^2}\partial_r(r^2\partial_r)\right)\left(F(t - r/c)/r\right) = -\frac{1}{r}f''(u) + \frac{c^2}{r^2}\partial_r\left(r^2\frac{-1}{c}\frac{f'(u)}{r} - r^2\frac{f(u)}{r^2}\right) \tag{4.32b}$$

$$= -\frac{f''(u)}{r} + \frac{c}{r^2}f'(u) - \frac{c}{r^2}\left(f'(u) - \frac{r}{c}f''\right) \equiv 0 \ . \tag{4.32c}$$

Thus, the exterior solution is a linear combination of functions $F(u)/r$, and it can be expressed by the STF expansion ($L = i_1 ... i_\ell$)

$$\phi^{\rm ext} = \sum_{\ell=0} \frac{(-1)^\ell}{\ell!} \partial_L \frac{F_L(u)}{r} \ . \tag{4.33}$$

The explicit expression for the F_L in terms of the multipoles of the source has been found by Blanchet and Damour (1989) by matching the exterior solution in Eq. (4.33) to Eq. (4.31). It reads

$$F_L(u) = \int d^3y y_L \int_{-1}^{1} dz \delta_\ell(z) \rho(u + \frac{z|y|}{c}, y) \ , \tag{4.34}$$

where

$$\delta_\ell(z) := \frac{(2\ell+1)!!}{2^{\ell+1}\ell!}(1-z^2)^\ell \ , \tag{4.35}$$

such that the integral $\int_{-1}^{1} dz\delta_\ell(z) = 1$ and $\delta_\ell(z) \to \delta(z)$ for $\ell \to \infty$. Differently from Eq. (4.15b), Eq. (4.34) involves a weight time average that is physically due to the finite propagation of the solution within the extended source. This average is negligible far away from the source, i.e. for $\rho(u + z|y|/c, .) \sim \rho(u, .)$. Note the time-average integral is the sum of a series of derivatives of the function

$$\int_{-1}^{1} dz\delta_\ell(z)\rho(u + \frac{z|y|}{c}, y) = \sum_{k=0}^{\infty} \frac{(2\ell+1)!!}{2^k k!(2\ell+2k+1)!!} \left(\frac{|y|}{c}\partial_u\right)^{2k} \rho(u, y) \, . \tag{4.36}$$

Hence, it admits a solution in powers of $1/c$. Analogous STF solutions exist for vectors and tensors wave equations, and they are summarized in the following without proof.

Vectors. The general exterior solution to

$$\Box A_\mu = -\frac{4\pi}{c} J^\mu \ , \tag{4.37}$$

is given by

$$A_0(u) = \sum_{\ell=0} \frac{(-1)^\ell}{\ell!}\partial_L \frac{F_L(u)}{r} \tag{4.38a}$$

$$A_i(u) = \sum_{\ell=0} \frac{(-1)^\ell}{\ell!}\partial_L \frac{G_{Li}(u)}{r} \ , \tag{4.38b}$$

where the $F_L(u)$ is the same as Eq. (4.34), i.e. the 0-component behaves like a scalar potential, and

$$G_{Li}(u) := \int d^3y y_L \int_{-1}^{1} dz\delta_\ell(z) J_i(u + \frac{z|y|}{c}, y) \ . \tag{4.39}$$

The tensor G_{Li} is STF with respect to the multi-index $L = i_1...i_\ell$ but not in the index i. Hence, it is usually re-expressed as a combination of STF tensors with $L+1$ indexes (an irreducible representation) as

$$G_{Li} = U_{iL} + \frac{\ell}{\ell+1}\epsilon_{ki\langle i_\ell} C_{L-1\rangle} + \frac{2\ell-1}{2\ell+1}\delta_{i\langle i_\ell} D_{L-1\rangle} \tag{4.40}$$

with

$$U_{L+1} := G_{\langle L+1\rangle} \ , \quad C_L := G_{kl\langle L-1}\epsilon_{i_\ell\rangle kl} \ , \quad D_{L-1} := G_{kkL-1} \ . \tag{4.41}$$

Intuition for this formulas for the case $\ell = 1$ can come by proving that a generic rank-2 tensor can be decomposed into a scalar, a vector and a rank-2 STF tensor, and by explicitely constructing the decomposition [exercise].

Damour and Iyer (1991) showed that a gauge transformation that preserves the Lorentz gauge,

$$A_\mu \to A_\mu + \partial_\mu\theta \ : \ \Box\theta = 0 \ , \tag{4.42}$$

allows one to set to zero the D_{L-1} term, but changes the expansion of the 0-component. The final result is

$$A_0 = \sum_{\ell=0} \frac{(-1)^\ell}{\ell!}\partial_L \frac{Q_L(u)}{r} \tag{4.43a}$$

$$A_i = -\frac{1}{c}\sum_{\ell=1} \frac{(-1)^\ell}{\ell!}\partial_{L-1}\left[\frac{Q^{(1)}_{iL-1}(u)}{r} + \frac{\ell}{\ell+1}\epsilon_{ikl}\partial_k\left(\frac{M_{lL-1}(u)}{r}\right)\right] \ , \tag{4.43b}$$

where the *electric* and *magnetic moment* are defined as

$$Q_L(u) := \int d^3y y_L \int_{-1}^{1} dz \left[\delta_\ell(z) y_L \rho(u + \frac{z|y|}{c}, y) - \frac{1}{c^2}\frac{2\ell+1}{(\ell+1)(2\ell+3)}\delta_{\ell+1}(z) y_{iL} J^{(1)}(u + \frac{z|y|}{c}, y)\right] \tag{4.44a}$$

$$M_L(u) := \int d^3y y_L \int_{-1}^{1} dz \left[\delta_\ell(z) y_{\langle L-1}\epsilon_{i\ell\rangle jk} y_j J_k(u + \frac{z|y|}{c}, y)\right] \tag{4.44b}$$

and superscripts indicate derivatives w.r.t. to retarded time,

$$Q^{(1)}_{iL-1} := \frac{d}{du} Q_{iL} \ , \quad J^{(1)} := \frac{d}{du} J_i \ . \tag{4.44c}$$

The electromagnetic field is thus decomposed in time-dependent STF electric and magnetic multipoles of the source.

Tensors. A similar results applies to tensors whose components satisfy the wave equation

$$\Box \bar{h}_{\mu\nu} = \frac{16\pi G}{c^4} T_{\mu\nu} \ . \tag{4.45}$$

One starts from the expansions

$$\bar{h}_{00} \sim \sum_\ell \partial_L \frac{F_L}{r} \ , \quad \bar{h}_{0i} \sim \sum_\ell \partial_L \frac{G_{Li}}{r} \ , \quad \bar{h}_{ij} \sim \sum_\ell \partial_L \frac{H_{Lij}}{r} \ , \tag{4.46}$$

and expresses G_{Li} and H_{Lij} by means of full STF tensors. After a transformation that preserves the Hilbert (Lorentz) gauge one gets (Damour and Iyer, 1991)

$$\bar{h}_{00} = \frac{4G}{c^2} \sum_{\ell=0} \frac{(-1)^\ell}{\ell!} \partial_L \frac{M_L(u)}{r} \tag{4.47a}$$

$$\bar{h}_{0i} = \frac{4G}{c^2} \sum_{\ell=1} \frac{(-1)^\ell}{\ell!} \partial_{L-1} \left[\frac{M^{(1)}_{iL-1}(u)}{r} + \frac{\ell}{\ell+1} \epsilon_{ikl} \partial_k \left(\frac{S_{lL-1}(u)}{r} \right) \right] \tag{4.47b}$$

$$\bar{h}_{ij} = \frac{4G}{c^2} \sum_{\ell=2} \frac{(-1)^\ell}{\ell!} \partial_{L-2} \left[\frac{M^{(2)}_{ijL-2}(u)}{r} + \frac{2\ell}{\ell+1} \epsilon_{ikl} \partial_k \left(\frac{\epsilon_{kl(i} S^{(1)}_{j)lL-1}(u)}{r} \right) \right] \ . \tag{4.47c}$$

The gravitational fields far away form the source is expressed in terms of a STF expansion with two sets of multipolar moments $M_L(u)$ and $S_L(u)$ (and their derivatives). They are related to the *active mass density*, *active current density* and *active stress tensors*

$$\sigma := \frac{1}{c^2}(T^{00} + T^{ii}) \ , \quad \sigma_i := \frac{1}{c} T^{0i} \ , \quad \sigma_{ij} := T^{ij} \ , \tag{4.48}$$

by the integrals (Damour and Iyer, 1991; Maggiore, 2007)

$$M_L(u) := \int d^3y \int_{-1}^{1} dz \left[\delta_\ell(z) y_L \sigma - \frac{4(2\ell+1)}{c^2(\ell+1)(2\ell+3)} \delta_{\ell+1}(z) y_{iL} \sigma^{(1)}_i + \frac{2(2\ell+1)}{c^4(\ell+1)(\ell+2)(2\ell+5)} \delta_{\ell+2}(z) y_{ijL} \sigma^{(2)}_{ij} \right] \tag{4.49a}$$

$$S_L(u) := \int d^3y \int_{-1}^{1} dz \left[\delta_\ell(z) \epsilon_{\langle kli_\ell} y_{L-1\rangle k} \sigma_l - \frac{(2\ell+1)}{c^2(\ell+1)(2\ell+3)} \delta_{\ell+1}(z) \epsilon_{\langle kli_\ell} y_{L-1\rangle km} \sigma^{(1)}_{lm} \right] \ . \tag{4.49b}$$

Example 4.2.1. □ *[TODO: Derive the quadrupole formula from the general solution.]*

Remark 4.2.1. *The result above holds for the linear GR theory, but the same structure carries over on general backgrounds. In PN theory the formulas remain the same with an appropriate substitution of $T_{\mu\nu}$ with the effective stress-energy tensor $\tau_{\mu\nu}$ that includes the nonlinearities of the gravitational field.*

4.3 Tensor spherical harmonics

To introduce tensor spherical harmonics it is useful to take a "quantum mechanical" approach. Given a field of spin s, its total angular momentum is the sum of the orbital angular momentum and of the spin, $J^i = L^i + S^i$. The operators J^2, J_z, L^2 and S^2 commute and can be diagonalized simulataneously.

Definition 4.3.1. *Tensor spherical harmonics* $\mathbf{Y}$ *of a field of spin s can be defined as the simultaneous eigenfunctions of the operators J^2, J_z, L^2 and S^2:*

$$J^2\mathbf{Y} = j(j+1)\mathbf{Y} \ , \quad J_z\mathbf{Y} = j_z\mathbf{Y} \ , \quad L^2\mathbf{Y} = l(l+1)\mathbf{Y} \ , \quad S^2\mathbf{Y} = s(s+1)\mathbf{Y} \ . \tag{4.50}$$

The state of the system belongs to a space that is the tensor product of the space of dimension $(2l_z+1)$ spanned by the states $|ll_z\rangle$ with the space of dimension $(2s_z+1)$ spanned by the states $|ss_z\rangle$:

$$|ll_z ss_z\rangle = |ll_z\rangle \otimes |ss_z\rangle \ . \tag{4.51}$$

The total state is thus expanded as

$$|jj_z\rangle = \sum_{l_z=-l}^{l} \sum_{s_z=-s}^{s} |ll_z ss_z\rangle \, \langle ll_z ss_z | jj_z\rangle \ , \tag{4.52}$$

where $\langle ll_z ss_z | jj_z\rangle$ are the Clebsh-Gordan coefficients. The total angular momentum eigenvalues can take the values

$$|l-s| \leq j \leq l+s \ . \tag{4.53}$$

The tensor spherical harmonics can be explicitely constructed from the eigenfunctions of the orbital angular momentum, the (scalar) spherical harmonics and of the spin operator,

$$L^2 Y_{ll_z} = l(l+1) Y_{ll_z} \ , \quad S^2 \mathbf{X}_{ss_z} = s(s+1)\mathbf{X}_{ss_z} \ , \tag{4.54}$$

as

$$\mathbf{Y} = \sum_{l_z=-l}^{l} \sum_{s_z=-s}^{s} \langle ll_z ss_z | jj_z\rangle Y_{ll_z} \mathbf{X}_{ss_z} \ . \tag{4.55}$$

The tensor spherical harmonics carry 4 labels $\mathbf{Y}^{ls}_{jj_z}$ (omitted above) and describe the angular distribution and the polarization of the field of spin s. Since L^2 is part of the Laplacian, the tensor spherical harmonics can be used to separate the wave equation for tensor fields, thus generalizing the scalar case. Note the spin eigenfunctions $\mathbf{X}_{ss_z}$ are tensor with indexes that depend on the spin; these tensor indexes are understood in the bold notation. For $s = 1/2$ they carry a spinor index; for $s = 1$ a vector index, and for $s = 2$ a pair of indexes.

Vectors. For $s = 1$, $\mathbf{X}_{1\, s_z}$ with $s_z = 0, \pm 1$ can be constructed from the Cartesian unit vectors

$$\mathbf{X}_{1\,\pm 1} = \mp \frac{1}{\sqrt{2}} (\hat{x} \pm \mathrm{i}\hat{y}) \ , \quad \mathbf{X}_{1\,0} = \hat{z} \ . \tag{4.56}$$

The tensor spherical harmonics are thus vectors for $s = 1$. They can be used to solve the wave equation for the electromagnetic potential.

These $\mathbf{Y}^{l\,s=1}_{jj_z}$ vector spherical harmonics have no special properties with respect to the vector n^i, in particular they are neither purely transverse not longitudinal. For this reason, the vector spherical harmonics expansion of the electromagnetic potential is usually expressed in terms of combinations of $\mathbf{Y}^{l1}_{jj_z}$ that highlights the transverse/longitudinal charater of the terms, i.e. the relation to the unit vector n^i along the direction of propagation of the wave. To write such an expansion, one defines the *pure-spin vector spherical harmonics*

$$\mathbf{Y}^{R}_{jj_z} := \sqrt{2j+1}\left[j^{1/2} \mathbf{Y}^{j-1}_{jj_z} - (j+1)^{1/2} \mathbf{Y}^{j+1}_{jj_z} \right] \tag{4.57a}$$

$$\mathbf{Y}^{E}_{jj_z} := \sqrt{2j+1}\left[(j+1)^{1/2} \mathbf{Y}^{j-1}_{jj_z} + j^{1/2} \mathbf{Y}^{j+1}_{jj_z} \right] \tag{4.57b}$$

$$\mathbf{Y}^{B}_{jj_z} := \mathrm{i}\mathbf{Y}^{j}_{jj_z} \ , \tag{4.57c}$$

where the $s = 1$ index in $\mathbf{Y}^{ls}_{jj_z} = \mathbf{Y}^{l1}_{jj_z} = \mathbf{Y}^{l}_{jj_z}$ is omitted and one has to remember that $j = l-1, l-l+1$ ($j = 1$) for $l \neq 0$ ($l = 0$). These basis functions are orthonormal in all the indexes and are the physically more appropriate to describe the polarization states of the vector field [1]. The definition of the pure-spin vector spherical harmonics can be now expressed in terms of scalar spherical harmonics in order to make explicit their relation with $\hat{n}$:

$$\mathbf{Y}^{R}_{\ell m} = Y_{\ell m}\hat{n} \ , \quad \mathbf{Y}^{E}_{\ell m} = \sqrt{\ell(\ell+1)} r \nabla Y_{\ell m} \ , \quad \mathbf{Y}^{B}_{\ell m} = \sqrt{\ell(\ell+1)}\mathrm{i}\mathbf{L} Y_{\ell m} = \sqrt{\ell(\ell+1)} r \hat{n} \times \nabla Y_{\ell m} = \hat{n} \times \mathbf{Y}^{E}_{\ell m} \ . \tag{4.58}$$

Note we have conventionally renamed the total angular momentum: $(j, j_z) \mapsto (\ell, m)$. The above formulas show the $\mathbf{Y}^{E}_{\ell m}$ and $\mathbf{Y}^{B}_{\ell m}$ are transverse w.r.t. $\hat{n}$ while $\mathbf{Y}^{R}_{\ell m}$ is longitudinal. A generic vector field satisfying the wave equation is finally expanded as

$$V^i(t,r,\theta,\varphi) = \sum_{\ell=0} \sum_{m=-\ell}^{\ell} R_{\ell m}(t,r)(Y^R_{\ell m})^i(\theta,\varphi) + \sum_{\ell=1} \sum_{m=-\ell}^{\ell} \left[E_{\ell m}(t,r)(Y^E_{\ell m})^i(\theta,\varphi) + B_{\ell m}(t,r)(Y^B_{\ell m})^i(\theta,\varphi) \right] \ . \tag{4.59}$$

Under reflection, $\hat{n} \mapsto -\hat{n}$ [2], the parity of $Y^E_{\ell m}$ and $Y^B_{\ell m}$ are respecitvely $(-1)^\ell$ and $(-1)^{\ell+1}$. Since these are the transformation properties of the electric and magnetic fields, the $Y^E_{\ell m}$ and $Y^B_{\ell m}$ are called respectively of *electric*-type and *magnetic*-type. Note the second sum in Eq. 4.59 starts with $\ell = 1$, since the basis functions are defined for $\ell \geq 1$.

Exercise 4.3.1. *Compute the parity of the quantities in Eq. 4.58.*

[1] Note $\mathbf{Y}^{E}_{jj_z}$ and $\mathbf{Y}^{R}_{jj_z}$ are not eigenfunctions of L^2

[2] In spherical coordinates this is

$$r \mapsto r \ , \ \theta \mapsto \pi - \theta \ , \ \phi \mapsto \phi + \pi \tag{4.60}$$

Tensors. The logic to obtain an expansion of rank-2 tensors in tensor spherical harmonics follows closely the one presented above for vectors. Many steps are here omitted; a full account can be found in (Thorne, 1980). The $\mathbf{Y}^{l2}_{jj_z}$ ($s=2$) are STF tensors build similarly to above by taking as eigenfunctions $\mathbf{X}_{2s_z}$ the appropriate combination of two $s=1$ eigenfunction $\mathbf{X}_{1s_z}$ combined with Clebsh-Gordan coefficients. *Pure-spin $s=2$ spherical harmonics* are then introduced as linear combination of $\mathbf{Y}^{l2}_{jj_z}$. The cheme below shows from which tensor spherical harmonics are obtained and what is their relations to the scalar spherical harmonics. Note again the total angular momentum indexes are renamed: $(j, j_z) \mapsto (\ell, m)$.

$$\mathbf{Y}^{j+2}_{jj_z}, \mathbf{Y}^{j}_{jj_z}, \mathbf{Y}^{j-2}_{jj_z} \to (\mathbf{Y}^{S0}_{\ell m})_{ij} = (n_i n_j - 1/3\delta_{ij})\, Y_{\ell m} \tag{4.61a}$$

$$\mathbf{Y}^{j+2}_{jj_z}, \mathbf{Y}^{j}_{jj_z}, \mathbf{Y}^{j-2}_{jj_z} \to (\mathbf{Y}^{E1}_{\ell m})_{ij} = (\frac{2}{\ell(\ell+1)})^{1/2}(r/2)(n_i\partial_j + n_j\partial_i)Y_{\ell m} \tag{4.61b}$$

$$\mathbf{Y}^{j+2}_{jj_z}, \mathbf{Y}^{j}_{jj_z}, \mathbf{Y}^{j-2}_{jj_z} \to (\mathbf{Y}^{E2}_{\ell m})_{ij} = (\frac{2}{\ell(\ell+1)})^{1/2}(\mathrm{i}/2)(n_i L_j + n_j L_i)Y_{\ell m} \tag{4.61c}$$

$$\mathrm{i}\mathbf{Y}^{j+1}_{jj_z}, \mathrm{i}\mathbf{Y}^{j-1}_{jj_z} \to (\mathbf{Y}^{B1}_{\ell m})_{ij} = (2\frac{(\ell-2)!}{(\ell+2)!})^{1/2} r^2 \Lambda_{ij,i'j'}\partial_{i'}\partial_{j'}Y_{\ell m} \tag{4.61d}$$

$$\mathrm{i}\mathbf{Y}^{j+1}_{jj_z}, \mathrm{i}\mathbf{Y}^{j-1}_{jj_z} \to (\mathbf{Y}^{B2}_{\ell m})_{ij} = (2\frac{(\ell-2)!}{(\ell+2)!})^{1/2}(\mathrm{i}/2)(\partial_{i'}L_{j'} + \partial_{j'}L_{i'})Y_{\ell m}\ . \tag{4.61e}$$

where the $s=2$ index in $\mathbf{Y}^{ls}_{jj_z}$ is omitted. The five function set above are STF tensors basis for the five possible polarization of a field of spin $s=2$ [3]. The two transverse polarizations are

$$n^i(\mathbf{Y}^{E2}_{\ell m})_{ij} = 0 = n^i(\mathbf{Y}^{B2}_{\ell m})_{ij}\ . \tag{4.62}$$

The gravitational field in TT gauge solution of the homogeneous wave equation of linearized GR is expanded in tensor spherical harmonics as follows,

$$h^{\rm TT}_{ij}(t,r,\theta,\varphi) = \frac{G}{c^4}\frac{1}{r}\sum_{\ell=2}\sum_{m=-\ell}^{\ell}\left[u_{\ell m}(t,r)(\mathbf{Y}^{E2}_{\ell m})_{ij}(\theta,\varphi) + v_{\ell m}(t,r)(\mathbf{Y}^{B2}_{\ell m})_{ij}(\theta,\varphi)\right]\ . \tag{4.63}$$

The expansion in tensor spherical harmonics of $h^{\rm TT}_{ij}$ can be now compared to the multipolar expansion in Eq. (3.57) of Chap. 3 in order to express the $u_{\ell m}, v_{\ell m}$ coefficients in terms of the momenta of the stress-energy tensor. The computation involves some nontrivial integrals of type $\sim \int d\Omega (\mathbf{Y}^{E/B2\ *}_{\ell m})_{ij} n_{i_1}...n_{i_\alpha}$, and the use of the basis $\mathcal{Y}^{\ell m}_{i_1\dots i_\ell}$ introduced in Sec. 4.1.

The starting point is the two expressions for the TT wave far away from the source

$$h^{\rm TT}_{ij} = \frac{G}{c^4}\frac{1}{r}\Lambda_{ij,kl}\sum_{\alpha=0}\frac{1}{\alpha!}(\partial_t^\alpha S^{kl,i_1\dots i_\alpha})n_{i_1}...n_{i_\alpha} \tag{4.64a}$$

$$= \frac{G}{c^4}\frac{1}{r}\sum_{\ell=2}\sum_{m=-\ell}^{\ell}\left[u_{\ell m}(t,r)(\mathbf{Y}^{E2}_{\ell m})_{ij}(\theta,\varphi) + v_{\ell m}(t,r)(\mathbf{Y}^{B2}_{\ell m})_{ij}(\theta,\varphi)\right]\ . \tag{4.64b}$$

To express the coefficient $u_{\ell m}$ in terms of the source multipoles one equates both lines, multiply by $(\mathbf{Y}^{E2\ *}_{\ell m})_{ij}$ and integrates on the solid angle. The orthogonality of the tensors spherical harmonics isolates $u_{\ell m}$ on the l.h.s., and gives that the latter is equal to an integral that can be solved to leading order in v/c (Thorne, 1980; Maggiore, 2007):

$$u_{\ell m} = \sum_{\alpha=0}\frac{1}{\alpha!}(\partial_t^\alpha S^{kl,i_1\dots i_\alpha})\int d\Omega\ \underbrace{(\mathbf{Y}^{E2\ *}_{\ell m})_{ij}\Lambda_{ij,kl}}_{=(\mathbf{Y}^{E2\ *}_{\ell m})_{kl}} n_{i_1}...n_{i_\alpha} \sim \mathcal{Y}^{\ell m\ *}_{i_1\dots i_\ell}(\partial_t^{\ell-2}S^{i_1 i_2, i_3\dots i_\ell}) + \mathcal{O}((v/c)^2)\ . \tag{4.65}$$

Using the conservation of the stress-energy tensor and the symmetries of the tensors, the contraction between the $\mathcal{Y}$ and the multipoles S can be written in terms of the contractions with the mass and current multipoles, e.g.

$$\mathcal{Y}^{\ell m\ *}_{i_1\dots i_\ell} S^{i_1 i_2, i_3\dots i_\ell} \sim \mathcal{Y}^{\ell m\ *}_{i_1\dots i_\ell}\ddot{M}^{i_1\dots i_\ell}\ . \tag{4.66}$$

The final results is

$$u_{\ell m} = \frac{d^\ell}{dt^\ell}I_{\ell m}\ ,\quad \text{with}\quad I_{\ell m} \sim \mathcal{Y}^{\ell m\ *}_{i_1\dots i_\ell}M^{i_1\dots i_\ell} \sim \int d^3x r^\ell T^{00}Y^*_{\ell m}\ . \tag{4.67}$$

[3] The labels $0, 1, 2$ in the names marks the helicity for massless fields.

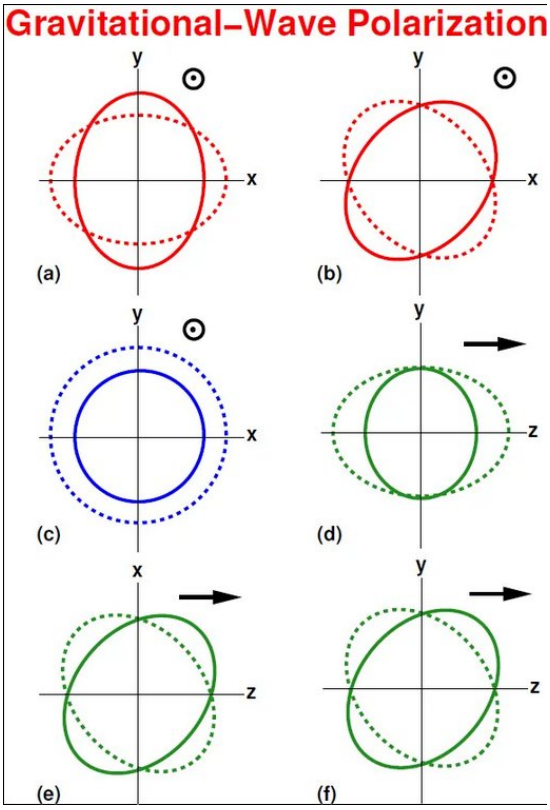

Figure 4.1: Effect on a ring of test masses on the $x-y$ plane at the passage of a GW in a generic metric theory of gravity. The wave propagaes in the perpendiculr direction in panel (a-c), while in the direction of the arrow in panels (d-f). Panels (a,b) are the transverse modes as in Fig. 3.1. Panel (c) is the transverse breathing mode A_s predicted for example by scalar-tensor theories. Panel (d) is the longitudinal mode A_L, predicted for example by massive scalar-tensor theories. Panels (e,f) are the $A_{1,2}$ The Einstein-Aether theory is an example that predict all six modes. From Will (2014).

A similar procedure can be followed for the $v_{\ell m}$ coefficients and leads to

$$v_{\ell m} = \frac{d^\ell}{dt^\ell} S_{\ell m} \ , \quad \text{with} \quad S_{\ell m} \sim \mathcal{Y}^{\ell m\ *}_{i\, i_1 \dots i_{\ell-1}} \epsilon_{ijk} P^{j,k\, i_1 \dots i_{\ell-1}} \sim \int d^3x r^\ell T^{0i} (\mathbf{Y}^B_{\ell m})_i \ . \tag{4.68}$$

Remark 4.3.1. *In GR, all the other components of the generic tensor spherical harmonics expansion can be eliminated by a gauge choice because there exist only two polarizations and their are both transverse degree of freedom. In alternative theories of gravity where the metric encodes the gravitational field there exist up to six different polarizations exist. The measure of the GW polarization thus provides a powerful test for theories of gravity (Will, 2014). A GW detector, whose scale is small compared to the gravitational wavelength, measures the local components of a symmetric* 3×3 *tensor given by the components of the Riemann tensor* $S_{ij} = -R_{0i0j}$ *via the equation of geodesic deviation,*

$$\ddot{x}_i = -R_{0i0j} x^j = S_{ij} x^j = \begin{pmatrix} A_S + A_+ & A_\times & A_1 \\ * & A_S - A_+ & A_2 \\ * & * & A_L \end{pmatrix}_{ij} x^j \ . \tag{4.69}$$

In general, S_{ij} *has six independent components that can be expressed in terms of polarizations. The polarization modes* A_L *and* $A_{1,2}$ *are longitudinal, with* A_L *an axially symmetric stretching mode in the propagation direction, and* $A_{1,2}$ *are quadrupolar modes in each of the two orthogonal planes containing the propagation direction. The polarization modes* $A_{+,\times}$ *are the transerve modes of GR while* A_S *is a transverse breathing mode. The effect of these polarization on a ring of test masses is shown in Fig. 4.1.*

In order to measure all these polarization an array of at least six suitably oriented GW antennas is necessary. Actually, there are eight unknowns in the problem: six polarizations and two direction cosines determinig the source skye position. The latter can be determined either via time-delays between different detectors or other observations (electromagnetic). With fewer detectors one can hope to measure at most particular combinations of the polarizations.

5. GWs energy

Discussion on the concept of energy in GR, gravitational-wave energy, the GW stress-energy tensor and the formula for GW luminosity.

Suggested readings. *Chap. 1,3 of Maggiore (2007). Chap. 4 of Wald (1984); Chap. 4 of Carroll (1997); Chap. 7-8 of Schutz (1985);*

5.1 Energy of the gravitational field

The physical reality of GW was investigated by Einstein already in 1916 and was finally established in the 60s with the fundamental work of Bondi, Goldberg, Newmann, Penrose, Pirani, Robison, Sachs, Trautman and many others. This theoretical work clarified GWs are not coordinate effects and can transport energy [1] Experimental evidence for GWs came afterwards with the Taylor & Hulse pulsar observation starting 1974.

Let us start with some considerations on the definition of energy of the grav. field in GR.

(i) In GR there is *no local definition of energy density for the gravitational field.* Roughly speaking, Einstein's equivalence principle allows us to eliminate gravitational forces at a point of the spacetime. This is implemented in the diffeorphism invariance of the theory, according to which we can always chosen normal coordinates such that the metric at a point p is flat,

$$g_{\mu\nu}(p) = \eta_{\mu\nu}\,. \tag{5.1}$$

(ii) Specifically thinking about GW energy, there is another difficulty. According to GR, any source of energy generates curvature via a stresst-energy tensor (SET). However, GWs have been defined - so far - as perturbation of a flat background that, by definition, cannot be curved. As a consequence, it appears necessary to generalize the concept of GW as perturbation of "generic background". A formal procedure fot that has been introduced by Isaacson in the 60s and it relies on separation of scales of variation of the metric (*short wave approximation*) to identify a background part on which the dynamical degrees of freedom (waves) propagate,

$$\boldsymbol{g} \sim \text{background metric} + \text{waves},\,. \tag{5.2}$$

It should be immediately stressed that, in general, the above separation is not possible and the applicability of such procedure needs to be evaluated case-by-case by identifying the scales in the particular physical system under consideration. However, when applicable, it allows us to define a suitable SET for the GWs.

(iii) A notion of *global energy characterizing the spacetime* exists in the special cases of stationary spacetimes and other spacetimes describing isolated bodies (See Rem. 5.1.1). If the spacetime posses a *timelike Killing vector (KV)* K^a, there exists a conserved current J^a (Komar current, $\nabla_a J^a = 0$) and an associated mass (Komar charge). The Komar mass is a globally conserved in the sense that its value does not vary during the time development of a spatial hypersurface in the GR Cauchy problem. An importat example of this global energy is the mass M parameter of the Schwarzschild solution. More generally, a notion of global energy can be constructed for a class of spacetimes called *asymptotically flat (AF)* that describe isolated objects. This is an advanced topic, see e.g. Chap. 11 of (Wald, 1984), but the basic intuition suggests that the spacetime of an isolated star or a black hole approaches the flat spacetime sufficiently far away from the object. Hence, in an asymptotical sense, the spacetime posses a time symmetry (approximate timelike KV) similar to that of Minkowski and stationary spacetimes, and this structure allows to define a conserved energy. Arnowitt, Deser e Misner (ADM, 1959) developed this idea in the context of the Hamiltonian formulation of GR and developed the concept of *ADM energy-momentum* associated to AF spacelike hypersurfaces. For the Schwarzschild solution the ADM mass coincide with the parameter M. Similarly, global notions of energy and momentum carried by the GWs have been developed by Bondi, Sachs, Penrose and others considering AF null hypersurfaces.

Remark 5.1.1. *We always work with* globally hyperbolic spacetimes*. This class of spacetimes are a restricted class of solutions of EFE obtained by postulating some general properties on the causal structure. In these cases it is possible*

[1] The famous conference Chapel Hill in 1957 where this topic was debated triggered the Weber experimental work and also led to a famous thought experiment `https://en.wikipedia.org/wiki/Sticky_bead_argument`.

to construct a foliation on the manifold that allows to prove the well-posedness of the Cauchy problem for EFE. Most of the spacetimes of astrophysical interest are globally hyperbolic spacetimes. Examples are given by the spacetimes of isolated compact objects.

5.2 Komar and ADM energy

We start a brief review of the concepts of Komar and ADM energy in GR from the well-known Newtonian case:

Remark 5.2.1. *The* mass of an isolated system in Newtonian gravity *can be defined as the gravitational flux through a close surface S containing the material body (source) using the following expression*

$$M = \int_V dV\, \rho = \int_V dV\, \Delta\phi = \frac{1}{4\pi} \oint_S ds\, n^i\, \partial_i \phi\,. \tag{5.3}$$

The fact that the system is isolated implies that $\Delta\phi = 0$ in the exterior of the source and that the last integral is independent on the choice of S. Since the gradient of the potential $\partial_i\phi$ is the force to hold in place a unit test mass, the mass definition canbe interpreted as the force to hold in place tes matter with unit mass density on S. Alternatively, M could be defined as the leading order coefficient of the multipolar expansion of the gravitational field far away from the source,

$$\phi \sim -\frac{M}{r} + \mathcal{O}(1/r^2)\,. \tag{5.4}$$

These definitions help to generalize the concept of mass to GR (Wald, 1984).

Komar mass. Similarly to the Newtonian case, a symmetry of the spacetime implies the existance of a conserved charge defined as the flux of the Killing field through a 2D closed, spacelike surface S:

$$\mathcal{L}_K \boldsymbol{g} = 0 \quad \Rightarrow \quad E_K := -\frac{1}{8\pi} \oint_S ds_{ab}\, \nabla^a K^b\,. \tag{5.5}$$

This is a standard result in GR that employs the properties of KVs and that reveals that the definition of E_K does not depend on S, provided the latter contains all the matter fields of the isolated source. Hence, E_k is a globally conserved quantity. The key bit of the calculation is to establish that the antisymmetric derivative of the 2-form $\alpha_{ab} := \epsilon_{abcd}\nabla^c K^d$ constructed with the 4D volume element $\boldsymbol{\epsilon}$ is zero in the exterior region,

$$\nabla_{[e}(\epsilon_{ab]cd}\nabla^c K^d) = \frac{2}{3} R^c_f K^f \epsilon_{ceab} \underbrace{\qquad}_{\text{exterior}, R_{ab}=0} = 0 \qquad \Rightarrow \quad \mathbf{d}\boldsymbol{\alpha} = 0 \text{ (exterior)}\,. \tag{5.6}$$

The vanishing of $\mathbf{d}\boldsymbol{\alpha}$ plays the same role as the vanishing of the Newtonian Laplacian $\Delta\phi$, as it can be appreciated from the following expression that uses Gauss-Stokes theorem:

$$E_K = -\frac{1}{8\pi}\oint_S \boldsymbol{\alpha} = -\frac{1}{8\pi}\int_\Sigma \mathbf{d}\boldsymbol{\alpha} = \frac{1}{4\pi}\int_\Sigma dV\, R_{ab} n^a K^b = 2\int_\Sigma dV\, \left(T_{ab} - \frac{1}{2} T g_{ab}\right) n^a K^b\,. \tag{5.7}$$

Above, Σ is the 3D volume of the spatial hypersurface bounded by S [2], and the last line employs EFE to express the Komar charge as a volume integral of the matter's SET. The derivation above is completely general, but in case K^a is a timelike KV the natural interpretation of E_K is that of an energy because the conservation is a consequence of time-translation invariance of the spacetime. In an analogous way, a symmetry by spatial translation defines the Komar momentum as conserved charge.

Example 5.2.1. *For the* Schwarzschild *metric $K^\alpha = (1,0,0,0)$ and the unit normal vectors that projects on 2-spheres have nonzero components $n_t = (1-2M/r)^{1/2}$ and $s_r = (1-2M/r)^{-1/2}$. The integrand of the Komar mass is*

$$ds_{ab}\nabla^c K^d = r^2 d\Omega\, (n_a s_b - n_b s_a)\nabla^a K^b = -2r^2 d\Omega\, \nabla^t K^r = -2\, M\, d\Omega\,, \tag{5.8}$$

where we used that $\nabla^t K^r = g^{tt}\nabla_t K^r = g^{tt}\Gamma^r_{tt}$ with $\Gamma^t_{rr} = M/r^2(1-M/r)$. From which integration on the 2-sphere gives $E_k = M$ independently on the choice of the sphere.

How to extend the energy definition to more general cases? From the heuristic consideration also mentioned above, one expects that a gloabal energy-momentum could be defined if the spacetime has "sufficient" (to be defined) asymptotic symmetries described by asymptotic killing vectors. It should be also clear from the Newtonian and Komar case that a global energy could exist for isolated systems. The next step is thus to define "how to go to ∞" and what is the minimal structure "of infinity" that allows the definition of meaningful quantities. There are two infinity: spatial infinity (i_0) and null infinity ($\mathcal{I}^+$).

[2] Note however the definition of Komar mass is geometrical and does not need S to embedded in Σ.

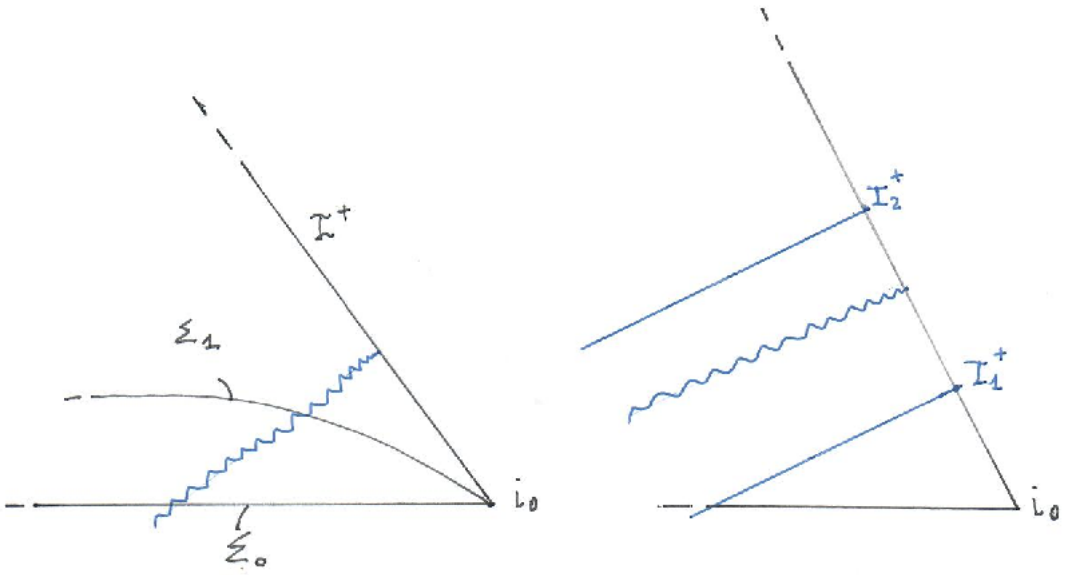

Figure 5.1: Illustration of asymptotic spatial and null infinity.

ADM mass. The concep of ADM mass applies to *asymptotically flat (AF) spacetimes at spatial infnity* i_0. A way to define these AF spacetimes is to ask that far from strong field region, there exist a coordinate system such that the metric is close to flat and the perturbation respectsfall-off conditions [3]

$$\boldsymbol{g} \sim \boldsymbol{\eta} + \boldsymbol{h} \;\text{ for } r\to\infty \quad : \quad h_{ij} = \mathcal{O}(1/r)\,, \text{ and } \;\partial_k h_{ij} = \mathcal{O}(1/r^2)\,. \tag{5.9}$$

The asymptotic transformations that preserve the AF structure are of the form

$$x^{'\mu} = \Lambda^\mu_\nu x^\nu + c^\mu(\theta,\phi) + \mathcal{O}(1/r^2)\,, \tag{5.10}$$

tha include Poincare transformations (Lorentz and boosts, $c^\mu = 0$), translations ($\Lambda^\mu_\nu = \delta^\mu_\nu$ and $c^\mu = const$), and angle-dependent translations (*supertranslations*, $\Lambda^\mu_\nu = \delta^\mu_\nu$ and $c^\mu \neq const$). This group of transformations is infinite dimensional and is called *Spi group*.

For AF spacetimes it is possible to define a conserved global energy corresponding to time-translations by considering integrals on asymptotic 2-spheres (outwards normal s^i),

$$E_{\rm ADM} := \frac{1}{16\pi}\lim_{r\to\infty}\oint_{S_r} r^2 d\Omega\, s^i \left(\partial_j h_{ij} - \partial_i h^k_k\right) \quad \text{Cartesian coordinates} \tag{5.11}$$

$$= -\frac{1}{8\pi}\lim_{r\to\infty}\oint_{S_r} (\kappa - \kappa_0)\,. \tag{5.12}$$

The first lines is the original definition of ADM and holds only in Cartesian coordinates , the second line is a geometrical definition that involves the trace of the extrisinc curvature of the asymptotic 2-surfaces embedded in the hypersurface minus a similar contribution given by considering an embedding in a flat hypersurface. Note the first integral exists thank to the fall-off behaviour. A similar definition applies for the momentum, for which each spatial translation generate the elements $P^i_{\rm ADM}$ that asymptotically transforms as a vector. Hence, we can define a 4-momentum and a mass as

$$M_{\rm ADM} := \sqrt{E_{\rm ADM} - P_i P^i}\,. \tag{5.13}$$

The key result is that $M_{\rm ADM}$ is a conserved quantity and, if the matter fields respect the dominant energy condition (DEC), then the ADM mass is positive definite (Schon and Yau, 1979, 1981; Witten, 1981)

$$M_{\rm ADM} \geq 0 \quad (=0,\ \text{iff } \boldsymbol{g} = \boldsymbol{\eta})\,, \tag{5.14}$$

In presence of a KV, this mass definition gives the same result as the Komar mass if the foliation is chosen such that $n^a = K^a = (\partial_t)^a$.

[3] This statement is not very rigorous although sufficient for our purposes. Appropriate fall-off conditions should be postulated on the 3-metric (hypersurfaces) and on the extrisic curvatures and their derivatives. A geometrical definition of spatial infinity that does not require introducing coordinates also exists.

Bondi energy. Let us move to the Bondi-Sachs mass. This concept refers to null infinity and allows us to quantify the energy carried by GWs (Bondi, 1960; Bondi et al., 1962; Sachs, 1962). Analogously to the ADM case, it is possible to define AF conditions for $\mathcal{I}^+$ by introducing Bondi coordinates adapted to outgoing null cones and prescribing appropriate asymptotic fall-off conditions for the metric components (see below). Note that a gemetrical definition of asymptotic flatness for $\mathcal{I}^+$ and covariant definition of gravitational radiation field were given by Newman and Penrose (1962); Penrose (1963). The asymptotic transformations that preserve the AF structure of $\mathcal{I}^+$ form the *BMS group* that, similarly to Spi, is infinite dimensional, contains Poincare' and supertranslations (Newman and Penrose, 1966). The BMS group has a unique set of 4-translations that allows the definition of a global energy-momentum. A way to introduce the Bondi mass is thus to postulate a formula similar to the Komar mass,

$$E_{\rm B} := -\frac{1}{8\pi} \lim_{S_r\to\mathcal{I}^+} \oint_{S_r} \boldsymbol{\alpha}\,, \tag{5.15}$$

but where S_r is a sequence of 2-spheres that approaches a section of $\mathcal{I}^+$ and the KV K^a is a generator of the asymptotic time translations that are paret of the BMS group.

There are two key results about the Bondi mass. The first is that the energy difference calculated from two successive sections of $\mathcal{I}^+$, e.g. $\mathcal{I}^+_1$ and $\mathcal{I}^+_2$, as shown in the right panel of Fig. 5.1, is negative:

$$E_{\rm B}[\mathcal{I}^+_2] - E_{\rm B}[\mathcal{I}^+_1] = -\oint f\,, \quad \text{with } f \geq 0\,. \tag{5.16}$$

This allows us to interpret the function f as the *GW flux* and the decrease of $E_{\rm B}$ as the energy radiated by GWs at null infinity. The second is that the Bondi mass is positive definite under DEC conditions (Schon and Yau, 1982; Horowitz and Perry, 1982),

$$E_{\rm B} \geq 0 \quad (=0,\ \text{iff } f\equiv 0)\,. \tag{5.17}$$

Example 5.2.2. *Consider* Maxwell equations *as a toy problem (Mädler and Winicour, 2016). The Minkowski metric can be written*

$$\eta = -du^2 - 2drdu + r^2 q_{AB} dx^A dx^B\,, \tag{5.18}$$

where u is the retarded time coordinate ($u=$ const are the outgoing light cones), r a radial coordinate, and $q_{AB} =$ $\mathrm{diag}(1,\sin^2\theta)$ with $A,B=1,2$ is the metric of unit 2-spheres with covariant derivative $\eth_A$. The Maxwell tensor in terms of the vector potential is $F_{ab} = \partial_a A_b - \partial_b A_a$ and it is invariant under a gauge transformation of the vector potential of type $A_a \mapsto A_a + \partial_a\chi$. It is possible to choose the gauge such that $A_r \equiv 0$, that implies the electric field is given by $E_r = F_{ru} = \partial_r A_u$ (note there is remaininng gauge freedom after this transformation). Maxwell equations are given by $M^b = \partial_a F^{ab} = 0$ or

$$0 = M^A: \quad \textit{Evolution eq.} \tag{5.19a}$$
$$0 = M^u : \partial_r(r^2\partial_r A_u) = \partial_r(\eth_B A^B) \quad \textit{Hypersurface eq.} \tag{5.19b}$$
$$0 = M^r : \partial_u(r^2\partial_r A_u) = \eth_B(\partial_r A_B - \partial_u A_B + \eth_B A_u) \quad \textit{Supplementary eq.}\,. \tag{5.19c}$$

The antisymmetry of the Maxwell tensor implies the identity

$$0 \equiv \partial_b M^b = \partial_u M^u + r^{-2}\partial_r(r^2 M^r) + \frac{1}{\sqrt{q}}\eth_C(\sqrt{q}M^C)\,. \tag{5.20}$$

The identity and the first two Maxwell equations imply that $0 = \partial_r(r^2 M^r)$, thus the supplementary equation is identically satified if it is satisfied at a given r. The hypersurface equation can be formally integrate up to a function $q(u,X^A)$ called the charge aspect*; this gives the total charge as a surface integral of the charge aspect,*

$$E_r = \partial_r A_u = \frac{1}{r^2}\left(q(u,a^A) + \partial_B A^B\right) \quad\Rightarrow\quad Q(u) := \frac{r^2}{4\pi}\oint_S E_r d\Omega = \frac{1}{4\pi}\oint_S q(u,X^A) + \underbrace{\frac{1}{4\pi}\oint_S \eth_B A^B}_{=0}\,. \tag{5.21}$$

Then, the supplementary equation implies the charge conservation

$$\frac{dQ}{du} = \frac{1}{4\pi}\oint_S \partial_u q(u,X^A) = \oint_S \partial_u(r^2\partial_r A_u) = \oint_S \eth_B(...)^B = 0\,. \tag{5.22}$$

Let us expand on the Bondi-Sach formalism building on the previous example (see e.g. (Mädler and Winicour, 2016)). The metric in Bondi coordinates is

$$g = -\frac{V}{r}e^{2\beta}du^2 - 2e^{2\beta}dudr + r^2 h_{AB}(dx^A - U^A du)(dx^B - U^B du)\,. \tag{5.23}$$

The asymptotic behaviour of the solution is given by the fall-off conditions

$$\beta = \mathcal{O}(1/r^2) \quad U^A = \mathcal{O}(1/r^2) \tag{5.24a}$$

$$V/r \sim 1 \ : \ V \sim r - 2m(u, X^A) + \mathcal{O}(1/r) \tag{5.24b}$$

$$h_{AB} \sim q_{AB} + \frac{1}{r} C_{AB}(u, x^A) + \mathcal{O}(1/r^2)\,, \tag{5.24c}$$

where m is called the *mass aspect* and satisfies

$$2\partial_u m = \eth_A \eth_B N^{AB} - N_{AB} N^{AB}\,. \tag{5.25}$$

Note that the mass aspect is the coefficient in a $1/r$ expansion of the g_{uu} metric function. This suggest an expression for the Bondi energy of type

$$E_{\rm B}(u) = \frac{1}{4\pi} \oint_S m(u, X^A) d\Omega\,, \tag{5.26}$$

that indeed is correct and can be obtained by a formal integration of EFE for the Bondi metric (Cf. the charge definition in terms of the charge aspect in Maxwell theory). The tensor appearing in Eq. (5.25) is called the *news tensor*

$$N_{AB} := \frac{1}{2} \partial_u c_{AB}\,, \tag{5.27}$$

and Penrose (1963) proved that it is independent on the $u = const$ foliation, i.e. it is geometrically defined tensor field at $\mathcal{I}^+$. Introduce now complex dyad on the unit sphere (tangent to null surfaces) $q^A \propto (1, \mathrm{i}\sin\theta)$ such that $q^{AB} = q^A \bar{q}^B + q^B \bar{q}^A$ [4] and define the *news function* N as

$$N := q^A q^B N_{AB} = \frac{1}{2} q^A q^B \partial_u C_{AB} = \partial_u (\frac{1}{2} q^A q^B C_{AB}) =: \partial_u \sigma_0\,. \tag{5.28}$$

The quantity σ_0 is a complex pseudoscalar that describes the shear of outgoing null hypersurfaces. Taking a derivative ∂_u of Eq. (5.26) and using Eq. (5.25) one obtains that the Bondi mass can only decrease,

$$\frac{dE_{\rm B}}{du} = -\frac{1}{4\pi} \oint_S |N|^2 d\Omega \leq 0\,. \tag{5.29}$$

The square of the news function is thus the GW energy flux at $\mathcal{I}^+$ mentioned above. Finally, a direct calculation using the Bondi metric and Eq. (3.31) reveals that the real and imaginary part of the shear are the GW polarizations, as also found by Newman and Penrose (1962); Penrose (1963):

$$\Im(\sigma_0)\,, \Re(\sigma_0) \quad \leftrightarrow \quad h_+\,, h_\times\,. \tag{5.30}$$

5.3 GW SET

Any form of energy must generate curvature through a SET. Having clarified that GW trasport energy, the next question is: Does a SET for the GW exist? Consider an AF spacetime of an isolated system. There are two main issues towards the definition of GW SET:

(i) Energy must be quadratic in the perturbation field. This implies that we must consider a perturbative expansion to *second order* in $\boldsymbol{h}$.

(ii) The Minkowski metric cannot be curved. We must consider perturbations of *generic background metric* and set up a procedure to separate the background part from the waves.

Second order expansion on generic background. We postulate a formal expansion of type

$$\boldsymbol{g} = \boldsymbol{\eta} + \boldsymbol{h}^{(1)} + \boldsymbol{h}^{(2)} + \mathcal{O}(3) \ \text{ with } \ |h^{(n)}_{\mu\nu}| \approx \epsilon^n |\eta_{\mu\nu}|\,, \tag{5.31}$$

where $\epsilon \ll 1$ is a parameter whose smallness will be defined later and $\boldsymbol{\eta}$ is a generic background metric with connection $\boldsymbol{\partial}$, i.e. not necessarily the flat metric. The Ricci tensor admits a similar expansion

$$R_{\mu\nu} = R^{(0)}_{\mu\nu} + R^{(1)}_{\mu\nu} + R^{(2)}_{\mu\nu} + \mathcal{O}(3)\,. \tag{5.32}$$

At first order this expansion is formally the same as the weak field equation, see Eq. (2.10c). The solution of linearized EFE for $\boldsymbol{h}^{(1)}$ can be found, up to a gauge choice, by solving (in vacuum, for simplicity):

$$0 = R^{(1)}_{\mu\nu}[\boldsymbol{h}^{(1)}]\,, \tag{5.33}$$

[4] The Newmann-Penrose tetrad vector $\boldsymbol{m}$ can be written as $m^a_{\rm NP} = 1/r(0, 0, q^A)$.

At second order, the Ricci contains several second order terms in the perturbation that are not present in $R^{(1)}_{\mu\nu}$, i.e.

$$2R^{(2)}_{\mu\nu} = \frac{1}{2}\partial_\mu h_{\alpha\beta}\partial_\nu h^{\alpha\beta} + h^{\alpha\beta}\partial_\mu\partial_\nu h_{\alpha\beta} \tag{5.34}$$
$$- 2h^{\alpha\beta}\partial_\beta\partial_{(\mu}h_{\nu)\alpha} + 2\partial^\alpha h^\beta_\nu\partial_{[\alpha}h_{\beta]\nu} + \partial_\alpha(h^{\alpha\beta}\partial_\beta h_{\mu\nu}) - \frac{1}{2}\partial^\alpha h\partial_\alpha h_{\mu\nu} - (2\partial_\alpha h^{\alpha\beta} - \partial^\beta h)\partial_{(\mu}h_{\nu)\beta}$$

This implies that the EFE at second order can be solved by adding to the first order $\boldsymbol{h}^{(1)}$ solution a term $\boldsymbol{h}^{(2)}$ that solves (in vacuum)

$$0 = R^{(1)}_{\mu\nu}[\boldsymbol{h}^{(2)}] + R^{(2)}_{\mu\nu}[\boldsymbol{h}^{(1)}]\,. \tag{5.35}$$

The first term is the linearized Ricci expression applied to the second order perturbation term, the second term is the second order Ricci expression applied to the first order perturbation term. Eq. (5.35) can be written as "an Einstein equation" for the second-order metric by simply introducing the Einstein tensor $G^{(2)}_{\mu\nu}$ in place of the Ricci $R^{(2)}_{\mu\nu}$ and re-arranging the term $R^{(2)}_{\mu\nu}$ in the r.h.s (to be treated as a "known term"):

$$G^{(1)}_{\mu\nu}[\boldsymbol{h}^{(2)}] = -G^{(2)}_{\mu\nu}[\boldsymbol{h}^{(1)}] =: 8\pi\tau_{\mu\nu}[\boldsymbol{h}^{(1)}] \tag{5.36}$$

The term $\tau_{\mu\nu}$ in the r.h.s. is symmetric and quadratic in $\boldsymbol{h}$, thus a candidate for the GW SET. Moreover, it is locally conserved on the background

$$\partial^\mu\tau_{\mu\nu} = 0\,, \tag{5.37}$$

if $\boldsymbol{h}^{(1)}$ satisfies the vacuum linearized EFE. However, the symmetry and conservation properties of $\tau_{\mu\nu}$ do not change by the addition of a term $\partial^\alpha\partial^\beta U_{\mu\nu\alpha\beta}$ with $U_{\mu\nu\alpha\beta} = \mathcal{O}(2)$ such that $U_{\mu\nu\alpha\beta} = U_{\mu\alpha[\nu\beta]} = U_{[\mu\alpha]\nu\beta} = U_{\nu\beta\mu\alpha}$. Worse, the second order expression is not invariant under an infinitesimal coordinate transformation [exercise]. In summary, we "almost" have a GW SET but the list does not fully check:

- ✓ Symmetric;
- ✓ Conserved on the background;
- ✓ Quadratic in $\boldsymbol{h}$, $\mathcal{O}(2)$;
- ✗ Not unique;
- ✗ Not gauge invariant.

Remark 5.3.1. *An alternative approach to the GW SET is the* Landau-Lifshitz pseudotensor. *The latter can be defined introducing the "gothic metric" tensor density* $\mathfrak{g}^{\alpha\beta} := \sqrt{-g}g^{\alpha\beta}$ *and the related tensor density*

$$\mathcal{H}^{\alpha\mu\beta\nu} := \mathfrak{g}^{\alpha\beta}\mathfrak{g}^{\mu\nu} - \mathfrak{g}^{\alpha\nu}\mathfrak{g}^{\beta\mu}\,. \tag{5.38}$$

$\mathcal{H}$ *has the same symmetries as the Riemann, in particular it is antisymmetric in* α *and* μ. *Taking two derivatives, one obtains the Einstein tensor multiplied by the metric determinant plus another symmetric term that defines the Landau-Lifshitz pseudotensor,*

$$\partial_\mu\partial_\nu\mathcal{H}^{\alpha\mu\beta\nu} = 2(-g)G^{\alpha\beta} + 16\pi(-g)\tau^{\alpha\beta}_{\rm LL} = 16\pi(-g)\left(T^{\alpha\beta} + \tau^{\alpha\beta}_{\rm LL}\right)\,. \tag{5.39}$$

Working in vacuum, the antisymmetry of $\mathcal{H}^{\alpha\mu\beta\nu}$ *implies a conservation law for the Landau-Lifshitz pseudotensor,*

$$0 = \partial_\alpha\partial_\mu\partial_\nu\mathcal{H}^{\alpha\mu\beta\nu} = \partial_\alpha\left((-g)\tau^{\alpha\beta}_{\rm LL}\right)\,. \tag{5.40}$$

*The specification to the weak field limit and the use of the TT leads to the same result of Eq. (**??**) after the short-wave averaging (see below).*

We also note that a stress-energy tensor for the gravitational field can be derived from a field theoretical formulation of the general relativity (as opposed to the standard geometrical picture; see also Sec. 6.2), in which gravity is treated as a nonlinear tensor field on flat spacetime, e.g. Babak and Grishchuk (2000); Maggiore (2007). Interestingly, the numerical values of the components of this tensor in the simplest gauge where the flat metric is $\mathrm{diag}(-1,1,1,1)$ *match those of the Landau-Lifshitz pseudotensor,* $(-g)\tau^{\alpha\beta}_{\rm LL}$.

Short-wave approximation. To proceed, we need to consider the issue of separating the background from the perturbation. In general, this separation is not necessarily possible. However, there might be systems in which a spacetime can be clearly composed of two parts that admits different scales of variation, see Fig. 5.2. The slowly varying component would then be naturally be associated to a background, while the rapidly varying component would be then associated to the perturbation. Concretely thinking of *spatial variation*, the background metric would be the part of the metric that vary on the long scale L, while the waves would be the part varying at short scales of the wavelength $\lambda \ll L$. Similarly, is *temporal scales* are cnsidered, one would associate the background to the low frequency varying component $\sim F$ and the waves to the high frequency component such that $f \gg F$. We stress that if a system admits a separation based on short/long wavelengths, it does not necessary implies it admits also a high/low frequency separation (and viceversa, see the following example.).

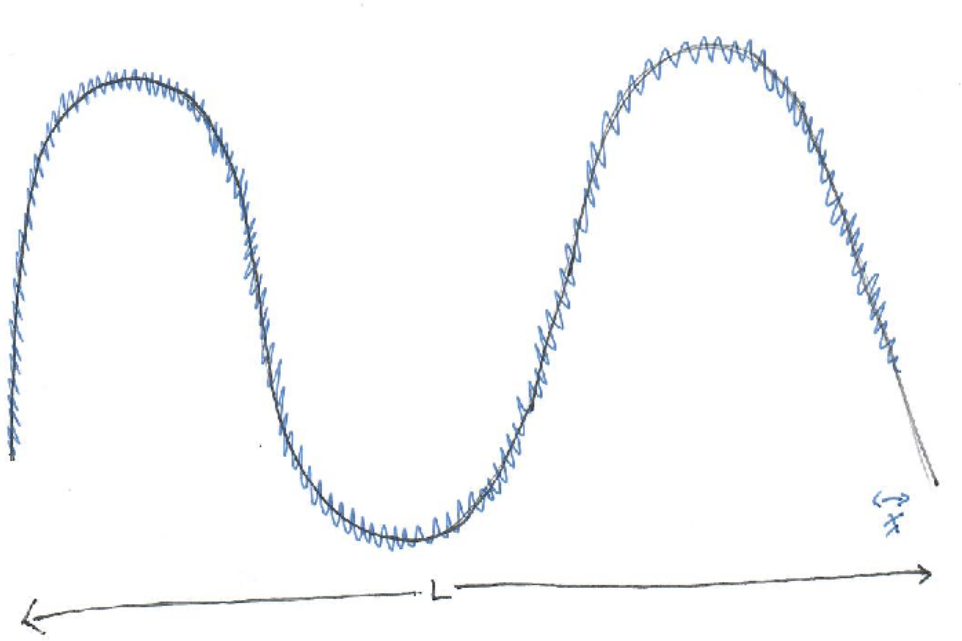

Figure 5.2: Illustration of spatial scale variations.

Example 5.3.1. GW experiments on Earth measure temporal, not length variations. *While the frequency and wavelength of a wave are related by $\lambda = c/f$, the temporal and spatial scales of variation of the background metric are* ***not*** *necessarily related. For example, consider a GW with $f \sim 10^3$ Hz, $\lambda\!\!\!^{-} \sim 50$ km and $|h| \sim 10^{-21}$ in the grav. field of Earth $\phi_\oplus \sim GM_\oplus/R_\oplus c^2 \sim 10^{-6}$. $\phi_\oplus$ is not smooth at lengthscales $\lambda\!\!\!^{-}$ because it has variations of order $deltaL/Lsim10^{-9} \gg |h|$ due to e.g. mountains; moreover the length of the laboratory apparatus to detect GW is $\ll \lambda$. It is not possible to separate the length scales of the Earth's grav. field and the GW! However, $\phi_\oplus$ is static with frequency $\ll f$. In this sense the grav. field of Earth can be separated from the GW.*

Let us analyse the hierarchy of perturbative equations outlined above in presence of a separation of scales. We focus on long/short spatial scales with $\lambda\!\!\!^{-} \ll L$, but the discussion is identical low/high frequencies. Considering the scalings

$$\partial \boldsymbol{\eta} \sim \mathcal{O}(1/L)\ , \quad \partial \boldsymbol{h}^{(1)} \sim \mathcal{O}(\epsilon^1/\lambda\!\!\!^{-})\ ;\ \partial^2 \boldsymbol{\eta} \sim \mathcal{O}(1/L^2)\ ,\ \partial^2 \boldsymbol{h}^{(1)} \sim \mathcal{O}(\epsilon^1/\lambda\!\!\!^{-2})\ , \tag{5.41}$$

The Ricci at different orders scale as

$$R^{(0)}_{\mu\nu} \sim \boldsymbol{\eta}\partial^2\eta \sim \mathcal{O}(1/L^2) \quad \text{Long wavelength (low freq.)} \tag{5.42}$$
$$R^{(1)}_{\mu\nu} \sim \boldsymbol{\eta}\partial^2 \boldsymbol{h}^{(1)} \sim \mathcal{O}(\epsilon/\lambda\!\!\!^{-2}) \quad \text{Short wavelength (high freq.)} \tag{5.43}$$
$$R^{(2)}_{\mu\nu} \sim \boldsymbol{\eta}\partial^2 \boldsymbol{h}^{(2)} + \boldsymbol{h}^{(1)}\partial^2 \boldsymbol{h}^{(1)} \sim \mathcal{O}(\epsilon^2/\lambda\!\!\!^{-2}) + \mathcal{O}(\epsilon^2/L^2) \quad \text{Long and short wavelengths}\,. \tag{5.44}$$

The second-order Ricci can contain both long and short wavelenghts contributions because the short wavelength combinations can result in a long wavelength mode if the two wavenumbers are comparable but have opposite signs, i.e. $h_{\alpha\beta}h_{\mu\nu} \sim e^{k_1 x}e^{-k_2 x} = e^{(k_1-k_2)x} \sim 1$ for $|k_1| \sim |k_2|$. Hence, the equations can be formally separated into a long/short parts:

$$R^{(1)}_{\mu\nu} = -\left[R^{(2)}_{\mu\nu}\right]^{\text{short}} + 8\pi\left[\bar{T}_{\mu\nu}\right]^{\text{short}} \tag{5.45a}$$
$$R^{(0)}_{\mu\nu} = -\left[R^{(2)}_{\mu\nu}\right]^{\text{long}} + 8\pi\left[\bar{T}_{\mu\nu}\right]^{\text{long}}\ , \tag{5.45b}$$

where the bar over the matter's SET $\boldsymbol{T}$ indicates the trace reverse. The short wave equation describes the propagation of the perturbation on the curved background. The long wavelengths equation describes the effet of GWs on the background curvature.

Let us comment on the validity of the above equations. The latter equate terms with different powers of ϵ. To be consistent, these powers must be compensated by the other expansion parameter $\lambda\!\!\!^{-}/L$. Interestingly, by requiring consistency we find a condition on the amplitude parameter ϵ that determines the validity of the approssimation. Consider first the long wavelength equation in vaccum $\bar{T}_{\mu\nu} = 0$ or equivalently in a situation where the curvature is

dominated by GW. The power counting gives

$$\frac{1}{L^2} \sim \epsilon^2 k^2 = \frac{\epsilon^2}{\lambda\!\!\!^{-2}} \quad \Rightarrow \quad \epsilon \sim \frac{\lambda\!\!\!^{-}}{L} \,. \tag{5.46}$$

In the opposite case, where the $\bar{T}_{\mu\nu}$ dominates over $R^{(2)}_{\mu\nu}$, one has

$$\frac{1}{L^2} \sim \epsilon^2 k^2 + (\text{matter}) \gg \epsilon^2 k^2 \quad \Rightarrow \quad \epsilon \ll \frac{\lambda\!\!\!^{-}}{L} \,. \tag{5.47}$$

In summary, the formalism is valid for small wave amplitudes up to the order for which the short/long wavelengths separation is valid, as shown in Fig. 5.2.

Remark 5.3.2. Breakdown of expansion on Mikowski and of scales separation. *Eq. (5.46) indicates that the metric expansion on Mikowski cannot be pushed beyond linear order. For flat spacetime $1/L = 0$ (stricly zero), and no GW of finite amplitude can exist. In other terms, the expansion in powers of ϵ has no domain of validity. More in general, Eq. (5.47) indicates that if the GW amplitude becomes too large, then the hypothesis of scale separation breaks and it is not possible to define wave-like perturbation on a background.*

Finally, we implement the scale separation and show that the term $-[R^{(2)}_{\mu\nu}]^{\text{long}} = 8\pi\tau_{\mu\nu}$ in the long-scales equation leads to a well-defined GW SET. Scale separation is computed by an *averaging operator* on lengths ℓ much larger than $\lambda\!\!\!^{-}$ and much smaller than L indicated as

$$\langle ... \rangle \text{ average on length scale } \ell \quad : \quad \lambda\!\!\!^{-} \ll \ell \ll L \,. \tag{5.48}$$

See Misner et al. (1973) 35.14 and the appendix of the Isaacson PhD thesis for more mathematical details on the averaging operator. The key consequence of the averaging procedure is that we can integrate by parts and discard surface terms because they are high order in $\lambda\!\!\!^{-}/L$. Far from the source, the integration by part can be performed also in time because the metric components are functions of the retarded time and

$$\int g(t-r)\partial_t f(t-r) = -\int g(t-r)\partial_x f(t-r) = \cancel{[...]} + \int \partial_x g(t-r) f(t-r) = -\int \partial_t g(t-r) f(t-r) \,. \tag{5.49}$$

The relevant averaging of the second order Ricci in the long-scale equation can be performed starting from Eq. (5.34) and specifying to (i) far from the matter source, (ii) harmonic gauge, and (iii) flat background. Most of the terms in Eq. (5.34) can be eliminated by integrating by parts and fixing the gauge; only the first two survive (first line) and combine to one term,

$$\left[2R^{(2)}_{\mu\nu}\right]^{\text{long}} := \langle 2R^{(2)}_{\mu\nu}\rangle = \langle \frac{1}{2}\partial_\mu h_{\alpha\beta}\partial_\nu h^{\alpha\beta}\rangle + \underbrace{\langle h^{\alpha\beta}\partial_\mu\partial_\nu h_{\alpha\beta}\rangle}_{=\langle \partial_\mu h_{\alpha\beta}\partial_\nu h^{\alpha\beta}\rangle} - 2\,\underbrace{\langle h^{\alpha\beta}\partial_\beta\partial_{(\mu}h_{\nu)\alpha}\rangle}_{=\langle \partial_\beta h^{\alpha\beta}\partial_{(\mu}h_{\nu)\alpha}\rangle = 0} + ... \tag{5.50}$$

The result is the *Isaacson tensor*, the effective SET for GWs:

$$\tau_{\mu\nu} := \frac{c^4}{32\pi G}\langle \partial_\mu h_{\alpha\beta}\partial_\nu h^{\alpha\beta}\rangle = \frac{c^4}{32\pi G}\langle \partial_\mu h^{\text{TT}}_{ij}\partial_\nu h^{\text{TT}\,ij}\rangle \tag{5.51}$$

Notably, this expression is gauge invariant because the integration by parts allows us to kill the terms introduced by an infinitesimal coordinate transformation. This implies also that the quantity depends ony onthe physical modes and we can specify to the TT gauge, as done in the second line. All the items on the list now check.

GW luminosity. Using the above formula, it is possible to compute the GW luminosity. The calculation employs the conservation law for $\tau_{\mu\nu}$,

$$0 = \int d^3x\,(\partial_0\tau^{00} + \partial_i\tau^{0i}) = \frac{1}{c}\dot{E} + \int d^3x\,\partial_i\tau^{0i} = \frac{1}{c}\dot{E} + \oint d^2y\, n_i\tau^{0i} = \frac{1}{c}\dot{E} + \frac{c^4r^2}{32\pi G}\oint d^2y\, n_r\tau^{0r} = \tag{5.52a}$$

$$= \frac{1}{c}\dot{E} + \frac{c^4r^2}{32\pi G}\oint d^2y\,\langle \partial^0 h_{ij}\partial_r h^{ij}\rangle = \frac{1}{c}\dot{E} + \frac{c^4r^2}{32\pi G}\oint d^2y\,\langle \partial_0 h_{ij}\partial_0 h^{ij}\rangle \,. \tag{5.52b}$$

The surface integrals are taken on a spherical surface of radius r and we exchanged spatial with time derivatives using the retarded time dependency $h(t-r/c)/r$, i.e. $\partial_r h(t-r/c) = -\partial_t h(t-r)/c = +\partial^t h(t-r)/c$ (or using the TT gauge condition $\tau^{0r} = \tau^{00}$). The GW luminosity is then given by changing sign to the first term to account for the emitted energy and introducing a factor c^2 from $x^0 = ct$,

$$\frac{dE}{dt} = \frac{c^3}{32\pi G} r^2 \int d\Omega \langle \partial_t h^{\rm TT}_{ij} \partial_t h^{{\rm TT}\ ij} \rangle = \frac{c^3}{16\pi G} \langle \dot{h}^2_+ + \dot{h}^2_\times \rangle = \frac{G}{5c^5} \langle \dddot{Q}_{ij} \dddot{Q}^{ij} \rangle . \tag{5.53}$$

The formulas above employ the quadrupole formulas; it it left as [exercise] to work out the integration of the Λ projector on the solid angle. It is sometimes useful to consider the power per unit solid angle, that is given by

$$\frac{dE}{dtd\Omega} = \frac{c^3}{32\pi G}\, r^2\, \langle \partial_t h^{\rm TT}_{ij} \partial_t h^{{\rm TT}\ ij} \rangle = \frac{c^5}{8\pi G} \langle \ddot{\dot{Q}}_{ij} \ddot{\dot{Q}}^{ij} \rangle \ . \tag{5.54}$$

Remark 5.3.3. The two faces of GW luminosity. *The dimension analysis of the luminosity formula starts from*

$$[Q] = aML^2 \ , \quad [\ddot{Q}] = aML^2T^{-3} \sim a\Omega^3 ML^2 \ , \quad [G/c^5] = TE^{-1} \ , \tag{5.55}$$

where a dimensionless factor a and an angular frequency Ω are introduced for later convenience. From the above one notices that the numerically small factor G/c^5 in front of the formula is the inverse of a power. If $\ddot{Q}$ has typical values of laboratory experiments, then the GW luminosity generated in these experiments is ridiculously small. However, Weber (an optimist) suggested to re-express the formula in terms of

$$c^5/G \sim 10^{52}\ W \tag{5.56}$$

which is an enormous luminosity factor. We use, as usual, R as the typical size of the sources, $\sigma = GM/c^2R$ as a measure of the source's self-gravity, $M = c^2R\sigma/G$ the mass of the source, $v = \Omega R$ the source's velocity. One gets

$$\dot{E} \sim \frac{G}{c^5} a^2\Omega^6 M^2 R^4 = a^2 \frac{G}{c^5} \left(\frac{v}{c}\right)^6 \left(\frac{c}{R}\right)^6 \frac{c^4R^2\sigma^2}{G^2} R^4 = a^2 \frac{c^5}{G} \left(\frac{v}{c}\right)^6 \sigma^2 = a^2 \frac{c^5}{G} \left(\frac{v}{c}\right)^6 \left(\frac{GM}{c^2R}\right) \ . \tag{5.57}$$

The last formula above shows that a source with strong self-gravity $\sigma \sim 1$ and high-velocity $v \sim c$ can generate GWs corresponding to the most luminous radiation in the Universe.

Example 5.3.2. Binary stars system in circular orbit. *The scaling formula $\dot{E} \sim \frac{G}{c^5} a^2\Omega^6 M^2 R^4$ gives the exact formula for the power emitted by a binary in circular orbit if one takes*

$$a = \frac{32}{5} \ , \quad \Omega \ : \ \textit{Orbital frequency} \ , \quad M \mapsto \mu \ : \ \textit{reduced mass} \ , \quad R \ : \ \textit{Orbital radius} \ . \tag{5.58}$$

The derivation follows from the previously derived waveform formula for binaries and the general expression of the power; it is left as [exercise]. The total power is

$$\dot{E} = \frac{32}{5} \frac{G\mu^2}{c^5} R^4\Omega^3 = \frac{1}{10} \frac{G\mu^2}{c^5} \Omega^6 \tag{5.59}$$

and by averaging over one orbit $\langle \dot{E} \rangle = 64/5 G\mu^2/R(v/c)^5$. The total power per unit solid angle is given by

$$\frac{E}{dtd\Omega} = \frac{24\mu^2R^4\Omega^6}{\pi c^5} g(\theta) \ , \quad g(\theta) = \left(\frac{1+\cos^2\theta}{2}\right)^2 + \cos^2\theta \ . \tag{5.60}$$

It is interesting to note that the emission is never zero for any angle of view of the source.

Example 5.3.3. *How does the emission of radiation influence the motion of the binary? A simple argument for the* inspiral motion*. Using Kepler's law to remove the radius dependence, the GW power is*

$$P = \dot{E}_{\rm GW} = \frac{32G}{5c^5} \mu^2 m^{3/4} \Omega^{10/3} \sim \Omega^{10/3} \ , \tag{5.61}$$

where the last line single out the frequency dependency specifying to equal masses $m_1 = m_2 = m/2$. Compare to the orbital energy

$$E = \frac{1}{2}\mu(\Omega R)^2 - \frac{m\mu}{R} = -\frac{1}{2}\frac{\mu m}{2R} \sim -\Omega^{2/3} \ , \tag{5.62}$$

where again one uses Kepler's law specifying to equal masses. The formula above indicates that if E becomes more negative due to the emission of GW, then the radius becomes smaller and the orbital frequency increases. In presence of radiation a circular orbit does not remain circular. The orbit is actually an accelerating inspiral during which the larger is the amount of radiation emitted, the larger the binary accelerates. The stars gets closer to each other and more relativistic as they radiate GW. This is the basic mechanism at the origin of the period decay of the Hulse& Taylor pulsar. The motion can only terminate with the collision of the stars and the merger *of the two. GW150914 is a signal generated by the merger of two black holes.*

Let us derive a simple equation describing the frequency evolution during the inspiral motion. Starting from $E \propto \Omega^{2/3}$*, take the log and derive both sides*

$$\frac{d}{dt}\ln E = \frac{d}{dt}\ln \Omega^{2/3} \quad \Rightarrow \quad \frac{2}{3}\frac{\dot\Omega}{\Omega} = \frac{\dot E}{E} = \frac{P}{E} \quad \Rightarrow \quad \dot\Omega = \frac{3}{2}\Omega\frac{\dot E}{E} = \frac{3}{2}\Omega\frac{P}{E} \sim \Omega^{11/3} \ . \tag{5.63}$$

Because the energy subtracted to the motion is the one radiated, we have used the energy balance $\dot E = P$*. If we had kept all the factors in equations, we would have obtained for the GW frequency the expression [exercise]*

$$-P = \dot E = \frac{dE}{d\Omega}\Omega \quad \Rightarrow \quad \frac{\dot\omega}{\omega^2} = \frac{96}{5}\left(\frac{1}{2}\frac{G\mathcal{M}_c}{c^3}\omega\right)^{5/3} = \frac{96}{5}\nu\left(\frac{1}{2}\frac{Gm}{c^3}\omega\right)^{5/3} \ . \tag{5.64}$$

The second expression is obtained using $\mathcal{M}_c = m\nu^{3/5}$*. Note that in both sides of the equation the frequency can be substitute with the mass-rescaled quantities* $\hat\omega := m\omega$ *(the derivative is then understood as taken with* $\hat t := t/M$*.) As anticipated in Chap. 3, the GW frequency (thus the phase) scales trivially with the binary mass and they key quantity is thus the mass ratio. The l.h.s. of Eq. (5.64) is an important quantity called* adiabaticity parameter*,*

$$Q_\omega^{-1} := \frac{\dot\omega}{\omega^2} = -3\frac{\dot R}{R\Omega} \ . \tag{5.65}$$

If $Q_\omega^{-1} \ll 1$ *(*$Q_\omega \gg 1$*), the radial velocity is much smaller than the tangential velocity, and the motion can be well approximated by an (adiabatic) sequence of circular orbits. It is trivial to manipulate Eq. (5.64) and express the chirp mass* $\mathcal{M}_c$ *in terms of the GW frequency* $f = \omega/2\pi$ *and its derivatives,*

$$\mathcal{M}_c = \frac{c^3}{G}\left(\left(\frac{5}{96}\right)^3 \pi^{-8} f^{-11}\dot f^3\right)^{1/5} \ . \tag{5.66}$$

Moreover, Eq. (5.64) can be integrated to obtain an explitic expression of the frequency evolution as a function of time [exercise]. The chirp signal observed in GW170817 is show in Fig. 5.3.

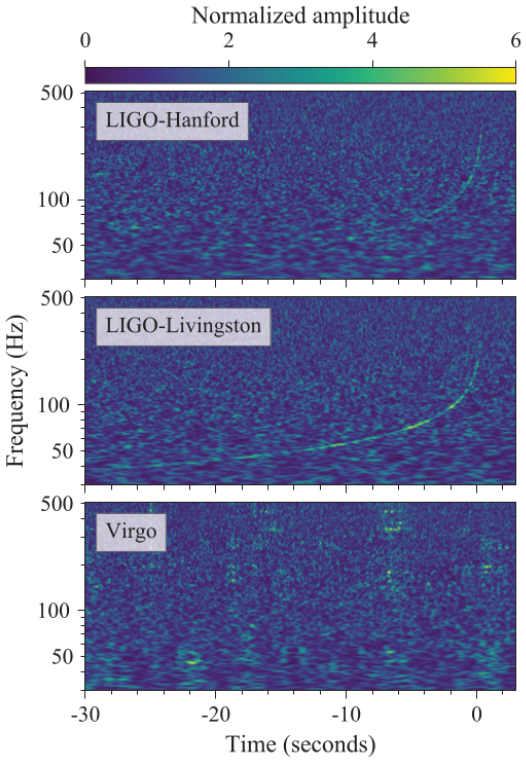

Figure 5.3: Observation of GW170817. The spectrogram in LIGO-L clearly indicates that the GW frequency and amplitude monotonically increase in time.

6. Post-Newtonian formalism

Post-Newtonian formalism for self-gravitating sources. Relaxed EFE, 1PN metric, basic ideas behind the systematic expansion, basic results for the two-body problem and waveform approximants.

Suggested readings. *Chap. 4 of Maggiore (2007); Damour (1983, 1987); Damour and Deruelle (1986); Futamase and Itoh (2007); Blanchet (2014); Schaefer and Jaranowski (2018).*

6.1 GWs from gravitating sources

The definition of gravitational waves we gave within linearized gravity applies to non-gravitating sources. The spacetime's curvature in the region of the source (*near region*) must be always zero for that formalism to hold. This implies a clear separation between the source's velocity and the background's curvature: while the quadrupole formula can contain an arbitrary number of terms as an expansion in v/c, the background must remain the flat metric $\boldsymbol{\eta}$. Nonetheless, the quadrupole formula clearly indicates that self-gravitating (compact) and fast moving sources are the most likely sources of GWs. For a source of mass M, extension R, velocity v at a distance D from the detectors, we found the scaling relation

$$h \sim \left(\frac{R}{D}\right)\left(\frac{GM}{c^2 R}\right)\left(\frac{v}{c}\right)^2 . \tag{6.1}$$

The *post-Newtonian (PN) formalism* extends the GW theory to weakly self-gravitating systems with small velocities (and stresses, "internal velocities"). For a self-gravitating source, the gravitational field and the source's velocity are not anymore independent because the latter is related to the gravitational potential by the virial theorem

$$\left(\frac{v}{c}\right)^2 \sim \frac{2GM}{c^2 R} = \frac{R_S}{R} . \tag{6.2}$$

The basic idea of the PN formalism is to consider solutions of the EFE in an expansion in $\epsilon = v/c$. The weakly-gravitating and slowly-moving source is assumed described by a smooth stress-energy tensor with compact support in $r < R$ such that

$$\epsilon = \sup\left[\left(\frac{GM}{c^2 R}\right)^{1/2}, \left|\frac{T^{0i}}{T^{00}}\right|, \left|\frac{T^{ij}}{T^{00}}\right|^{1/2}\right] \ll 1 . \tag{6.3}$$

This formalism is the main building block to compute the GWs emitted by compact binaries, i.e. binary systems composed by black holes and neutron stars. Note there is no guarantee the PN formalism can be pushed at arbitrary high-order in ϵ.

A naive approach to the problem would be to compute $\mathcal{O}(\epsilon^n)$ corrections to the equations of motion and then calculate the radiation via the multipolar expansion (that is an expansion in ϵ.) However, this is not possible because

- Gravitational-wave emission subtract energy from the motion;
- Gravitational waves at a given PN order are sources of GWs at higher order.

The PN formalism is significantly more involved than analogous perturbative expansion of linear field theories.

The PN formalism was started by Einstein, Landau & Lifshitz, Droste, de Sitter and others. Notable early results are the Einstein-Infeld-Hoffmann 1PN Lagrangian for N bodies, and the applications to the binary pulsar PSR 1913+16 (Damour and Taylor, 1991; Damour and Taylor, 1992; Weisberg et al., 2010). A systematic approach to the problem was however obtained only in the the 90s by Blanchet & Damour and Will & Wiseman. The formalism prescribes how to compute consistently arbitrary corrections to dynamics and radiation by matching the PN expansion in the near region to exterior (far zone) solutions. The starting point of the formulation is the Landau and Lifshitz formulation of EFE in harmonic gauge Landau and Lifschits (1975), also known as *relaxed Einstein field equations*

Note that we here adopt the convention of calling call $\frac{n}{2}$PN terms corrections of order $\mathcal{O}(\epsilon^n) \sim \mathcal{O}(1/c^n)$. This is used in many modern references but not all of them.

6.2 Relaxed EFE

Define the field

$$\mathsf{h}^{\mu\nu} := \mathfrak{g}^{\mu\nu} - \eta^{\mu\nu} = \sqrt{-g}g^{\mu\nu} - \eta^{\mu\nu} \tag{6.4}$$

to be considered in place of the metric in the full theory (no approximation; $\mathsf{h}^{\mu\nu}$ is not small in general). The connection to the linearized gravity is obtained considering

$$g_{\mu\nu} = \eta_{\mu\nu} + h_{\mu\nu} + \mathcal{O}(2)\ , \quad -g = 1 + h\ , \quad g^{\mu\nu} = \eta^{\mu\nu} - h^{\mu\nu}\ , \tag{6.5}$$

and inserting these expression in h:

$$-\mathsf{h}^{\mu\nu} \simeq \eta^{\mu\nu} - (1+h)^{1/2}(\eta^{\mu\nu} - h^{\mu\nu}) = h^{\mu\nu} - \frac{1}{2}\eta^{\mu\nu}h = \bar{h}^{\mu\nu}\ . \tag{6.6}$$

The field h reduces to minus the trace-reversed linear perturbation in the weak field limit.

The harmonic gauge in terms of the gothic metric is

$$0 = \partial_\mu \mathfrak{g}^{\mu\nu} = \partial_\mu \mathsf{h}^{\mu\nu} \quad \text{(Harmonic gauge)}\,. \tag{6.7}$$

In this gauge, and using the field $\mathsf{h}^{\mu\nu}$ the exact EFF read

$$\boxed{\Box \mathsf{h}^{\mu\nu} = \frac{16\pi G}{c^4}\tau^{\mu\nu} = \frac{16\pi G}{c^4}(-g)\left(T^{\mu\nu} + t^{\mu\nu}_{\rm LL} + t^{\mu\nu}_{\rm H}\right) \quad \text{(REFE)}\ ,} \tag{6.8}$$

where

$$T^{\mu\nu} \quad \text{(stress energy tensor)} \tag{6.9a}$$

$$t^{\mu\nu}_{\rm LL}[\mathsf{h}^{\mu\nu}, \partial\mathsf{h}^{\mu\nu}] \quad \text{(Landau-Lifshiz energy-momentum psedotensor)} \tag{6.9b}$$

$$(-g)t^{\mu\nu}_{\rm H} = \frac{c^4}{16\pi G}(\partial_\alpha \mathsf{h}^{\beta\mu}\partial_\beta \mathsf{h}^{\alpha\nu} - \mathsf{h}^{\alpha\beta}\partial_\alpha\partial_\beta \mathsf{h}^{\mu\nu}) \tag{6.9c}$$

Eq. (6.8) and Eq. (6.7) are equivalent to EFE and are written in terms of partial derivatives instead of covariant. It is immediate to verify that the harmonic gauge condition implies

$$\partial_\mu\left((-g)t^{\mu\nu}_{\rm H}\right) = 0\,, \tag{6.10}$$

and also the local conservation law

$$\partial_\mu \underbrace{\left[(-g)\left(T^{\mu\nu} + t^{\mu\nu}_{\rm LL} + t^{\mu\nu}_{\rm H}\right)\right]}_{=:\tau^{\mu\nu}} = \partial_\mu \tau^{\mu\nu} = 0\,. \tag{6.11}$$

The equation above simply follows from the fact that the flat wave operator in Eq. (6.8) commutes with the partial derivatives. The formal solution of Eq. (6.8) can be immediately written down in therms of the retarded Green function (exactly as in the linearized theory or in electromagnetism):

$$\boxed{\mathsf{h}^{\mu\nu} = \mathsf{h}^{\mu\nu}_{\rm hom} - \frac{4G}{c^2}\int d^3x' \frac{\tau^{\mu\nu}(t - |x-x'|/c, x')}{|x-x'|}\ .} \tag{6.12}$$

Differently from the linearized theory, now $\tau^{\mu\nu}$ contains the field $\mathsf{h}^{\mu\nu}$ and the formula above cannot be employed to directly compute the solution. Note we included the homogeneous solution of the flat wave equation, $\mathsf{h}^{\mu\nu}_{\rm hom}$. A possible approach is then to obtain a solution by iteration: a starting approximation for $\mathsf{h}^{\mu\nu}$ can be plugged into $\tau^{\mu\nu}$ and used in the r.h.s. of Eq. (6.12) to compute a new approximation for $\mathsf{h}^{\mu\nu}$. Note that a solution of Eq. (6.12) alone, i.e. obtained by specifying a r.h.s., is not necessarily a solution of EFE because it does not satisfy the gauge condition Eq. (6.7). This justifies the name *relaxed* EFE. A possible procedure for the solution is to first solve the REFE and then specify the gauge. This guarantees that the matter source obeys the correct EOM in the computed metric because the harmonic gauge is equivalent to Eq. (6.11).

The homogeneous solution of the wave equation given smooth initial data can be expressed via the Kirchoff's formula,

$$\mathsf{h}^{\mu\nu}_{\rm hom} = \frac{1}{4\pi}\oint d\Omega\ \left[\partial_r\left(r\mathsf{h}^{\mu\nu}_{\rm hom}\right) + \partial_t\left(r\mathsf{h}^{\mu\nu}_{\rm hom}\right)\right]\ , \tag{6.13}$$

where the integration is performed on the boundary of the past light cone. This solution is usually discarded (at low PN orders) because the requirement of no incoming radiation into the domain of dependence corresponds to setting to zero the integrand (for $r \to \infty$ and keeping $u = const$).

Post-Minkowskian iteration. A possible way to solve the REFE is to postulate a *post-Minkowskian (PM) expansion* in the gravitational constant G,

$$\mathsf{h}^{\mu\nu} = G\,\mathsf{h}^{\mu\nu}_{(1)} + G^2\,\mathsf{h}^{\mu\nu}_{(2)} + \mathcal{O}(G^3)\,, \tag{6.14}$$

and look for an iterative solution order by order in G. This approach is naturally adapted for spacetimes that do not deviate too much from Minkowski spacetime. Hence, it can be considered to obtain an expansion of the metric in the asymptotic wave zone far from the source. The starting point of the expansion is the flat metric, so the first approximation $\mathsf{h}^{\mu\nu}_{(1)}$ is determined by solving Eq. (6.12) with $\tau^{\mu\nu} = T^{\mu\nu}[\boldsymbol{\eta}]$ in the r.h.s. This is the usual linearized solution that can be expressed as a multipolar STF series discussed in Chap. 4. The second correction $\mathsf{h}^{\mu\nu}_{(2)}$ is determined by solving Eq. (6.12) with $\tau^{\mu\nu}$ calculated from $t^{\mu\nu}_{\rm LL}[\mathsf{h}^{\mu\nu}_{(1)}]$ and $T^{\mu\nu}[\boldsymbol{g}]$ with $\boldsymbol{g} = \boldsymbol{\eta} + \mathcal{O}(G)$. At the end of the required iterations, the harmonic gauge must be imposed.

6.3 Post-Newtonian expansion

Another possible iterative approach to solve the REFE is to postulate a *post-Newtonian (PN) expansion*,

$$\mathsf{h}^{\mu\nu} = \epsilon^1\,{}_{(1)}\mathsf{h}^{\mu\nu} + \epsilon^2\,{}_{(2)}\mathsf{h}^{\mu\nu} + \mathcal{O}(\epsilon^3)\,. \tag{6.15}$$

A direct comparison with the weak field metric in Eq. (2.24) and Eq. (2.33) reveals that the Newtonian order (0PN) is given by

$$\mathsf{h}^{00} = -\frac{2\phi}{c^2} + \mathcal{O}(\epsilon^4) \tag{6.16a}$$

$$\mathsf{h}^{0i} = \mathcal{O}(\epsilon^3) \tag{6.16b}$$

$$\mathsf{h}^{ij} = \mathcal{O}(\epsilon^4)\,. \tag{6.16c}$$

These are the lowest possible terms in the PN perturbation. Proceeding to the first iteration, these terms should be used to compute the r.h.s. of Eq. (6.12) to obtain the 1PN equations

$$\Box\mathsf{h}^{00} = \frac{16\pi G}{c^4}\left(1+\frac{4V}{c^2}\right)T^{00} - \frac{14}{c^2}\partial_k V\partial^k V + \mathcal{O}(\epsilon^6) \tag{6.17a}$$

$$\Box\mathsf{h}^{0i} = \frac{16\pi G}{c^4}T^{0i} + \mathcal{O}(\epsilon^5) \tag{6.17b}$$

$$\Box\mathsf{h}^{ij} = \frac{16\pi G}{c^4}T^{ij} + \frac{4}{c^4}\left(\partial^i V\partial^j V - \frac{1}{2}\delta^{ij}\partial_k V\partial^k V\right) + \mathcal{O}(\epsilon^6)\,, \tag{6.17c}$$

where we introduced a common PN notation $V = -\phi/c^2$ (at this order) and highlighted the correct order of the approximation without justification (see below). The 1PN equations now contains new but known metric terms at the r.h.s. and could be in principle solved in terms of a multipolar STF series discussed in Chap. 4. Clearly, these multipoles are different multipoles from those of the PM expansion considered above.

1PN metric. Before considering a systematic iterative solution of the REFE in the PN formalism, we discuss a simpler calculation for the 1PN metric that highlights some important points. At Newtonian order the weak and static metric is Eq. (2.24), i.e.

$$g_{00} = -1 + 2\frac{U}{c^2}\,,\quad g_{0i} = 0\,,\quad g_{ij} = \delta_{ij}\,. \tag{6.18}$$

where the static potential U is minus the Newtonian potential, i.e. the solution of the Poisson equation

$$U = \frac{G}{c^2}\int d^3y\,\frac{T^{00}(y)}{|x-y|}\,. \tag{6.19}$$

As anticipated above without explanation, at a given a PN order, different metric coefficients must be expanded up to different powers of ϵ in order for EFE to be fullfilled at that given order. This can be understood by the following argument. The stress-energy tensor component scale as

$$\left|\frac{T^{0i}}{T^{00}}\right| = \mathcal{O}(\epsilon)\,,\quad \left|\frac{T^{ij}}{T^{00}}\right| = \mathcal{O}(\epsilon^2)\,, \tag{6.20}$$

as we have assumed and as expected by common matter models, e.g. a perfect fluid or point particles. Consequently, using EFE $G_{\mu\nu} \sim \Box g_{\mu\nu} \simeq GT_{\mu\nu}/c^4$, one sees that if $g_{00} = \mathcal{O}(\epsilon^n)$ then the contribution to the same order of the other metric components must be $g_{0i} = \mathcal{O}(\epsilon^{n+1})$ and $g_{ij} = \mathcal{O}(\epsilon^{n+2})$.

We further assume that at this order we can neglect backreaction of the GWs. This assumption turns out to be correct. Without radiation reaction, the metric must be symmetric under time reversal (Chandrasekhar and Esposito,

1970). For $t \mapsto -t$ ($v \mapsto -v$), the metric coefficient g_{00}, g_{ij} are even while the metric coefficients g_{0i} are odd. Hence, g_{00}, g_{ij} must contain even powers of v, while g_{0i} must contain odd powers. Indeed, complete calculations show that that if terms with the "wrong" parity under time reversal are included, then these terms satisfy homogenous wave equations and can be gauged away. We conclude that the power counting in the PN metric (in absence of backreaction) must be of type

Component	0PN	1PN	2PN	
g_{00}	$-1+g_{00}^{(2)}$	$g_{00}^{(4)}$	$g_{00}^{(6)}$	...
g_{0i}		$g_{0i}^{(3)}$	$g_{0i}^{(5)}$	...
g_{ij}	δ_{ij}	$g_{ij}^{(2)}$	$g_{ij}^{(4)}$	...

where $g_{\mu\nu}^{(n)}$ indicates the metric components at order $\mathcal{O}(\epsilon^n)$.

Following Blanchet and Damour (1989), the 1PN metric can be computed starting from the full EFE in harmonic gauge and by simplifying the quadratic nonlinear terms using the Newtonian values

$$g_{00}+1=\mathcal{O}(\epsilon^2)\ ,\quad g_{0i}=\mathcal{O}(\epsilon^3)\ ,\quad g_{ij}-(g_{00}+2)\delta_{ij}=\mathcal{O}(\epsilon^4)\,, \tag{6.21}$$

and the fact that time derivatives are half-PN order larger than spatial derivatives,

$$\partial_0 g_{\mu\nu}=\mathcal{O}(\epsilon)\partial_i g_{\mu\nu}\,. \tag{6.22}$$

This implies that only the quadratic terms of the g_{00} component needs to be considered. The latter can be re-absorbed by introducing a logarithmic variable $\ln g_{00}$ to obtain linear equations for the 1PN order:

$$\Box \ln g_{00}=\frac{8\pi G}{c^4}\left(T^{00}+T^k_k\right)+\mathcal{O}(\epsilon^6) \tag{6.23}$$

$$\Box g_{0i}=\frac{16\pi G}{c^4}T^{0i}+\mathcal{O}(\epsilon^5) \tag{6.24}$$

$$\Box g_{ij}=-\frac{16\pi G}{c^4}\left(T^{00}+T^k_k\right)+\mathcal{O}(\epsilon^4)\,. \tag{6.25}$$

These equations can be directly solved in terms of retarded integrals since the source is compact. It is useful to define

$$\sigma:=\left(T^{00}+T^k_k\right)/c^2 \quad \text{active gravitational mass density} \tag{6.26}$$

$$\sigma_i:=T^{0i}/c \qquad \text{active gravitational current density}\,, \tag{6.27}$$

such that the 1PN can be expressed in terms of the two retarded potentials

$$V:=G\int d^3y\,\frac{\sigma(u,y)}{|x-y|} \tag{6.28}$$

$$V_i:=G\int d^3y\,\frac{\sigma_i(u,y)}{|x-y|}\,. \tag{6.29}$$

The metric is

$$g_{00}=-e^{-2V/c^2}+\mathcal{O}(\epsilon^6)=-1+\frac{2V}{c^2}-\frac{2V^2}{c^4}+\mathcal{O}(\epsilon^6) \tag{6.30a}$$

$$g_{0i}=-\frac{4V_i}{c^3}+\mathcal{O}(\epsilon^5) \tag{6.30b}$$

$$g_{ij}=\delta_{ij}(1+\frac{2V}{c^2})+\mathcal{O}(\epsilon^4)\,. \tag{6.30c}$$

This is the same metric one would obtain solving the 1PN REFE for $\mathsf{h}^{\mu\nu}$, except that iterating the REFE give h^{ij} up to $\mathcal{O}(\epsilon^6)$.

Remark 6.3.1. *Futamase and Schutz (1983) proposed a definition of the PN expansion based on GR's initial value problem. In this approach one considers a sequence of GR solutions such that the initial data satisfy the Newtonian scalings*

$$T^{00}\sim\rho\sim\mathcal{O}(\epsilon^2)\ ,\quad T^{0i}\sim v^i\sim\mathcal{O}(\epsilon^3)\ ,\quad T^{ij}\sim P\sim\mathcal{O}(\epsilon^4)\ ,\quad g^{00}\sim\phi\sim\mathcal{O}(\epsilon^2)\,. \tag{6.31}$$

This scaling can be found from Euler equations and Newton gravitational law, $\Delta\phi\sim\rho$. The solutions in the sequence are identified and mapped one into the other using the same spatial coordinates and the Newtonian time $\tau:=\epsilon t$. This parameter encodes the fact that the weaker gravity is, the longer the system's timescale becomes. The terms of the PN expansion are defined as the relativistic terms of the Taylor series in ϵ along the sequence of solutions. This approach clarifies some conceptual and mathematical features for the PN formalism. First, the PN limit involves both weak gravity and slow motion: the motion must remain slow as gravity weakens. It should be also clear that there is no

Newtonian limit in vacuum since the spacetime must be Minkowski for $\epsilon \to 0$. Second, the PN limit must be singular because GR's hyperbolic equations turn into elliptic equations as $c \to \infty$. Also, the singular limit cannot be uniform for all times because any weak gravity system will eventually develop strong gravity at sufficiently long times due to nonlinearities of EFE (This is the reason why one requires the Newtonian scaling for the initial data rather than for the solutions). Third, standard Taylor theorem guaranteed that the PN expansion (defined along the sequences) about $\epsilon \approx 0$ is an asymptotic expansion [1]*. Finally, it is easy to understand why the PN expansion, defined in this way, is composed of regular terms. The key feature is that the retarded integrals in (τ, y^i) coordinates have domain of dependence the past light cone $C = \{(\tau, \vec{y}) : 0 \leq |\vec{x} - \vec{y}| \leq c\tau/\epsilon\}$. The fact that the domain C is finite and increases as $1/\epsilon$ for $\epsilon \to 0$ is crucial to prevent divergences and highlights that retardation effects must be always taken into account. To see this, consider the integral of a function of the retarded time $u = \tau - \epsilon r$ and Taylor expand about $u \sim \tau$,*

$$\int dr\, f(\tau - \epsilon r) \simeq \int dr\, f(\tau) - \epsilon \int dr\, r\, \dot{f}(\tau) + \dots . \tag{6.32}$$

This expansion is essentially equivalent to Eq. (6.22) and it is justified by the slow motion assumption. The second term is usually dropped since it is higher order... however, the dropping is not generically possible because $r \to 1/\epsilon$ for $\epsilon \to 0$ and the term $\epsilon r \dot{f} \sim \dot{f}$ is not uniformly small. The second term might be discarded only when $\dot{f}$ falls off sufficiently rapidly; this happens at low PN order, but at higher order divergences of type $\epsilon^n \ln \infty$ appear. However, such divergences might be eliminated by considering that in (τ, y^i) coordinates the upper bound of the integral behaves as $1/\epsilon$, and thus one would get $\sim \epsilon^n \ln \epsilon$. This suggests that the PN expansion can involve logarithms and might not be differentiable in ϵ for $\epsilon = 0$ but also that divergences might be removed.

6.4 Einstein-Infeld-Hoffmann Lagrangian

Combining the 1PN metric with the stress-energy tensor for N particles leads to *Einstein-Infeld-Hoffmann Lagrangian*, which is briefly presented without derivation.

The first step is to take the stress-energy tensor for a system of N particles

$$T^{\mu\nu} = \frac{1}{\sqrt{-g}} \sum_{a=1}^{N} m_a \frac{d\tau_a}{dt} \frac{dx_a^\mu}{dt} \frac{dx_a^\nu}{dt} \delta^{(3)}(x^i - x_a^i) \ , \tag{6.33}$$

and to compute the contributions $T^{00}_{(0)}$, $T^{00}_{(2)}$, $T^{ij}_{(2)}$, $T^{0i}_{(1)}$ summing up all the particles except one, say $a = b$. From the latter quantities one obtains the metric generated on particle b by all the other particles. The Lagrangian for particle b is then derived from the action associated to this metric,

$$S = -mc^2 \int dt \sqrt{-g_{00} - 2g_{0i}\frac{v^i}{c} - g_{ij}\frac{v^i v^j}{c^2}} \ . \tag{6.34}$$

The result is expressed as $L = L_0 + L_1/c^2$ where

$$L_0 = \sum_{a=1}^{N} \frac{1}{2} m_a v_a^2 + \sum_{a \neq b} \frac{G m_a m_b}{2 r_{ab}} \tag{6.35a}$$

$$L_1 = \sum_{a=1}^{N} \frac{1}{8} m_a v_a^4 - \sum_{a \neq b} \frac{G m_a m_b}{4 r_{ab}} (7 v_a^i v_b^i + \frac{(r_{ab}^j v_a^j)(r_{ab}^j v_b^j)}{r^2}) + \frac{3G}{2} \sum_a \sum_{b \neq a} \frac{m_a m_b v_a^2}{r_{ab}} - \frac{G^2}{2} \sum_a \sum_{b \neq a} \sum_{c \neq a} \frac{m_a m_b m_c}{r_{ab} r_{ac}} \ . \tag{6.35b}$$

Example 6.4.1. 1PN EOM and the PSR B1913+16 mass. *The 1PN EOM for a binary system were solved by Damour and Deruelle (1986) and were key to obtain the timing formulas for PSR B1913+16. Since the action is invariant under time translations and rotation, there exists two first integrals of the EOM representing the energy and the angular momentum. In the center of mass frame* [2] *the energy and angular momentum per reduced mass $\mu = m_1 m_2/m$ are*

$$\frac{E}{\mu} = \frac{1}{2} v^2 - \frac{Gm}{r} + \frac{3}{8}(1 - 3\nu)\frac{v^4}{c} + \frac{Gm}{2c^2 r}[(3 + \nu)v^2 + \nu \frac{(r^i v_i)}{r} + \frac{Gm}{r}] \tag{6.36a}$$

$$\frac{J^i}{\mu} = [1 + \frac{1}{2}(1 - 3\nu\frac{v^2}{c^2} + (3 + \nu)\frac{Gm}{c^2 r}]\epsilon_{ijk} r^j v^k \ , \tag{6.36b}$$

where $\nu = \mu/m$ is the symmetric mass ratio. *The radial and azimutal angle EOM can be recast to equations formally identical to the Newtonian equations by redefining parameters and coordinates. Thus, they can be solved analytically and the motion is defined by the usual Keplerian orbit parameters plus an additional set of post-Keplerian parameters.*

[1] Some assumptions on the smoothness in ϵ and the existance of some limites are needed, see (Futamase and Schutz, 1983) for details.
[2] Actually it is a center of energy, and differs from the Newtonian definition.

One finds that the periastron advance is a function of $1/r$; the derivative of its angular position ω averaged over one orbit is predicted to be

$$\langle \dot{\omega} \rangle = 2.11353 \left(\frac{m_1 + m_2}{M_\odot} \right)^{2/3} \ deg/yr \ . \tag{6.37}$$

Because $\langle \dot{\omega} \rangle$ can be measured from the pulsar data, the comparison with the theory gives the binary mass.

6.5 Radiation reaction

The backreaction on the matter due to the emission of GWs needs to be taken into account at sufficiently high PN order. At this order, the invariance under time-reversal is broken and the power couting done above for the 1PN metric.

A way to estimate the PN order at which backreaction enters the expansion is to use the energy balance equation and equating the power lost by a source of energy E to the GW power as calculated in linearized theory. We find

$$E = K + V \simeq -\frac{1}{2}V + V = \frac{1}{2}V = -K = -\frac{1}{2}Mv^2 \quad \Rightarrow \quad \dot{E} = -Mv\dot{v} \tag{6.38a}$$

$$P = \dot{E}_{\rm GW} \simeq \frac{GM^2}{c^5}\frac{v^6}{r} \, , \tag{6.38b}$$

where the first line uses the virial theorem. Thus

$$\dot{E} = P = \dot{E}_{\rm GW} \quad \Rightarrow \quad \dot{v} \simeq \frac{GM}{r^2}\left(\frac{v}{c}\right)^5 \tag{6.38c}$$

indicating the radiation backreaction enters at ϵ^5, i.e. at 2.5PN. This estimate is correct, and the quadrupole formula does give the correct leading order result. Note that in a nonlinear theory is not guaranteed that the energy balance holds.

Example 6.5.1. *Backreaction is present also in electromagnetism. The dynamics of a N charges produces electromagnetic waves propagating to infinity. The energy propagated with the waves is draned by the motion of the charges that must experience a radiation reaction force. Let us show that the work of the radiation reaction force corresponds to the radiated power by the ensamble of charges. The electromagnetic Lagrangian for charge q_a with mass m_a is*

$$L_a = -m_a c^2 \sqrt{1 - \frac{v_a^2}{c^2}} - q_a \phi + \frac{q_a}{c} v_a^i A_i \ , \tag{6.39}$$

where the potential $A_\mu = (\phi, A_i)$ is generated by the current $J_\mu = (\rho, J_i)$ produced by all the charges and calculated along the particle a trajectory. To solve for the motion one can proceed with a near-zone–v/c expansion. The potentials can be computed via a multipolar near-zone expansion

$$\phi = \Box^{-1}[\rho] \simeq \frac{1}{r}\int d^3x' \, \rho(x') + \frac{n_i}{cr^2}\frac{d}{dt}\int d^3x' \, \rho(u, x') x'^i + ... = \sum_a \frac{q_a}{r} + ... \tag{6.40a}$$

$$A_i = \Box^{-1}[J_i] \simeq \frac{1}{cr}\int d^3x' \, J_i(u, x') + ... = -\frac{1}{cr}\sum_a q_a x_a^i + ... \tag{6.40b}$$

The Lagrangian can be expanded in v/c and one finds that: (i) the term linear in v/c vanishes because charge conservation; (ii) the Lagrangian depends only on positions and velocities up to $(v/c)^2$ (is conservative), and (iii) at $(v/c)^3$ the dipole of the charge distribution $d^i = \sum_a q_a x_a^i$ generates an electric field $E^i = 2/(3c^2)\dddot{d}^i$ that in turn exerts a Lorentz force $F^i = q_a E^i$ on the point mass a. The total work performed on all the charges is

$$W = \sum_a F_a^i v_{a\,i} = \frac{2}{3c^3}\sum_a q_a v_a^i \dddot{d}_i \ . \tag{6.41}$$

Taking the time-average power one verifies that the average work equals the total radiated power

$$\bar{W} = -\frac{2}{3c^3}\langle \ddot{d}^i \rangle \ . \tag{6.42}$$

□ *[TODO: Expand on calculations (Maggiore P.275; LandauLifshitz 65-75)]*

6.6 Systematic PN expansion

Going to higher PN orders turn out to be significantly complex due to presence of new source terms from the GW SET. These terms are a consequence of nonlinearities of EFE and require a careful mathematical treatement of the

retarded solutions. A difficulty is that the higher-order source terms have non compact support. This is immediately evident from the last equation of Eq. (6.17), whose formal solution involves the integration over the field V. In the specific case, it is possible to check the integral is convergent due to the fall-off of V at large radii, but higher order iterations introduce divergences. The key issue is that the PN expansion is valid only in the near zone of the source and cannot be applied far away. The PN formalism utilizes different approximate solution of the REFE in different zones and combines them to obtain a valid solution to a given order in ϵ.

PN: a near zone expansion. A key step in the above 1PN metric derivation is the assumption in Eq. (6.22). The equation implies that retardation effects are "small" in the PN expansion and can be discarded as higher-order terms. The PN expansion of a function is an expansion of type

$$F(u) = F(t - r/c) = F(t) - \frac{r}{c}\dot{F}(t) + \frac{1}{2}\frac{r^2}{c^2}\ddot{F}(t) + \dots , \tag{6.43}$$

where each time derivatives carries (in the Fourier space) a factor proportional to the characteristic frequency of variation $\omega = c/\lambda\!\!\!^{-}$,

$$\mathcal{F}[F(t - r/c)] = \tilde{F}(\omega)\left(1 - \frac{r\omega}{c} + \frac{1}{2}\frac{r^2\omega^2}{c^2} + \dots\right) = \tilde{F}(\omega)\left(1 - \frac{r}{\lambda\!\!\!^{-}} + \frac{1}{2}\frac{r^2}{\lambda\!\!\!^{-2}} + \dots\right) . \tag{6.44}$$

Hence, the PN expansion on the small velocity $\epsilon \sim 1/c \ll 1$ is an *near zone* expansion $r/\lambda\!\!\!^{-} \ll 1$, where $\lambda\!\!\!^{-}$ is the reduced wavelength of the radiation. As evident from Eq. (6.43) the terms of the series in powers of $1/c$ blow up in r for $r \to \infty$. This is unphysical if F represent a metric potential of a AF spacetime. The PN expansion is indeed an *asymptotic expansion* where the coefficients depend on a second scale (parameter) and the series is not uniformly convergent.

□ [TODO: connect to 1PN, quadrupole formula and divergent integrals, example dipole radiation?]

PM: a wave zone expansion. The PM formalism provides a natural alternative for an expansion in the wave zone. At lowest order in G, one obtains the solution $\mathsf{h}^{\mu\nu}_{(1)}$ as a multipole expansion. Let us consider only the 00 component as an illustrative toy model. The multipole expansion of the field far from the source of Eq. (4.47) is

$$\mathsf{h}^{00}_{(1)} \simeq \frac{4G}{c^2}\left[\underbrace{\frac{M(u)}{r}}_{0PN} + \underbrace{\frac{1}{2}\partial_i\partial_j\frac{M^{ij}(u)}{r}}_{1PN} - \underbrace{\frac{1}{6}\partial_i\partial_j\partial_k\frac{M^{ijk}}{r}}_{\frac{3}{2}PN} + \dots\right] . \tag{6.45}$$

As indicated in the equation, each of these multipoles correspond to a different PN order. This can be verified directly considering the multipoles are functions of the retarded time and the spatial derivatives can be substituted by time derivatives. For example, the quadrupole term has the structure

$$\frac{G}{c^2}\partial_i\partial_j\frac{M^{ij}(u)}{r} \sim \frac{G}{c^2}\left(\frac{M^{ij}(u)}{r^3} + \frac{\dot{M}^{ij}(u)}{cr^2} + \frac{\ddot{M}^{ij}(u)}{c^2 r}\right) , \tag{6.46}$$

where the angular dependency is omitted. Introducing the source's characteristic mass M, radius R and velocity $v \sim R/T$, the quadrupole term M^{ij} is of order $\sim MR^2$, the characteristic wavelenght of the radiation is $\lambda\!\!\!^{-} \sim cT$, and the PN power counting of the quadrupole term is

$$\frac{G}{c^2}\partial_i\partial_j\frac{M^{ij}(u)}{r} \sim \frac{GM}{c^2 r}\frac{R^2}{c^2T^2}\left(1 + \frac{cT}{r} + \frac{c^2T^2}{r^2}\right) \sim \frac{GM}{c^2 r}\left(\frac{v}{c}\right)^2\left(1 + \frac{\lambda\!\!\!^{-}}{r} + \left(\frac{\lambda\!\!\!^{-}}{r}\right)^2\right) . \tag{6.47}$$

The quadrupole term has a leading order PN term that is $\mathcal{O}(\epsilon^2)$ with respect to the leading mass term $GM/(c^2R)$, hence it is 1PN. A second, important comment is that the multipolar solution is divergent for $r \to 0$, i.e. the asymptotic expansion does not apply down to $r < R$.

Given the solution at first order, one can proceed to the higher order solutions. Here one should note that, differently from the homogenous equation for $n = 1$, the sources $\tau^{\mu\nu}_{(n>1)}$ extend to the whole space. Because all the multipoles in $\mathsf{h}^{\mu\nu}_{(1)}$ diverge for $r \to 0$, the $\mathsf{h}^{\mu\nu}_{(1)}$ will also diverges as all the other corrections. In other words, the solutions that are valid for $r > R$ (strictly positive) cannot be extended down to $r \to 0$.

The general method to compute higher-order PM solution is as follows. One observes that $\mathsf{h}^{\mu\nu}_{(n)}$ is not needed as a full multipolar series but only as a truncated sum up to a required PN order. If one considers the truncated expansion, then the retarded integral defined as

$$I^{\mu\nu}_{(n)}(B) := \Box^{-1}_{\rm ret}(r^B\tau^{\mu\nu}_{(n)}) \tag{6.48}$$

is finite for a sufficiently large $B \in \mathbb{R}^+$ (One can always find a B such that ...) Crucially, the integral $I^{\mu\nu}_{(n)}(B)$ admits a unique analytical continuation to the B-complex plane except at some integer values and at the origin. In

particular, for $B \to 0$ the integral admits a Laurent expansion, whose term $\propto B^0$ is a particular finite solution of the inhomogenous equation $\Box \mathsf{h}_{(n)} = \tau_{(n)}$. This solution is indicated as the *partie finie*

$$\mathrm{FP}_{B=0} I^{\mu\nu}_{(n)}(B) = \mathrm{FP}_{B=0}\left[\Box^{-1}_{\rm ret}(r^B \tau^{\mu\nu}_{(n)})\right] . \tag{6.49}$$

The FP reduces to the retarded Green function integral if the source has compact support. The general solution of the iteration is given by summing up the particular FP solution with the general homogeneous solution.

The behaviour at $\mathcal{I}^+$ of the PM solution $\mathsf{h}^{\mu\nu}_{(n)}$ is

$$\mathsf{h}^{\mu\nu}_{(n)}(u) \sim \sum_{k=1}^{n-1}\sum_{p=0} G^{\mu\nu}_{L\,(k,p,n)}(u)\frac{\hat{n}_L (\log r)^p}{r^k} , \tag{6.50}$$

where the $\log(r)$ terms are due to the use of harmonic coordinates. In order to compute the waveform in TT gauge, the field $\mathsf{h}^{\mu\nu}$ needs to be turned into radiative coordinates (denoted with capital letters, except for the retarded time) where one recovers the structure

$$H^{\mu\nu}_{(n)}(u) \sim \sum_{k=1} K^{\mu\nu}_{L\,(k,n)}(u)\frac{\hat{N}_L}{R^k} . \tag{6.51}$$

The transformation to radiative coordinates must be obtained order-by-order in G by explicit computation. The $1/R$ part of the expansion is then selected and projected using the τ tensors. The final expression is

$$H^{\rm TT}_{ij} = \frac{4G}{c^2 R}\tau_{ij,kl}(\hat{N})\sum_{\ell=2}\frac{1}{c^\ell \ell!}\left[N_{L-2}U_{klL-2}(u) - \frac{2\ell}{(\ell+1)}N_{mL-2}\epsilon_{mn(k}V_{l)nL-2}(u)\right] , \tag{6.52}$$

where U_L and V_L are called the *radiative multipolar moments*. To lowest order they are expressed as derivatives of the multipoles introduced in Eq. (4.49a),

$$U_L(u) = M^{(\ell)}_L(u) = \frac{d^\ell}{du^\ell}M_L(u) , \quad U_L(u) = S^{(\ell)}_L(u) = \frac{d^\ell}{du^\ell}S_L(u) . \tag{6.53}$$

Higher order computations reveal the appearance of *hereditary* terms that are given as integrals in the retarded time from ∞ to u of the multipole moments. These terms are a consequence of the propagation of waves on a curved background. The hereditary terms are of two types. There are *tail terms* that quantify the contributions of the source from the past to u physically corresponding to the backscattering of the GW off the background curvature. The other type is composed of *memory terms*, physically interpreted as the re-radiation of the stress-energy of the propagating waves, and that contribute to a nonzero wave amplitude even after the generating source has switched off.

Two zones and Matching. The systematic PN calculation is performed by employing PN and PM expansions in their respective regions of validity. The solution of the equations are first considered in two domains: an *inner zone* that includes the entire source and extends just outside of that, and a *wave zone* that includes infinity and extends down towards the source without reaching it. If R is the radius of the source and λ the wavelength of the radiation, the inner zone extends up to a radius $r^{\rm in}$ such that $R < r^{\rm in} \ll \lambda$. The wave zone extends from radii $r^{\rm out} > R$ (strictly larger). In each domain it is possible to calculate the PN and PM multipolar expansions, respectively. The two domains overlap in the region $R < r < r^{\rm in}$. In a second step, the PM multipolar expansion is matched to the PN multipolar expansion in this region, up to the given order in ϵ.

Remark 6.6.1. *The construction can be mathematically rather involved. Blanchet and Damour (1989) first derived the quadrupole formula at 1PN using a rigorous approach that follows the above ideas. Starting from the 1PN metric $\boldsymbol{g}^{\rm in}$ of Eq. (6.30a) that is valid in the inner zone, they considered a multipolar expansion of the type in Eq. (4.38) where the potentials V, V_i outside the matter source are expressed in terms of multipoles F_L, G_{iL}. The multipoles are then expanded in Taylor series of $z|y|/c$ and expressed as moments of the source terms σ, σ_i. A coordinate transformation to another harmonic system allows to express the 1PN metric in the overlap region in terms of two STF multipoles I_L, J_L (and their derivatives) to the given PN order. Next, they considered a PM solution in the wave zone. The first iteration is given by a multipolar expansion of the type in Eq. (4.47), where M_L, S_L and derivatives are called the* algorithmic multipoles. *The second PM iteration requires the regularization via FP of the solution of the quadratic GW SET terms and to add the solution of the homogeneous equation. This gives an external metric $\boldsymbol{g}^{\rm out}$ valid in the overlap region in terms of the algoritmic multipoles M_L, S_L (and derivatives). The "in" and "out" metrics must be then connected by a coordinate transformation. The latter is determined by requiring imposing the $(0i0j)$ component of the linearized Riemann tensor to be consistent, and gives the algorithmic moments in terms of the source moments, $M_L = I_L + \mathcal{O}(1/c^4)$ and $S_L = J_L + \mathcal{O}(1/c^4)$. Finally, the multipoles of the external metric in radiative (TT) gauge (Eq. (6.52)) are connected to the algorithmic multipoles of the external metric in harmonic coordinate to find $I^{\rm rad}_L = M_L + \mathcal{O}(1/c^3)$ and $J^{\rm rad}_L = S_L + \mathcal{O}(1/c^3)$ that implies $I^{\rm rad}_L(u) = I_L(u) + \mathcal{O}(1/c^3)$ $J^{\rm rad}_L(u) = J_L(u) + \mathcal{O}(1/c^3)$. The result is a complete 1PN expression of the GW in terms of the time-retarded moments of the source that is valid for weakly self-gravitating systems.*

6.7 Compact binaries

Applications of the PN formalism to the dynamics and radiation from compact binaries are further discussed in the Blanchet (2014) and the Schaefer and Jaranowski (2018) reviews. The starting point is the GR action with the stress-energy tensor of Eq. (6.33),

$$S = S_{\rm GR} + S_{\rm pointmasses} = \frac{c^3}{16\pi G}\int {\rm d}^4x\, R\sqrt{|g|} - \sum_a m_a c^2 \int {\rm d}s_a \ , \tag{6.54}$$

where ${\rm d}s_a = (-g_{\mu\nu}(dx^\mu_a/dt)(dx^\nu_a/dt)/c^2)^{1/2}{\rm d}t$ is calculated on the trajectory of body a. This action is also the starting point for the Einstein-Infeld-Hoffman 1PN approach. Differently from there high-order PN computations, require the regularization of the point-particles described by Dirac deltas. This can be done with field theory tools like dimensional regularization. We do not discuss here this technical aspects and refer instead the interested reader to the above reviews. In the following, we give an overview of the results for circular binaries and show how GW approximants are constructed from these results.

Consider a circular binary with objects with masses $m_1 \geq m_2$ and dimensionless spins $\chi_i = S_i/m^2$ $i = 1, 2$. We define the additional spin parameters

$$\tilde{a}_i := \frac{a_i}{m} = \frac{S_i}{m\, m_i} = \frac{\chi_i m_i}{m} \ , \quad \hat{a}_0 := \tilde{a}_1 + \tilde{a}_2 \ , \quad \tilde{a}_{12} := \tilde{a}_1 - \tilde{a}_2 \ . \tag{6.55}$$

For $m_1 \gg m_2$ ($\nu \to 0$) $\tilde{a}_1 \to S_1/(m_1)^2$ is the dimensionless spin of the large black hole and $\tilde{a}_{12} \to 0$. In place of the GW frequency, it is useful to introduce the parameter

$$x := \left(\pi \frac{Gm}{c^3} f\right)^{2/3} = \left(\frac{1}{2}\frac{Gm}{c^3}\omega\right)^{2/3} = \left(\frac{Gm}{c^3}\Omega\right)^{2/3} \sim \mathcal{O}((v/c)^2) \ , \tag{6.56}$$

where the scaling in ϵ simply follows from $(Gm/c^3\,\Omega)^{2/3} \sim ((Gm/r\,(r\Omega)c^3)^{2/3} \sim (v^2\, v/c^3)^{2/3}$. The energy of circular orbits can be written as

$$E(x) = E_{\rm orb}(x) + E_{\rm SO}(x) + E_{\rm SS}(x) \ , \tag{6.57a}$$

where the different terms describe the orbital, spin-orbit and spin-spin interactions. The leading order contribution is $E_{\rm Newt} = -\mu c^2 x/2$. The orbital energy is known at 4PN (Damour et al., 2014, 2016; Bernard et al., 2017)

$$\begin{aligned}\frac{E_{\rm orb}(x)}{E_{\rm Newt}} &= 1 - \left(\frac{3}{4} + \frac{\nu}{12}\right)x + \left(-\frac{27}{8} + \frac{19\nu}{8} - \frac{\nu^2}{24}\right)x^2 + \left(-\frac{675}{64} + \left(\frac{34445}{576} - \frac{205\pi^2}{96}\right)\nu - \frac{155\nu^2}{96} - \frac{35\nu^3}{5184}\right)x^3 \\ &+ \left[-\frac{3969}{128} + \left(\frac{9037\pi^2}{1536} - \frac{123671}{5760} + \frac{448}{15}(2\gamma_E + \ln(16x))\right)\nu + \left(\frac{3157\pi^2}{576} - \frac{498449}{3456}\right)\nu^2 + \frac{301\nu^3}{1728} + \frac{77\nu^4}{31104}\right]x^4 \\ &+ ...\end{aligned} \tag{6.57b}$$

with $\gamma_E = 0.577...$ is the Euler constant. Work towards 5PN computation is ongoin with different techniques Bern et al. (2019); Bini et al. (2019). The spin sector expansions start with

$$E_{\rm SO} = -\frac{1}{6}(7\hat{a}_0 + \tilde{a}_{12}\sqrt{(1-4\nu)})\nu x^{5/2} + ... \quad ; \quad E_{\rm SS} = \frac{1}{2}\hat{a}_0^2\nu x^3 + ... \quad . \tag{6.57c}$$

and terms in the spin-orbit sector are know up to 4.5PN Levi et al. (2020); Antonelli et al. (2020).

The gravitational waveform for nonspinning binaries and generic masses is complete at 3.5PN order. Let $P_{\rm Newt}(x) = 32c^5/(5G)\,\nu^2 x^5$, the expression of the GW power (flux) is

$$\begin{aligned}\frac{P(x)}{P_{\rm Newt}(x)} &= 1 + \left(-\frac{1247}{336} - \frac{35}{12}\nu\right)x + 4\pi x^{3/2} + \left(-\frac{44711}{9072} + \frac{9271}{504}\nu + \frac{65}{18}\nu^2\right)x^2 + \left(-\frac{8191}{672} - \frac{583}{24}\nu\right)\pi x^{5/2} \\ &+ \left[\frac{6643739519}{69854400} + \frac{16}{3}\pi^2 - \frac{1712}{105}\gamma_E - \frac{856}{105}\log(16x) + \left(-\frac{134543}{7776} + \frac{41}{48}\pi^2\right)\nu - \frac{94403}{3024}\nu^2 - \frac{775}{324}\nu^3\right]x^3 \\ &+ \left(-\frac{16285}{504} + \frac{214745}{1728}\nu + \frac{193385}{3024}\nu^2\right)\pi x^{7/2} + ...\end{aligned} \tag{6.58}$$

Terms in the SO sector are known up to 4PN Marsat et al. (2014), 3PN at S^2 Bohé et al. (2015), and 3.5PN at S^3 Marsat (2015).

Taylor waveform approximants. In order to illustrate the application of the PN formalism to GW modeling from binary systems we go back to Example 5.3.2. The integration of Eq. (5.64) gives an equation for the GW frequency evolution in time, $\omega \sim (t_c - t)^{-3/8}$, where t_c is an integration constant called the *coalescence time*. The frequency formally diverges at $t = t_c$ but in those conditions the slow motion approximation is not valid anymore. The frequency evolution is then usually expressed in term of the parameter $x \sim \omega^{2/3}$ by introducing the dimensionless time

$$\tau := \nu \frac{c^3}{GM}(t_c - t) \quad \Rightarrow \quad x(t) = \frac{1}{4}\tau^{-1/4} \ . \tag{6.59}$$

The leading order GW phase can be then immediately calculated by integration,

$$\phi_{\rm Newt}(t) = \int_0^{t_0} dt' \omega(t') = \phi_0 - \frac{1}{\nu}\tau^{5/8} = \phi_0 - \frac{x^{-5/2}}{32\nu} \ . \tag{6.60}$$

This procedure can be now extended to high PN order using the PN expanded expressions for the orbital energy and the flux and using the energy balance. The time-domain phase is an expansion in x

$$\frac{\phi(t)}{\phi_{\rm Newt}(t)} = 1 + \mathcal{O}(x) + \mathcal{O}(x^{3/2}) + \mathcal{O}(x^2) + \mathcal{O}(x^{5/2} + \mathcal{O}(x^3) + ... \tag{6.61a}$$

$$= 1 + \left(\frac{3715}{1008} + \frac{55}{12}\nu\right) x - 10\pi x^{3/2} + \left(\frac{15293365}{1016064} + \frac{27145}{1008}\nu + \frac{3085}{144}\nu^2\right) x^2 + ... \ . \tag{6.61b}$$

The second line indicates the first terms for nonspinning binaries. The expansion for nonspinning binaries is fully known up to 3.5PN, i.e. $\mathcal{O}(x^{7/2})$, with several high-order terms known.

Waveform approximants build in this way are called *Taylor approximants*. The following example describe how to calculate analytically the Taylor approximants in frequency domain. The latter form is useful for gravitational-wave data analysis.

Remark 6.7.1. *The* saddle point/stationary phase method *approximates the definite integral (limits are not indicated)*

$$I(\lambda) = \int dt A(t) e^{\lambda \phi(t)} \tag{6.62}$$

where $A(t), \phi(t)$ are real functions, for $\lambda \ll 1$ ($\lambda > 0$), assuming the integration domain contains a stationary point $\phi'(t_0) = 0$. Around the stationary point, the Taylor expansion of the functions is

$$\lambda\phi(t) = \lambda\left(\phi(t_0) + \frac{1}{2}\phi''(t_0)(t - t_0)^2 + \mathcal{O}(2)\right) = \lambda\phi_0 + \frac{1}{2}\phi_0'' x^2 + \mathcal{O}(2) \tag{6.63a}$$

$$A(t) = A(t_0) + \mathcal{O}(1) = A_0\left(1 + \frac{x}{\sqrt{\lambda}}\frac{A_0'}{A_0} + \mathcal{O}(2)\right) \tag{6.63b}$$

where functions evaluated at t_0 are indicates with a subscript $_0$ and where the second line changes to the (integration) variable to $x := \sqrt{\lambda}(t - t_0)$. The integral is thus

$$I(\lambda) = \frac{A_0}{\sqrt{\lambda}} e^{-\lambda\phi_0} \int dx e^{-\frac{1}{2}\phi_0'' x^2} \left[1 + \mathcal{O}(1/\sqrt{\lambda})\right] = \frac{A_0}{\sqrt{\lambda}} e^{-\lambda\phi_0} \sqrt{\frac{2\pi}{\phi_0''}} \left[1 + \mathcal{O}(1/\sqrt{\lambda})\right] \ , \tag{6.64}$$

where one observe that for $\lambda \ll 1$ the contributions in brakets are progressively smaller, and that the first integral is dominated by the saddle point $x \simeq 0$ and that it can be approximated by a Gaussian integral on the real axis. The method can be extended to the complex functions. In this case, one must take a complex integral on a countour around the zero(s) $\phi'(z) = 0$ where $\Re(\phi)$ looks like a saddle. The result is the same as above; the detailed steps can be checked in analysis books.

Example 6.7.1. Stationary phase approximation (SPA) of GW. *The data analysis of GW data requires frequency-domain waveforms. Given a time-domain real waveform, $h_+(t) = A(t)\cos\phi(t)$, the complex Fourier transform is*

$$\tilde{h}(f) = \int dt A(t)\cos(t) e^{{\rm i}2\pi f t} = \frac{1}{2}\int dt A(t)\left(e^{{\rm i}\phi(t)} + e^{-{\rm i}\phi(t)}\right) e^{{\rm i}2\pi f t} \tag{6.65}$$

where we consider only $f > 0$ since $\tilde{h}(-f) = \tilde{h}^*(f)$. Looking for a SPA solution, the contribution $\propto e^{{\rm i}\phi(t) + {\rm i}2\pi t t}$ has no stationary points and is always oscillating and can be discarded. The stationary point of the other contribution is

$$2\pi f = \dot{\phi}(t_f) = \omega(t_f) \ , \tag{6.66}$$

and the SPA solution is

$$\tilde{h}(f) \simeq \frac{1}{2}\left(\frac{2\pi}{\ddot{\phi}(t_f)}\right)^{1/2} A(t_f)\, e^{{\rm i}\Psi_+(f)} \tag{6.67}$$

where

$$\Psi_+(f) = 2\pi f t_f - \phi(t_f) - \frac{\pi}{4} \ . \tag{6.68}$$

The phase of the Fourier transform of the time-domain (quadrupolar) waveform is thus simply the Legendre transform of the quadrupolar time-domain phase $\phi(t)$. Using now Eq. (6.59) to substitute $t_f(\tau_f(f)) \sim f^{-8/3}$ into the Newtonian expressions for $A(t_f)$ and $\ddot{\phi}(t_f)$ one obtains that at leading order

$$\tilde{h}(f) = \tilde{A}(f) e^{-\mathrm{i}\Psi(f)} \sim f^{-7/6} e^{-\mathrm{i}\Psi(f)} \ . \tag{6.69}$$

Details and factors are left as [exercise]. Differentiating Eq. (6.68) twice with respect to f leads to

$$\frac{d^2\Psi_{\rm SPA}}{dw^2} = \frac{Q_\omega(w)}{w^2} \ , \tag{6.70}$$

where $w = 2\pi f$ $(\neq \omega)$ is the Fourier domain circular frequency. Hence, the frequency-domain phase in the SPA can be calculated by integrating term-by-term the PN expansion of the Q_ω obtained from the energy balance,

$$Q_\omega = -\omega^2 \frac{\dot{E}}{P} = \frac{5}{48\nu} x^{-5/2} \left(1 + \frac{743 + 924\nu}{336} - 4\pi x^{3/2} + \mathcal{O}(x^2) \right) \ . \tag{6.71}$$

Remark 6.7.2. *The Q_ω quantity also measures the number of GW cycles spent by the binary system within an octave of the GW frequency ω. It is therefore analogous to the "quality factor" of a damped oscillator. The accumulated time-domain phase between frequencies (ω_1, ω_2) is given by the following integral*

$$Q_\omega = \frac{\omega^2}{\dot{\omega}} = \frac{d\phi(t)}{d\ln\omega} \quad \Rightarrow \quad \phi = \int_{\omega_1}^{\omega_2} Q_\omega d\ln\omega \ . \tag{6.72}$$

A change of Q_ω of the order ± 1 during a frequency octave $\ln\omega_2/\omega_1 = 1$ corresponds to a local dephasing (around ω) of $\Delta\phi = \pm 1$ rad. Moreover, it can be shown that the squared signal-to-noise ratio (Chap. 9) can be written as (Damour et al., 2000),

$$\rho^2 = 4 \int d\ln\omega \frac{Q_\omega(\omega) A^2(\omega)}{\omega S_n(\omega)} \ , \tag{6.73}$$

where A is the amplitude of the time-domain waveform and S_n the one-sided noise power spectral density.

Finite size effects. The motion of bodies that have an internal structure and can be deformed (like neutron stars) is affected by the presence of tidal forces. We start with recalling how finite structure effect are described in Newtonian gravity.

Remark 6.7.3. Newtonian EOM for N perfect-fluid bodies. *The Newton potential of N fluid bodies with density ρ and pressure P is*

$$U = \sum_{b=1}^{N} \int_{V_b} d^3x' \, \frac{\rho(t,x')}{|x - x'|} \ , \tag{6.74}$$

where V_b is the volume where the densitiy of body b is nonzero. The potential for body a is thus given by an "external" contribution from the other bodies and a "self" contribution,

$$U_a = \int_{V_a} d^3x' \, \frac{\rho(t,x')}{|x - x'|} + \sum_{b=1, b\neq a}^{N} \int_{V_b} d^3x' \, \frac{\rho(t,x')}{|x - x'|} =: U_a^{(\rm self)} + U_a^{(\rm ext)} \ . \tag{6.75}$$

The force on body is also separated into a self-contribution and an external contirbution; the self- contribution also contains the pressure of the fluid body (see next equation). Because the force is $F \sim Gm^2/r^2$, the external force is $\sim GM/D^2$ where D is the characteristic distance between the bodies and M the total mass, while the self-force is $\sim GM^2/R_a^2$ where R_a is the characteristic size of body a; one would estimate that

$$\frac{F_a^{(\rm self)}}{F^{(\rm ext)}} \sim \left(\frac{D}{R_a} \right)^2 \ll 1 \ . \tag{6.76}$$

However, the self force is identically zero because in the integral

$$F_a^{(\rm self)\,\mathrm{i}} = \int_{V_a} d^3x' \, \left(-\partial_i P + \rho \partial_i U_a^{(\rm self)} \right) = 0 - \int d^3x \int d^3x' (x - x')^i \frac{\rho(t,x)\rho(t,x')}{|x' - x'|^3} \equiv 0 \tag{6.77}$$

both terms are zero. The first term is zero because the pressure is zero at the surface; the second term vanishes because the integrand is odd under exchange $x' \leftrightarrow x$, while the domain of integration is invariant under the same exchange. Note the densities ρ in the integrand are conceptually distinct: one is the source of the grav. field (the one in $U^{(\rm ext)}$),

while the other is the "passive" density that measure the response to the external field. The external force acting on body a is

$$F_a^{(\mathrm{ext})\,\mathrm{i}} = \int d^3x\, \rho \partial_i U_a^{(\mathrm{ext})}(t,x) = \int d^3y\, \rho \partial_i U_a^{(\mathrm{ext})}(t, z_a + y) \tag{6.78a}$$

$$= \int d^3y\, \rho \left[\partial_i U_a^{(\mathrm{ext})}(t,z_a) + y^j \partial_i \partial_j U_a^{(\mathrm{ext})}(t,z_a) + \frac{1}{2} y^j y^k \partial_i \partial_j \partial_k U_a^{(\mathrm{ext})}(t,z_a) + ... \right] \tag{6.78b}$$

where in the second passage one introduces the center of mass of coordinate $z_a(t)$ and a new coordinate y around it $y = x - z_a$; and in the last passage a multipolar expansion around the center of mass is performed. Hence, the EOM for body a is

$$m_a \frac{d^2 z_a^i}{dt^2} = m_a \partial_i U_a^{(\mathrm{ext})}(t,z_a) + \frac{1}{2} Q_a^{jk} \partial_j \partial_k U_a^{(\mathrm{ext})}(t,z_a) + ... \,, \tag{6.79}$$

where Q_a^{jk} is the quadrupole of body a and the dipole term is zero in the center of mass frame. Considering that $\partial U^{(\mathrm{ext})} \sim 1/D^2$ and $Q \sim \varepsilon M R^2$ where $\varepsilon \leq 1$ is the ellipticity of the body, it is immedate to estimate that $Q\partial^3 U^{(\mathrm{ext})} \sim R^2/D^2$ and

$$\frac{Q_a^{jk} \partial_j \partial_k U_a^{(\mathrm{ext})}}{\partial_i U_a^{(\mathrm{ext})}} \sim \varepsilon \frac{R_a^2}{D^2} \ll 1 \,. \tag{6.80}$$

The above formula indicates the order of magnitude of the quadrupole correction to the EOM [3].

The above remark suggests that for a structured body in a binary system, the field of the companion induces, at leading order, a quadrupole moment that, in turn, modifies the orbit. A Newtonian argument indicate that the correction to the point-mss dynamics due to finite size enter at 5PN order. The Newtonian tidal force exterted by body a on body b of size R when they are separated by a distance D is of order

$$F_{a\to b}^{(\mathrm{tidal})} \sim \frac{GMR_b}{D^3}. \tag{6.81}$$

Body b is distorted by this force and deforms; the first relevant correction for the dynamics is given by the quadrupole, $Q \sim \varepsilon m R^2$. The ellipticity ε can be estimated as the ratio of te tidal force to the self-force of the body,

$$\varepsilon_b \sim \frac{F_{a\to b}^{(\mathrm{tidal})}}{F_b^{(\mathrm{self})}} \sim \left(\frac{R_b}{D}\right)^3 \,. \tag{6.82}$$

The quadrupole of body b induces a correction to the force $F_{ab}^k \sim m_b \partial_k U^{(\mathrm{ext})}$ acting on body b. The induced force on body a is of order

$$F_{b\to a}^{(\mathrm{quad})\,\mathrm{k}} \sim \frac{Q_b^{ij}}{m_b} \partial_i \partial_j F_{ab}^k \sim \varepsilon \frac{R_b^2}{D^2} F_{ab}^k \tag{6.83}$$

from which

$$\frac{F_{b\to a}^{(\mathrm{quad})\,\mathrm{k}}}{F_{ab}^k} \sim \varepsilon \frac{R_b^2}{D^2} \sim \frac{R_b^5}{D^5} \sim \left(\frac{v}{c}\right)^{10} \,. \tag{6.84}$$

In the last passage one estimates the radius of a compact object as close to Schwarzschild one, and uses the virial theorem $r \sim GM/c^2 \sim v^2/c^2$. The estimate above is correct: tidal effects enter the action at order 5PN and several PN terms have been calculated for the dynamical and for the waveform up to 7.5PN (Damour, 1987; Damour et al., 2012).

The description of tidal interactions in the PN dynamics of self-gravitating and deformable bodies was formulated in a series of works by Damour, Soffel and Xu in the '90s (Damour, 1983; Damour et al., 1991, 1992, 1993, 1994). They developed a multi-chart approach whereby an *outer problem*, in which the bodies are "skeletonized" as worldlines with global properties, is matched to an *inner problem*, in which the effects of the other bodies in the worldtube around a given body are included.

In the case of compact binaries, the inner problem corresponds to the description of the tidal response of a NS due to the external gravitational field of the companion. The matching with the outer problem allows one to include the effect of the tidal deformations on the orbital dynamics and the GW radiation. The presentation here follows closely that of Refs. (Damour and Nagar, 2009, 2010). A fully relativistic treatment of the *inner problem* was developed in (Damour, 1983; Hinderer, 2008; Damour and Nagar, 2009; Binnington and Poisson, 2009). In the local frame of body A, the internally-generated mass M_L^A and spin S_L^A multipole moments, $L = i_1 i_2 ... i_\ell$ being a multi-index, are related to the external gravitoelectric G_L^A and gravitomagnetic H_L^A tidal moments[4] by the *tidal polarizability coefficients*,

$$M_L^A = \mu_\ell G_L^A \quad , \quad S_L^A = \sigma_\ell H_L^A \,. \tag{6.85}$$

[3] The interested reader could, at this point, estimate the effect of the Sun's quadrupole moment on the Mercury perielion and compare to the GR correction.

[4] The tidal moments are defined as the symmetric-trace-free projection of the derivatives of the externally-generated parts of the local gravitoelectric $\bar{E}_a$ and gravitomagnetic fields $\bar{B}_a$, e.g. $G_L^A = \partial_{\langle L-1} \bar{E}^A_{a_\ell\rangle}|_{X^a\to 0}$, where X^a are local coordinates (Damour and Nagar, 2009).

The gravitoelectric (gravitomagnetic) coefficient $G\mu_l$ has dimension $[\text{length}]^{2\ell+1}$ and measures the ℓ-th-order mass (spin) multipolar moment induced in the NS by the external ℓ-th-order gravitoelectric (gravitomagnetic) field. The dimensionless relativistic Love numbers are defined as

$$k_\ell = \frac{(2\ell-1)!!}{2}\frac{G\mu_\ell}{R^{2\ell+1}} \ , \ j_\ell = \frac{(2\ell-1)!!}{2}\frac{G\sigma_\ell}{R^{2\ell+1}} \ , \tag{6.86}$$

with R being the NS radius. Note that the many works in the literature focus on the dominant quadrupole $\ell = 2$ gravitoeletric coefficient and drop the subscript, e.g. Hinderer (2008). For BH $\mu_\ell^{\rm BH} = \sigma_\ell^{\rm BH} = 0$ (Damour and Nagar, 2009; Binnington and Poisson, 2009; Grlebeck, 2015). Nevertheless BH can also be tidally polarized (Damour and Lecian, 2009). In practice, the calculation of the Love numbers reduces to the solution of stationary perturbations of spherical relativistic stars, because it is assumed that the external field varies sufficiently slowly ("adiabatic tides"). The tidal coefficients have a strong dependency on the NS compactness. Thus, Love numbers must be computed in GR, and not in the Newtonian limit. Love numbers depend on the EOS employed to construct the equilibrium NS. Hence, they carry the imprint of the EOS on the binary dynamics. We will see the definition of the Love numbers and how they are calculated in Chap. 7.

Finite-size effects are incorporated into the PN two-body dynamics by augmenting the effective action S with the nonminimal (worldline) couplings

$$S_{\rm nonminimial} = \sum_a \frac{\mu_\ell^a}{2\ell!}\int (G_L^a)^2 {\rm d}s_a + \frac{\ell\,\sigma_\ell^a}{\ell! 2(\ell+1)}\int (H_L^a)^2 {\rm d}s_a \ . \tag{6.87}$$

The additional term alter the dynamics at 5PN in a way that is linear in the tidal deformations. The tidal contribution to the two-body Lagrangian at leading PN (Newtonian) order contains only the $\ell = 2$ gravitoelectric terms and reads

$$L_{\rm tidal}^{\rm LO} = k_2^A G M_B^2 \frac{R_A^5}{r^6} + (A \leftrightarrow B) \ , \tag{6.88}$$

where r is the separation between the stars in the binary. Eq. (6.88) indicates that tidal corrections are attractive and short range. The effect of tides can be illustrated considering the modification to the Kepler law given by the quadrupolar gravitoelectric term

$$\Omega^2 r^3 = GM\left[1 + ... + 12\frac{M_A}{M_B}\frac{R_A^5}{r^5}k_2^A + (A \leftrightarrow B)\right] \ . \tag{6.89}$$

At a given radius the frequency is higher if the tidal interactions are present. In other words, the motion is accelerated by tidal effects and the system merges earlier and at a lower frequency. The contact GW frequency of the two NS can be estimated setting $r = R_A + R_B$ and finding $2GM\Omega \simeq 2(M_B/(MC_B) + M_B/(MC_B))^{-3/2}$ (Damour and Nagar, 2010). For equal masses the latter relation translates to

$$f_{\rm GW}^{\rm contact} \simeq 1.327\left(\frac{C}{0.15}\right)^{3/2}\left(\frac{M}{2.8{\rm M}_\odot}\right) \text{kHz} \ . \tag{6.90}$$

Simulations show that the contact between the two NS happens approximately $2-4$ GW cycles prior to merger at an even lower frequency $f_{\rm GW}^{\rm NR,contact} \simeq 700\ (M/2.8{\rm M}_\odot)$ Hz (Bernuzzi et al., 2012).

7. Perturbations of spherical spacetimes

Basic ideas on the gauge-invariant perturbations framework, Regge-Wheeler-Zerilli equations, solutions containing quasi-normal-modes, stability of black holes, and Love numbers of relativistic stars.

Suggested readings. *Chap. 4 of Chandrasekhar (1985). Reviews: Kokkotas and Schmidt (1999); Nollert (1999); Nagar and Rezzolla (2005); Berti et al. (2009).*

7.1 Gauge invariant perturbation theory

Linear perturbations of spherical spacetimes describe

- Gravitational wave propagation on curved background;
- Stability of black holes solutions and spherical star equilibria;
- Deformation of spherical stars and relativistic Love numbers;
- Gravitational waves from black holes and neutron star out of equilibrium;
- Dynamics and GWs from small objects moving in black hole spacetime (in the test mass limit).

In linearized gravity around flat spacetime, one choses the Mikowski brackground metric in some global inertial coordinates and considers small perturbations in the sense that the components of the perturbed metric in those coordinates are smaller than those of the the background. Infinitesimal coordinate transformations are still possible as far as the coordinates' variation does not change the background metric and it is of the same order as the perturbation.

For spherically symmetric spacetimes one can proceed similarly taking, for example, the Schwarzschild metric for the background and explicitely fixing the gauge. This was the first approach to the problem by Regge and Wheeler (1957); Zerilli (1970), where the *Regge-Wheeler (RW)* gauge was defined. Moncrief (1974a,b) and other authors have later proposed a gauge-invariant approach to the perturbation problem (Gerlach and Sengupta, 1979, 1980; Gundlach and Martin-Garcia, 2000; Martin-Garcia and Gundlach, 2001). Under an infinitesimal coordinate transformation

$$x^\mu \mapsto x^{\mu'} = x^\mu + \xi^\mu \ , \tag{7.1}$$

the perturbative tensor field changes as $\boldsymbol{h} \mapsto \boldsymbol{h}' = \boldsymbol{h} + \mathcal{L}_\xi \boldsymbol{h}$ and it is called gauge invariant iff

$$\mathcal{L}_\xi \boldsymbol{h} = 0 \ . \tag{7.2}$$

Starting from a general infinitesial coordinate transformation, Gerlach and Sengupta (1979, 1980) cast all the possible linear perturbations into gauge-invariant quantities and write down the linearized Einstein equations for these gauge-invariant perturbation (See Sec. II of Gundlach and Martin-Garcia (2000) for a review of the formalism).

The main steps to compute spherical spacetime perturbations are:

1. *2+2 split.* Write the general spherically symmetric spacetime as a manifold $\mathcal{M} = M^2 \times S^2$, where M^2 is a Lorenztian 2D manifold with metric $g_{AB}(t,r)$ $(A,B,... = 0,1)$ and S^2 is the 2-sphere with metric $\gamma_{ab}(\theta,\varphi)$ $(a,b,.., = 2,3$ in this chapter) such that $g_{\mu\nu} = \mathrm{diag}(g_{AB}, r^2\gamma_{ab})$. Introduce covariant derivatives in M^2 and S^2 and a analogous decomposition of the stress-energy tensor. The spherically symmetric EFE are then re-written as equations for g_{AB} for the M^2 manifold.
2. *Even/odd and multipole decomposition.* Linear perturbation are decomposed into scalar, vector or tensor fields on M^2 times scalar, vector or tensor spherical harmonic on S^2. Under a parity transformation

$$\theta \mapsto \pi - \theta \ , \quad \varphi \mapsto \varphi + \pi \ , \tag{7.3}$$

the perturbations pick either a factor $(-1)^\ell$ (even) or a factor $(-1)^{\ell+1}$ (odd). Because the background metric is invariant under a parity transformation, the two sectors do not mix. Thus, the generic perturbations decouple into *even* (or *polar*) and *odd* (or *axial*).

The perturbations are not spherically symmetric (they are general) but their angular dependence is fully encoded in the tensor spherical harmonics in which they are expanded. Linearized EFE equations for the perturbative fields on M^2 apply to each multipole that are thus labelled by (ℓ, m). Note however that gauge-invariant metric perturbations are possible only for $\ell \geq 2$.

3. *Gravitational waves.* The GW degrees of freedom in this formalism are encoded in the odd and even-parity Regge-Wheeler-Zerilli (RWZ) master functions $\Psi^{(o/e)}_{\ell m}$. These fields satisfy wave equations on M^2 for each (ℓ, m) multipole. The RWZ equations contain characteristic potentials that are determined by the background spacetime.

2+2 split. □ [TODO: To be written.]

Even/odd perturbation of spherical spacetimes. Tensor perturbations of spherical spacetimes are naturally developed in tensor spherical harmonics and spherical coordinate taking advantage of the symmetries of the background. The tensor spherical harmonics needed here are a generalization of those discussed in Chap. 4. Maggiore (2018) (Sec. 12.2) discusses their explicit construction that consists in (i) an extension to four indexes of the $(\mathbf{Y}^x_{\ell m})_{ij}$ with $x = S0, E1, E2, B1, B2$ [1], (ii) their expression in terms of derivatives of the the scalar $Y_{\ell m}$ (extension of Eq. (4.61)), and (iii) change of coordinate to spherical components. The computations are trivial but lengthy and are not reported here.

The tensor spherical harmonics form a complete basis on the 2-sphere to expand a tensor field of any rank. The spherical harmonics $Y_{\ell m}$ form a basis for scalar fields on S^2. A vector basis can be constructed by taking the covariant derivative of the scalar spherical harmonics on S^2 (indicated as $_{|a}$),

$$Z^{\ell m}_a := Y^{\ell m}_{|a} \; ; \quad S^{\ell m}_c := \epsilon_{cd}\gamma^{de} Y^{\ell m}_{|e} \; , \tag{7.5}$$

where the first (second) expression should be used for even (odd) perturbation, see below. Above $\boldsymbol{\epsilon}$ is the volume form in the 2-sphere, $\epsilon^{ac}\epsilon_{bc} = \gamma_{ab}$. A basis for even and odd symmetric tensors on S^2 is given by

$$\gamma_{ab} Y^{\ell m} \; , \quad Z^{\ell m}_{ab} := Y_{|ab} + \frac{\ell(\ell+1)}{2}\gamma_{ab} Y_{\ell m} \; ; \quad S^{\ell m}_{ab} := \frac{1}{2}(S^{\ell m}_{a|b} + S_{b|a}) \; . \tag{7.6}$$

Note the even basis is formed by a pure trace and a traceless tensor. Explicit expressions in terms of the partial derivatives of $Y_{\ell m}(\theta, \varphi)$ can be found in e.g. Appendix A of Nagar and Rezzolla (2005).

The tensor spherical harmonics components in spherical coordinates for tensors on $\mathcal{M} = M \times S^2$ are then expressed in terms of the above quantities. Explicit expression can be found in Sec. 12.2.1 of Maggiore (2018). Advanced software for symbolic algebraic computation has been developed to this purpose [2] A generic tensor perturbation of spherical spacetime expanded in tensor spherical harmonics decomposes in even and odd

$$h_{\mu\nu} = h^{(e)}_{\mu\nu} + h^{(o)}_{\mu\nu} \, , \tag{7.7}$$

where the even expansion contains contributions from $(\mathbf{Y}^x_{\ell m})_{\mu\nu}$ with $x = tt, Et, Rt, L0, T0, E1, E2$ and the odd expansion with $x = Bt, B1, B2$. The metric perturbation is a special case. In terms of the basis functions for the 2-sphere discussed above, each term in the even and odd multipolar series is

$$(h^{(e)}_{\ell m})_{\mu\nu} = \left[\begin{array}{cc|c} H_0 Y_{\ell m} & H_1 Y_{\ell m} & h^{(e)}_A Z^{\ell m}_a \\ * & H_2 Y_{\ell m} & \\ \hline * & & r^2 K Y_{\ell m}\gamma_{ab} + r^2 G\, Z^{\ell m}_{ab} \end{array}\right] \; , \quad (h^{(o)}_{\ell m})_{\mu\nu} = \left[\begin{array}{c|c} 0 & h^{(o)}_A S^{\ell m}_a \\ \hline * & h S^{\ell m}_{ab} \end{array}\right] \tag{7.8}$$

The even/odd perturbations are thus described by the functions (indexes ℓm are omitted for brevity)

$$(H_0, H_1, H_2, h^{(e)}_A, K, G) \; , \quad (h^{(o)}_A, h) \; , \tag{7.9}$$

There are 3 odd and 7 even metric and matter perturbations. There are 1 odd and 3 even infinitesimal coordinate transformation. Thus, there are $3-1=2$ odd gauge-invariant perturbations, in the form of a vector field on M^2, and $7-3=4$ even gauge-invariant metric perturbations, in the form of a symmetric tensor and a scalar. The RW gauge can be specified by taking

$$G = h^{(e)}_A = h = 0 \, . \tag{7.10}$$

The gauge invariant fields are not those listed in Eq. but suitable combinations of them. The gauge-invariant combinations relevant for the following are

$$k_A := h^{(o)}_A - h_{|A} + \frac{2h}{r} r_{|A} \; , \quad \kappa_1 := K + e^{-2b}\left(r\partial_r G - \frac{2}{r} h^{(e)}_1\right) \; , \quad \kappa_2 := \frac{1}{2}\left[e^{-2b} H_2 - e^b \partial_r (r e^b K)\right] \; , \tag{7.11}$$

where the background metric of M^2 is $\bar{g} = -e^{2a}\mathrm{d}t^2 + e^{2b}\mathrm{d}r^2$. A similar decomposition holds for the stress-energy tensor.

[1] For the 00 component of a rank-2 tensor one uses the scalar $\delta^0_\mu \delta^o_\nu Y_{\ell m}$, while for the $0i$ component one uses the vector spherical harmonics. The basis function is still denoted as $\mathbf{Y}^x_{\ell m})_{ij}$ but with

$$x = tt, Et, Bt, Rt, L0, T0, E1, E2, B1, B2 \, . \tag{7.4}$$

The extension is here indicated as $(\mathbf{Y}^x_{\ell m})_{\mu\nu}$ with an abuse of notation. These quantities correspond to the $(\mathbf{t}^x_{\ell m})_{\mu\nu}$ of Sec. 12.2 in Maggiore (2018).

[2] The `Mathematica` package for computer algebra `xPert` is specifically design for metric perturbation theory, see `http://www.xact.es/xPert`).

7.2 Regge-Wheeler-Zerilli (RWZ) equations

The Regge-Wheeler-Zerilli equations describe perturbation of the Schwarzschild black hole. The background metric is taken in Schwarzschild coordinates with $e^{2a} = e^{-2b} = (1 - R_S/r) = (1 - 2GM/(c^2 r)) =: A(r)$. It is useful to introduce the tortoise coordinate

$$r_* = r + R_s \ln\left(\frac{r}{R_s} - 1\right) , \tag{7.12}$$

that maps the Schwarzschild exterior $[R_s, \infty)$ to $(-\infty, +\infty)$ [3]

Let $\Lambda = \ell(\ell+1)$, the odd (RW) and even (Zerilli) master functions for each multipoles are defined as the gauge-invariant quantities (ℓm are omitted for brevity)

$$\Psi^{(o)} := \frac{r}{\Lambda}\left[\partial_t h_1^{(o)} - r^2 \partial_r\left(\frac{h_0^{(o)}}{r^2}\right)\right] , \quad \Psi^{(e)} := \frac{r^2(\Lambda\kappa_1 + 4e^{-4b}\kappa_2)}{\Lambda[r(\Lambda-2)+6M]} . \tag{7.13}$$

These functions have dimensions of length. The linearized EFE lead, for both odd and even master functions, to wave equations of type

$$-\Psi^{\ell m}_{tt} + \Psi^{\ell m}_{r_* r_*} - V_\ell(r_*)\Psi^{\ell m} = S_{\ell m} , \tag{7.14a}$$

where the potentials are

$$V_\ell^{(o)} := A(r)\left(\frac{\Lambda}{r^2} - \frac{6M}{r^3}\right) \tag{7.14b}$$

$$V_\ell^{(e)} := A(r)\frac{\Lambda(\Lambda-2)^2 r^3 + 6(\Lambda-2)^2 M r^2 + 36(\Lambda-2)M^2 r + 72M^3}{r^3((\Lambda-2)r+6M)^2} \tag{7.14c}$$

These potentials are written in terms of the Schwarzschild radial coordinate not in terms of r_*. The potentials $V_\ell^{(e/o)}(r_*)$ decays exponentially near the horizon ($r_* \to \infty$) and as $1/r_*^2 \sim 1/r^2$ for $r_* \to \infty$; and they have maximum for $r_* \sim 2M$ ($r \sim 3M$), Fig. 7.1. Chandrasekhar (1985) has shown that one can transform the odd equation to the corresponding one for even modes via a transformation involving differential operations. It can also be shown that both odd and even perturbations are connected to the Bardeen-Press perturbation equation derived via the Newman-Penrose formalism. The source term $S_{\ell m}$ comes from the perturbation stress-energy tensor. Here, we mostly discuss the vacuum case $S_{\ell m} \equiv 0$, but a notable example of nonzero source is a particle perturbation. Note also that different conventions for the RWZ functions are used in the literature; we follow Nagar and Rezzolla (2005) where the different notations are also summarized.

Example 7.2.1. *An equation similar to the RWZ can be easily obtained for scalar perturbations of Schwarzschild by considering the box operator of the background metric,*

$$0 = \Box_{\bar{g}}\phi = (-\bar{g})^{1/2}\partial_\mu((-\bar{g})^{1/2}\bar{g}^{\mu\nu}\partial_\nu\phi) . \tag{7.15}$$

Expanding the solution in spherical harmonics

$$\phi(t, r, \theta, \varphi) = \frac{1}{r}\sum_{\ell=0}\sum_{m=-\ell}^{\ell}\phi_{\ell m}(t, r)Y_{\ell m}(\theta, \varphi) , \tag{7.16}$$

one finds that the cofficients $\phi_{\ell m}(t, r)$ satisfy the same equation as for odd tensor perturbation with a very similar potential (and $S_{\ell m} \equiv 0$).

7.3 Asymptotic waves

Let us sketch the connection between the odd and even-parity RWZ master functions and the plus and cross polarization amplitudes of the GWs in the TT gauge. The basic idea for computing the radiative part of the metric at null infinity is to consider retarded coordinates (u, r, θ, ϕ) and take the limit for $r \to \infty$ while keeping $u = const$. If the perturbed metric is expanded in $1/r$, then the radiative part is the part that decays as $1/r$ in asymptotically Cartesian coordinates. A procedure is the following:

[3] Note that inverse transformation is given by Lambert W-function $r = W(\pm e^{r_*-1}) + 1$, where $\pm$ are to be used for the exterior and interior respectively.

1. Transform the metric to Cartesian components $h_{\hat{\mu}\hat{\nu}}$,
$$h_{\hat{\mu}\hat{\nu}} = e^{\mu}_{\hat{\mu}} e^{\nu}_{\hat{\nu}} h_{\mu\nu} \ , \quad \text{with} \quad \boldsymbol{e} = \text{diag}\left(e^{a}, e^{-b}, r^{-1}, (r\sin^{-1}\theta)\right) \ ; \tag{7.17}$$
2. Require that the TT Cartesian components $h_{\hat{\theta}\hat{\theta}}, h_{\hat{\theta}\hat{\varphi}}, h_{\hat{\varphi}\hat{\varphi}}$ behave $\sim f(t-r)/r$ and satisfy the traceless condition $h_{\hat{\theta}\hat{\theta}} + h_{\hat{\varphi}\hat{\varphi}} = 0 + \mathcal{O}(1/r)$, while the others are $\mathcal{O}(1/r^2)$;
3. Infer the leading-order dependency of the metric perturbation in Eq. 7.1for large r;
4. For both odd and even parity perturbations take the plus and cross components as
$$h_{+}^{(o/e)} := \frac{1}{2}\left(h_{\hat{\theta}\hat{\theta}}^{(o/e)} + h_{\hat{\varphi}\hat{\varphi}}^{(o/e)}\right) \ , \quad h_{\times}^{(o/e)} := h_{\hat{\theta}\hat{\varphi}}^{(o/e)} \ . \tag{7.18}$$

Comparing the expression of the Cartesian components in term of the metric perturbation to the assumed asymptotic expressions leads to

$$h \sim \mathcal{O}(r) \ , \quad h_A^{(o)} \sim \mathcal{O}(1/r) \ ; \quad H_2 \sim \mathcal{O}(1/r^2) \ , \quad h_1^{(e)} \sim \mathcal{O}(1/r) \ , \quad K \sim \frac{\Lambda}{2}G + \mathcal{O}(1/r^2) \ , \quad rG \sim \mathcal{O}(1) \ . \tag{7.19}$$

Next, one needs to connect the perturbations above to the master function making use of the gauge-invariant equations. Specifically, for the odd parity one can use the linearized Hamiltonian constraint while for the even parity it is sufficient to calculate the asymptotic expression of the $\kappa_{1,2}$ quantities. The result is

$$\partial_t h = e^a \partial_r (r\Psi^{(o)}) + h_0^{(o)} \quad \Rightarrow \quad \frac{h}{r} \sim -\Psi^{(o)} + \mathcal{O}(1/r) \tag{7.20a}$$
$$\Psi^{(e)} \sim \frac{r}{2}G + \mathcal{O}(1/r^2) \, . \tag{7.20b}$$

Hence, the asymptotic expressions of the master functions are found to be $\Psi^{(e/o)} \sim 1$. Note that, although the Ψ have length dimension, they do not aymptotically depend on the radius. Putting together things in Eq. 7.18, one gets

$$h_{+}^{(o)} := \frac{1}{2}\left(h_{\hat{\theta}\hat{\theta}}^{(o)} + h_{\hat{\varphi}\hat{\varphi}}^{(o)}\right) = \frac{h}{r^2}(S^{\ell m}_{\theta|\theta} - \frac{1}{\sin^2\theta}S^{\ell m}_{\varphi|\varphi}) + \mathcal{O}(1/r^2) \tag{7.21a}$$
$$h_{\times}^{(o)} := h_{\hat{\theta}\hat{\varphi}}^{(o)} = \frac{h}{r^2}\frac{1}{\sin\theta}S^{\ell m}_{(\varphi|\theta)} + \mathcal{O}(1/r^2) \tag{7.21b}$$
$$h_{+}^{(e)} := \frac{1}{2}\left(h_{\hat{\theta}\hat{\theta}}^{(e)} + h_{\hat{\varphi}\hat{\varphi}}^{(e)}\right) = \frac{G}{2}(Y^{\ell m}_{|\theta\theta} - \frac{1}{\sin^2\theta}Y^{\ell m}_{|\varphi\varphi}) + \mathcal{O}(1/r^2) = \frac{G}{2}W^{\ell m} + \mathcal{O}(1/r^2) \tag{7.21c}$$
$$h_{\times}^{(e)} := h_{\hat{\theta}\hat{\varphi}}^{(e)} = G\frac{1}{\sin\theta}Y^{\ell m}_{|\theta\varphi} + \mathcal{O}(1/r^2) = \frac{G}{2}\frac{X^{\ell m}}{\sin\theta} + \mathcal{O}(1/r^2) \ . \tag{7.21d}$$

As a final step, it is useful to define

$$W^{\ell m} := \frac{1}{\sin\theta}S^{\ell m}_{(\varphi|\theta)} = \partial_{\theta\theta}Y_{\ell m} - \cot\theta\partial_\theta Y_{\ell m} - \frac{1}{\sin^2\theta}\partial_{\varphi\varphi}Y_{\ell m} \tag{7.22a}$$
$$X^{\ell m} := -\sin\theta\left(S^{\ell m}_{\theta|\theta} - \frac{1}{\sin^2\theta}S^{\ell m}_{\varphi|\varphi}\right) \tag{7.22b}$$

and the *spin weighted spherical harmonics of spin* $s = -2$

$${}^{2}Y_{\ell m}(\theta,\varphi) := \sqrt{\frac{(\ell-2)!}{(\ell+2)!}}\left(W_{\ell m}(\theta,\varphi) - \mathrm{i}\frac{X_{\ell m}(\theta,\varphi)}{\sin\theta}\right) \ . \tag{7.23}$$

The final result is the expression of the GW in the TT gauge far from the source in terms of the RWZ master functions

$$h_+ - \mathrm{i}h_\times = \frac{G}{c^4 r}\sum_{\ell=2}\sum_{m=-\ell}^{\ell}\underbrace{\sqrt{\frac{(\ell+2)!}{(\ell-2)!}}\left(\Psi^{(e)}_{\ell m} + \mathrm{i}\Psi^{(o)}_{\ell m}\right)}_{=:h_{\ell m}} {}^{-2}Y_{\ell m}(\theta,\varphi) + \mathcal{O}(1/r^2) \, . \tag{7.24}$$

Remark 7.3.1. *In general the* spin weighted spherical harmonics of spin s *are defined as*

$${}^{s}Y_{\ell m}(\theta,\varphi) := e^{\mathrm{i}m\varphi}(-1)^2\sqrt{\frac{2\ell+1}{4\pi}}d^{\ell}_{m,-s}(\theta) \tag{7.25}$$

where $d^{\ell}_{m,-s}$ *are the Wigner small-d matrices. They generalize the spherical harmonics for scalar functions on* S^2 *to functions on* S^2 *with spin weight* s*. The latter transform under a rotation of an angle* α *about the poles as* $F \mapsto e^{\mathrm{i}s\alpha}F$*. These functions represent fields with an additional U(1) symmetry. In case of GWs, one can see this by considering the transformation of the shear pseudoscalar* σ_0 *under a rotation of the real and imaginary part of the Newmann-Pensrose tetrad vector* $m^a = 1/\sqrt{2}(\hat{\theta} + \mathrm{i}\hat{\phi})^a$*.*

Remark 7.3.2. Connection to the multipolar waveform. *The multipoles $h_{\ell m}$ in Eq. (7.24) can be expressed as a PN series using the formalism of Chap. 4 and Chap. 6. The starting point are the expressions of the TT waveforms in terms of STF multipoles (Eq. (6.52)) and spherical tensor harmonics (Eq. (4.63)). Recalling the relations between STF tensors and spherical components of Chap. 4, the relations between the radiative multipole moments in Eq. (6.52) and the coefficients of the tensor spherical harmonics expansion in Eq. (4.63) are*

$$u_{\ell m} \propto U_L \mathcal{Y}^L_{\ell m} \ , \quad v_{\ell m} \propto V_L \mathcal{Y}^L_{\ell m} \ , \tag{7.26}$$

where the constants and ℓ-dependent factors are omitted. It is now sufficient to recall the expression of the spherical harmonics in terms of the STF spherical harmonics for a given unit vector N^i, Eq. (4.22)

$$Y_{\ell m} = \mathcal{Y}^L_{\ell m} N_L \ , \tag{7.27}$$

and combine Eq. (7.24), Eq. (4.63),Eq. (4.22), and Eq. (4.63) to find that the multipoles $h_{\ell m}$ are a combination of the multipoles of the tensor spherical harmonics decomposition Kidder (2008)

$$h_{\ell m} = \frac{G}{\sqrt{2} R c^{\ell+2}} \left(u_{\ell m} - \frac{\mathrm{i}}{c} v_{\ell m} \right) \ . \tag{7.28}$$

To lowest order the $u_{\ell m}, v_{\ell m}$ are given by Eq. (4.67) and Eq. (4.68). In particular,

$$u_{2m} \propto \frac{d^2}{dt^2} \int d^3x \, r^2 T^{00} Y^*_{\ell m} \ , \tag{7.29}$$

thus indicating that the $\ell = 2$ terms to lowest order reproduce the quadrupole formula.

7.4 Initial-boundary value problem (IBVP) for the RWZ

Let us now discuss the IBVP for the gravitational perturbations. Since the RWZ potential goes to zero for $r_* \to \pm\infty$, the RWZ equation without sources reduces to the a one dimension "free" wave equation for large $|r_*|$. The most general asymptotic solution at large radii $r_* \to \infty$ is thus described by the linear combination of an ingoing and an outgoing wave moving on the light cones of Mikowski spacetime. For example, if the solution is composed of a single Fourier mode, $\Psi \sim e^{-\mathrm{i}\omega(t \pm r_*)}$, then the outgoing to (ingoing from) infinity part is the one with the - (+). A standard boundary condition imposed at $r_* \to \infty$ is that the solution is composed of the outgoing wave solely. The asymptotic general solution near the horizon ($r_* \to -\infty$) can be also be described by the superposition of an ingoing and an outgoing wave. Because no signals can come from the the horizon, the physical boundary condition to be imposed for $r_* \to -\infty$ is that the solution is composed of the ingoing wave solely [4].

Further insights on the IBVP can be grasped by introducing the Fourier transform in time $\tilde{\Psi}(\omega, r_*) = \mathcal{F}[\Psi(t, r_*)]$. Letting $x = r_*/c$, the RWZ equation becomes

$$\tilde{\Psi}_{xx} + \left(\omega^2 - V_\ell(x)\right) \tilde{\Psi} = 0 \ . \tag{7.30}$$

The boundary conditions discussed above translate into the requirements

$$\tilde{\Psi} \sim e^{\pm \mathrm{i}\omega x} \ , \quad x \to \pm\infty \ . \tag{7.31}$$

for each Fourier mode. Eq. (7.30) is similar to the Schroedinger equation for stationary states. The choice of "the others" boundary conditions, namely in/out-going for $x \to \pm\infty$, would imply $\tilde{\Psi} = 0$ at the boundaries, and would map into a Schroedinger problem for bound states. But because the RWZ potential is positive, such bound states cannot exist (for any ω^2).

The physical situation described by the RWZ with these boundary conditions is the following. At an initial time one has a nonzero profile (an external perturbation or a matter source term in case $S_{\ell m} \neq 0$) of $\Psi(t = 0, r_*)$ localized on a spatial interval of the r_* domain. The solution of the IBVP determines how the wave propagates on the Schwazrschild background (represented by the V_ℓ potential) up to infinity and down to the horizon. The qualitative behaviour of the solution can be expected from a basic argument. Imagine the initial profile has compact spatial support on the right of the potential's peak and sufficiently far away such that V_ℓ is small. If $\partial_t \Psi(t = 0, r_*) = 0$, the solution will initially propagate by separating in the in/outgoing waves (i.e. the characteristics) on the approximately flat spacetime. The outgoing wave will reach infinity by keeping its amplitude approximately constant [5]. A detector at very large radius would thus record a first burst of radiation. The ingoing wave will instead interact with a larger and larger potential as time advances; part of it will continue down to the horizon but part of it could be reflected back to infinity [6]. This behaviour can be also interpreted as a wave on flat background with an effective refraction index $\omega^2_{\text{eff}} = \omega^2 - V_\ell$. The detector at very large radius would thus record a second burst of radiation different from the previous because modified by its interaction with the potential Fig. 7.1. We shall see below that this burst can carry information about the black hole spacetime.

[4] This boundary condition also follows from requiring smoothness of the solution.

[5] This is due to the use of the tortoise coordinates that "hide" the $1/r$ asymptotic behaviour of the spherical wave.

[6] One would be tempted to consider an analogy to the Schroedinger for scattering states. In those problems, however, one considers incoming waves from infinity that are not compatible with the outgoing boundary condition discussed above. A different boundary should be used for scattering.

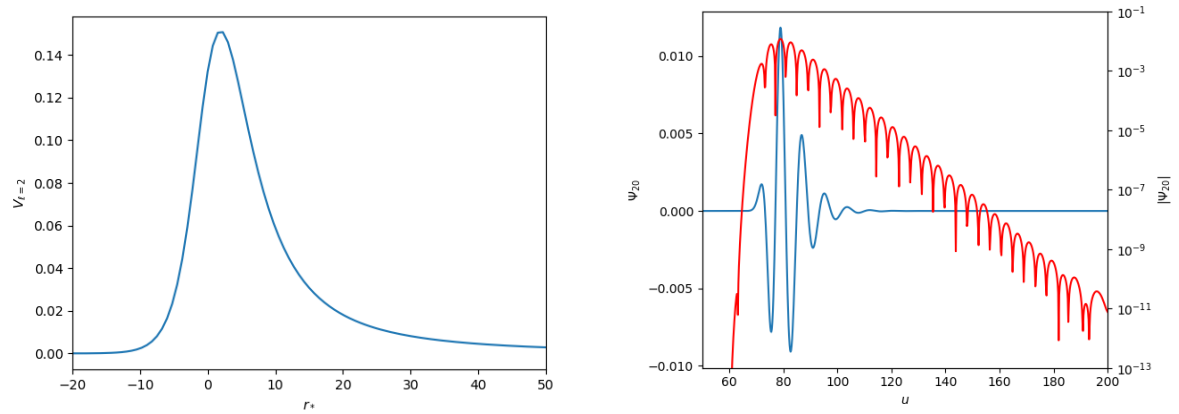

Figure 7.1: RW potential for $\ell = 2$ amd $M = 1$ as function of the tortoise coordinate (left) and time domain solution for $\Psi^{(o)}_{20}$ in vacuum as a function of the retarded time $u = t - r_*$ given a time-symmetric pulse as initial data (right). The solution is composed by precursor-burst and the ringdown (power law tails are not visible in the plot).

7.5 Quasi-normal-modes (QNMs)

Quasi-normal modes (QNMs) are damped and oscillating (exponentials with complex frequencies) solutions of a large class of mathematical problems describing physical "open systems". Examples of such systems are waves on an infinite string, resonances in a particles scattering experiment or gravitational emission from vibrating black holes. Note the spectrum of the differential operators describing these problems is purely continuous. QNMs are reviewed by many authors (Kokkotas and Schmidt, 1999; Nollert, 1999; Berti et al., 2009).

In perturbations of black holes, QNMs complex frequencies carry information on the mass (and spin) of the background BH solutions. Since these frequencies characterize the GW, they are observable and are of primary importance to probe black-hole spacetimes. The QNMs of the RWZ master function are visible in Fig. 7.1 as the exponentially damped oscillations starting at $u \sim 80$. QNMs can be studied considering the Fourier transform of the the RWZ. In this approach, the boundary conditions discussed above are imposed on the general solution of the RWZ for $\tilde{\Psi}$ and they select these discrete frequencies in a similar way the regularity/junctions condition determine the quantum levels of a quantum mechanical system described by the Schroedinger equation for stationary states. A more rigorous approach involves the use of the Laplace transform. This method allows one to solve the IBVP via Green functions including the initial data. The QNM complex frequencies emerge here as complex poles of the Green function (see below).

Let us start from the Fourier approach for the RWZ (Leaver, 1985). Using the Schwarzschild radial coordinates rescaled to the black hole mass (equivalent to let $M = 1$) the frequency-domain RWZ equation writes

$$r(r-1)\tilde{\Psi}_{rr} + \tilde{\Psi}_r + \left[\frac{\omega^2 r^2}{r-1} - \Lambda + \frac{\epsilon}{r}\right]\tilde{\Psi} = 0 \ , \tag{7.32}$$

where $\epsilon = -1, 0, 3$ for scalar, electromagnetic and gravitational perturbations. The equation above is known as the *generalized spheroidal wave equation*. The boundary conditions discussed above in the Schwarzschild radial coordinates are

$$\Psi \sim (r-1)e^{-\mathrm{i}\omega} \ , \quad r \to 1 \quad ; \quad \tilde{\Psi} \sim e^{\mathrm{i}\omega(r+\ln r)}, \quad r \to +\infty \ . \tag{7.33}$$

The problem admits a general solution given by the series

$$\tilde{\Psi} = (r-1)^s r^{-2s} e^{-s(r-1)} \sum_{n=0}^{\infty} a_n \left(\frac{r-1}{r}\right)^n \ , \tag{7.34a}$$

where $s := -\mathrm{i}\omega$ and the series' prefactor incorporates the boundary conditions that are satisfied if the series converges. The a_n coefficients satisfy the recursion relations

$$a_0 = 1 \ , \quad \alpha_0 a_1 + \beta_0 a_0 = 0 \ , \quad \alpha_n a_{n+1} + \beta_n a_n + \gamma_n a_{n-1} = 0 \ , \tag{7.34b}$$

with

$$\alpha_n = n^2 + (2s+2)n + 2s + 1 \tag{7.34c}$$
$$\beta_n = -(2n^2 + (8s+2) + 8s^2 + 4s + \Lambda - \epsilon) \tag{7.34d}$$
$$\gamma_n = n^2 + 4sn + 4s^2 - \epsilon - 1 \ . \tag{7.34e}$$

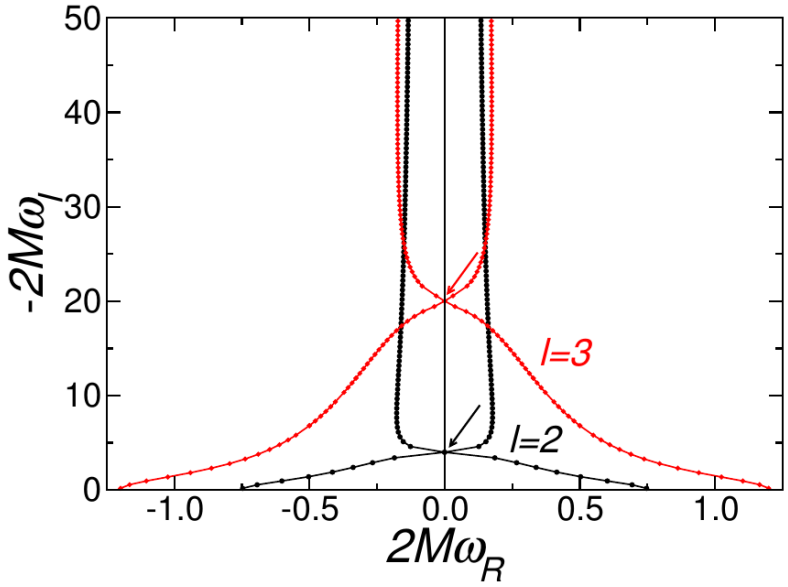

Figure 7.2: The spectrum of QNM for a Schwarzschild black-hole, for $\ell = 2$ (diamonds) and $\ell = 3$ (crosses). The arrow indicate the purely imaginary frequency. From Berti et al. (2009).

A further condition to impose is that the series converges and it is finite. The behaviour of the series at infinity,

$$\frac{a_{n+1}}{a_n} \sim 1 \pm \sqrt{\frac{2s}{n}} + \frac{2s - 3/4}{n} + \dots \quad n \to \infty \,, \tag{7.35}$$

indicates that uniform convergence is obtained only with the minus sign. This condition selects particular values of s in the following way. The convergence condition of the series translates into the convergence of the continued fraction,

$$\frac{a_{n+1}}{a_n} = \cfrac{-\gamma_{n+1}}{\beta_{n+1} - \cfrac{\alpha_{n+1}\gamma_{n+2}}{\beta_{n+2} - \cfrac{\alpha_{n+2}\gamma_{n+2}}{\beta_{n+3} + \dots}}} \,. \tag{7.36}$$

For a given frequency s, the three-term recurrence relation for a_n possesses two linearly independent solutions. The solution that converges to zero for $n \to \infty$, called the minimal solution, is obtained for the values of s that satify the $n = 0$ continued fraction equation. The QNM are then defined by the infinite roots s of the infinite continued fraction equation

$$0 = -\frac{\beta_0}{\alpha_0} = \frac{a_1}{a_0} = \cfrac{-\gamma_1}{\beta_1 - \cfrac{\alpha_1\gamma_2}{\beta_2 - \cfrac{\alpha_2\gamma_2}{\beta_3 + \dots}}} \,. \tag{7.37}$$

Their explicit determination require to truncate the recursion and a numerical method to find the root.

Figure 7.2 shows some of the modes of the Schwarzschild black hole. Tables and scripts to compute them are available on e.g. Berti's website (Berti et al., 2009). The number of modes (overtones) for each harmonic index ℓ is infinite Bachelot and Motet-Bachelot (1993). The imaginary part of the frequency is negative and grows very quickly (this is also true for the higher ℓ modes): this means that the higher modes do not contribute significantly in the emitted gravitational wave signal. Note the real part is not monotonically decreasing with the overtones and it is largest for the fundamental tone. This is in contrast to the picture of a vibrating and damped string for which the fundamental mode has the lowest frequency and longest damping time and the overtone have a monotonic dependence. An interpretation of QNMs in terms of forced hamornic oscillator modes is discussed in Maggiore (2008). There is also a special purely imaginary QNM frequency whose value increases with ℓ [7].

Example 7.5.1. *A toy model reproducing the key feature of QNMs is the RWZ master equation with the* Pöschl-Teller potential

$$V(x) = \frac{V_0}{\cosh^2(\alpha x - x_0)} \tag{7.38}$$

where $V_0 = V(x_0)$ is the maximum of the RWZ potential and $\alpha^2 := -V''(x_0)/(2V_0)$. This potential is rapidly decaying for $x \to \pm\infty$ and allows one to find the QNM analytically. Introduce now a new independent variable and a rescale the master function as

$$\xi := (1 + e^{-2\alpha(x - x_0)})^{-1} \,, \quad y := \tilde{\Psi}/(\xi(1-\xi))^{\mathrm{i}\omega/2\alpha} \,. \tag{7.39}$$

[7] The curious reader can find more about this starting from the various reviews referenced in the notes.

Near infinity ($\xi = 1$) $1-\xi \sim e^{-2\alpha(x-x_0)}$ and near the horizon ($\xi = 0$) $\xi \sim e^{2\alpha(x-x_0)}$. Eq. (7.30) reduces to a hypergeometric equation

$$\xi(1-\xi)\partial_{\xi\xi} y + [c - (a_+ + a_- + 1)\xi]\partial_\xi y - a_+ a_- y = 0 \ , \tag{7.40}$$

where $a_\pm = [\alpha \pm \sqrt{\alpha^2 - 4V_0} - 2\mathrm{i}\omega]/(2\alpha)$, $c = 1 - \mathrm{i}\omega/\alpha$. The solution is therefore expressed via the hypergeometric series $F(a,b,c,z)$ as

$$\tilde{\Psi} = A\xi^{\mathrm{i}\omega/2\alpha}(1-\xi)^{-\mathrm{i}\omega/2\alpha}F(a_+ - c + 1, a_- - c + 1, 2 - c, \xi) + B(\xi(1-\xi))^{-\mathrm{i}\omega/2\alpha})F(a_+, a_-, c, \xi) \ , \tag{7.41}$$

where A, B are two constants determined by the properties of the hypergeometric function and by the boundary conditions. Because $F(a,b,c,0) = 1$ and $\xi e^{\mathrm{i}\omega/2\alpha} \sim e^{\mathrm{i}\omega x}$, the boundary condition at the horizon implies that $A \equiv 0$. To impose the boundary condition at infinity one observes that $\Psi \sim Be^{\mathrm{i}\omega x}F$, and thus the latter translates in to a sort of "quantization rule" for the parameter $q_\pm$. By considering the transformation of $F(a,b,c,\xi)$ under $\xi \to 1-\xi$, (Abramowitz and Stegun, 1964),

$$F(a,b,c,z) = (1-z)^{c-a-b}\frac{\Gamma(c)\Gamma(a+b-c)}{\Gamma(a)\Gamma(b)}F(c-a,c-b,c-a-b+a,1-z) + \frac{\Gamma(c)\Gamma(c-a-b)}{\Gamma(c-a)\Gamma(c-b)}F(a,b,-c+a+b+1,1-z) \ , \tag{7.42}$$

the "B" term of the solution is consistent with the boundary condition if it a constant. Since $c - a_+ - a_- = \mathrm{i}\omega/\alpha$ and $(1-\xi)^{c-a_+-a_-} \sim e^{-\mathrm{i}\omega x}$, one must demand that $1/\Gamma(a_\pm) = 0$. The QNM of the Pöschl-Teller potential follows from this condition,

$$\omega = \pm\sqrt{V_0 - \alpha^2/4} - \mathrm{i}\alpha(2n+1)/2 \ , \quad n = 0, 1, 2, ... \tag{7.43}$$

The first overtone approximate rather well the RWZ value $M\omega = 0.3737 - \mathrm{i}0.0890$.

Example 7.5.2. *An approximate analytic expression for the QNM can be found by applying the* Wentzel-Kramers-Brillouin (WKB) *method of quantum mechanics. The physical scenario is the following. Eq. (7.30) is analgous to a 1D Schrödinger equation for a mass m in a potential barrier $V(x)$*

$$\tilde{\Psi}_{xx} + Q(x)\tilde{\Psi} = 0 \ , \quad \textit{with} \ \ Q(x) := \frac{2m[E - V(x)]}{\hbar} \ . \tag{7.44}$$

The potential (and $Q(x)$) tends to constant values for $x \pm \infty$. One considers an energy below the peak of the potential, a wave package comes-in from $x \sim +\infty$ and gets in part reflected and in part transmitted. The reflected amplitude is generally comparable to the incident amplitude, while the transmitted amplitude is much smaller. In the WKB approach one formally multiplies the Ψ_{xx} by a small parameter and looks for a series solution of the small transmitted wave whose leading order term is given by the solution of the Eikonal equation,

$$(\tilde{\Psi}^{(0)}_x)^2 = -Q \quad \Rightarrow \quad \tilde{\Psi}^{(0)} = \int dx\sqrt{-Q(x)} \ . \tag{7.45}$$

The transmitted amplitude is obtained by integrating $(-Q)^{1/2}$ between the turning points of the potential barrier $V(x)$. The gravitational problem is different in the sense that there is no incoming wave from infinity (the boundary condition there is outgoing) but some gravitational perturbation is initially prescribed. Thus, in general, one does not expect the transmitted wave to be smaller than the reflected but of approximately the same amplitude. However, there exists a quantum mechanical case similar to this: the case $\max[Q] \sim 0$, i.e. for the energies in the quantum mechanics (squared frequencies for the BH case) comparable to the peak of the potential. Following this idea, Schutz and Will (1985) consider $\max[Q] \gtrsim 0$ and propose to match the two WKB solutions, valid for $x < x_1$ and $x > x_2$ such that $Q(x_{1,2}) = 0$, to an approximate solution in the region $x_1 < x < x_2$ around $x = x_0$, the point of $\max[Q]$. This gives QNM frequencies approximated by the value of the potential and its second derivative at the peak,

$$(M\sigma)^2 \approx V_\ell(r_0) - \mathrm{i}(n + \frac{1}{2})\left(-2V''_\ell(r_0)\right)^{1/2} \ , \tag{7.46}$$

where n is the quantum number labelling the overtones. This method works well for estimating the fundamental mode and can be applied also to other than gravitational perturbations.

Remark 7.5.1. *Nollert and Schmidt (1992) pointed out that the asymptotic boundary conditions in Eq. (7.31)* are not sufficient to specify a unique solution *of the IVBP. This is simple to see. Consider the boundary at $x \to \infty$ and the solution $\tilde{\Psi}_1$ of the IVBP corresponding to the boundary $\tilde{\Psi}_1 = e^{-\mathrm{i}\omega x}(1 + \mathcal{O}(1/x))$. Now take another solution corresponding to the asymptotic behaviour $\tilde{\Psi}_0 = e^{+\mathrm{i}\omega x}(1 + \mathcal{O}(1/x))$, and combine it to the first,*

$$\tilde{\Psi}_2 = \tilde{\Psi}_1 + \tilde{\Psi}_0 = e^{-\mathrm{i}\omega x}\left[1 + \mathcal{O}(1/x) + e^{+2\mathrm{i}\omega x}\left(1 + \mathcal{O}(1/x)\right)\right] = e^{-\mathrm{i}\omega x}\left(1 + \mathcal{O}(1/x)\right) \ . \tag{7.47}$$

This is another solution since the term $e^{+2\mathrm{i}\omega x}$ for positive imaginary part of ω vanishes faster than any power of x. This counter-example suggests that, differently from the normal modes of the finite string, if complex modes $e^{\mathrm{i}\omega x}$ with $\Im(\omega) > 0$ appears as possible solution, then the specification of the asymptotoc behaviour does not guarntee uniqueness. Moreover, these modes become unbounded at both the horizon and spatial spatial infinity. This fact is a consequence of the fact that for generic potentials the differential operator associated to the problem is not self-adjoint and the Fourier modes do not represent a complex set. A Laplace analysis clarifies these issues.

Laplace transform approach to solve the Cauchy problem. We discuss the Laplace method for the general solution of the initial value (Cauchy) problem and then specialize it to the case of the RW equation.

Let us consider the Cauchy problem for the wave equation for $\Psi(t,x)$ with $x\in\mathbb{R}$ and $t\in\mathbb{R}^+$

$$\Psi_{tt}-\Psi_{xx}+V(x)\Psi=0 \tag{7.48a}$$
$$\Psi(0,x)=\psi(x) \tag{7.48b}$$
$$\Psi_t(0,x)=\psi_t(x) \tag{7.48c}$$

with a potential $V(x)>0$ that is real, continuous and decays as $V(x)\sim\mathcal{O}(1/|x|)$ for large x, If the initial data have compact support or are sufficiently localized, then the solution Ψ is bounded and admits a Laplace transform. The Laplace transform of the solution $\Psi(t,x)$ is

$$\phi(s,x)=\mathcal{L}[\Psi]:=\int_0^\infty e^{-st}\Psi(t,x)dt \tag{7.49}$$

and it is defined for $\Re(s)>0$ and can be analytically continued into $\Re(s)<0$. By integrating the equation for Ψ one finds that the function $\phi(s,t)$ satisfies the equation

$$-\phi_{xx}+\left(s^2+V(x)\right)\phi=F(s,x)\ , \tag{7.50}$$

with F defined by the problem's initial data

$$F(s,x):=s\psi(x)+\psi_t(x)\ . \tag{7.51}$$

Given two independent solutions, $f^\pm(s,x)$, of the homogeneous equation ($F=0$), the solution of Eq. (7.50) is

$$\phi(s,x)=\int_{-\infty}^{+\infty}\hat{G}(s;x,x')F(s,x')dx'\ , \tag{7.52}$$

where the Green function generated from the homogeneous independent solutions is defined as

$$\hat{G}(s;x,x'):=\frac{1}{W(s)}\left[\theta(x-x')f^-(s,x')f^+(s,x)+\theta(x'-x)f^-(s,x)f^+(s,x')\right]=\frac{f^-(s,x_<)f^+(s,x_>)}{W(s)}\ , \tag{7.53}$$

with $x_<=\min(x,x')$, $x_>=\max(x,x')$, and the *Wronkskian* is defined as

$$W(s):=f^-(s,x)f^+_x(s,x)-f^-_x(s,x)f^+(s,x)\ . \tag{7.54}$$

Note $W(s)$ does not depend on x because $W_x=0$, which follows by the fact that $f^\pm$ are solutions of the homogeneous equation:

$$W_x=\cancel{f^-_x f^+_x}+f^-f^+_{xx}-f^+_x f^-_x-\cancel{f^+f^-_{xx}}=(V+s^2)(f^+f^--f^+f^-)\equiv 0\ . \tag{7.55}$$

It is straightforward to verify that the Green function satisfy an equation like Eq. (7.50) with Dirac's source term $F(x)=\delta(x)$ [exercise]. The formal solution of the Cauchy problem is then obtained from the inverse Laplace transform of ϕ

$$\psi(t,x)=\mathcal{L}^{-1}[\phi]:=\frac{1}{2\pi\mathrm{i}}\lim_{R\to\infty}\int_{\epsilon-\mathrm{i}R}^{\epsilon+\mathrm{i}R}e^{st}\phi(s,x)ds \tag{7.56a}$$
$$=\frac{\partial}{\partial t}\int_{-\infty}^{+\infty}G(t;x,x')\psi(x')dx'+\int_{-\infty}^{+\infty}G(t;x,x')\psi_t(x')dx' \tag{7.56b}$$

where

$$G(t;x,x'):=\mathcal{L}^{-1}[\hat{G}]=\frac{1}{2\pi\mathrm{i}}\lim_{R\to\infty}\int_{\epsilon-\mathrm{i}R}^{\epsilon+\mathrm{i}R}e^{st}\hat{G}(s;x,x')ds\,. \tag{7.57}$$

In the inverse Laplace calculation, ϵ is a real number greater than the real part of all singularities of $\phi(s)$. In practice, the integral is evaluated by chosing a closed path enclosing on the left the singularities of $\phi(s)$ and using Cauchy's residue theorem.

The above formal solution of the Cauchy problem highlights that the Green function $G(t;x,x')$ propagates the initial data at times $t>0$. The expression also contains the requirement that the solution is bounded; this condition is implemented in the two solutions $f^\pm(s,x)$ of the homogeneous equation that must be chosen as bounded functions (or, in general, as functions fullfilling the problem's boundary conditions on the spatial domain).

Example 7.5.3. *The immediate application of the Laplace method is the* wave equation for a string with fixed ends *at $x=0,\pi$. Here one takes the wave equation with zero potential, arbitrary initial data and boundary conditions given by $\Psi(\cdot,x=0)=0=\Psi(\cdot,x=\pi)$ (at all times). The formalism described above applies with the only change that the*

spatial integrals must be restricted to the domain $\Omega = [0, \pi]$ and the homogeneous solutions must satisfy the boundary conditions at $x = 0, \pi$.

It is well known that the general solution to this problem is given by a superposition of normal modes *(NMs)*

$$\Psi(t, x) = \sum_{n=1}^{\infty} A_n \sin(nx) e^{int} \tag{7.58}$$

where the constants A_n are determined by the initial data. The result above can be directly verified using the separation of variable technique [exercise]. This problem is self-adjoint and the NMs form a complete set for the solutions' space.

Apply now the the Laplace method to obtain the same result. The two independent solutions of the homogeneous equation in Laplace space that satisfy the boundary conditions at $x = 0, \pi$ are

$$f^-(s, x) = e^{sx} - e^{-sx} \propto \sin(sx) \quad , \quad f^+(s, x) = e^{sx} - e^{-sx+2\pi s} \ . \tag{7.59}$$

They are entire functions of s, hence $\hat{G}$ is meromorphic on the whole complex plane and the only poles are those of the Wronskian. The Wronskian is

$$W = -2s \left(e^{\pi s} - s^{-\pi s}\right) \tag{7.60}$$

and has zeros $s_n = \mathrm{i}n$ with $n \in \mathbb{Z}$. The Taylor expansion of W near its zeros is $W \sim -[n\pi \cos(n\pi)](s - n)$, so the Green function $\hat{G}(s; x, x')$ has simple poles at s_n. The homogeneous solutions calculated at s_n are not anymore independent but

$$f^+(s_n, x) \propto f^-(s_n, x) = f_n(x) := \sin(nx) \, . \tag{7.61}$$

The asymptotic behaviour of the Green function for $|s| \gg 1$ is

$$\hat{G}(s; x, x') \sim \begin{cases} -\frac{e^{+s|x-x'|}}{2s} & \Re(s) < 0 \\ +\frac{e^{-s|x-x'|}}{2s} & \Re(s) > 0 \, . \end{cases} \tag{7.62}$$

The calculation of the inverse laplace transform $G(t; x, x') = \mathcal{L}^{-1}[\hat{G}]$ requires to chose a contour in the complex s-plane. The vertical line at $\epsilon > 0$ can be closed with a contour on the right or on the left. Eq. (7.62) for $\Re(s) < 0$ implies that the integral over the left semicircle vanishes for $t > 0$. However, the left contour encloses the poles, so the contribution of the residuals gives

$$G(t; x, x') = -\sum_n \mathrm{Res}\left(e^{st} \frac{f^-(s, x_<) f^+(s, x_>)}{W(s)}\right) = \sum_n \mathcal{N}_n e^{s_n t} f_n(x) f_n(x') \, , \tag{7.63}$$

wher $\mathcal{N}_n \propto 1/W'(s_n)$ is a normalization constant. The right contour does not contain poles but the integral over the right semicircle vanishes only for $t < |x - x'|$ (Eq. (7.62) for $\Re(s) > 0$). Hence, $G(t; x, x') = 0$ for $t < |x - x'|$ that indicates the sum in the previous equation must converge to zero at early times. Combining these findings the Green function can be written as

$$G(t; x, x') = \theta(t - |x - x'|) \sum_n \mathcal{N}_n e^{s_n t} f_n(x) f_n(x') \, , \tag{7.64}$$

from which the causal structure of the solution emerges. Finally, using Eq. (7.56a) the solution can be immediately written as in Eq. (7.58) where the amplitudes are given by

$$A_n = \mathcal{N}_n \int_0^{\pi} \left[s_n \psi(x) + \psi_t(x)\right] f_n(x') dx' \, . \tag{7.65}$$

Summarizing: (i) the poles s_n are the normal oscillation frequencies of the string, (ii) the homogeneous solutions at the poles $f_n(x) := \sin(nx)$ are the NM of the solution that evolve in time as $e^{s_n t}$, (iii) the NM evolution is determined uniquely by the Green function and the boundary conditions, and includes the causal behaviour, (iv) the excitation coefficients are determined uniquely by the initial data. These results carry over in presence of a potential provided the boundary conditions remains the same.

QNMs in the Laplace approach. Let us see how QNMs generically emerge in the solution of the Cauchy problem obtained with the Laplace method. The asymptotic ("boundary") conditions for the no-incoming radiation (either from the horizon or spatial infinity) are specified on the homogenous functions and for $\Re(s) > 0$ as

$$f^{\mp} \sim e^{\pm sx} \quad \text{for } x \to \mp\infty \, . \tag{7.66}$$

These conditions guarantee that the solution is squared integrable at infinity for $\Re(s) > 0$. The operator defined by Eq. (7.50) with $F \equiv 0$ and the above conditions is not self-adjoint. As such, the eigenvalues $-s^2$ are not necessarily real. We might now follow similar steps to the fixed string but we would immediately realize that the computation of the Green function and its analytical continuation for $\Re(s) < 0$ become significantly more complex and depends on the shape of the potential. Hence, let us start with a few simplified hypotheses that allows us to stay as close as possible to the derivation of the normal modes but necessarily departs from the case of Schwarzschild perturbations. This instructive because it highlights some of the issues that arise when computing and interpreting QNMs.

We will first assume the following holds:

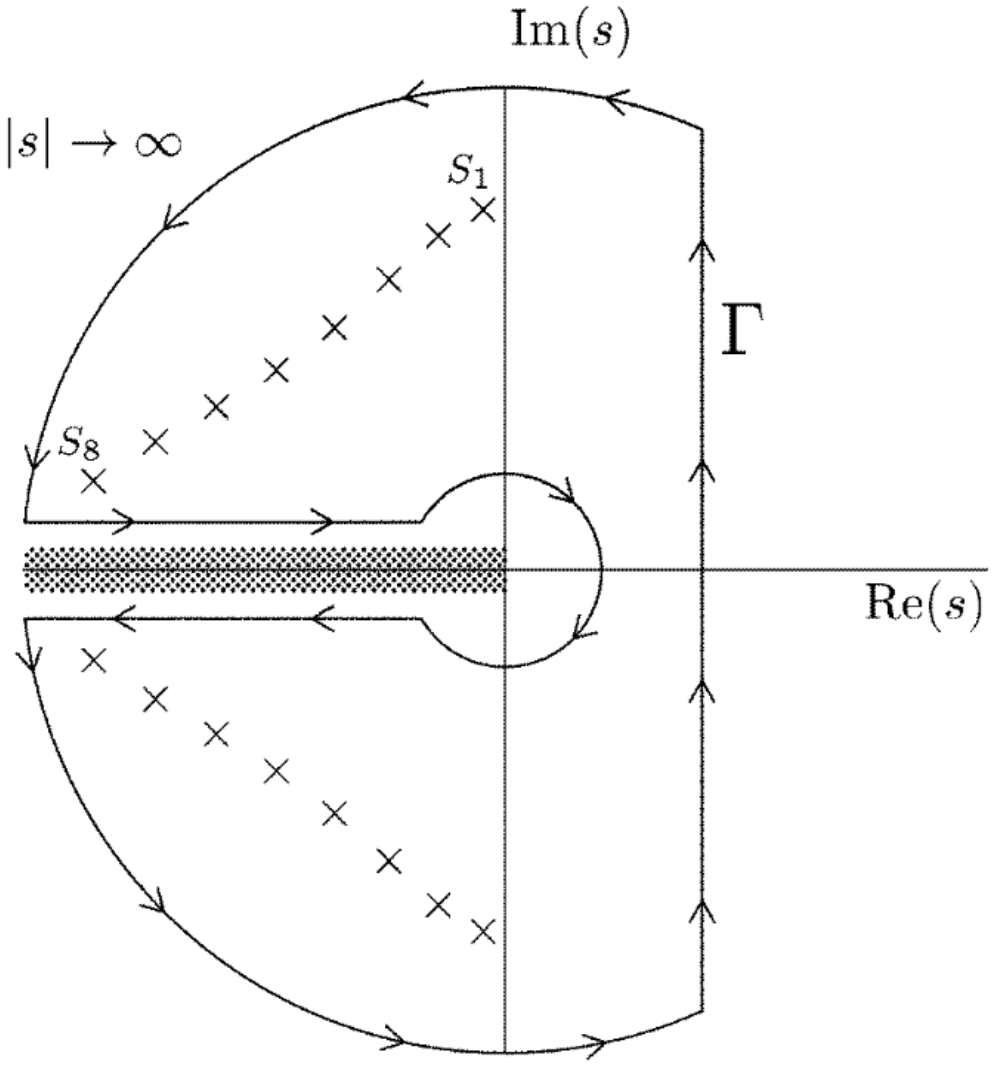

Figure 7.3: Contour of integration of the Green function for Schwarzschild QNMs. (From (Nollert, 1999).)

1. There are no essential singularities;
2. The homogeneous solutions $f^{\pm}(s,x)$ are analytic;
3. The integral on the left semicircle vanishes;
4. The initial data has compact support.

Under these conditions we can perform all the steps done for the finite string and formally obtain a similar result in the form

$$G(t;x,x') = \sum_n \mathcal{N}_n e^{s_n t} f_n(x) f_n(x')\,, \tag{7.67}$$

but where now s_n are *complex* poles on the left complex s-plane and the quasi normal modes have asymptotic behaviour $f_n \sim e^{-s_k|x|}$ for $|x| \to \infty$. These quasi-normal modes are now defined by analytical continuation to $\Re(s) < 0$, which implies they are bounded because they have the same expressions as those (bounded) defined for $\Re(s) > 0$. Hence, the solution does not respect the square integrability condition for $\Re(s) < 0$. The solution of the problem requires to consider the calculation of the amplitudes A_n, now with the complex QNMs f_n, and also to carefully consider the time development of the initial data. The physical interpretation of the solution must consider the particular physics scenario and the particular potential $V(x)$. Nonetheless, the analytical continuation guarantees the solution is unique (differently from the Fourier approach) and the complex poles of the Green function provides a robust deiniftion of QNMs. This definition immediately connects with the Fourier transform approch by letting $s = i\omega$.

QNMs of Schwarzrschild BH. In the case of Schwarzschld perturbations, the RW $V(x)$ decays exponentially for $x \to -\infty$, it reaches a maximum and then decays as $1/x^2$ for $x \to +\infty$. Leaver (1985); Bachelot and Motet-Bachelot (1993) proved that

1. $f^{-}(s,x)$ is analytic;
2. $f^{+}(s,x)$ has an essential singularity in $s = 0$, a brunch cut in the negative real axis, $\Re(s) < 0$ and $\Im(s) = 0$, and poles in the plane $\Re(s) < 0$.

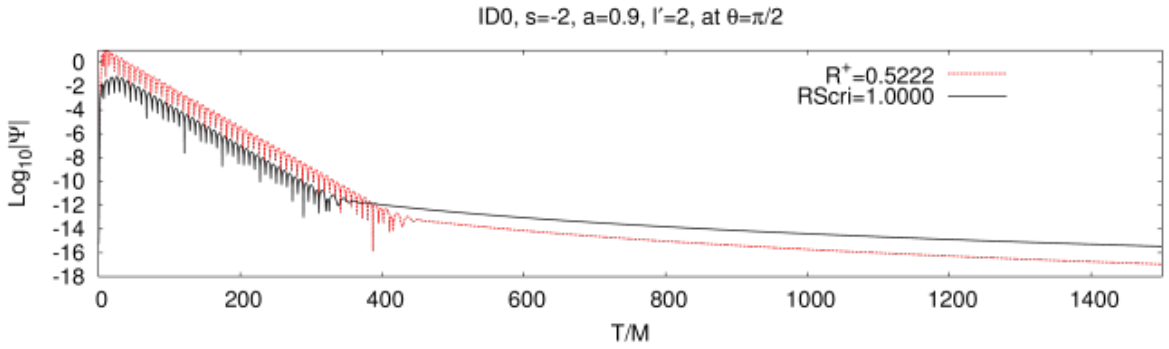

Figure 7.4: Perturbations of a Kerr BH with dimensionless spin $a = 0.9$. The perturbative field is in this case the Weyl scalar Ψ_4 decomposed into axizimuthal $m-$ modes and evolved according to the Teukolsky equation. The field is extracted at null infinity and at a large distance. One can appreciate the same structure as for Schwarzschild perturbations and that the power-law tails have different exponents depending on wether they are extracted at null infinity or finite distance. (From (Harms et al., 2013).)

The contour for inverse Laplace transform is shown in Fig. 7.3. It must be chosen as made of a segment $[\epsilon - \mathrm{i}R, \epsilon + \mathrm{i}R]$ parallel and on the right of the imaginary s-axis, a small circle γ_r around the origin and two segments $\delta_r^{\pm}$ above and below the negative real axis. The contour is closed with two quarters of a circle $\Gamma_R^{\pm}$ in the IV and III quadrants of the complex plane. The solution is now schematically given by

$$\Psi \sim \int_{\epsilon-\mathrm{i}R}^{\epsilon+\mathrm{i}R}(...) = \underbrace{\int_{\Gamma_R^+}(...) + \int_{\Gamma_R^-}(...)}_{\text{early times}} - \underbrace{\sum_k \mathrm{res}(..., s_k)}_{\text{QNMs}} + \underbrace{\int_{\delta_r^+}(...) + \int_{\delta_r^-}(...) + \int_{\gamma_r}(...)}_{\text{late times}} \,. \tag{7.68}$$

The different integrals contribute to the solution at different times. They compose the structure *precursor, burst, ringdown and tail* we see in Fig. 7.1. The precursor and the burst are early time contributions, and they dependent on the initial data. QNMs follow the peak of the radiation. The late time solution (not shown in the figure) is determined by the fall-off faster behaviour of the potential. A potential that at large radii falls-off as a power or x, generates power-law tails in the solution $\Psi \sim t^{-p}$, with p dependent on the multipolar index ℓ, on the perturbation's spin. The solution's power-law tail also depend on the class of initial data and on the spatial position at which the time solution is evaluated, Fig. 7.4. For example, tail decays are different for scalar and gravitational perturbations, for the solutions at scri and at finite radius. Power-law tails are not present for compact support potentials [8]. QNMs are generate at intermediate times by the interaction of the wave with the peal of the potential (Cf. Poschl-Teller and WKB). Hence, they carry the signature of the background spacetime from the region of largest curvature.

7.6 Effectiveness of perturbation theory

Perturbation theory is important to describe astrophysical processes.

- 'Scattering" of GWs. Vishveshwara (1970a) first pointed that the response of a black hole to a perturbation is of the type summarized in Fig. 7.1, and that the ringdown waveform carries in the QNM the "signature" of the BH.
- Plunges of small objects (particles) into a BH. Davis et al. (1999) studied the waveform produced by the radial plunge of a particle, Fig. 7.6. The waveform has the same structure precursor-burst-ringdown-tail highlighted by Vishveshwara.
- In a series of works Ipser and Thorne (1968); Thorne (1969); Campolattaro and Thorne (1970) studied perturbations of spherical neutron stars thus starting the field of GW asteroseismology (Andersson and Kokkotas, 1998).
- Deformation (polarization coefficients) of neutron stars (Damour, 1983; Hinderer, 2008; Damour and Nagar, 2009; Binnington and Poisson, 2009);
- Nonspherical Gravitational collapse to BH. Cunningham et al. (1978, 1979); Seidel (1990) have computed with perturbation theory the main feature of the waveform generated in the gravitational collapse (see below).

The above results are also relevant to understand the main features of more complex astrophysical processes, e.g.

- The black hole's ringdown is a generic late-time feature in any binary black hole collisions.
- Numerical relativity simulations of rotational collapse to black holes shown that the waveform morphology is the same predicted by perturbation theory, see Fig. 7.6.

[8] The Poschl-Teller potential mimics the peak of the Regge-Wheeler potential but has exponential decay for $x \to \infty$; no tails are present.

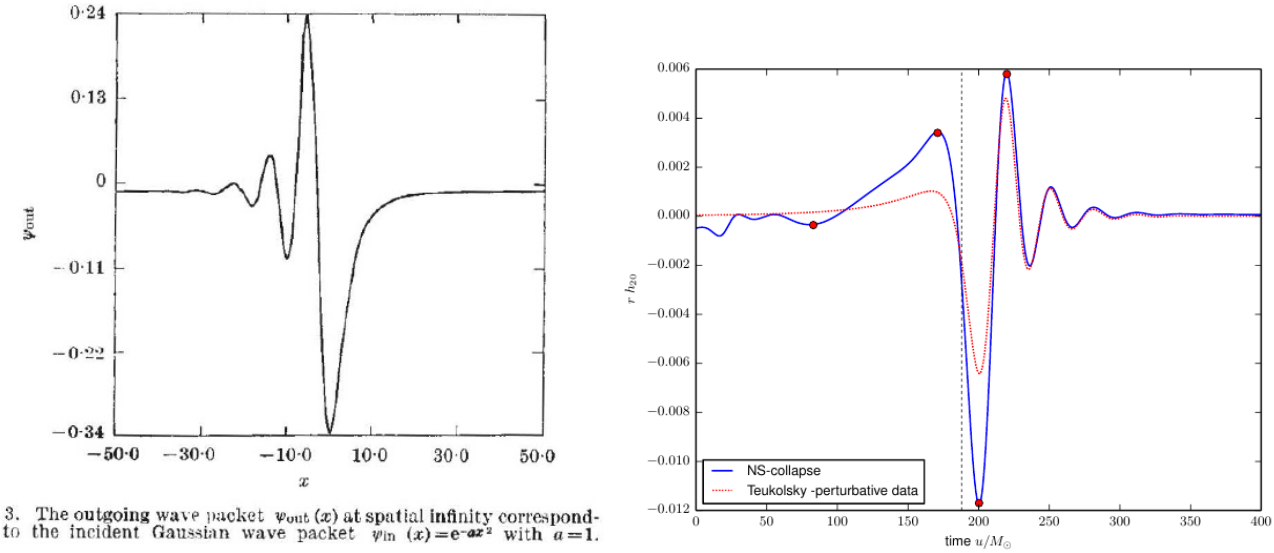

Figure 7.5: Left: The original plot of Vishveshwara (1970a). Note the x-axis is not not the asymptotic (null) time but the space coordinate, thus the "opposite" sign ($u = t - x$). Right: Ψ_{20} waveform from a 3+1 simulation of gravitational collapse to BH in numerical relativity and a waveform from a particle's radial plunge on a Kerr black hole with the same spin (From (Dietrich and Bernuzzi, 2015)).

- GW asteroseismology is relevant to understand the properties and the signatures of radiating isolated neutron stars but also the proto- neutron star resulting from the core collapse supernovae remnants. The ultimate applications are related to constratining the nuclear equation of of state and the explosion mechanism.

7.7 Stability of black hole spacetimes

A fundamental question about exact stationary solutions of EFE like Minkowski, Schwarzschild or Kerr is their stability under small perturbations. Stability is key for assessing the relevance of these solutions. Rigorous proofs are very nontrivial and usually build on several results. A very rough scheme is the following:

- Linear mode stability: within linear perturbation theory one should prove that the time evolution of each mode $\Psi_{\ell m}$ is bounded (in some norm) for a suitable class of initial data (say, with compact support).
- Linear stability: mode stability does not, in general, guarantee that a solution composed of an infinite sum of modes remains bound. One should prove that all solutions to the linearised EFE remain bounded for all time by a suitable norm of their initial data. Note that mode stability is a necessary condition to linear stability.
- Nonlinear stability: here one considers the more general Cauchy problem in GR with initial data given by Minkowski/Schwarzschild or Kerr plus small deviation. For example, nonlinear stability of Mikowski for asymptotically flat vacuum initial data has been proven by Christodoulou and Klainerman (1993).

The question of stability for black hole spacetimes is still open, although many positive results are available. An incomplete list of results follows.

- Regge and Wheeler (1957); Vishveshwara (1970b) proposed the first arguments for mode stability. The solutions of the RWZ equation composed of QNM and power law tails discussed above suggests that the perturbations radiate away and decay in time.
- Linear stability of scalar perturbation to Schwarzschild has been proven by Kay and Wald (1987).
- Linear stability of Schwarzschild was proven by Dafermos et al. (2019).
- Nonlinear stability of Schwarzschild was proven by Klainerman and Szeftel (2017) for a class of nontrivial perturbations.
- Mode stability of Kerr was proven by Whiting (1989).
- Linear stability of scalar perturbation of nonextremal Kerr BH was proven by Dafermos et al. (2014).
- All extremal Kerr BH are unstable to gravitational perturbation along their event horizon (Aretakis, 2015).
- Non-linear stability of the Schwarzschild black hole family (Dafermos et al., 2021)

7.8 Tidal Love numbers

Perturbations of spherical spacetimes can be used to calculate the response of a (spherical) compact object to an external gravitational field. An important application for gravitational-wave astronomy, already mentioned above, is the study of the oscillations and deformations of neutron stars (Nollert, 1999; Kokkotas and Schmidt, 1999; Stergioulas, 2003). For example, stationary perturbations of Tolmann-Oppenheimer-VOlkoff (TOV) star spacetimes can be used

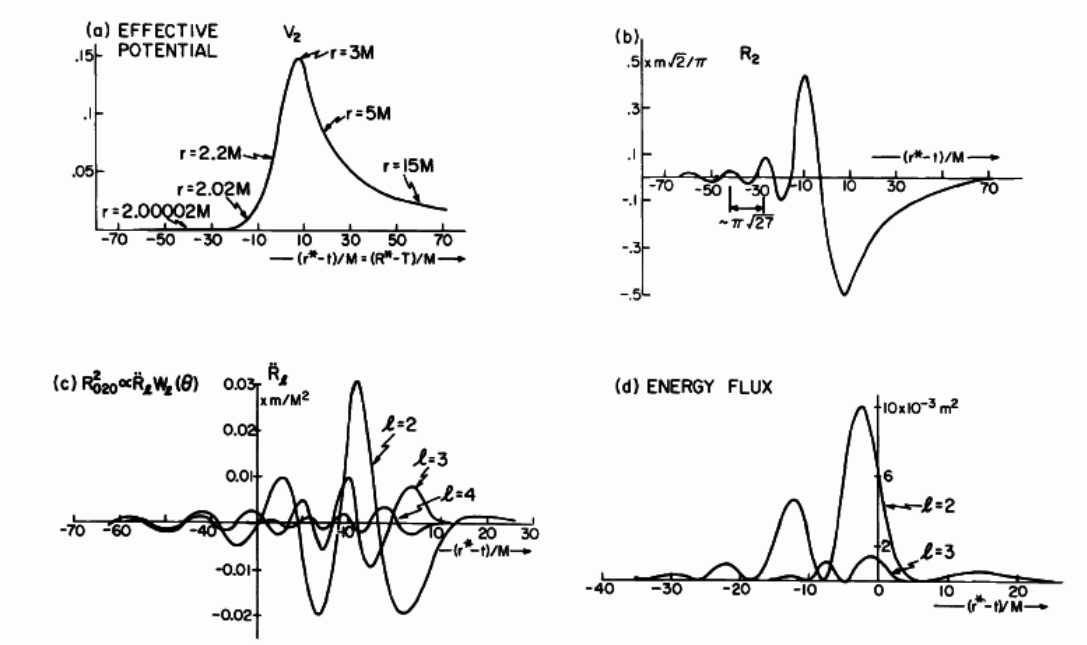

FIG. 1. Asymptotic behavior of the outgoing burst of gravitational radiation compared with the effective potential, as a function of the retarded time $(t-r^*)/M$. (a) Effective potential for $l=2$ in units of M^2 as a function of the retarded time $(t-r^*)/M=(T-R^*)/M$. For selected points the value of the Schwarzschild coordinate r is also given. (b) Radial dependence of the outgoing field $R_l(r,t)$ as a function of the retarded time for $l=2$. (c) $\ddot{R}_l(r^*,t)$ factors of the Riemann tensor components (see text) given as a function of the retarded time for $l=2,3,4$. (d) Energy flux integrated over angles for $l=2,3$; the contributions of higher l are negligible.

Figure 7.6: Davis et al. (1999) results for the waveform from particle's radial plunge into Schwarzschild.

to describe the tidal interactions of a neutron star in an external gravitationl field. They are relevant in compact binary mergers involving neutron stars (at least one).

The neutron star in the binary interacts with the companion and can deform, or "gravitationally polarize" (Damour, 1983; Damour and Nagar, 2009) (and see e.g. Damour and Lecian (2009) for the black hole case.) In general relativity, the motion of a system of well separated, strongly self-gravitating (compact), bodies can be described by a "matching" approach which consists in splitting the problem into two (Damour, 1983; Damour et al., 1991):

(i) the *outer problem* where one solves field equations in which the bodies are "skeletonized" by worldlines endowed with some global characteristics (such as mass, spin or higher-multipole moments);

(ii) the *inner problem* where one obtains the near-worldline behavior of the outer solution from a study of the influence of the other bodies on the structure of the fields in an inner world tube around each body.

This approach can be used to obtain binary black hole dynamics in post-Newtonian (PN) formalism and to prove that the bodies' finite-size correction enters at 5PN □ [TODO: REF]. In the following we focus on the inner problem and the definition of Love numbers that describe the response of the neutron star to the external field (Damour, 1983; Damour and Nagar, 2009).

Definition of multipolar tidal coefficients. Consider a static, spherically symmetric star of mass M perturbed by a stationary, external gravitational quadrupolar field $E_{ij}\sim\partial_i\partial_j\phi^{\rm external}$. The star is expected to respond to the external field by developing a quadrupole moment Q_{ij}. This phenomeon is analogous to the electric polarizability of a medium that, placed in an external electric field, develops a dipole moment. Assuming a linear response, an (eletric-type) quadrupolar tidal coefficient is defined as (Damour, 1983; Hinderer, 2008; Damour and Nagar, 2009)

$$Q_{ij}=\mu_2 E_{ij}\,. \tag{7.69}$$

A more general definition of μ_2 (valid also for other other multipoles) and the framework for the actual calculation can be obtained by the following argument. In the star local frame and for large radii, the metric coefficient g_{00} (gravitational potential in the weak field) can be written as

$$\frac{1-g_{00}}{2}=-\frac{M}{r}+\frac{3}{2}\frac{Q_{ij}}{r^3}\left(n^in^j-\frac{1}{3}\delta^{ij}\right)+\mathcal{O}\left(\frac{1}{r^4}\right)+\frac{1}{2}E_{ij}x^ix^j+\mathcal{O}(r^3)\,. \tag{7.70}$$

The above expression shows that the tidal coefficient $\mu_2$in Eq.(7.69) can be obtained by matching the term growing as $\sim r^2$ to the term falling as $\sim 1/r^3$ of the asymptotics expression of the (perturbed) metric coefficient.

This procedure can be generalized (Damour and Nagar, 2009). In the local frame of the body, define the *external gravitoelectric and gravitomagnetic tidal moments*

$$G_L:=G_{i_1\dots i_\ell}\quad H_L:=H_{i_1\dots i_\ell} \tag{7.71}$$

as those *multipoles* of the perturbed metric that grow as r^ℓ. Similarly, the *internal mass and spin multipoles moments*

$$M_L \qquad S_L \tag{7.72}$$

are those that decay as $r^{-(\ell+1)}$. The multipolar tidal coefficients of the body are then postulated as those relating the linear response of the internal moments to the external ones

$$M_L = \mu_\ell G_L \qquad S_L = \sigma_\ell H_L \,. \tag{7.73}$$

In a linearly perturbed, stationary star spacetime the asymptotic behaviour of the field uniquely defines these moments (Note: this is different from the vacuum case). In the following only the gravitoeletric sector is discussed since the magnetic sector is analogous.

Calculation of tidal Love number. Consider even parity, stationary perturbations of the TOV metric $g^{(0)}_{\alpha\beta}$

$$g_{\alpha\beta} = g^{(0)}_{\alpha\beta} + h^{(e)}_{\alpha\beta} \,. \tag{7.74}$$

The $h^{(e)}_{00}$ coefficient of the perturbed metric can be expressed in terms of a function H that is directly related to the logarithm of the enthalpy perturbation. The perturbative equation for H is

$$H'' + C_1 H' + C_0^{(\ell)} H = 0 \tag{7.75}$$

with

$$\begin{aligned} C_0^{(\ell)} &= e^{2\lambda}\left[\frac{\ell(\ell+1)}{r^2} + 4\pi(\rho+P)\frac{d\rho}{dP} + 4\pi(5\rho+9P)\right] - 4\phi'^2 \\ C_1 &= \frac{2}{r} + e^{2\lambda}\left[\frac{2m}{r} + 4\pi r(p-\rho)\right] . \end{aligned}$$

(A similar equation hold for odd parity perturbations). In the star interior, Eq.(7.75) needs to be solved numerically together with the background equations and by specifying a equation of state (EOS). In the star exterior, $\rho = P = 0$ and $m = M$, and the equation reduces to the *associated Legendre equation* with variable $x = r/M - 1$. The general solution can be expressed in terms of the *associated Legendre functions*

$$H^{\rm outer} = a_P \hat{P}_{\ell 2}(x) + a_Q \hat{Q}_{\ell 2}(x) \,. \tag{7.76}$$

The coefficients a_P and a_Q are to be determined by the boundary conditions, in particular by the matching with the interior solution. The ratio $a_\ell := a_Q/a_P$ can be determined by requiring the continuity of the logarithmic derivative at the surface

$$y_\ell(r) = \frac{rH'(r)}{H(r)} \tag{7.77}$$

i.e.

$$y_\ell^{\rm inner}(R) = y_\ell^{\rm outer}(R) = (1+x_R)\frac{\hat{P}'_{\ell 2}(x_R) + a_\ell \hat{P}_{\ell 2}(x_R)}{\hat{Q}'_{\ell 2}(x_R) + a_\ell \hat{Q}_{\ell 2}(x_R)} \tag{7.78}$$

with $x_R = R/M - 1 = 1/C - 1$. Note this is a nontrivial statement to check, since it depends on the EOS (and the regularity of the matter fields at the surface, e.g. the sound speed) and on the fact that the perturbed star surface does not coincide with the background star radius. Solving Eq.(7.78) for a_ℓ gives

$$a_\ell = -\frac{\hat{P}'_{\ell 2}(x_R) + C y_\ell(R)\hat{P}_{\ell 2}(x_R)}{\hat{Q}'_{\ell 2}(x_R) + C y_\ell(R)\hat{Q}_{\ell 2}(x_R)} \,. \tag{7.79}$$

This coefficient can be now directly related to the tidal coefficient μ_ℓ. The asymptotic behaviour of the outer solution is determined by

$$\hat{P}_{\ell 2}(x) \sim \left(\frac{r}{M}\right)^{\ell+1} \qquad \hat{Q}_{\ell 2} \sim \left(\frac{M}{r}\right)^{\ell+1} , \tag{7.80}$$

such that the growing and falling part of the perturbation are

$$(h^{(e)}_{00})^{\rm growing} \sim a_P \left(\frac{r}{M}\right)^{\ell+1} Y_{\ell m} \qquad (h^{(e)}_{00})^{\rm falling} \sim a_P \left(\frac{r}{M}\right)^{-(\ell+1)} Y_{\ell m} \,. \tag{7.81}$$

The matching gives (reintroducing the constants G and c)

$$(2\ell-1)!! G\mu_\ell = a_\ell \left(\frac{GM}{c^2}\right)^{2\ell+1} . \tag{7.82}$$

$G\mu_\ell$ has dimension of [length]$^{2\ell+1}$. The *tidal Love numbers* are defined as the dimensionless combination

$$k_\ell := \frac{1}{2} a_\ell C^{2\ell+1} = -\frac{1}{2} C^{2\ell+1} \frac{\hat{P}'_{\ell 2}(R/M-1) - C y_\ell(R) \hat{P}_{\ell 2}(R/M-1)}{\hat{Q}'_{\ell 2}(R/M-1) + C y_\ell(R) \hat{Q}_{\ell 2}(R/M-1)} \tag{7.83}$$

The *tidal polarizability parameters* of a star often employed in gravitational-wave astronomy are defined as

$$\Lambda_\ell := \frac{2k_\ell}{(2\ell-1)!! C^{2\ell+1}} \,. \tag{7.84}$$

☐ [TODO: Figure of $\Lambda_\ell(C)$]

8. Effective-one-body framework

The effective-one-body (EOB) is an Hamiltonian formalism that allows one to map the general-relativistic two-body problem into the dynamics of an effective particles in an effective metric. It is a powerful formalism that incorporates results from PN, black hoe perturbation theory (including Gravitational Self-Force, GSF) and numerical relativity to provide gravitational wave templates.

Suggested readings. *Damour (2012) review; Papers: (Buonanno and Damour, 1999, 2000).*

8.1 General idea

The key components of the EOB formalism are

1. the effective Hamiltonian for the conservative dynamics;
2. the radiation reaction force;
3. the waveform.

In prescribing each of the three component, one starts from the PN knowldge but tries to introduce suitable resummations of the PN Taylor series in x.

Starting points of the method and basic building blocks:

1. PN Hamiltonian in ADM coordinate and related results (Damour and Schäfer, 1988; Damour et al., 2015) (50+ years of efforts starting from the works of Arnowitt et al. (1960); Kimura (1961) and summarized by Schaefer and Jaranowski (2018))

$$\hat{H} = \frac{H}{\mu} = H_{\rm N} + H_{\rm 1PN} + H_{\rm 2PN} + ... \tag{8.1a}$$

$$H_{\rm N} = \frac{p^2}{2} - \frac{1}{q} \tag{8.1b}$$

$$H_{\rm 1PN} = \frac{1}{8}(3\nu - 1)(p^2)^2 - \frac{1}{2}[(3+\nu)p^2 + \nu(n\cdot p)^2] + \frac{1}{2q^2} \tag{8.1c}$$

...

2. Hamitonian of a test-mass on Schwzrschild;
3. Pade' resummation of the circular GW flux (Damour et al., 1998, 2000, 2001);
4. The smooth transition plunge-ringodwn studied in Davis et al. (1999) and following works.

Here, the presentation of the formalism focuses on nonspinning circular binaries, although the method has been extended to spinning binaries and noncircurlar motion. Before starting we review some classical mechanics (and a bit of quantum) with the following

Remark 8.1.1. *In classical mechanics, periodic systems with a time-independent Hamiltonian can be described using Hamilton-Jacobi (HJ) equations and the* action-angle *variables. Let us briefly remind these concepts and their connection to the Bohr-Sommerfeld quantization rule.*

For a time-independent Hamiltonian H the action can be written in terms of Hamilton's characteristic function W, that satisfies the HJ equation (time-independent eigenvalue problem)

$$S(p,q,t) = W(q,p) - Et \ ; \quad W \ : \ H(q, \frac{\partial W}{\partial q}) = E \ . \tag{8.2}$$

Solutions of the HJ can be searched for using separation of variables. If one of the q coordinates is cyclic, then it can be always be separated. If additionally the motion is periodic [1] *one introduces (for each q) the action variable*

$$J := \frac{1}{2\pi}\oint q dq = \oint \frac{\partial W}{\partial q} dq = const \ , \tag{8.3}$$

[1] Periodic motion refer to phase space periodicity. This includes closed orbits (oscillations, q and p are period functions with same frequency) but also rotations (p period but q unbounded).

where the integral is taken over one period in the phase space. The conjugate variable $\theta := \partial W/\partial J$ evolves linearly in time at the characteristic frequency of the motion $\theta \propto \Omega t$ with $\Omega = \partial H/\partial J$. Note that J has dimension of an angular momentum and θ has no dimension. The Bohr-Sommerfeld quantization rule is

$$J = \hbar n \ . \tag{8.4}$$

Let us apply the formalism to the Coulomb potential $V(r) = -\alpha/r$, specifying for simplicity to in-plane $\theta = \pi/2$ motion from the beginning. The Hamiltonian and the HJ equations are

$$H = \frac{m}{2}(p_r^2 + \frac{p_\varphi^2}{r^2}) + V(r) \ ; \quad (\frac{\partial W_r}{\partial r})^2 + \frac{1}{r^2}(\frac{\partial W_\varphi}{\partial \varphi})^2 = 2m(E - V(r)) \ . \tag{8.5}$$

The variable φ is cyclic, so $p_\varphi = const$. For $E < 0$ the motion is periodic. The action variables are

$$J_\varphi := \frac{1}{2\pi}\oint p_\varphi d\varphi = p_\varphi \ , \quad J_r := \frac{1}{2\pi}\oint \sqrt{2m(E - V(r) - \frac{p_\varphi^2}{r^2}}dr = -J_\varphi + (\alpha/2)\sqrt{2m/E} \ . \tag{8.6}$$

The second integral gives [2]

$$E = -\frac{\alpha^2 m}{2(J_r + J_\varphi)^2} \ . \tag{8.7}$$

The above equation the correct orbital frequency in a bound Kepler orbit, $\Omega_r = \partial E/\partial J_r = \alpha^2(J_r + J_\varphi)^{-3} = 1/(\alpha)\sqrt{-2E^3/m}$. Note that $\Omega_\varphi = \Omega_r$. The application of the Bohr-Sommerfeld quantization rule to Eq. (8.7)

$$E_n = -\frac{\alpha^2 m}{2\hbar^2(n_r + \ell)^2} = -\frac{\alpha^2 m}{2\hbar^2 n^2} \tag{8.8}$$

where $n := n_r + \ell$ is the principal quantum number (Coulomb degeneracy).

8.2 EOB Hamiltonian

The EOB is a relativistic generalization of the well-known Newtonian property that the relative motion is equivalent to the motion of a particle of mass $\mu = \nu M$ in an effective potential. The GR dynamics can, in fact, be mapped into the motion of an effective particle μ into an effective metric. Here we see how to construct such a dictionary between the real Hamiltonian for the relative motion and the effective motion,

$$\text{Real Hamiltonian (relative motion)} \quad \leftrightarrow \quad \text{Effective EOB Hamiltonian} \ . \tag{8.9}$$

The EOB Hamiltonian is built in three conceptual steps.

1. *Delaunay PN ADM Hamiltonian.* The ADM PN Hamiltonian for the relative motion is written in terms of the action variables. It is convenient for notation purposes (but not only, see Rem. 8.2.1) to indicate the action variables using their quantum numbers n, ℓ. Let $\alpha = GM\mu/\hbar$, the expression to 2PN is (Damour et al., 1998)

$$E_{\rm real} = -\frac{\mu}{2}\frac{\alpha^2}{n^2}\left[1 + \frac{\alpha^2}{c^2}\left(\frac{c_{11}}{n\ell} + \frac{c_{20}}{n^2}\right) + \frac{\alpha^4}{c^4}\left(\frac{c_{13}}{n\ell^3} + \frac{c_{22}}{n^2\ell^2} + \frac{c_{31}}{n^3\ell} + \frac{c_{40}}{n^4}\right) + ...\right] \tag{8.10}$$

   with $c_{n\ell} = c_{n\ell}(\nu)$ known PN coefficients.

2. *Effective metric and Delaunay Hamiltonian.* Consider the effective metric

$$g_{\rm eff} = -A(R;\nu)\mathrm{d}T^2 + B(R;\nu)\mathrm{d}R^2 + R^2\mathrm{d}\Omega^2 \tag{8.11a}$$

$$A(R;\nu) = 1 + \tilde{a}_1(\nu)\frac{GM}{c^2R} + \tilde{a}_2(\nu)\left(\frac{GM}{c^2R}\right)^2 + ... = 1 + \tilde{a}_1(\nu)u + \tilde{a}_2(\nu)u^2 + ... \tag{8.11b}$$

$$B(R;\nu) = 1 + \tilde{b}_1(\nu)\frac{GM}{c^2R} + \tilde{b}_2(\nu)\left(\frac{GM}{c^2R}\right)^2 + ... = 1 + \tilde{b}_1(\nu)u + \tilde{b}_2(\nu)u^2 + ... \ , \tag{8.11c}$$

   with unknown metric potentials A, B given by a PN series in $u := \frac{GM}{c^2R}$. The Newton limit for $u \to 0$ fixes $\tilde{a}_2 = 2$; while the Schwarzschild limit $\nu = 0$ fixes $A(R, \nu = 0) = 1 - 2GM/R = B^{-1}(R, \nu = 0)$. The Delaunay Hamiltonian of an (effective) particle of mass μ on this metric is (quantum number N, L)

$$\mathcal{E}_{\rm eff} = \mu c^2 - \frac{1}{2}\mu\frac{\alpha^2}{N}\left[1 + \frac{\alpha^2}{c^2}\left(\frac{C_{11}}{NL} + \frac{C_{20}}{N^2}\right) + \frac{\alpha^4}{c^4}\left(\frac{C_{13}}{NL^3} + \frac{C_{22}}{N^2L^2} + \frac{C_{31}}{N^3L} + \frac{C_{40}}{N^4}\right) + ...\right] \ , \tag{8.12}$$

   where the coefficients are combinations of the tilde coefs, $C_{NL} = C_{NL}(\tilde{a}_i, \tilde{b}_i)$.

[2] The integral should be familiar from mechanics classes. Because the motion is confined in $r \in [r_0, r_1]$ it can be calculated using

$$\oint \sqrt{...} = \int_{r_0}^{r_1} \sqrt{(1 - r_0/r)(r_1/r - 1)} = \pi/2(r_1 - r_0) - \pi\sqrt{r_0 r_1} \ .$$

3. *Dictionary between energy levels.* The EOB Hamiltonian is defined by the map that conect the real (known as a PN expansion) and the effective problem. The map is constructed by first demanding that

$$n = N \ , \quad \ell = L \ , \tag{8.13}$$

and then searching for a relation $E_{\rm real} \leftrightarrow \mathcal{E}_{\rm eff}$. The Hamiltonias (energy levels) of the two problems are schematically given by

$$E = Mc^2 + E_{\rm real} = Mc^2 + \text{Newt} + 1PN + 2PN + ... \tag{8.14a}$$
$$\mathcal{E}_{\rm eff} = \mu c^2 + \text{Newt} + 1PN + 2PN + ... \tag{8.14b}$$

Buonanno and Damour (1999) postulate

$$\frac{\mathcal{E}_{\rm eff}}{\mu c^2} = 1 + f(\frac{E_{\rm real}}{\mu c^2}) = 1 + \frac{E_{\rm real}}{\mu c^2}\left(1 + \alpha_1 \frac{E_{\rm real}}{\mu c^2} + \alpha_2 \left(\frac{E_{\rm real}}{\mu c^2}\right)^2 + ...\right) \tag{8.15}$$

with unknown coefficients $\alpha_i(\nu)$. The above equation translates into a relation between the unknown coefficients at each PN order,

$$C_{NL}(\tilde{a}_i, \tilde{b}_i) \leftrightarrow \alpha_i(\nu) \ . \tag{8.16}$$

For example, at 2PN there are six algebraic equations connecting the set of six coefficients

$$(\tilde{a}_2, \tilde{a}_3, \tilde{b}_1, \tilde{b}_2, \alpha_1, \alpha_2) \ . \tag{8.17}$$

Assuming $\tilde{b}_1 = +2$, implies that (i) the effective metric coincides with Schwzarschild at this order and that (ii) there exists a unique solution for the 2PN coefficients, given by

$$\tilde{b}_1 = +2 \ \Rightarrow \ \tilde{a}_1 = 0 \ , \ \ \tilde{a}_3 = 2\nu \ , \ \ \tilde{b}_2 = 2 - 6\nu \ , \ \ \alpha_1 = \nu/2 \ , \ \ \alpha_2 = 0 \ . \tag{8.18}$$

The 2PN A-potential is

$$A_{\rm 2PN} = 1 - 2u + 3\nu u^3 \ , \tag{8.19}$$

while the 2PN energy map is

$$\frac{\mathcal{E}_{\rm eff}}{\mu c^2} = 1 + \frac{E_{\rm real}}{\mu c^2}\left(1 + \frac{\nu}{2}\frac{E_{\rm real}}{\mu c^2}\right) = \frac{s - m_1^2 c^4 - m_2 c^4}{2 m_1 m_2 c^4} \ ; \quad s := (Mc^2 + E_{\rm real})^2 \ . \tag{8.20}$$

A similar derivation can be performed also at 3PN and leads to the same map for the energy. After verifying this order, one assumes the maps holds also at any order.
The EOB Hamiltonian is found by solving Eq. (8.20) for $E_{\rm real}$ and then by solving the effective Hamilton-Jacobi equation to get $\mathcal{E}_{\rm eff}$ in terms of the effective phase space coordinates. Defining the coordinates

$$t := \frac{T}{GM} \ , \ \ r := \frac{R}{GM} \ , \ \ R_* := \int \mathrm{d}R \, \frac{B}{A} \ , \ \ p_{r_*} := \frac{P_{R_*}}{\mu} \ , \ \ p_\varphi := \frac{P_\varphi}{\mu G M} \ , \tag{8.21}$$

The Hamiltonian reads

$$H_{\rm EOB} = Mc^2 \sqrt{1 + 2\nu(\hat{H}_{\rm eff} - 1)} \ , \tag{8.22a}$$

where

$$\hat{H}_{\rm eff} = \frac{H_{\rm eff}}{\mu} = \sqrt{A(u;\nu)(1 + p_\phi^2 u^2 + 2\nu(4 - 3\nu)u^2 p_{r*}^4) + p_{r*}^2} \ . \tag{8.22b}$$

One can immediately very that for $\nu \to 0$, $H_{\rm EOB} \to H_{\rm eff}$ and the the effective Hamiltonian $H_{\rm eff}$ reduces to the Hamiltonian of a particle in Schwarszchild spacetime, where $A(u;0) = 1 - 2u$. Also, for small u

$$H_{\rm EOB} \simeq Mc^2 + \frac{\mu}{2}P^2 + \frac{\mu}{2}(A - 1) = Mc^2 + \frac{\mu}{2}P^2 - \frac{GM\mu}{c^2 R} \ . \tag{8.23}$$

The metric potential $A(u)$ is thus interpreted as the inter-binary energy.

Remark 8.2.1. *Following from Rem. 8.1.1, it should be clear that the EOB map can be interpreted from a quantum-mechanical point of view. The construction presented above is done in such a way the gauge invariant energy levels of the two conservative dynamics match each other, Fig. 8.1.*

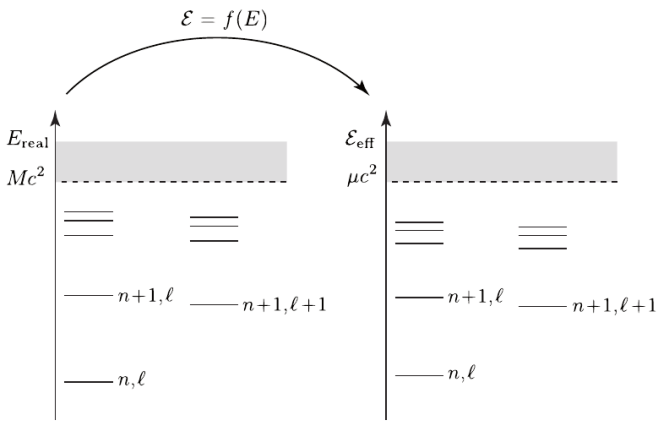

Figure 8.1: Quantum interpretation of the EOB dictionary for the conservative dynamics. From Damour (2012).

Metric potentials and resummation. At 3PN the metric potentials calculated from the EOB dictionary are (Damour, 2012)

$$A_{\rm 3PN} = 1 - 2u + 3\nu u^3 + a_4(\nu)u^4 \ , \quad a_4(\nu) = \left(\frac{94}{3} - \frac{41\pi}{32}\right)\nu \ . \tag{8.24}$$

and

$$D_{\rm 3PN} := \frac{A_{\rm 3PN}}{B_{\rm 3PN}} = 1 - 6\nu u^2 + 2(3\nu - 26)\nu u^3 \ . \tag{8.25}$$

It is remarkable that the 3PN Hamiltonian within the EOB formalism can be written in such a compact form (Cf. the starting ADM Hamiltonian given e.g. in (Damour, 2012)). The double-square-root structure of Eq. (8.22) is a first example of resummation in the EOB formalism. The EOB Hamiltonian contains by construction all the PN but in a more compact form. Moreover, since the square roots contains all the infinite terms of their Taylor expansion, one can hope that more information than the PN series is present in the EOB Hamiltonian [3].

The convergence properties of the 3PN EOB Hamiltonian can be improved introducing a further resummation. One can observe that the coefficient $a_4(\nu)$ becomes rather large for $\nu = 1/4$, and wonder whether this is a real feature of the (unknown) exact effective metric or an unwanted feature introduced by the PN series. How to assess this? There is a simple way: continuity. We expect that the dynamics is smooth in the parameter ν. In fact, this should be required, as there is no fundamental reason to expect a different behaviour. The Schwarzschild's test-mass dynamics then provides an exact limit for $\nu \to 0$. Thus, we expect that for $\nu \neq 0$ the structure of the $A(u;\nu)$ and the Hamiltonian must be similar to Schwarschild and must be a continuous-in-ν deformation of the Schwarschild expressions. For example, the Schwarzschild spacetime as an horizon at $R_S = 2GM/c^2$ ($u = 0.5$) and a last stable orbit (LSO) at $R = 6M/c^2$. The effective spacetime should also posses these features albeit at different coordinate locations (corrected/deformed by functions of the mass ratio, ν). Inspection of the 3PN potential shows that $A_{\rm 3PN}(u,\nu)$ diverges for $\nu \to 1/4$ and does not admit any zero, Fig. 8.1. By constrast the 2PN potential follows qualitatively the behaviour of the Schwarzschild potential and admit a horizon (zero). A possible way to improve the model is, for example, to apply a Pade' function to the 3PN potential,

$$A_{\rm 3PN}(u) \mapsto P^1_3[A_{\rm 3PN}(u)] = \frac{1 + n_1 u}{1 + d_1 u + d_2 u^2 + d_3 u^3} \ , \tag{8.26}$$

where the n_1, d_1, d_2, d_3 can be algebraically computed from the coefficients of $A_{\rm 3PN}(u)$ by requiring that the first four terms of the Taylor expansion of $P^1_3[A(u)]$ in powers of u coincide with $A_{\rm 3PN}$ [4]. As shown in Fig. 8.2 this potential is much closer to the 1PN and 2PN potential and retains similar properties.

For finite mass ratio the function $A(u;\nu)$ is completely known analytically up to 4PN (Damour et al., 2015) with few terms known at 5PN (and even beyond in the test-mass limit). The expression at 4PN is remarkably simple

$$A_{\rm 4PN} = 1 - 2u + \nu(2u^3 + a_4 u^4 + a_5(\nu, \ln u)u^5) \ , \tag{8.27}$$

where $a_5(\nu, \ln u)$ is a linear function of ν and $\ln u$. Unknown terms at 5PN are currently parametrized by one or few free coefficients that can be fixed by comparing gauge invariant quantities like the waveform or the energetics to numerical relativity simulations. Moreover, the metric potentials in the EOB Hamiltonian are always employed in

[3] We have started from PN series and obtained a result that (potentially) contains more information than the starting one. The accuracy/faithfulness of the resummation is essentially a guess and must be verify against all the available exact results. But there is no trick and, on the contrary, this is a well known/defined approach for asymptotic series. A relevant example is given by Pade' approximants. The latter are rational polinomials known to give a better approximation of functions than the respective truncated Taylor series. In fact these approximants can work where the Taylor series does not converge. Pase' approximants are a well known technique used extensively also in computer calculations.

[4] A fast way to obtain these coefficients is to use computer algebra, e.g. with `Mathematica` `https://mathworld.wolfram.com/PadeApproximant.html`.

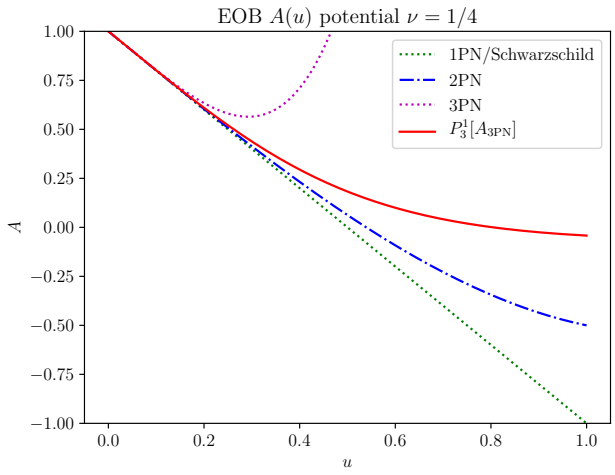

Figure 8.2: EOB potential at various PN order and the resummation ofthe 3PN potential.

some resummed form. For example, the $A(u)$ potential can be resummed with P_3^1 at 3PN, with P_4^1 at 4PN and with P_5^1 at 5PN, and the resulting "resummed PN series" shows a smooth behaviour in the PN order and in ν. The 3PN D potential

$$D_{3\mathrm{PN}}(u) \mapsto P_3^0[D_{3\mathrm{PN}}(u)] = \frac{1}{1+6\nu u^2 - 2\nu(3\nu-26)u^3} \ . \tag{8.28}$$

The above expression guarantees that the D function remains positive when $R \to 0$ as demanded by the fact that $D(\nu \to 0) \to 1$.

Example 8.2.1. Circular orbits *are given by setting* $p_{r_*} \equiv 0$ *in the Hamiltonian and looking for the stationary point,*

$$\hat{H}_{\mathrm{eff}} = \sqrt{A(u)(1+p_\varphi^2 u^2)} \ , \quad \frac{d}{du}\left(A(u)(1+p_\varphi^2 u^2)\right) = 0 \ . \tag{8.29}$$

The angular momentum of the circular orbits is thus given by $(d/du = ')$

$$p_\varphi^2 = j_0^2 = -\frac{A'(u)}{(u^2 A(u))'} \ . \tag{8.30}$$

One can now recall that the effective potential for Schwarzschild geodesics is given by

$$V_j^{(s)} = A(R)\left(\frac{j^2}{R^2} + s\right) \tag{8.31}$$

where $s = 1(0)$ *for timelike(null) geodesics and* j *is the angular momentum. Within EOB the concepts of LSO and light-ring can be generalized by simply considering* $A(u) \mapsto A(u;\nu)$ *and using the same formulas of the Schwarzschild spacetime. It is left as [exercise] to study the LSO and the LR for the potentials given above.*

8.3 Radiation reaction force & Factorized circular waveform

The Hamiltonian EOM from the EOB Hamiltonian are

$$\dot{r} = \left(\frac{A}{B}\right)^{1/2} \frac{\partial \hat{H}_{\mathrm{EOB}}}{\partial p_{r_*}} \tag{8.32a}$$

$$\dot{\varphi} = \frac{\partial \hat{H}_{\mathrm{EOB}}}{\partial p_\varphi} := \Omega \tag{8.32b}$$

$$\dot{p}_{r_*} = -\left(\frac{A}{B}\right)^{1/2} \frac{\partial \hat{H}_{\mathrm{EOB}}}{\partial r_*} \tag{8.32c}$$

$$\dot{p_\varphi} = \hat{\mathcal{F}}_\varphi = -\frac{1}{\Omega} F^{\ell_{\max}} \ , \tag{8.32d}$$

The last equation contains a new ingredient: the *radiation reaction force* expressed in terms of the circular GWflux truncated at some multipole $\ell_{\max}$. The latter is given in terms of the modulus of the multipolar waveform discussed in Rem. 7.3.2,

$$F^{\ell_{\max}} = \frac{2}{16\pi G} \sum_{\ell=2}^{\ell_{\max}} \sum_{m=1}^{\ell} (m\Omega)^2 |R h_{\ell m}|^2 \ . \tag{8.33}$$

The mutlipolar waveform introduced in Rem. 7.3.2 specified for circular orbits is written in general as Kidder (2008)

$$h_{\ell m}(x) = h^{\rm N}_{\ell m}(x)\,\hat{h}_{\ell m}(x)\ ; \quad h^{\rm N}_{\ell m} = \frac{GM\nu}{c^2 R} n_{\ell m} c_{\ell+\epsilon} x^{(\ell+\epsilon)} Y_{\ell-\epsilon,-m}(\frac{\pi}{2},\phi)\ , \tag{8.34}$$

where x is the PN frequency parameter; $\epsilon = \pi(\ell+m)$ denotes the parity of $\ell+m$, i.e. $\epsilon=0$ for even-parity (mass-generated) and $\epsilon=1$ for odd-parity (current-generated) ones multipoles; $n_{\ell m}$ and $c_{\ell+\epsilon}(\nu)$ are numerical coefficients given in e.g. (Damour and Nagar, 2011); and $Y_{\ell m}$ the spherical harmonics. The subleading order term is given by a PN expression in the Taylor form

$$\hat{h}^{\rm Taylor}_{\ell m} = 1 + c^{\ell m}_1 x + c^{\ell m}_{3/2} x^{3/2} + c^{\ell m}_2 x^2 + ...\ . \tag{8.35}$$

Damour et al. (2009) proposed a way to resumm the above Taylor series and thus improve its convergence properties in the high-velocities (high-frequencies) regime. This waveform is known as *factorized waveform* because is it the product of several factors. Specifically it writes

$$\hat{h}^{\rm DIN\ (\epsilon)}_{\ell m} = \hat{S}^{(\epsilon)}_{\rm eff}\, T_{\ell m}\, e^{{\rm i}\delta_{\ell m}}\, f_{\ell m}\ . \tag{8.36}$$

In the above expression the first two terms are known and are specific (factorized) contributions to the PN waveform [5], while the last terms are calculated by dividing the Taylor form with the known factors. The different terms in the factorized waveform are

- *Effective source factor.* Derived from leading order contributions to the circular waveform in the test-mass limit. For even parity it is chosen as the effective energy since the leading order source of gravitational radiation is given by the energy density. For odd parity it is taken as the circular angular momentum.

$$\hat{S}^{(0)}_{\rm eff}(x) = \hat{H}_{\rm eff}\ , \quad \hat{S}^{(1)}_{\rm eff}(x) = \sqrt{x} j(x)\ . \tag{8.37}$$

- *Tail factor.* A resummed expression for an infinite number of "leading logarithms" entering the transfer function between the near-zone multipolar wave and the farzone one, due to tail effects linked to its propagation in a Schwarzschild background of mass $M_{\rm ADM} = H_{\rm EOB}$ (circular orbits):

$$T_{\ell m} = \frac{\Gamma(\ell+1-2{\rm i}\hat{\hat{k}})}{\Gamma(\ell+1)} e^{\pi\hat{\hat{k}}} e^{2{\rm i}\hat{\hat{k}}\ln(2kr_0)} \tag{8.38}$$

  where $k := m\Omega$, $\hat{\hat{k}} := GM_{\rm ADM}k$, and $r_0 = 2GM/\sqrt{e}$.
- *Phase factor.* Computed as $\delta_{\ell m} = \arg[\hat{h}^{\rm Taylor}_{\ell m}/(\hat{S}_{\rm eff}\, T_{\ell m})]$;
- *Amplitudes.* Computed as the ration of the moduli, $f_{\ell m}(x) = |\hat{h}^{\rm Taylor}_{\ell m}/(\hat{S}_{\rm eff}\, T_{\ell m})|$, they have a PN form $f_{\ell m}(x) = 1 + f^{\ell m}_1 x + f^{\ell m}_2 x^2 + ...$ that is further resummed with various techniques (Damour, 2012).

There are several design choices in the factorized waveform that are currently subject of research and being explored/improved. A crucial aspect is the verification of the convergence of the analytical flux using exact result at high frequencies. These results are mostly available in the test-mass limit $\nu \to 0$ from the solution of the RWZ (or Teukolsky) equations. An early study in this direction is shown in Fig. 8.3.

8.4 Binary black hole (BBH) waveforms

The EOB formalism successfully predicted the waveform emitted by binary black holes and it is nowadays the most sophisticated approach to compute high-precision templates. Let us discuss the the main steps to compute EOB waveform for BBHs.

(i) Define the *moment of merger* t_m as the instant at which the orbital frequency $\Omega(t)$ reaches its maximum. This happens in the vicinity of the EOB (ν-deformed) adiabatic (no rad.reac. force) lightring. This can be seen by explicitely writing the EOM equation for Ω

$$\Omega = \frac{Au^2 p_\varphi}{\nu \hat{H}_{\rm EOB}\hat{H}_{\rm eff}}\ , \tag{8.39}$$

and observing that the maximum in $A(u)u^2$ on a circular orbit corresponds to a maximum of Ω. The maximum of Ω (or a neighbour) is a natural point where to stop the EOB dynamics. The circular waveform can be thus evaluated on the EOB dynamics obtaining $\hat{h}^{\rm insp}$.

(ii) Close to the moment of merger the amplitude of the EOB $(2,2)$ waveform also has an absolute maximum that marks the end of the chirp signal. Note both the max of Ω and the max of the waveform cannot be predicted by the PN waveform, but they are observed in the GW computed by numerical relativity simulations. Comparing to the latter, the EOB circular waveform describing the circular inspiral motion $\hat{h}^{\rm insp}$ is the least

[5] This expression has no formal derivation, but was proposed based on physical intuition. Some of the motivations are technical and are mentioned in Damour et al. (2009). The factors essentially absorb terms that would otherwise make the PN coefficients to diverge faster.

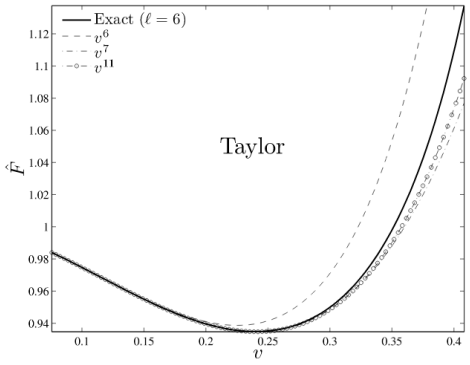

Fig. 3 The extreme-mass-ratio limit ($\nu = 0$): the Newton-normalized energy flux emitted by a particle on circular orbits. The figure illustrates the scattering of the standard Taylor expansion of the flux around the "exact" numerical result (computed up to $\ell = 6$) obtained via perturbation theory.

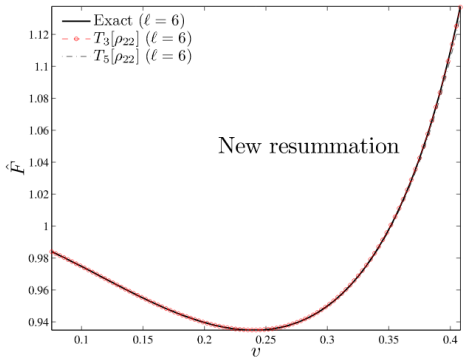

Fig. 6 Performance of the new resummation procedure described in Ref. [50]. The total GW flux $\hat{F}$ (up to $\ell_{\rm max} = 6$) computed from inserting in Eq. (62) the factorized waveform (41) with the Taylor-expanded $\rho_{\ell m}$'s (with either 3PN or 5PN accuracy for ρ_{22}) is compared with the "exact" numerical data.

Figure 8.3: Factorized circular flux compare to exact data in the test-mass limit ($\nu \to 0$, Left: PN waveform truncated at different PN order. Note the divergence from the exact result and the oscillatory character of the PN series. Right: Factorized waveform. From Damour and Nagar (2011).

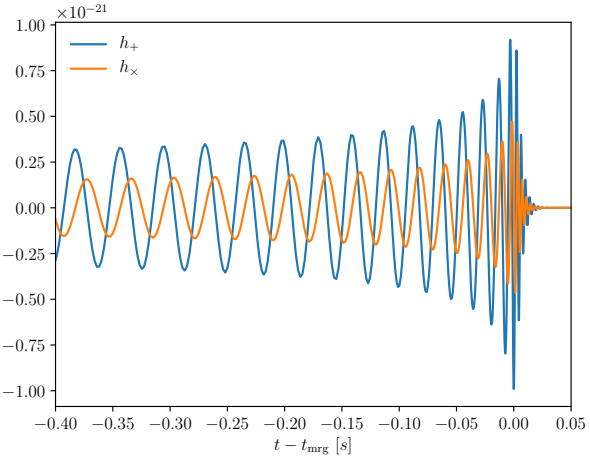

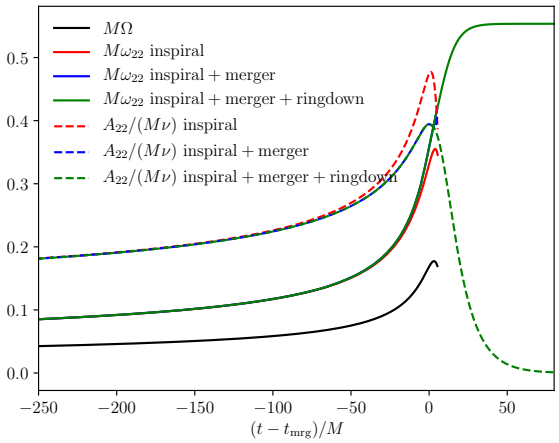

Figure 8.4: EOB BBH waveforms. Left: EOB waveform compatible with GW150914. Right: EOB $(2, 2)$ waveform around at merger. The different contributions to the waveform are highlighted.

accurate towards the end of the inspiral. Beside the fact that the dynamics is reaching the highest velocity regime, another source of inaccuracy is that the motion is not circular. A way to improve the waveform is to introduce multiplicative corrections to the circular waveform called *Next-to-Quasi-Circular (NQC)* corrections. This defines the inspiral+plunge waveform, that for the $(2, 2)$ looks

$$\hat{h}^{\rm insplunge} = \hat{h}^{\rm insp}\,\hat{h}^{\rm NQC} = \hat{h}^{\rm insp}\,\left(1 + a_1\frac{p_{r_*}^2}{(r\Omega)^2} + a_2\frac{\ddot{r}}{r\Omega^2}\right) e^{{\rm i}(b_1 p_{r_*}/(r\Omega) + b_2 p_{r_*} r\Omega)}\,, \tag{8.40}$$

where the coefficients $a_{1,2}, b_{1,2}$ (4 for each multipoles and dependent on ν) can be fixed by comparing to selected numerical data.

(iii) The $h^{\rm insplunge}$ waveform is then smoothly connected to the *ringdown* waveform,

$$h^{\rm ringdown}(M_f, a_f) = \sum_n C_n e^{\sigma_n (t - t_m)}\,. \tag{8.41}$$

The matching point (or interval) is chosen around t_m (maximum of Ω) as suggested by Davis et al. (1999). Here one needs a prediction for the final Kerr BH mass M_f and spin a_f, from which the Kerr QNM frequencies can be calculated, and a prescription for determining the excitation amplitudes C_n. Quantitative models of the ringdown make use of numerical relativity data.

An example of BBH waveform is shown in Fig. 8.4.

8.5 Tidal interactions

Damour and Nagar (2010) incorporated the treatment of tidal effect into the formalism, thus extending the model's

applicability to binaries with neutron stars. Tidal interactions are included by augmenting the EOB potential

$$A \mapsto A + A_{\rm tidal} \ , \tag{8.42}$$

with an expression inferred from the tidal Lagrangian Eq. (6.88), (Bini et al., 2012).

The tidal potential has the form

$$A_{\rm tidal} = \sum_{\ell\geq 2} \left[\kappa^{A+}_\ell u^{2\ell+2}(1+\alpha_1^{(\ell+)}u + \alpha_2^{(\ell+)}u^2 + ...) + \kappa^{A-}_\ell u^{2\ell+3}(1+\alpha_1^{(\ell-)}u + ...) + (A\leftrightarrow B)\right] \tag{8.43}$$

where $\alpha_i^{(\ell)}(\nu)$ are coefficients and

$$\kappa^{A+}_\ell := 2k^A_\ell \left(\frac{M_A}{MC_A}\right)^{2\ell+1} \frac{M_B}{M_A} \ , \quad \kappa^{A-}_\ell := 2j^A_\ell \left(\frac{M_A}{MC_A}\right)^{2\ell+1} \frac{M_B}{M_A} \ , \tag{8.44}$$

are the *multipolar tidal polarizability coupling constants*. The current analytical knowledge comprise gravitoelectric terms $\ell = 2, 3$ up to the next to next leading order (NNLO; coefficients $\alpha_{1,2}^{(2+,3+)}$) and gravitomagnetic terms up to NLO (coefficient $\alpha_1^{(2-)}$) (Vines and Flanagan, 2010; Damour et al., 2012; Bini et al., 2012; Bini and Damour, 2014).

Taking the Newtonian limit illustrates the meaning of the above coefficients,

$$H_{\rm EOB} \simeq Mc^2 + \frac{\mu}{2}P^2 + \frac{\mu}{2}(A-1) = Mc^2 + \frac{\mu}{2}P^2 + \frac{\mu}{2}\left(-\frac{2GM}{c^2R^2} + ... - \frac{\kappa^T_2}{R^5}\right) \ . \tag{8.45}$$

The constant $\kappa^T_2 = \kappa^A_2 + \kappa^B_2$ encodes the effect of tidal interactions at leading order. For a large span of EOS, masses in $[1,2]\mathrm{M}_\odot$ and mass ratios in $q\in[1,2]$ its values are $\kappa^T_2 \sim [50, 500]$. A common alternative notation uses the quantities $\Lambda^i_2 \equiv 2/3 k^i_2 (c^2 R_i/GM_i)^5$ with $i\in\{A,B\}$, in place of the κ^A_2 and defines

$$\tilde\Lambda = \frac{16}{13}\frac{(M_{\rm A}+12M_{\rm B})M^4_{\rm A}}{M^5}\Lambda_{\rm A} + (A\leftrightarrow B) \ . \tag{8.46}$$

Note that using the κ quantities leads to more compact formulas.

Tidal corrections are introduced also in the waveform (Flanagan and Hinderer, 2008; Vines et al., 2011; Damour et al., 2012; Banihashemi and Vines, 2018) At leading order the stationary phase approximation of the waveform reads

$$\tilde h(f) = \tilde A f^{-7/6} e^{-i(\Psi_0(x)+\Psi_{\rm tidal}(x))} = \tilde A f^{-7/6} e^{-i(\Psi_0(x) - 39/4\kappa^T_2 x^{5/2})} \ , \tag{8.47}$$

where $x(f) = (\pi GMf/c^3)^{2/3}$ and $\Psi_0(x)$ is the point-mass phase. Note that the tidal contribution at leading order is again fully determined by κ^T_2. For this reason, the latter (or equivalently $\tilde\Lambda$) is the quantity that is best measured from GW observations.

The EOB formalism is currently the only method to obtain an accurate GW measurement of tidal parameters and thus constraints on the neutron star matter. The reason is that the measurement of κ^T_2 is more sensitive at high frequencies where post-Newtonian approximants but most of the signals are detected at frequencies that are too low for performing relativity simulations.

9. Experiments and data analysis

Discussion on the GW detectors and on characterization of noise curves. Data analysis application based on match-filtering techniques.

Suggested readings. *Chap. 7,8,9 of Maggiore (2007); Abbott et al. (2019a).*

9.1 GW detectors

Experimental GW physics began in the 1960s with J. Weber, who proposed resonant bars detectors. Bar detectors have resonance frequencies tha can be excited by the passage of a GWs. The frequency range of sensitivity of these instruments is centered in a narrow interval around the resonance at kiloHertz frequencies. A bar dector with a mass of 2 tons can measure a relative displacement as small as $\Delta L/L \sim 10^{-18} - 10^{-19}$. No GW events were observed with these apparati. Detections of GW passing through Earth have been possible with *ground-based laser interferometers*. These experiments are kilometer-size Michelson-Morley interferometers with Fabry-Perot cavities started in the 1980s and operated by the LIGO and Virgo collaborations. More recently, the KAGRA collaboration has joined the experimental effort. Future experiments will include the spaced-based LISA mission and the ground-based next-generation (the third, hence 3G) detectors such as the Einstein Telescope (ET).

In the following, we discuss key aspects of ground-based laser interferometers, the main sources of noise, current GW antennas and the two most important GW events observed so far. Next-generation detectors are discussed briefly at the end.

Ground-based laser interferometers. A simple scheme of a ground-based interferometer used for GW detections is shown in Fig. 9.1. GW interferometers are instruments for measurements of light time-intervals.

The basic concept is the following: a monochromatic laser beam starts from its source and reaches a *beam-splitter*, which separates the light in a beam travelling along one arm and another beam traveling in a second orthogonal arm. At the end of each arm, a highly reflective mirror (test-mass) is located at a precise distance from the beam-splitter. After travelling forth and back, the two beams recombine at the beam-splitter and the resulting light is collected in a photodiode, which measures its intensity. If the two beams are reconstructed with a coherent phase, there is constructive interference. If the phases of the laser beams are not aligned, there is destructive interference.

Key components of the interferometers are:

- **Mode cleaners**: the beam is cleaned in input and in output in order to ensure a monochromatic light beam;
- **Recycling mirrors**: these instruments are located before and after the beam-splitter and they are useful to reintroduce the light beam into the interferometer in order to minimize the losses of power;
- **Fabry-Prot cavities**: the arms of the interferometers have Fabry-Prot cavities constituted by the input test-masses and the end test-masses. Here the light resonates many times in order to increase the effective length of its path and to boost the intensity of the laser (which reaches ∼50 kW);
- **Suspensions**: based on the concept of inverse pendulum, they are used to keep the test-masses in a fixed position, avoiding motions due to external unwanted contributions (e.g. seismic motions).

What does an interferometer measure? Let $\omega_{\rm lsr}, \mathbf{k}_{\rm lsr}$ the frequency and the wavenumber of the laser beam (different from the frequency of the GW we want to detect). The electric (and magnetic) field of the laser is (complex notation)

$$E(t, \mathbf{x}) = E_0 \, e^{-i\omega_{\rm lsr} t + i\mathbf{k}_{\rm lsr}\cdot\mathbf{x}} \, . \tag{9.1}$$

We denote L_x and L_y the lengths of the two arms and we assume that the beam-splitter divides the light in two equal beams. A photon that reaches the beam-splitter at time t_0, travels through an arm and comes back, arrives again at the beam-splitter at a time $t' = t_0 + 2L_x/c$ (or $t' = t_0 + 2L_y/c$, depending on the direction). Then, considering the reflection and transmission factors [1], we can write the electric fields of the two beams at the position of the

[1] The incoming field is divided in two at the beam-splitter. Here the first beam is reflected ($r = 1/\sqrt{2}$), then it goes through the interferometer arm, it reaches the perfectly reflecting end-mirror ($r = -1$) and it goes back to the beam-splitter where it is transmitted($t = 1/\sqrt{2}$). The other beam is immediately transmitter though the beam-splitter ($t = 1/\sqrt{2}$), then it also reaches the perfectly reflecting end-mirror ($r = -1$) and goes back to the beam-splitter, but here it is reflected from the other side of the mirror ($r = -1/\sqrt{2}$). The overall is $-1/2$ for the field in the x-arm and $+1/2$ for the field in the y-arm.

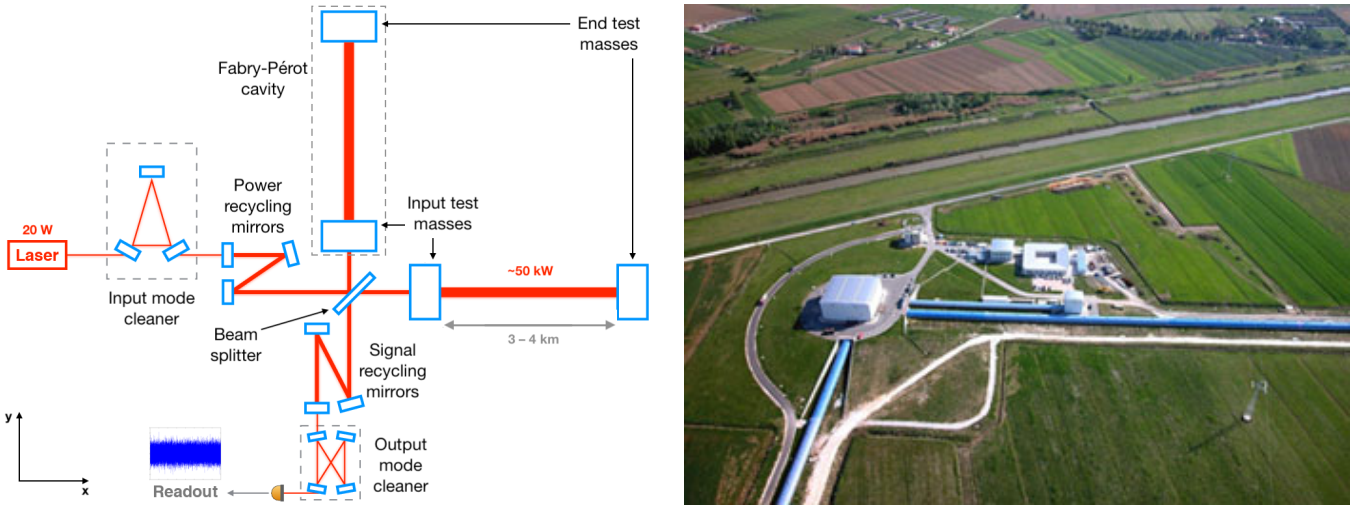

Figure 9.1: Characterization of GWs detectors. Left: Schematic example of ground-based laser interferometer, as LIGO or Virgo. The figure highlights the most important components of the instrument. Right: Picture of the European Gravitational Observatory (EGO) center and the Virgo interferometer, located near Pisa, Italy.

beam-splitter before the beams' recombination as

$$E_x(t) = -\frac{1}{2} E_0\, e^{-\mathrm{i}\omega_{\rm lsr} t + 2\mathrm{i} k_{\rm lsr} L_x} \ , \quad E_y(t) = \frac{1}{2} E_0\, e^{-\mathrm{i}\omega_{\rm lsr} t + 2\mathrm{i} k_{\rm lsr} L_y} \ . \tag{9.2}$$

The recombined field is $E_{\rm out}(t) = E_x(t) + E_y(t)$. Writing $2L_x = (L_x + L_y) + (L_x - L_y)$ and the same for $2L_y$, we see that

$$E_{\rm out} = -\mathrm{i} E_0\, \sin\left[k_{\rm lsr}(L_y - L_x)\right]\, e^{-\mathrm{i}\omega_{\rm lsr} t + \mathrm{i} k_{\rm lsr}(L_x + L_y)} \ , \tag{9.3}$$

and the power measured at the photodiode is proportional to

$$|E_{\rm out}|^2 = E_0^2\, \sin^2[k_{\rm lsr}\, \underbrace{(L_y - L_x)}_{=:\Delta L}] \ . \tag{9.4}$$

Therefore any variation in the flight-time of the beams (ΔL) results in a corresponding variation of the power at the photodetector.

During the scientific observation cycles (technically speaking when the detectors are *locked*), the interferometers work in the dark fringe: the phases of the light beams are taken to be anti-aligned in order to have destructive interference at the photodiode. This means that, in absence of GW signal in the detector, the laser power gathered at the photodiode is zero, on average. The dark fringe is used because it is easier to detect deviations from the null value. Indeed, what we want to measure is the fractional displacement of the arms $\Delta L/L \propto h(t)$, which is encoded in the phase of the recombined beam. Since this deviation is expected to be small, by expanding Eq. (9.4), at the lowest order we get $|E_{\rm out}|^2 \propto \Delta L^2/L^2$. At this point is clear that if we want to measure a small deviation which affect the detector at quadratic order, we need to set the interferometer in the most sensitive condition, and then the dark fringe is preferred.

Sources of noise. Noise can be roughly defined as the output of the detectors that is not a GW signal. Full characterization of the noise sources is essential to detect GW with amplitudes of the order of $\sim 10^{-20}$. There are many sources of noise in ground-based detectors, the main one are discussed in the following. The noise at each frequency is described by its power spectral density (PSD) $S_n(f)$ (which we will define in Sec. 9.2).

- **Seismic noise**: this contribution has a spectrum in all three dimensions close to $10^{-7}\ f^{-2}\ \mathrm{m}/\sqrt{\mathrm{Hz}}$. Isolation can be provided in a relatively simple way by making use of the fact that, for a simple pendulum system, the transfer function to the pendulum mass of the horizontal motion of the suspension point falls off as f^{-2} above the pendulum resonance. In a similar way, isolation can be achieved in the vertical direction by suspending a mass on a spring. In the case of the Virgo detector, operations are posisble to below 10 Hz. The system design is made of a seven-stage horizontal pendulum arrangement with six of the upper stages being suspended with cantilever springs to provide vertical isolation.
- **Gravity gradients**: this effect is caused by direct gravitational coupling of mass density fluctuations to the suspended mirrors. The dominant source of gravity gradients arise from seismic surface waves, where density fluctuations of the Earth's surface are produced near the location of the individual interferometer test masses. The seismic contribution to the PSD of the rms motion $\tilde{x}(f)$ of the test-masses can be shown to be

$$S_n^{\rm seism}(f) \propto \left(\frac{G\varrho}{\pi f^2}\right)^2 \ , \tag{9.5}$$

where ϱ is the Earths density near the test-masses. A monitor and subtraction method can be used to control this source of noise. An array of seismometers can be distributed strategically around each test mass to monitor the relevant ground motion (and ground compression) that would be expected to couple through local gravity. A subtraction signal can be developed from knowing how the observed density fluctuations couple to the motion of each test-mass, and can potentially allow a significant reduction in gravity-gradient noise.

- **Thermal noise**: The biggest contributions are associated with the mirror masses and the last stage of their suspensions, especially in the low frequency range. Current detector are limited by thermal noise at their most sensitive frequency band. In fact, above the operating range there are the internal resonances of the test masses. The thermal noise in the operating range comes from the tails of these resonant modes. In order to estimate the internal thermal noise of a test mass, each resonant mode of the mass can be regarded as a harmonic oscillator. Using a direct application of the fluctuation-dissipation theorem to the optically-sensed position of the mirror surface, one finds that the PSD of the test-masses position can be described by

$$S_n^{\rm therm}(f) = \frac{2\,k_{\rm B}T}{\pi^2 f^2}\,\frac{W_{\rm diss}}{F_0}\,, \tag{9.6}$$

where F_0 is the peak amplitude of the oscillatory force and $W_{\rm diss}$ is the power dissipated in the mirror. This expression highlights where mechanical dissipation is located with respect to the sensing laser beam. In particular, the thermal noise associated with the multi-layer dielectric mirror coatings, required for high reflectivity, will in fact limit the sensitivity of second-generation gravitational-wave detectors at their most sensitive frequency band. In order to keep thermal noise as low as possible the mechanical loss factors of the masses and pendulum resonances should be as low as possible. Furthermore, the test-masses must have a shape such that the frequencies of the internal resonances are kept as high as possible. They must be large enough to accommodate the laser beam spot without excess diffraction losses, and they must be massive enough to keep the fluctuations due to radiation pressure at an acceptable level.

- **Quantum noise**: There are two sources of quantum noise: the uncertainty of the number of detected photons in the photodiode, called shot-noise, and the perturbations due to the radiation pressure of the laser beam. An obvious point to choose is halfway up a fringe since the change in photon number produced by a given differential change in arm length is greatest at this point, and consequently we minimize the uncertainty in the dark fringe. It is possible to obtain the explicit expression for the PSD for the shot-noise assuming that the number of photon collected at the photodiode is a stochastic variable with Poissonian distribution. The result is

$$S_n^{\rm sh} = \frac{\hbar c^2}{I_0\omega_0}\,, \tag{9.7}$$

where I_0 and ω_0 are respectively the intensity and the frequency of the light beam inside of the detector. We can see that this term is not frequency-depended. For the radiation pressure contribution, one can use the classical relation for the light pressure $F_{\rm rp} = 2I_0/c$ and we get,

$$S_n^{\rm rp} = \frac{2\hbar I_0\omega_0}{m^2c^2(2\pi f)^4}\,, \tag{9.8}$$

where m is the mass of the mirror. From Eq. (9.7) and Eq. (9.8), it is possible to define an single quantum PSD as

$$S_n^{\rm quant} = \left(\kappa + \frac{1}{\kappa}\right)\frac{h_{\rm SQL}^2}{2} \geq h_{\rm SQL}^2\,, \tag{9.9}$$

where

$$\kappa = \frac{2I_0\omega_0}{m(\pi c f)^2}\,, \quad h_{\rm SQL} = \sqrt{\frac{2\hbar}{m(\pi L f)^2}}\,.$$

The quantity $h_{\rm SQL}$ determines the standard quantum limit, which represents a fundamental threshold for the observations. However, it is possible to exceed this limit using a particular optical technique, called *squeezing*. This method acts on the coherent states of the laser beam selecteing the quadrature of interenst and reducing the quantum fluctuations around this value.

Current detectors. Currently, the international network for GW observation is constituted of four operative ground-based interferometers. In U.S.A., there are the two LIGO (Laser Interferometer Gravitational-Wave Observatory) detectors: this machines have arms of 4 km and the laboratories are located in Hanford, Washington, and Livingston, Louisiana. The other two detectors are in Europe. One is GEO600 in Hannover, Germany, with arms of 600 m and founded by the Max Planck Society and the Science and Technology Facilities Council (STFC) Collaboration. This detector is smaller than the others and used to develop technology and "astrowatch" mode. The other one is Virgo with arms of 3 km and located near Pisa, Italy. It was funded by INFN (Italy) and CNRS (France) organizations and run by the the EGO (European Gravitational Observatory).

The initial LIGO and Virgo operations started in 2000s, but they did not detect any GWs. The inteferometers where subsequently upgraded to their "advanced" configurations. This first observation period O1 of the Advanced

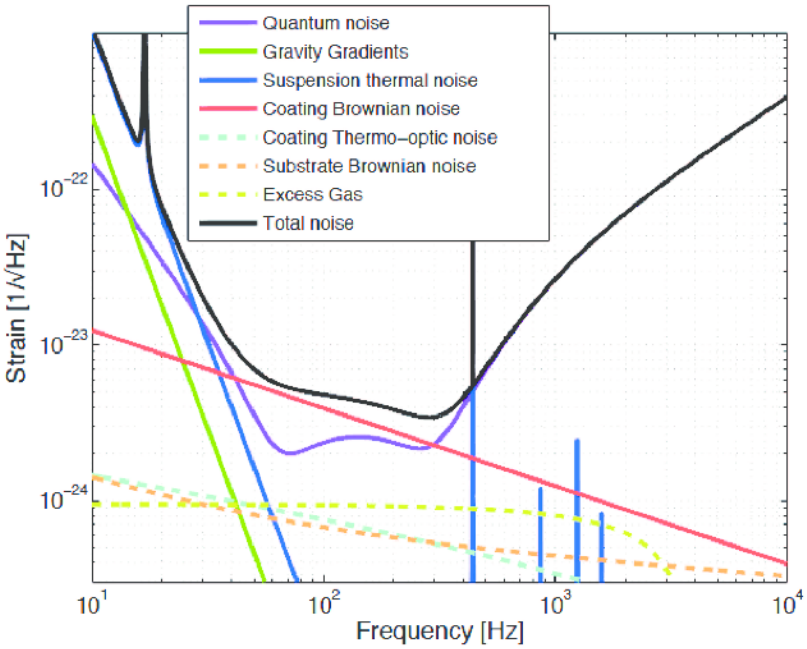

Figure 9.2: Amplitude spectral density of the design configuration planned and Advanced Virgo. The figure shows the different contributions of the several sources of noise present in the interferometers. At low frequency, the sensitivity is limited by the seismic motions, the several thermal contributions and the radiation pressure noise of the laser, while in the high frequency limit, the instruments are strongly limited by the quantum shot-noise. However, the realistic picture is more complex since many other external effects contribute in the noise and the ASDs show several high amplitude noise features. These peaks are due to several practical complications, e.g. the AC power grid (harmonics of 60 Hz in the U.S. and 50 Hz in Europe), mechanical resonances, injected calibration lines, contributions due to control systems and many others.

LIGO configurations started in 2015 and lasted for 3 months. Advanced Virgo started commissioning in 2016, joining the two LIGO detectors in May 2017 during the second observation period O2. In these two periods of observations (O1 and O2), the LIGO-Virgo collaboration (LVC) observed 11 gravitational transients coming from binary mergers of compact objects, such as black holes and neutron stars. These events are collected in a catalog and described in Abbott et al. (2019b). O3 runs started in 2019 and continued to spring 2020.

In 2020, another ground-based interferometer joined the network: KAGRA (Kamioka Gravitational Wave Detector) that is located in the Kamioka Observatoy, Japan, near the neutrino physics experiments. KAGRA is 3 km long and it implemented two new technologies: it is built underground to minimize the effect of seismic motions and it uses cryogenic temperatures in order to reduce the Brownian noise. Moreover, another proposal comes from the LIGO collaboration for a detector in India.

Binary-black-hole merger observation: GW150914. The first direct observation of a gravitational transient was made on 14 September 2015 and was announced by the LIGO and Virgo collaborations on 11 February 2016. Formally, this event was observed by the LIGO detector before O1, during an engineering run (i.e. period in which the performances of the detector are tested). The whitened strains observed by the LIGO interferometers are shown in Fig. 9.6 with the respective spectrograms. This event corresponds to a coalescence of two black holes with masses respectively of $\sim$35 $M_\odot$ and $\sim$30 $M_\odot$ located at $\sim$400 Mpc from the Earth. The spectrograms in Fig. 9.6 show that frequency increases with time coherently with the chirp-like evolution described in (Chap. 3) followed by a ringdown (Chap. 7). At the merger, the two objects reached a relative velocity of $\sim 0.55\,c$ emitting $\sim 3.6 \times 10^{49}$ W. After the merger, the collision generated a single remnant black hole with mass $\sim$62 $M_\odot$ and during the dynamics the system emitted in total $\sim 3\ M_\odot c^2$ through GWs.

This first direct observation was reported around the world as a remarkable accomplishment for many reasons and now it represents a milestone of modern physics. First of all, this is a second proof of the existence of gravitational radiation after the pulsars observations and the first detection of a GW passing through Earth. Furthermore, GW150914 demonstrates the existence of stellar-mass black holes more massive than 25 $M_\odot$, and establishes that binary black holes can form in nature and merge within a Hubble time. Thanks to the discovery of GWs, the 2017 Nobel Prize in Physics was awarded to Rainer Weiss, Barry Barish and Kip Thorne "[...] for decisive contributions to the LIGO detector and the observation of gravitational waves".

Binary neutron star observation: GW170817. GW170817 is a signal observed by the LIGO and Virgo detectors on 17 August 2017, originating from the shell elliptical galaxy NGC 4993. The GW was produced by the last minutes of two neutron stars spiralling closer to each other and finally merging. The two stars had a mass of $\sim$1.4 $M_\odot$ each

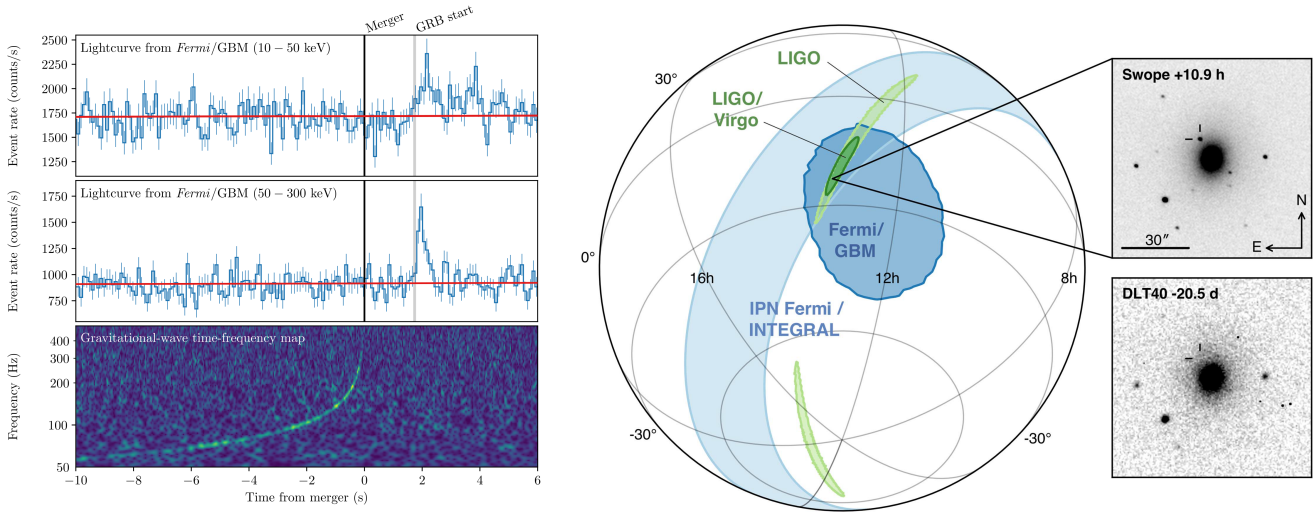

Figure 9.3: Left panel: the figure shows the coincident measurements of the gravitational signal GW170817 and the short gamma-ray burst GRB170817 observed ∼2 s after the GW peak by Fermi spacecraft. Right panel: combined measurment of the sky location of GW170817 source. It is possible to see that using the information from three detector it is possible to strongly constraint the position of the source with GWs.

and the system was located at ∼40 Mpc from the Earth. Neutron stars are very interesting objects since the matter that compose them has a density larger than the nuclear density, and its behaviour is currently not fully understood, and they represent natural laboratories in which we can test our theories.

The gravitational wave signal GW170817 lasted for approximately 100 seconds starting from a frequency of 24 Hz. It covered approximately 3000 cycles, increasing in amplitude and frequency to a few hundred hertz in the typical inspiral chirp pattern. An automatic computer search of the LIGO-Hanford datastream triggered an alert to the LIGO team about 6 minutes after the event. The gamma-ray burst (GRB) alert had already been issued at this point (16 seconds post-event), so the timing near-coincidence was automatically flagged. The LIGO/Virgo team issued a preliminary alert (with only the crude gamma-ray position) to astronomers in the follow-up teams at 40 minutes post-event. Sky localisation of the event requires combining data from the three interferometers; this was delayed by two problems. The Virgo data were delayed by a data transmission problem, and the LIGO Livingston data were contaminated by a brief burst of instrumental noise (called *glitch*) a few seconds before the peak of the signal. These required manual analysis and interpolation before the sky location could be announced about 4.5 hours post-event. The three detections localized the source to an area of ∼30 square degrees in the southern sky at 90% probability. This narrow sky region allowed the astronomical telescopes to locate the source of the signal and they were able to observe the electromagnetic counterpart of this violent collision. This light emitted by this source was observed by many observatories on the Earth and in the space, and in many observational bands, allowing us to perform the first multi-messenger observation with GW and light.

Next-generation detectors. Current detectors perform measurements in the frequency range 20 Hz to 1 kHz and at the threshold of the quantum noise. One one hand, there is a push to accessing higher frequencies and improve the current ground-based interferometer sensitivity. Higher frequencies are interesting for example for signal from neutron star mergers (not only inspiral). On the other hand, other frequency ranges can explore a variety of new sources like supermassive black holes or white dwarf. Other interferometric anthennas are being set up to start multi-band GW astronomy.

An ongoing project is LISA, acronym for Laser Interferometer Space Antenna. This is a mission led by the European Space Agency (ESA) and it would be the first dedicated space-based gravitational wave detector. The LISA concept has a constellation of three spacecraft arranged in an equilateral triangle with sides millions of killometers long, flying along an Earth-like heliocentric orbit. Each satellite corresponds to a test mass and the distance between them is measured with interferometric techniques. The size of this interferometer allows one to observe GWs in the frequency range from 0.1 mHz to 1 Hz. In this band, we expect to find the signals from heavy mass black holes, like galactic collisions, and the inspirals from extreme mass ratio binary coalescences. On December 2015, the ESA launched the LISA Pathfinder. In this mission, two test masses were placed in a nearly perfect gravitational free-fall and their relative motion was monitored. The laser interferometer measured the relative position and orientation of the masses to an accuracy of less than 0.01 nanometres. This was a result beyond the expectation and this accuracy is estimated to be sensitive enough to detect GWs by the follow-on mission. LISA is expected to be launched in 2034.

Another EU project GW observations is the Einstein Telescope (ET). This proposal is for an interferometer located underground in order to reduce seismic noise and gravity gradient noise (the same technique is adopted by the current interferometer KAGRA). The arms will be 10 km long, and like LISA, there will be three arms in an equilateral triangle, with two detectors in each corner. In order to measure the polarization of incoming gravitational waves and

avoid having an orientation to which the telescope is insensitive, a minimum of two detectors are required. While this could be done with two 90° interferometers at 45° to each other, the triangular form allows the arms to be shared. The 60° arm angle reduces each interferometer's sensitivity, but that is made up for by the third detector, and the additional redundancy provides a useful cross-check. Each of the three detectors would be composed of two interferometers, one optimized for operation below 30 Hz and one optimized for operation at higher frequencies. The low-frequency interferometers will use cooled optics, with a beam power of about 18 kW in each arm cavity. The high-frequency ones will use room-temperature optics and a much higher recirculating beam power of 3 MW. The ASD is expected to be a couple of orders of magnitude below the design sensitivity of the current detectors. This might allow us to see the post-merger dynamics of binary neutron star mergers, currently hidden by the high-frequency noise. These sources are expected to emit radiation in the band from 2 kHz to 6 kHz and these phenomena could reveal unknown aspects of the nuclear matter in high-density regimes.

Another proposal for a ground-based detector is Cosmic Explorer (CE). This mission is planned to be founded by U.S. contribution and the project is a 40 km L-shaped observatory. As ET, this detector will be able to determine the nature of the densest matter in the universe and reveal the universes binary black hole and neutron star populations throughout cosmic time, providing an independent probe of the history of the expanding universe. Thanks to its large size, CE is expected to perform measurements with high accuracy and it will be able to extend the band coverage of the current detectors, expecially in the low-frequency region.

9.2 Noise characterization

The output of a standard GW detector is a time series $s(t)$ which contains also the gravitational-wave time series $h(t)$ [2]. In general, $s(t)$ is not the signal detected at the photodiode: assuming an experimental apparatus with linear response, the output signal $s_{\rm out}$ is a linear function of the Fourier transform of the signal,

$$\tilde{s}_{\rm out}(f) = T(f)\tilde{s}(f) \ , \tag{9.10}$$

where $T(f)$ is the transfer function. If the apparatus is composed by different components, the resulting transfer function is the product of the $T_i(f)$ of each component. In absence of noise, $s(t) = h(t)$ and thus one expects that

$$\tilde{h}_{\rm out}(f) = T(f)\tilde{h}(f) \ . \tag{9.11}$$

In general $s(t) \neq h(t)$ because the detectors picks up many other signals that are not GW. All these other signals form the noise.

Power spectral density (PSD) and amplitude spectral density (ASD). To introduce the concept of *noise* imagine that each time the laser beam interacts with a detector component spurious signal fluctuations are generated. Let the output be a superposition of the gravitational signal and the noise,

$$s_{\rm out}(t) = h_{\rm out}(t) + n_{\rm out}(t) \ , \tag{9.12}$$

and define a fictitious input noise,

$$\tilde{n}(f) = T^{-1}(f)\tilde{n}_{\rm out}(f) \ . \tag{9.13}$$

as if all the noise is generated in input and propagates with the gravitational signal in the apparatus. Then we can write

$$s(t) = h(t) + n(t) \, , \tag{9.14}$$

and we can think that the detector output is generated by the signal $h(t)$ and the noise $n(t)$, both dimensionless quantities.

If the noise is stationary, i.e. its properties are time independent, the different Fourier components are uncorrelated, then

$$\langle \tilde{n}^*(f)\tilde{n}(f')\rangle = \frac{1}{2}\,\delta(f-f')\,S_n(f) \, , \tag{9.15}$$

where $\langle \dots \rangle$ denotes the average over a the ensemble [3] and $S_n(f)$ is the *power spectral density (PSD)*. Since $n(t)$ is real $\tilde{n}(-f) = \tilde{n}^*(f)$, $S_n(-f) = S_n(f)$. If $n(t)$ is dimensionless, the PSD has dimensions Hz^{-1}. Moreover, we observe that in a real scenario we work with finite segment of data of a given period T, and we are dealing with discrete functions fo time and frequency. Therefore the integral of the δ function does not diverge for $f = f'$;

$$\delta(f=0) \to \left[\int_0^T e^{2\pi \mathrm{i} f t}\mathrm{d}t\right] = T \, , \tag{9.16}$$

and from Eq. (9.15) we get

[2] The GW is described by a tensor, but reduces to a scalar time series once projected onto the detctor anthenna pattern.

[3] The average over the ensemble is the average over the possible realizations of our system. But we have only one possible system, i.e. our detector, then the average over the ensemble is replaced with the time average over a period T. The noise contained in the data is considered as one of the possible realizations. This is equivalent to the assumption of ergodic system. We also observe that the resolution of the Fourier transform $\tilde{n}(f)$ is $\Delta f = 1/T$.

$$\left\langle |\tilde{n}(f)|^2 \right\rangle = \frac{T}{2} S_n(f) \,. \tag{9.17}$$

The power spectral density can be introduced in a second, more rigorous, way. Assume the combination of all the noise sources in a detector produces a time series $n(t)$ that can be represented by a vector n_i, with components given by the discrete time samples $n_i = n(t_i)$. The noise is described as a stochastic process with statistical properties given by the probability distribution $p(n)$. This model can be used to define summary statistics such as the mean $\mu = E[n]$ (where E is defined as the expectation value) and covariance $C_{ij} = E\left[(n_i - \mu)(n_j - \mu)\right]$ where the expectation values are taken with respect to $p(n)$. The mean can be estimated from the data as

$$\mu = \frac{1}{N} \sum_{i=1}^{N} n_i \,, \tag{9.18}$$

where N is the total number of points. Note that, in practice, the analyses do not use all N samples at once, but rather use segments of contiguous data of various lengths from a few seconds up to hours depending on the application. Noise is referred to as *Gaussian* if the joint probability distribution follows a multi-variate normal distribution:

$$p(n) = \frac{1}{\sqrt{\det(2\pi C_{ij})}} \exp\left[-\frac{1}{2} \sum_{i,j} (n_i - \mu) C^{-1}_{ij} (n_j - \mu) \right] \,, \tag{9.19}$$

where C^{-1}_{ij} is the inverse covariance matrix. The noise is referred to as *stationary* if C_{ij} depends only on the lag $|i - j|$. Recalling that for every index i exists a related time t_i, the condition of stationarity can be written as

$$C_{ii+k} = C_{jj+k} \,, \;\; \forall i, j, k \,.$$

Stationary noise is characterized by the correlation function $C(\tau)$, where $\tau = |t_i - t_j|$ is the time lag, and then the mean value μ and the other statistical properties are constant with respect to time.

Transforming to the Fourier domain, where the labels i, j now refer to frequencies f_i, f_j, stationary noise has a diagonal covariance matrix $C_{ij} \to \delta_{ij} S_n(f)$, which defines the PSD $S_n(f)$. The power spectral density is given by the Fourier transform of the correlation function $C(\tau)$,

$$S_n(f) = 2 \int_{-\infty}^{+\infty} C(\tau)\, e^{+2\pi i f \tau} \, \mathrm{d}\tau \,, \tag{9.20}$$

and, on the other hand,

$$C(\tau) = \int_{0}^{\infty} S_n(f)\, e^{-2\pi i f t} \, \mathrm{d}f \,. \tag{9.21}$$

The last integral is limited to positive frequencies $f > 0$ because $C(\tau)$ is a real function and $S^*_n(f) = S_n(-f)$. Sometimes the *amplitude spectral density (ASD)* is also used to characterize the noise, this quantity corresponds to the square root of the PSD, $\sqrt{S_n(f)}$.

From the above argument, we understand that the analysis in the frequency-domain is better suited for our task, since the covariant $N \times N$ matrix is reduced in a diagonal form. Stationary noise is uncorrelated between frequency bins, and the noise $\tilde{n}(f)$ in each bin follows a Gaussian distribution with random phase and amplitude $S_n^{1/2}(f)$. However, the reality is more complex and LIGO-Virgo data analysis pipelines must take into account the effect of non-stationarity and non-Gaussian deviations.

The PSD is a key quantity in GW analyses but it is not known a priori, it must be estimated from the data. In order to estimate PSD of a noise segment of data, one can perform a complex Fourier transform of the entire data stream around some time to be searched for signals, but that yields to a result strongly affected by noise fluctuations. To overcome this, it is common to use some form of averaging and these methods can be used to reduce the variance in the estimated power spectrum, but at the cost of either reducing the frequency resolution or requiring longer stretches of data. An example is the *Welch averaging method.* If we have a noise time series of duration T, the method consists in dividing the strain in M chunks with a fixed duration of T/M and estimate the Fourier spectrum for all of them, then the final PSD is the average of the square amplitudes of the spectra of the different chunks.

Remark 9.2.1. *In order to estimate the PSD, the time-domain series should not include, in principle, a GW signal.*

Remark 9.2.2. *The technical tool used to estimate the Fourier spectrum of a data segment is the* fast Fourier transform (FFT) [4]*, a fast algorithm that reduces the complexity of computing the discrete Fourier transfrom (DFT)*

[4] `https://en.wikipedia.org/wiki/Fast_Fourier_transform`

of a time series of N points from $\mathcal{O}(N^2)$ (matrix-vector multiplication) to $\mathcal{O}(N\log(N))$. The DFT of a finite time series $a_i(t_i)$ $i=1,...,N$ is defined as

$$\tilde{a}_j(f_j) = \sum_{i=0}^{N} a_i\, e^{-\frac{2\pi \mathrm{i}}{N} ij}\,, \tag{9.22}$$

where $N = T\cdot F_s$ and F_s defines the sampling frequency. The DFT $\tilde{a}_j$ is thus defined on a range of frequencies $f_j \in [-\frac{F_s}{2}, +\frac{F_s}{2}]$ with a step of $\Delta f = \frac{1}{T}$. Thus, the length of the time- series T defines the resolution in the frequency domain. Note that the Fourier transform assumes a periodical signal, but in practical applications the DFT/FFT is always applied to a finite time series. A related issue in signal processing with the FFT is windowing, that is essential in order to avoid spectral leakage effects. This will be further discussed in Rem. 9.4.1.

9.3 Antenna pattern

The tensor $h_{ij}^{\mathrm{TT}}(t)$ is reduced to a scalar quantity $h(t)$ when it is projected onto the detector. The scalar $h(t)$ depends on the geometry of the detector and on the direction of origin of the GW. An interferometer has not the same sensitivity in all the directions.

From linearized GR, we know that we decompose write a GW signal in its polarizations,

$$h_{ij}(t,\mathbf{x}) = \sum_{A=+,\times} e_{ij}^{A}(\mathbf{n})\, h_A(t,\mathbf{x})\,, \tag{9.23}$$

where e_{ij}^{A} are the polarization matrix defined in Eq. (3.11), $\mathbf{n}$ is the unitary vector that defines the direction of propagation of the GW and $\mathbf{x} = (r,\theta,\phi)$ are the polar coordinates centred in the position of the interferometer. First of all, we note that we assume that the observed GWs have wavelengths much larger than the size of the detector (like it is for the ground-based interferometers). Then, we are allowed to neglect the spatial dependency of the GW.

In general the output of a GW detector is a scalar quantity $h(t)$. The measured strain is proportional to the emitted GW (which is a tensorial quantity) through the detector tensor D_{ij} as

$$h(t) = D_{ij}\, h_{ij}(t) = \sum_{A=+,\times} D_{ij}\, e_{ij}^{A}(\mathbf{n})\, h_A(t,\mathbf{x})\,, \tag{9.24}$$

where $D_{ij}(\mathbf{n})$ is a constant tensor which depends only the geometry of the detector. It is then convenient to define the *antenna pattern functions* $F_A(\mathbf{n})$,

$$F_A(\mathbf{n}) = D_{ij}\, e_{ij}^{A}(\mathbf{n})\,, \quad \text{for } A = +,\times\,. \tag{9.25}$$

The antenna pattern functions depend on the direction of propagation $\mathbf{n} = (\theta,\phi)$ of the incoming GW and thanks to them we can rewrite Eq. (9.24) as

$$h(t) = F_+(\mathbf{n})\, h_+(t) + F_\times(\mathbf{n})\, h_\times(t)\,. \tag{9.26}$$

The above equation implicitly assumes that we fixed a system of axes $(\mathbf{u},\mathbf{v})$ in the plane orthogonal to the propagation direction $\mathbf{n}$ of the wave, with respect to which the polarizations h_+ and $h_\times$ are defined. It is interesting to generalize this expression for any arbitrary set of axes, performing a rotation of ψ around $\mathbf{n}$. The the axes $(\mathbf{u},\mathbf{v})$ are rotated to new axes according to

$$\mathbf{u}' = \mathbf{u}\cos\psi - \mathbf{v}\sin\psi\,, \tag{9.27}$$

$$\mathbf{v}' = \mathbf{u}\sin\psi + \mathbf{v}\cos\psi\,. \tag{9.28}$$

In the new frame, the two polarizations change their amplitudes $h_{+,\times} \to h'_{+,\times}$ according to

$$h_+ = h_+\cos(2\psi) - h_\times\sin(2\psi)\,, \tag{9.29}$$

$$h_+ = h_\times\sin(2\psi) + h_+\cos(2\psi)\,. \tag{9.30}$$

Indeed, in the new frame, the polarization tensors are given by

$$\left(e_{ij}^{+}\right)' = u'_i u'_j - v'_i v'_j\,, \tag{9.31}$$

$$\left(e_{ij}^{\times}\right)' = u'_i v'_j + v'_i u'_j\,. \tag{9.32}$$

Combining the last equation with Eq. (9.27), it is possible to get the tranformation law Eq. (9.29). This equation tells us how the polarization angle affects the observed strain.

The pattern functions $F_{+,\times}$ depends on the polarization tensors $e_{ij}^{+,\times}$ through Eq. (9.25). Thus, it is convient to include the dependency on the polarization angle in the antenna functions,

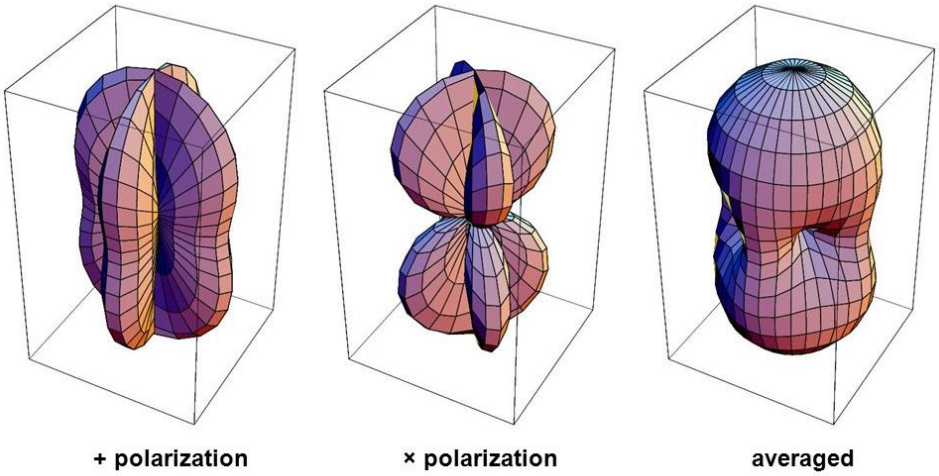

Figure 9.4: Antenna pattern functions for an L-shaped interferometer detector. The figures show the value of $F_A(\theta, \phi, \psi = 0)$ for $A = +, \times$ in cartesian coordinate, where the detector is located at the centre of the box. The average corresponds to the root-mean-square (rms) sensitivity, $F_{\rm rms} = (F_+^2 + F_\times^2)^{1/2}$.

$$F_+(\mathbf{n}, \psi) = F_+(\mathbf{n}, 0)\cos(2\psi) - F_\times(\mathbf{n}, 0)\sin(2\psi)\,, \tag{9.33}$$
$$F_\times(\mathbf{n}, \psi) = F_\times(\mathbf{n}, 0)\sin(2\psi) + F_+(\mathbf{n}, 0)\cos(2\psi)\,, \tag{9.34}$$

where $F_{+,\times}(\mathbf{n}, 0)$ are the functions previously defined. Of course, fixing the axes $(\mathbf{u}, \mathbf{v})$, the polarizagtion angle ψ is constant for an incoming GW signal and the antenna functions depend only on the direction of propagation. However, it is useful to keep the general notation in order to denote how the measured strain is modified by a rotation of ψ. A useful idedntity satisfied by the antenna functions, independently from the specific form of the detector tensor D_{ij}, is

$$\int F_\times(\mathbf{n}) F_+(\mathbf{n})\, \mathrm{d}\Omega = 0\,, \tag{9.35}$$

where $\mathrm{d}\Omega = \sin\theta \mathrm{d}\theta\, \mathrm{d}\phi$ is the integral over the solid angle. Moreover, it is interesting to observe that it is always possible to choose a frame (i.e. a value of ψ) where so that $F_\times$ vanishes and F_+ is non-zero, or viceversa. Note that integrating over the angle ψ we get

$$\int_0^{2\pi} F_+^2(\mathbf{n}, \psi)\, \mathrm{d}\psi = \int_0^{2\pi} F_\times^2(\mathbf{n}, \psi)\, \mathrm{d}\psi\,. \tag{9.36}$$

By studing in detail the interaction between the GWs and a laser interferometer using the equation of the geodesic deviation, it is possible to prove that the antenna pattern functions for such a detector have the following forms,

$$F_+(\mathbf{n}, \psi = 0) = \frac{1}{2}\left(1 + \cos^2\theta\right)\, \cos(2\phi)\,, \tag{9.37}$$
$$F_\times(\mathbf{n}, \psi = 0) = \cos\theta\, \sin(2\phi)\,, \tag{9.38}$$

where we expanded the dependency on the direction $\mathbf{n}$ using the polar anlges θ, ϕ.

As it is shown in Fig. 9.4, the antenna functions are relatively smooth functions of the position of the source in the sky. On one hand, this is an advantage because the detector has a good covarege of the sky, of almost 4π, except for some blind spots (differently from a conventional astronomic telescope). On the other hand, however, with a single detector it is impossible to locate the source in the sky. Indeed, Eq. (9.26) depends on four variables: the two polarizations $h_{+,\times}$ and the two angles θ, ϕ. Then, if we assume to use two interferometers, we have only three measurements: the strains $s_1(t)$, $s_2(t)$ observed by the detectors and the time delay between them τ_{12}. These quantitites are not enought to solve Eq. (9.26). However, if we use three detector, we will get five measured quantitites (the three strains $s_i(t)$, $i = 1, 2, 3$, and two independet delay times) and we are able to sove Eq. (9.26). Then it is possible to understand that a global network of interferometers is necessary to fully understand the nature of these signals.

9.4 Data analysis & Match filtering

We have seen that we can write the detector output as $s(t) = h(t) + n(t)$. For the typical GW event expected by astrophysical events and the sensitivity of the current ground-based detectors it holds that

$$|h(t)| \ll |n(t)| \ . \tag{9.39}$$

Then, we ask ourselves: How can we distinguish a signal in a recorded strain of data?

This is a problem of signal processing in which the noise is louder than our signal; an optimal technique to solve the problem is touse data *filtering*. To understand the idea of filtering, suppose that we know the form of $h(t)$ that we are looking for. Then we can average the quantity $s(t) \cdot h(t)$ over a period T of time,

$$\frac{1}{T}\int_0^T s(t)\cdot h(t)\,\mathrm{d}t = \frac{1}{T}\int_0^T h^2(t)\,\mathrm{d}t + \frac{1}{T}\int_0^T n(t)\cdot h(t)\,\mathrm{d}t\,. \tag{9.40}$$

If $h(t)$ and $n(t)$ are uncorrelated oscillating functions, then, the second integral will grow as $T^{-1/2}$ (as it is for systems behaving as random-walks),

$$\frac{1}{T}\int_0^T n(t)\cdot h(t)\,\mathrm{d}t \propto \frac{n_0 h_0}{\sqrt{T}}\ , \tag{9.41}$$

where h_0 and n_0 are respectively the characteristic amplitudes of the signal and the noise. On the other hand, the first integral is positive definite and it contributes as

$$\frac{1}{T}\int_0^T h^2(t)\,\mathrm{d}t \propto h_0^2\ . \tag{9.42}$$

Thus, for $T \to \infty$, the second term of Eq. (9.40) is averaged to zero and we have *filtered out* the contribution of the noise from the output. In a realistic scenario, we cannot use a infinite number of data points and we are limited to the observation time. Still, denoting with τ_0 the time-scale of a GW event, we see that this method is able to identify a signal against a given background noise in the regime $n_0\sqrt{\tau_0/T} \lesssim h_0$, digging below the noise threshold. To give an idea, if we consider a binary black hole coalescence with characteristic time-scale $\tau_0 \sim 0.02$ s, with a segment of $T = 16$ s we can observe GW amplitudes of 3 orders of magnitude below the ASD limit.

Matched filtering. Once clarified the basic idea, let us introduce a mathematical framework. We are interested in a quantify that defines the *loudness* of a recorded signal $s(t)$. Then, we write

$$\mathrm{S} = \int_{-\infty}^{+\infty} s(t)\,K(t)\,\mathrm{d}t = \int_{-\infty}^{+\infty} \tilde{s}^*(f)\,\tilde{K}(f)\,\mathrm{d}f\,. \tag{9.43}$$

where $K(t)$ is a filter function that has to *match* our signal s. For this equality we made use of the convolution product. The noise can be quantified as the standard deviation of the recorded strain within the assumption $h(t) = 0$,

$$\begin{aligned}
\mathcal{N}^2 &= \Big[\big\langle \mathrm{S}^2\big\rangle - \big\langle \mathrm{S}\big\rangle^2\Big]_{h=0} = \big\langle \mathrm{S}^2\big\rangle_{h=0} \\
&= \int_{-\infty}^{+\infty} K(t)\,K(t')\,\langle n(t)\,n(t')\rangle\ \mathrm{d}t\,\mathrm{d}t' \\
&= \int_{-\infty}^{+\infty} K(t)\,K(t')\int_{-\infty}^{+\infty} e^{2\pi \mathrm{i} t(f-f')}\,\langle \tilde{n}^*(f)\,\tilde{n}(f')\rangle\ \mathrm{d}f\,\mathrm{d}f'\,\mathrm{d}t\,\mathrm{d}t' \\
&= \frac{1}{2}\int_{-\infty}^{+\infty} S_n(f)|\tilde{K}(f)|^2\ \mathrm{d}f\,,
\end{aligned} \tag{9.44}$$

where we used $\langle n(t)\rangle = 0$ and Eq. (9.15).

Now, we assume to know how to describe the GW signal we are looking for (i.e. we have a model for $h(t)$) and we ask ourselves: Which is the best filter function $K(t)$ that maximises amount of signal S with respect to N? Averaging S over a time period T we get

$$\langle \mathrm{S}\rangle = \int_{-\infty}^{+\infty} \tilde{h}^*(f)\,\tilde{K}(f)\,\mathrm{d}f\,, \tag{9.45}$$

since $\langle n(t)\rangle = 0$. Then computing the ratio between them we obtain

$$\frac{\langle \mathrm{S}\rangle^2}{\mathcal{N}^2} = \frac{\left|\int_{-\infty}^{+\infty} \tilde{h}^*(f)\,\tilde{K}(f)\,\mathrm{d}f\right|^2}{\frac{1}{2}\int_{-\infty}^{+\infty} S_n(f)|\tilde{K}(f)|^2\ \mathrm{d}f} = \frac{\left|\int_{-\infty}^{+\infty}\left(\frac{\tilde{h}^*(f)}{\sqrt{S_n(f)}}\right)\left(\tilde{K}(f)\sqrt{S_n(f)}\right)\ \mathrm{d}f\right|^2}{\frac{1}{2}\int_{-\infty}^{+\infty} S_n(f)|\tilde{K}(f)|^2\ \mathrm{d}f}\,. \tag{9.46}$$

Using the Cauchy-Schwarz inequality, the ratio in Eq. (9.46) can be maximised as

$$\frac{\langle \mathrm{S}\rangle^2}{\mathcal{N}^2} = 2c\,\frac{\left(\int_{-\infty}^{+\infty}\frac{|\tilde{h}(f)|^2}{S_n(f)}\mathrm{d}f\right)\left(\int_{-\infty}^{+\infty}|\tilde{K}(f)|^2\,S_n(f)\,\mathrm{d}f\right)}{\int_{-\infty}^{+\infty}S_n(f)|\tilde{K}(f)|^2\,\mathrm{d}f} = 2c\int_{-\infty}^{+\infty}\frac{|\tilde{h}(f)|^2}{S_n(f)}\mathrm{d}f\,, \tag{9.47}$$

where c is a constant factor. This equation leads to the value of the optimal filter

$$\tilde{K}(f) = 4c\,\frac{\tilde{h}(f)}{S_n(f)}\,. \tag{9.48}$$

The above argument suggests to introduce the *Wigner scalar product* between two real functions $a(t)$ and $b(t)$

$$(a|b) = 4\int_0^\infty \frac{\tilde{a}^*(f)\,\tilde{b}(f)}{S_n(f)}\,\mathrm{d}f\,, \tag{9.49}$$

where the constant c has been fixed to $c = 1$ and the factor 4 comes from the limitation of the integral to positive frequencies $f \geq 0$. In general $(a|b)$ is a complex number, while $(a|a)$ is always real. Using this definition we can rewrite Eq. (9.43) as

$$\mathrm{S} = (s|h)\,, \tag{9.50}$$

and the same for Eq. (9.47),

$$\frac{\langle \mathrm{S}\rangle^2}{\mathcal{N}^2} = (h|h)\,, \tag{9.51}$$

An interesting interpretation of Eq. (9.49) is to split the PSD into two ASD terms that can be associated with the two time series, i.e.

$$(a|b) = 4\int_0^\infty \frac{\tilde{a}^*(f)}{\sqrt{S_n(f)}}\,\frac{\tilde{b}(f)}{\sqrt{S_n(f)}}\,\mathrm{d}f\,.$$

This ends up weighting both functions by the inverse of the ASD, which are the "whitened forms" of these functions: the integrand of scalar product weights each Fourier's component of the functions $a(t)$ and $b(t)$ with the intensity of the noise in that specific frequency bin. In other words, the Wigner scalar product is weighting the signals more at the frequencies observed at higher sensitivity, while it weights less the signals at frequencies at which the noise is loud. It is interesting to observe that, if we take a generic GW signal such that

$$h_+(t) = A(t)\cos\left(\phi(t)\right)\,, \quad h_\times(t) = A(t)\sin\left(\phi(t)\right)\,,$$

then it is possible to prove that

$$(h_+|h_\times) = 0\,. \tag{9.52}$$

This result leads to the conclusion that the product $(s|h)$ does not mix the contributions from different polarizations and its result is a linear combination of the projections of each component, i.e. if $h = a_+h_+ + a_\times h_\times$, where $a_{+,\times}$ are real constant values, then $(s|h) = a_+(s|h_+) + a_\times(s|h_\times)$.

The Wigner scalar product allows one to quantity the match (overlap) between a template and a signal and the concept of signal-to-noise ratio in the context of filtered analysis. The *overlap* between two time series $a(t)$ and $b(t)$ is defined as

$$\mathcal{O}[a,b] = \frac{|(a|b)|}{\sqrt{(a|a)(b|b)}}\,. \tag{9.53}$$

The quantity $\mathcal{O}$ takes value from 0 to 1 and it measures the agreement between the two time series. We observe that $(a|a)$ is proportional to the power spectrum of the whitened series $\tilde{a}(f)/\sqrt{S_n(f)}$, and the same for $b(t)$.

How can we estimate the loudness of the recorded signal assuming a given template $h(t)$? The quantity defined in Eq. (9.43) is able to quantify the agreement between the data and the GW template. If one is interested in the strength of the signal that matches the template h in the data s, one needs to normalize the overlap $(s|h)$ with the "length" of the template. The *signal-to-noise ratio (SNR)* is thus defined as

$$\rho := \frac{(s|h)}{\sqrt{(h|h)}}\,. \tag{9.54}$$

The SNR ρ is proportional to amplitude of the signal and independent from the amplitude of the template. The SNR is a fundamental quantity for GW data analysis since it estimates the amount of signal deposited in the recorded data s with respect to a given template h.

So far we have defined the overlap between s and h where we have assumed the template to be of the same length as our data. However, what we are actually interested in is the matched filter of s using h where the data $s(t)$ is an extended time series whose length is longer than the template time series $h(t)$. Then we are to choose a reference time t_0 and a reference phase angle ϕ_0 for $h(t; t_0, \phi_0)$ such that the SNR amplitude is maximized. Recalling the rules of Fourier functions, we can define the template with respect to arbitrary reference values $t_0 = \phi_0 = 0$ and then write in Eq. (9.54) the explicit dependency from these parameters as

$$\rho(t_0, \phi_0) = \frac{4}{\sqrt{(h|h)}} \int_0^\infty \frac{\tilde{s}^*(f)\, \tilde{h}(f)\, e^{-\mathrm{i}(2\pi f t_0 + \phi_0)}}{S_n(f)}\, \mathrm{d}f\,. \tag{9.55}$$

Moreover, it is interesting to note that for the case $n(t) = 0$, i.e. $s(t) = h(t)$, Eq. (9.54) returns the case of Eq. (9.51). For this reason, the square root of Eq. (9.51) is usually labelled as optimal SNR, $\rho_{\rm opt} = \sqrt{(h|h)}$. This computation is valid for in the case of a single detector; for the multiple detectors it is possible to compute the network SNR summing the squared SNRs of every detector,

$$\rho^2_{\rm net} = \sum_{k=\mathrm{L,H,V,...}} \rho^2_k\,. \tag{9.56}$$

Remark 9.4.1. *The Fourier transform is a key mathematical tool for signal processing. The discrete realization of the FFT is the DFT introduced in Rem. 9.2.2 that can be computed using the FFT algorithm. The FFT technique allows us to transform time series in frequency series, but it assumes that the input time series $a_i = a(t_i)$ is a periodic function of time. If we perform the FFT of a non-periodic signal, the computation will be biased by the squared window function implicitly assumed using a finite time segment. Then, the resulting $\tilde{a}_j$ will be the convolution product between a_i and the squared window function, which contributes in the spectrum as a $1/f^2$ factor (the Fourier transform of a step function, see Fig. 9.5). In order to avoid this problem, the time series must be multiplied by a smooth function that has zeros at the beginning and of the end of the series. The Fourier contribution of a smoother function decreases faster than the $1/f^2$ and then it does not affect the estimation of the FFT as much as the step function. estimation of the FFT gives us better results.This method is called windowing and an example is shown in Fig. 9.5.*

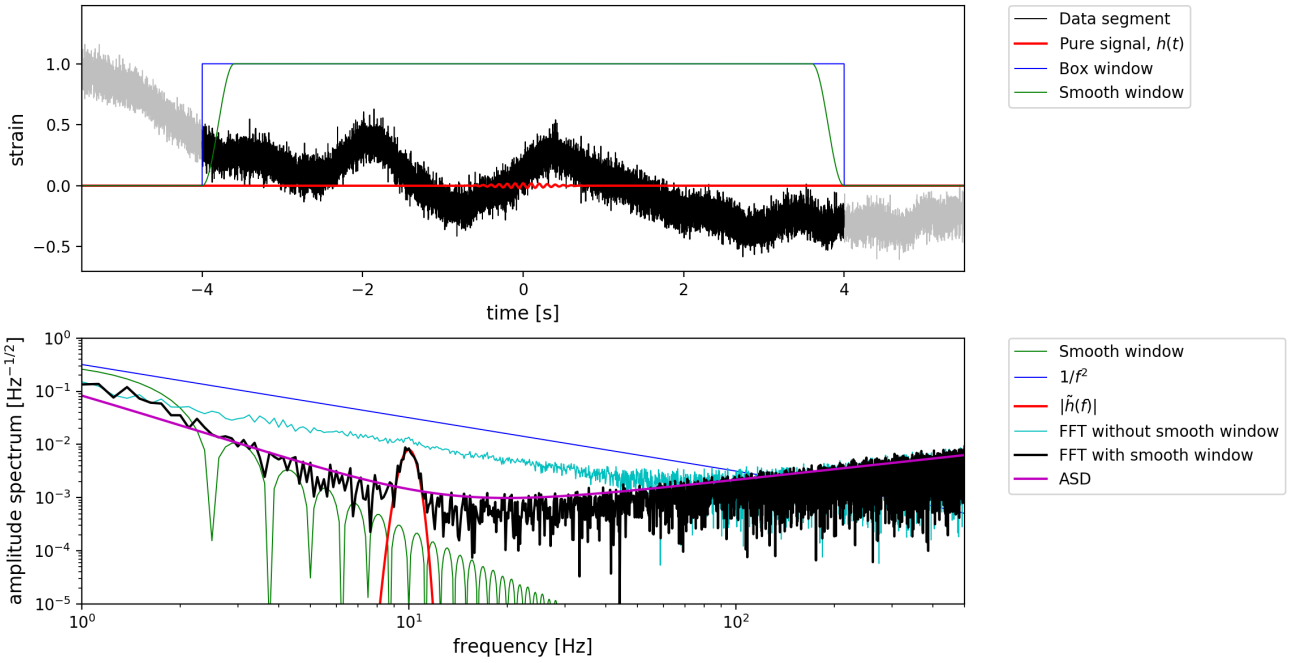

Figure 9.5: Top panel: the black line is a strain segment of artificial noise in which an fictitious signal (red) is injected. However, the signal is too small to be directly observed in the time-domain data. The blue function is the squared window implicitly applied in the choice of the segment, while the green function is a cosine-window, largely used in signal processing and known as Tukey window. Bottom panel: The purple line is the analytical ASD used to generate the noise and the red line is the amplitude spectrum of the pure injected signal. The cyan line is the spectrum of the data strain without windowing, i.e. the Tukey window is not applied. The black line is the spectrum of the same strain with the Tukey window. For the non-windowed strain, the low-frequency region is dominated by the *leakage*, proportional to $1/f^2$, due to not appropriate usage of the FFT and the contribution of the signal is not observable. On the other hand, the black line shows a clear deviation from the noise ASD. The spectrum of the Tukey window is plotted in green: it is possible to see that its contribution decrease much rapidly than $1/f^2$.

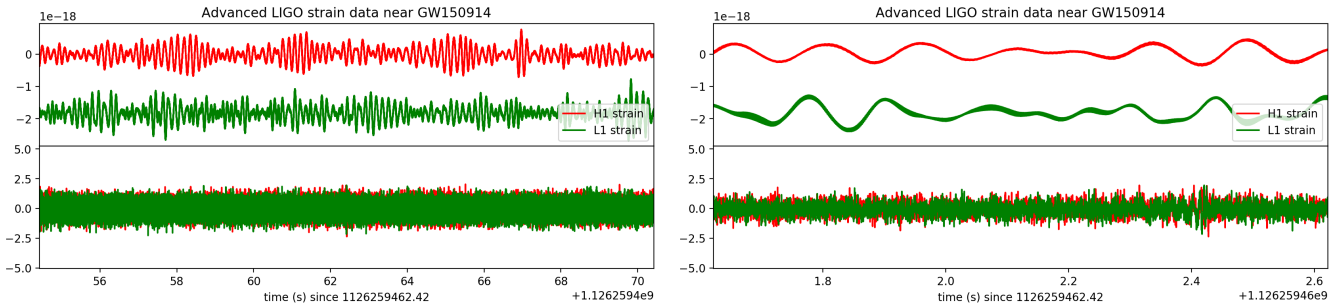

Figure 9.6: Left figure: top panel shows segments of 16 s extracted from the raw data of LIGO Hanford (red) and LIGO Livingston (green) centred around GW150914 trigger time. The bottom panel shows the same strain whitened with the respective PSDs. Right figure: The same as right, but zoomed on a period of 1 s. It is possible to see a correlation between the recorded strain of the two detectors.

Signal processing. Let us discuss the signal processing analysis of the first GW observation recorded by the LIGO detectors, GW150914. Data were recorded by two ground-based interferometers, labelled as H and L, and each of them returns a strain of data $s_{\rm H,L}(t)$. The data are time series segments with a finite length T and with a constant sampling frequency F_s, i.e. the inverse of the time difference between each point of the series. Then, our series contains $T \cdot F_s$ elements. A power excess in the data indicates that a signal $h(t)$ might e contained in $s_{\rm H,L}(t)$: How can we extract the GW signal?

The data are dominated by the noise contributions and their fluctuations are much larger than the ones due to a GWs. First of all, we have to estimate the PSD (or the ASD) of our detectors. The spectrum of the noise is estimate using data segments that do not contain the signal. The computation is performed with the Welch's method, previously discussed, and computing the Fourier transfrom using the FFT (See Rem. 9.2.2 and 9.4.1.) Second, we have to reweight the frequency components of the signal $s(t)$ on the ASD, in order to minimize the effects of the noise. This method is called *whitening*: the signal is rescaled in the frequency domain by the noise amplitude, in order to clean the time series and obtain constant noise contribution for each frequency bin (white noise, $S_n(f) = 1$). The whitened signal $s_{\rm w}(r)$ can be computed as

$$s_{\rm w}(t) = \int_{-\infty}^{+\infty} \frac{\tilde{s}(f)\, e^{+{\rm i}2\pi f t}}{\sqrt{S_n(f)}}\, {\rm d}f \ , \tag{9.57}$$

which is the anti-Fourier transform of $\tilde{s}(f)/\sqrt{S_n(f)}$.

The application of this procedure to GW150914 is shown in Fig. 9.6. The bottom-right panel of Fig. 9.6 shows a strong correlation between the fluctuations of the two detectors. In order to better visualise the signal, we shift the L signal of a time delay equal to the time taken by the light to travel between the two locations. Then we have also to invert L signal since the two LIGO detectors are oriented in opposite directions. In the end, we apply a band-pass filter (Butterworth of the fourth order) in order to remove the high-frequency and low-frequency noise contributions, since the spectrogram of GW150914 shows evidence of signal in the range between 30 Hz and 350 Hz. It is important to observe that usually LVC does not apply any further filter to the observed data, we are doing this now only for visualisation scopes. The final result is shown in Fig. (9.7): the two strains match perfectly and they agree with GR predictions.

Parameter estimation. After introducing the concepts of matched filtering and signal processing, let us focus on the methods used to estimate the parameters of the source using the matched filtering technique. The working asumption here is that the GW matches a waveform template $h(t;\boldsymbol{\theta})$, where $\boldsymbol{\theta}$ are the parameter of the source. In the case of a binary black hole merger we have 15 independent parameters: the two masses $m_{1,2}$ and the spins $\mathbf{s}_{1,2}$ of the two black holes , the inclination angle ι between the line of sight and the orbital plane, the luminosity distance D_L of the system from the Earth, the two angles for the sky location (α, δ), the polarization angle ψ, and the reference time t_0 and phase ϕ_0.

The parameter estimation methods are based on the Bayesian theory of probability. This framework is necessary in order to perform *inference* based on the measured data, recovering the posterior distribution for our parameters and quantifying the goodness of the template with respect to the data. The most important input quantities are the prior distribution of $\boldsymbol{\theta}$ and the likelihood function $p(s|\boldsymbol{\theta}, H)$. The prior distribution encodes the information or the assumptions that we have or make on the system (source) before making the measurement. The simplest and more agnostic prior for a parameter is a uniform distribution over a finite range. Then we have to define a likelihood function: this term quantifies the agreement between the experimental data and a template and it has to take into account the deviations due to instrumental noise. We recall that for every detector k we have the respective recorded strain of data $s_k(t)$ and the associated PSD $S_{n,k}(f)$ that describe the noise fluctuations. We can start imposing the assumption of Gaussian and stationary noise and rewrite Eq. (9.19) as

$$p(n) \propto e^{-\frac{1}{2}(n|n)} \ . \tag{9.58}$$

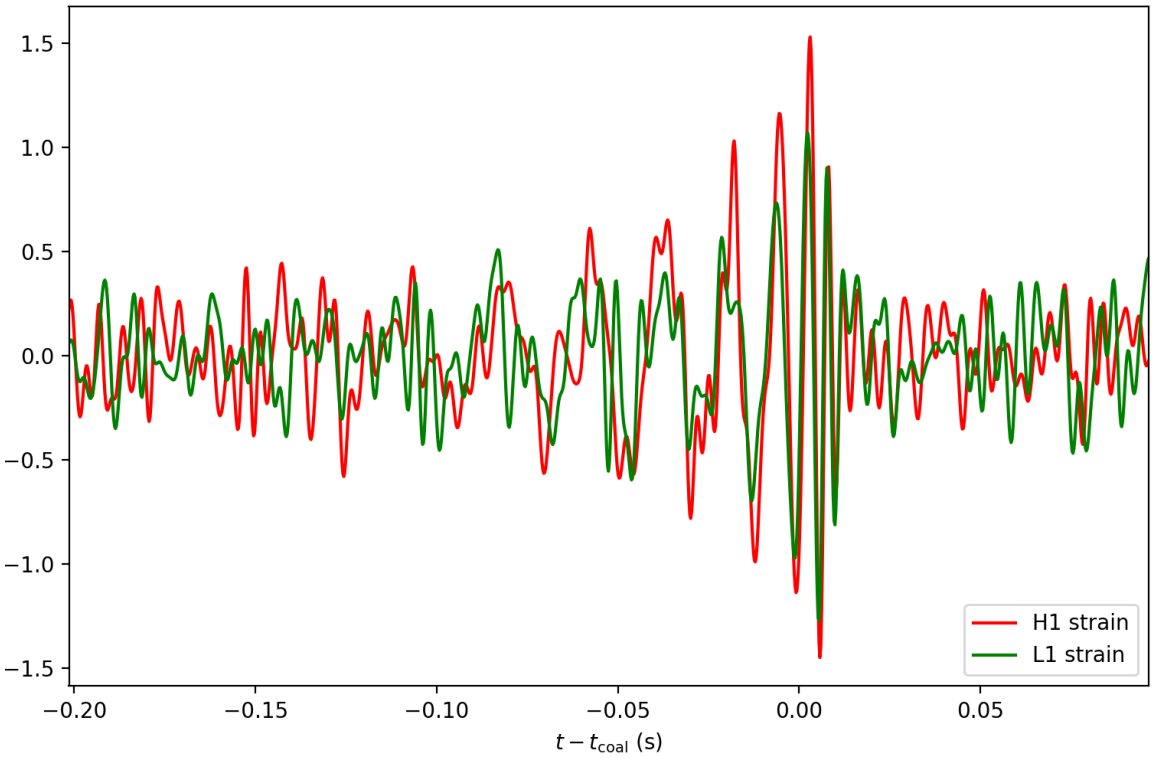

Figure 9.7: Whitened and band-pass-filtered strains of 0.3 s recorded by LIGO Hanford (red) and LIGO Livingston (green) centred around GW150914 trigger time. It is possible to see the chirp-like evolution of the frequency before merger (i.e. the amplitude peak) and then the signal is dissipated almost with constant frequency in the post-merger stage. The signal had a network SNR equal to 25, which is a very large value compared with the other detected transients.

Then it is natural to substitute $n(t) = s(t) - h(t;\boldsymbol{\theta})$, obtaining

$$p(s|\boldsymbol{\theta}, H, S_n) := A \cdot \exp\left[-\frac{1}{2}(s - h(\boldsymbol{\theta})|s - h(\boldsymbol{\theta}))\right] \to A \cdot \exp\left(-\frac{2}{T}\sum_{i=1}^{N}\frac{|\tilde{s}(f_i) - \tilde{h}(f_i;\boldsymbol{\theta})|^2}{S_n(f_i)}\right), \tag{9.59}$$

where A is the normalization constant. Eq. (9.59) defines the likelihood function of the observed data for a single detector and its approximation for discrete time series (where T is the period of the analysed strain and $N = T \cdot F_s$ is the number of elements of the series). In the discrete case, we can write the normalization constant of the likelihood function as

$$A = \prod_{i=1}^{N}\sqrt{\frac{2}{\pi T\, S_n(f_i)}}\,.$$

The likelihood function in Eq. (9.59) is defined real and positive for every value of the parameters' space and its logarithm is proportional to the inverse of the residual between our data and the template $h(t;\boldsymbol{\theta})$, which is the quantity we want to maximise. In the case of multiple detectors, the resulting likelihood is the product of the likelihood of the single detectors,

$$p(s_{\{\text{H,L,...}\}}|\boldsymbol{\theta}, H, S_{n,\{\text{H,L,...}\}}) = \prod_{k=\text{H,L,...}} p(s_k|\boldsymbol{\theta}, H, S_{n,k})\,. \tag{9.60}$$

Once obtained the prior distribution and the likelihood function, we can apply the Bayes' theorem and compute the posterior distribution for the parameters $\boldsymbol{\theta}$ with the model $h(t;\boldsymbol{\theta})$. Once we have likelihood function and prior distribution, we can apply the Bayes' theorem and get the posterior distribution for our parameters $\boldsymbol{\theta}$ as

$$p(\boldsymbol{\theta}|s_{\{\text{H,L,...}\}}, S_{n,\{\text{H,L,...}\}}, H) = \frac{p(s_{\{\text{H,L,...}\}}|\boldsymbol{\theta}, S_{n,\{\text{H,L,...}\}}, H)\cdot p(\boldsymbol{\theta}|H)}{p(s_{\{\text{H,L,...}\}}|S_{n,\{\text{H,L,...}\}}, H)}\,. \tag{9.61}$$

Exploring a parameter space of dimension $\gtrsim 15$ can be computationally challenging. Moreover, both the GW template the likelihood function are usually not analytically defined. For the reasons above, the posterior distributions are

usually calculated using Markov Chain Monte Carlo (MCMC) techniques. MCMC are methods for obtaining samples from a target probability distributions using iterative chains. An introduction on these numerical methods can be found on dedicated lecture notes on the course webpage.

Assuming a "best match" templates that maximize the posterior is found, it is interesting to study the associated uncertainty. Let us assume that $\boldsymbol{\theta}^*$ are the best combination of parameters such that $h(t;\boldsymbol{\theta}^*)$ is the best template matching $s(t)$. For a small variation $\Delta\boldsymbol{\theta}$ of the parameter, $\boldsymbol{\theta}^* \to \boldsymbol{\theta}^* + \Delta\boldsymbol{\theta}$, the waveform varies as

$$h(t;\boldsymbol{\theta}^*) \to h(t;\boldsymbol{\theta}^*) + \left.\frac{\partial h(t)}{\partial\theta_i}\right|_{\boldsymbol{\theta}=\boldsymbol{\theta}^*} \Delta\theta_i \,. \tag{9.62}$$

and Eq. (9.59) becomes

$$\log p(s|\boldsymbol{\theta}^*, \Delta\boldsymbol{\theta}, H, S_n) \propto -\frac{1}{2}\Gamma_{ij}\,\Delta\theta_i\,\Delta\theta_j \ . \tag{9.63}$$

Assuming a uniform prior distribution for $\Delta\boldsymbol{\theta}$, we can apply the Bayes' theorem and compute the posterior probability for the deviation parameters, $p(\Delta\boldsymbol{\theta}|s,\boldsymbol{\theta}^*,H,S_n)$, which will be identical to Eq. (9.63) unless a normalization constant. This probability density represents a Gaussian function with zero mean for each parameter $\Delta\theta_i$ with covariance matrix such that

$$\Gamma_{ij}(\boldsymbol{\theta}^*) = \left(\frac{\partial h}{\partial\theta_i}\middle|\frac{\partial h}{\partial\theta_j}\right)_{\boldsymbol{\theta}=\boldsymbol{\theta}^*} = 4\int_0^\infty \frac{1}{S_n(f)}\left[\left(\frac{\partial\tilde{h}(f)}{\partial\theta_i}\right)^*\left(\frac{\partial\tilde{h}(f)}{\partial\theta_j}\right)\right]_{\boldsymbol{\theta}=\boldsymbol{\theta}^*} \mathrm{d}f \,. \tag{9.64}$$

The matrix Γ_{ij} is usually called *Fisher information matrix* and its elements are functions of the chosen combination of parameters $\boldsymbol{\theta}^*$ though the dependencies of the template $h(t;\boldsymbol{\theta})$. Then it follows that the variance associated with the uncertainty $\Delta\theta_i$ can be computed as

$$\mathrm{Var}(\Delta\theta_i) = \left(\boldsymbol{\Gamma}^{-1}\right)_{ii} \ . \tag{9.65}$$

On the other hand, the integrals in Eq. (9.64) of the diagonal terms Γ_{ii} measure the amount of information that we gain for that particular parameter in every frequency bin. The integral of this quantity, i.e. Γ_{ii} itself, is then proportional to the cumulative information gained for the parameter θ_i.

Bibliography

Abbott, B. P. et al. (2019a). A guide to LIGO-Virgo detector noise and extraction of transient gravitational-wave signals.

Abbott, B. P. et al. (2019b). GWTC-1: A Gravitational-Wave Transient Catalog of Compact Binary Mergers Observed by LIGO and Virgo during the First and Second Observing Runs. *Phys. Rev.*, X9(3):031040.

Abramowitz, M. and Stegun, I. A. (1964). *Handbook of Mathematical Functions with Formulas, Graphs, and Mathematical Tables*. Dover, New York, ninth dover printing, tenth gpo printing edition.

Andersson, N. and Kokkotas, K. D. (1998). Towards gravitational-wave asteroseismology. *Mon. Not. Roy. Astron. Soc.*, 299:1059–1068.

Antonelli, A., Kavanagh, C., Khalil, M., Steinhoff, J., and Vines, J. (2020). Gravitational spin-orbit coupling through third-subleading post-Newtonian order: from first-order self-force to arbitrary mass ratios. *Phys. Rev. Lett.*, 125(1):011103.

Aretakis, S. (2015). Horizon Instability of Extremal Black Holes. *Adv. Theor. Math. Phys.*, 19:507–530.

Arnowitt, R. L., Deser, S., and Misner, C. W. (1960). Gravitational-electromagnetic coupling and the classical self-energy problem. *Phys. Rev.*, 120:313–320.

Babak, S. V. and Grishchuk, L. P. (2000). The Energy momentum tensor for the gravitational field. *Phys. Rev. D*, 61:024038.

Bachelot, A. and Motet-Bachelot, A. (1993). The Resonances of a Schwarzschild black hole. (In French). *Ann. Inst. H. Poincare Phys. Theor.*, 59:3–68.

Banihashemi, B. and Vines, J. (2018). Gravitomagnetic tidal effects in gravitational waves from neutron star binaries.

Bern, Z., Cheung, C., Roiban, R., Shen, C.-H., Solon, M. P., and Zeng, M. (2019). Scattering Amplitudes and the Conservative Hamiltonian for Binary Systems at Third Post-Minkowskian Order. *Phys. Rev. Lett.*, 122(20):201603.

Bernard, L., Blanchet, L., Bohé, A., Faye, G., and Marsat, S. (2017). Energy and periastron advance of compact binaries on circular orbits at the fourth post-Newtonian order. *Phys. Rev.*, D95(4):044026.

Bernuzzi, S., Nagar, A., Thierfelder, M., and Brügmann, B. (2012). Tidal effects in binary neutron star coalescence. *Phys.Rev.*, D86:044030.

Berti, E., Cardoso, V., and Starinets, A. O. (2009). Quasinormal modes of black holes and black branes. *Class. Quant. Grav.*, 26:163001.

Bini, D. and Damour, T. (2014). Gravitational self-force corrections to two-body tidal interactions and the effective one-body formalism. *Phys.Rev.*, D90(12):124037.

Bini, D., Damour, T., and Faye, G. (2012). Effective action approach to higher-order relativistic tidal interactions in binary systems and their effective one body description. *Phys.Rev.*, D85:124034.

Bini, D., Damour, T., and Geralico, A. (2019). Novel approach to binary dynamics: application to the fifth post-Newtonian level. *Phys. Rev. Lett.*, 123(23):231104.

Binnington, T. and Poisson, E. (2009). Relativistic theory of tidal Love numbers. *Phys. Rev.*, D80:084018.

Blanchet, L. (2014). Gravitational Radiation from Post-Newtonian Sources and Inspiralling Compact Binaries. *Living Rev. Relativity*, 17:2.

Blanchet, L. and Damour, T. (1989). Postnewtonian generation of gravitational waves. *Annales Poincare Phys.Theor.*, 50:377–408.

Bohé, A., Faye, G., Marsat, S., and Porter, E. K. (2015). Quadratic-in-spin effects in the orbital dynamics and gravitational-wave energy flux of compact binaries at the 3PN order. *Class. Quant. Grav.*, 32(19):195010.

Bondi, H. (1960). Gravitational Waves in General Relativity. *Nature*, 186(4724):535.

Bondi, H., van der Burg, M. G. J., and Metzner, A. W. K. (1962). Gravitational Waves in General Relativity. VII. Waves from Axi-Symmetric Isolated Systems. *Proceedings of the Royal Society of London Series A*, 269(1336):21–52.

Buonanno, A. and Damour, T. (1999). Effective one-body approach to general relativistic two-body dynamics. *Phys. Rev.*, D59:084006.

Buonanno, A. and Damour, T. (2000). Transition from inspiral to plunge in binary black hole coalescences. *Phys. Rev.*, D62:064015.

Campolattaro, A. and Thorne, K. S. (1970). Non-radial Pulsation of General-Relativistic Stellar Models. V. Analytic Analysis for L = 1. *Astrophys. J.*, 159:847.

Carroll, S. M. (1997). Lecture notes on general relativity.

Chandrasekhar, S. (1985). *The mathematical theory of black holes*.

Chandrasekhar, S. and Esposito, F. P. (1970). The $2\frac{1}{2}$-POST-NEWTONIAN Equations of Hydrodynamics and Radiation Reaction in General Relativity. *Astrophys. J.*, 160:153.

Christodoulou, D. and Klainerman, S. (1993). The Global nonlinear stability of the Minkowski space.

Cunningham, C. T., Price, R. H., and Moncrief, V. (1978). Radiation from collapsing relativistic stars. I - Linearized odd-parity radiation. *Astrophys. J.*, 224:643.

Cunningham, C. T., Price, R. H., and Moncrief, V. (1979). RADIATION FROM COLLAPSING RELATIVISTIC STARS. II. LINEARIZED EVEN PARITY RADIATION. *Astrophys. J.*, 230:870–892.

Dafermos, M., Holzegel, G., and Rodnianski, I. (2019). The linear stability of the Schwarzschild solution to gravitational perturbations. *Acta Math.*, 222:1–214.

Dafermos, M., Holzegel, G., Rodnianski, I., and Taylor, M. (2021). The non-linear stability of the Schwarzschild family of black holes. *Preprint*.

Dafermos, M., Rodnianski, I., and Shlapentokh-Rothman, Y. (2014). Decay for solutions of the wave equation on Kerr exterior spacetimes III: The full subextremal case —a— ¡ M.

Damour, T. (1983). Gravitational radiation and the motion of compact bodies. In Deruelle, N. and Piran, T., editors, *Gravitational Radiation*, pages 59–144. North-Holland, Amsterdam.

Damour, T. (1987). AN INTRODUCTION TO THE THEORY OF GRAVITATIONAL RADIATION. *NATO Sci. Ser. B*, 156:3–62.

Damour, T. (2012). The General Relativistic Two Body Problem and the Effective One Body Formalism. In *Proceedings, Relativity and Gravitation : 100 Years after Einstein in Prague*.

Damour, T. and Deruelle, N. (1986). General relativistic celestial mechanics of binary systems. II. The post-Newtonian timing formula. *Ann. Inst. Henri Poincaré Phys. Théor*, 44(3):263–292.

Damour, T. and Iyer, B. R. (1991). Multipole analysis for electromagnetism and linearized gravity with irreducible cartesian tensors. *Phys. Rev.*, D43:3259–3272.

Damour, T., Iyer, B. R., and Nagar, A. (2009). Improved resummation of post-Newtonian multipolar waveforms from circularized compact binaries. *Phys. Rev.*, D79:064004.

Damour, T., Iyer, B. R., and Sathyaprakash, B. (2000). Frequency domain P approximant filters for time truncated inspiral gravitational wave signals from compact binaries. *Phys.Rev.*, D62:084036.

Damour, T., Iyer, B. R., and Sathyaprakash, B. S. (1998). Improved filters for gravitational waves from inspiralling compact binaries. *Phys. Rev.*, D57:885–907.

Damour, T., Iyer, B. R., and Sathyaprakash, B. S. (2001). A Comparison of search templates for gravitational waves from binary inspiral. *Phys. Rev.*, D63:044023. [Erratum: Phys. Rev.D72,029902(2005)].

Damour, T., Jaranowski, P., and Schäfer, G. (2016). Conservative dynamics of two-body systems at the fourth post-Newtonian approximation of general relativity. *Phys. Rev.*, D93(8):084014.

Damour, T., Jaranowski, P., and Schfer, G. (2014). Nonlocal-in-time action for the fourth post-Newtonian conservative dynamics of two-body systems. *Phys. Rev.*, D89(6):064058.

Damour, T., Jaranowski, P., and Schfer, G. (2015). Fourth post-Newtonian effective one-body dynamics. *Phys. Rev.*, D91(8):084024.

Damour, T. and Lecian, O. M. (2009). On the gravitational polarizability of black holes. *Phys. Rev.*, D80:044017.

Damour, T. and Nagar, A. (2009). Relativistic tidal properties of neutron stars. *Phys. Rev.*, D80:084035.

Damour, T. and Nagar, A. (2010). Effective One Body description of tidal effects in inspiralling compact binaries. *Phys. Rev.*, D81:084016.

Damour, T. and Nagar, A. (2011). The Effective One Body description of the Two-Body problem. *Fundam. Theor. Phys.*, 162:211–252.

Damour, T., Nagar, A., and Villain, L. (2012). Measurability of the tidal polarizability of neutron stars in late-inspiral gravitational-wave signals. *Phys.Rev.*, D85:123007.

Damour, T. and Schäfer, G. (1988). HIGHER ORDER RELATIVISTIC PERIASTRON ADVANCES AND BINARY PULSARS. *Nuovo Cim.*, B101:127.

Damour, T., Soffel, M., and Xu, C.-m. (1991). General relativistic celestial mechanics. 1. Method and definition of reference systems. *Phys. Rev.*, D43:3273–3307.

Damour, T., Soffel, M., and Xu, C.-m. (1992). General relativistic celestial mechanics. 2. Translational equations of motion. *Phys. Rev.*, D45:1017–1044.

Damour, T., Soffel, M., and Xu, C.-m. (1993). General relativistic celestial mechanics. 3. Rotational equations of motion. *Phys. Rev.*, D47:3124–3135.

Damour, T., Soffel, M., and Xu, C.-m. (1994). General relativistic celestial mechanics. 4: Theory of satellite motion. *Phys. Rev.*, D49:618–635.

Damour, T. and Taylor, J. H. (1991). On the Orbital Period Change of the Binary Pulsar PSR 1913+16. *Astrophys. J.*, 366:501.

Damour, T. and Taylor, J. H. (1992). Strong field tests of relativistic gravity and binary pulsars. *Phys. Rev.*, D45:1840–1868.

Davis, M., Ruffini, R., and Tiomno, J. (1999). Pulses of gravitational radiation of a particle falling radially into a schwarzschild black hole. *Phys. Rev.*, D60:124004.

Dietrich, T. and Bernuzzi, S. (2015). Simulations of rotating neutron star collapse with the puncture gauge: end state and gravitational waveforms. *Phys.Rev.*, D91(4):044039.

Everitt, C. W. F. et al. (2011). Gravity Probe B: Final Results of a Space Experiment to Test General Relativity. *Phys. Rev. Lett.*, 106:221101.

Flanagan, E. E. and Hinderer, T. (2008). Constraining neutron star tidal Love numbers with gravitational wave detectors. *Phys.Rev.*, D77:021502.

Futamase, T. and Itoh, Y. (2007). The post-Newtonian approximation for relativistic compact binaries. *Living Rev. Rel.*, 10:2.

Futamase, T. and Schutz, B. F. (1983). Newtonian and post-Newtonian approximations are asymptotic to general relativity. *Phys. Rev. D*, 28(10):2363.

Gerlach, U. H. and Sengupta, U. K. (1979). Gauge invariant perturbations on most general spherically symmetric space-times. *Phys. Rev.*, D19:2268–2272.

Gerlach, U. H. and Sengupta, U. K. (1980). Gauge invariant coupled gravitational, acoustical, and electromagnetic modes on most general spherical space- times. *Phys. Rev.*, D22:1300–1312.

Gundlach, C. and Martin-Garcia, J. M. (2000). Gauge-invariant and coordinate-independent perturbations of stellar collapse. I: The interior. *Phys. Rev.*, D61:084024.

Grlebeck, N. (2015). No-hair theorem for Black Holes in Astrophysical Environments. *Phys. Rev. Lett.*, 114(15):151102.

Harms, E., Bernuzzi, S., and Brügmann, B. (2013). Numerical solution of the 2+1 Teukolsky equation on a hyperboloidal and horizon penetrating foliation of Kerr and application to late-time decays. *Class.Quant.Grav.*, 30:115013.

Hinderer, T. (2008). Tidal Love numbers of neutron stars. *Astrophys.J.*, 677:1216–1220.

Horowitz, G. T. and Perry, M. J. (1982). GRAVITATIONAL ENERGY CANNOT BECOME NEGATIVE. *Phys. Rev. Lett.*, 48:371.

Ipser, J. R. and Thorne, K. S. (1968). Relativistic, Spherically Symmetric Star Clusters. I. Stability Theory for Radial Perturbations. *Astrophys. J.*, 154:251–+.

Jackson, J. D. (1975). *Classical electrodynamics; 2nd ed.* Wiley, New York, NY.

Kay, B. S. and Wald, R. M. (1987). Linear Stability of Schwarzschild Under Perturbations Which Are Nonvanishing on the Bifurcation Two Sphere. *Class. Quant. Grav.*, 4:893–898.

Kidder, L. E. (2008). Using Full Information When Computing Modes of Post- Newtonian Waveforms From Inspiralling Compact Binaries in Circular Orbit. *Phys. Rev.*, D77:044016.

Kimura, T. (1961). Fixation of Physical Space-Time Coordinates and Equation of Motion of Two-Body Problem. *Progress of Theoretical Physics*, 26(2):157–172.

Klainerman, S. and Szeftel, J. (2017). Global Nonlinear Stability of Schwarzschild Spacetime under Polarized Perturbations.

Kokkotas, K. D. and Schmidt, B. G. (1999). Quasi-normal modes of stars and black holes. *Living Rev. Rel.*, 2:2.

Landau, L. D. and Lifschits, E. M. (1975). *The Classical Theory of Fields*, volume Volume 2 of *Course of Theoretical Physics*. Pergamon Press, Oxford.

Leaver, E. W. (1985). An Analytic representation for the quasi normal modes of Kerr black holes. *Proc. Roy. Soc. Lond.*, A402:285–298.

Levi, M., Mcleod, A. J., and Von Hippel, M. (2020). N^3LO gravitational spin-orbit coupling at order G^4.

Mädler, T. and Winicour, J. (2016). Bondi-Sachs Formalism. *Scholarpedia*, 11:33528.

Maggiore, M. (2007). *Gravitational Waves. Vol. 1: Theory and Experiments*. Oxford Master Series in Physics. Oxford University Press.

Maggiore, M. (2008). The Physical interpretation of the spectrum of black hole quasinormal modes. *Phys. Rev. Lett.*, 100:141301.

Maggiore, M. (2018). *Gravitational Waves. Vol. 2: Astrophysics and Cosmology*. Oxford University Press.

Marsat, S. (2015). Cubic order spin effects in the dynamics and gravitational wave energy flux of compact object binaries. *Class. Quant. Grav.*, 32(8):085008.

Marsat, S., Bohé, A., Blanchet, L., and Buonanno, A. (2014). Next-to-leading tail-induced spin?orbit effects in the gravitational radiation flux of compact binaries. *Class. Quant. Grav.*, 31:025023.

Martin-Garcia, J. M. and Gundlach, C. (2001). Gauge-invariant and coordinate-independent perturbations of stellar collapse. II: Matching to the exterior. *Phys. Rev.*, D64:024012.

Misner, C. W., Thorne, K. S., and Wheeler, J. A. (1973). *Gravitation*. W. H. Freeman, San Francisco.

Moncrief, V. (1974a). Gravitational perturbations of spherically symmetric systems. I. The exterior problem. *Ann. Phys.*, 88:323–342.

Moncrief, V. (1974b). Gravitational perturbations of spherically symmetric systems. ii. perfect fluid interiors. *Ann. Phys.*, 88(2):343 – 370.

Nagar, A. and Rezzolla, L. (2005). Gauge-invariant non-spherical metric perturbations of Schwarzschild black-hole spacetimes. *Class. Quant. Grav.*, 22:R167.

Newman, E. and Penrose, R. (1962). An Approach to gravitational radiation by a method of spin coefficients. *J. Math. Phys.*, 3:566–578.

Newman, E. T. and Penrose, R. (1966). Note on the Bondi-Metzner-Sachs Group. *Journal of Mathematical Physics*, 7(5):863–870.

Nollert, H.-P. (1999). TOPICAL REVIEW: Quasinormal modes: the characteristic 'sound' of black holes and neutron stars. *Class. Quant. Grav.*, 16:R159–R216.

Nollert, H.-P. and Schmidt, B. G. (1992). Quasinormal modes of Schwarzschild black holes: Defined and calculated via Laplace transformation. *Phys. Rev. D*, 45(8):2617.

Penrose, R. (1963). Asymptotic properties of fields and space-times. *Phys. Rev. Lett.*, 10:66–68.

Regge, T. and Wheeler, J. A. (1957). Stability of a Schwarzschild singularity. *Phys. Rev.*, 108:1063–1069.

Sachs, R. K. (1962). Gravitational Waves in General Relativity. VIII. Waves in Asymptotically Flat Space-Time. *Proceedings of the Royal Society of London Series A*, 270(1340):103–126.

Schaefer, G. and Jaranowski, P. (2018). Hamiltonian formulation of general relativity and post-Newtonian dynamics of compact binaries. *Living Rev. Rel.*, 21(1):7.

Schon, R. and Yau, S.-T. (1979). On the Proof of the positive mass conjecture in general relativity. *Commun. Math. Phys.*, 65:45–76.

Schon, R. and Yau, S.-T. (1981). Proof of the positive mass theorem. 2. *Commun. Math. Phys.*, 79:231–260.

Schon, R. and Yau, S.-T. (1982). PROOF THAT THE BONDI MASS IS POSITIVE. *Phys. Rev. Lett.*, 48:369–371.

Schutz, B. F. (1985). *A First Course in General Relativity*. Cambridge Univ. Pr., Cambridge, UK.

Schutz, B. F. and Will, C. M. (1985). BLACK HOLE NORMAL MODES: A SEMIANALYTIC APPROACH. *Astrophys. J.*, 291:L33–L36.

Seidel, E. (1990). Gravitational radiation from even parity perturbations of stellar collapse: Mathematical formalism and numerical methods. *Phys. Rev.*, D42:1884–1907.

Stergioulas, N. (2003). Rotating stars in relativity. *Living Rev. Rel.*, 6:3.

Thorne, K. S. (1969). Non-radial Pulsation of General-Relativistic Stellar Models. III. Analytic and Numerical Results for Neutron Stars. *Astrophys. J.*, 158:1.

Thorne, K. S. (1980). Multipole Expansions of Gravitational Radiation. *Rev. Mod. Phys.*, 52:299–339.

Vines, J., Flanagan, E. E., and Hinderer, T. (2011). Post-1-Newtonian tidal effects in the gravitational waveform from binary inspirals. *Phys. Rev.*, D83:084051.

Vines, J. E. and Flanagan, E. E. (2010). Post-1-Newtonian quadrupole tidal interactions in binary systems. *Phys. Rev.*, D88:024046.

Vishveshwara, C. V. (1970a). Scattering of Gravitational Radiation by a Schwarzschild Black-hole. *Nature*, 227:936–938.

Vishveshwara, C. V. (1970b). Stability of the schwarzschild metric. *Phys. Rev.*, D1:2870–2879.

Wald, R. M. (1984). *General relativity*. The University of Chicago Press, Chicago.

Weisberg, J., Nice, D., and Taylor, J. (2010). Timing Measurements of the Relativistic Binary Pulsar PSR B1913+16. *Astrophys.J.*, 722:1030–1034.

Whiting, B. F. (1989). Mode stability of the Kerr black hole. *Journal of Mathematical Physics*, 30:1301–1305.

Will, C. M. (2014). The Confrontation between General Relativity and Experiment. *Living Rev. Rel.*, 17:4.

Witten, E. (1981). A Simple Proof of the Positive Energy Theorem. *Commun. Math. Phys.*, 80:381.

Zerilli, F. J. (1970). Effective potential for even parity Regge-Wheeler gravitational perturbation equations. *Phys. Rev. Lett.*, 24:737–738.